



HAL
open science

Design of hybrid nano-composite adsorbent for recovery of Pd And Au from electronic wastewater

An Trieu

► **To cite this version:**

An Trieu. Design of hybrid nano-composite adsorbent for recovery of Pd And Au from electronic wastewater. Other. Université de Lyon, 2018. English. NNT : 2018LYSE1314 . tel-03083322

HAL Id: tel-03083322

<https://theses.hal.science/tel-03083322>

Submitted on 19 Dec 2020

HAL is a multi-disciplinary open access archive for the deposit and dissemination of scientific research documents, whether they are published or not. The documents may come from teaching and research institutions in France or abroad, or from public or private research centers.

L'archive ouverte pluridisciplinaire **HAL**, est destinée au dépôt et à la diffusion de documents scientifiques de niveau recherche, publiés ou non, émanant des établissements d'enseignement et de recherche français ou étrangers, des laboratoires publics ou privés.



N°d'ordre NNT : 2018LYSE1314

THESE de DOCTORAT DE L'UNIVERSITE DE LYON

opérée au sein de
l'Université Claude Bernard Lyon 1

Ecole Doctorale ED206
Chimie, Procédés, Environnement

Spécialité de doctorat : Chimie

Discipline : Chimie

Soutenue publiquement le 18/12/2018, par :

Quoc-An TRIEU

DESIGN OF HYBRID NANO-COMPOSITE ADSORBENT FOR RECOVERY OF Pd AND Au FROM ELECTRONIC WASTEWATER

Devant le jury composé de :

Mme. GIROIR-FENDLER Anne, Enseignant-chercheur/CARE	Présidente-Examinatrice
M. HESEMANN Peter, Directeur de Recherche /ICGM Montpellier	Rapporteur
M. TREBOUET Dominique, Professeur des Universités/IPHC Strasbourg	Rapporteur
Mme. LEBEAU Bénédicte, Directeur de recherche/IS2M Mullhouse	Examinatrice
M. DANIELE Stéphane, Professeur des Universités /IRCELYON	Directeur de thèse
M. PELLET-ROSTAING Stéphane, Directeur de Recherche /ICSM	Co-directeur de thèse
M. TRAORE Youssouf, Manager R&D/ MORPHOSIS	Invité

TO MY FATHER AND MY MOTHER

ACKNOWLEDGMENT

During this thesis that I've conceived as a risk-taking activity, I have been blessed, influenced and supported by many individuals, and organizations.

First and foremost, I'm greatly indebted to my supervisor – Prof. Stéphane DANIELE – for your valuable time, your huge enthusiasm, your unceasing encouragement, and your stoic resilience. With the lack of experiences in material chemistry, I have learned a lot of knowledge in this field through this research under your supervision. Although embarking on this research was to deal with different challenges and obstacles, you've walked me through this adventure eventually.

I am grateful to Prof. Stéphane PELLET-ROSTAING for being my co-supervisor in this thesis and having taken your valuable time to inspire me with the ideas about ligands' structures and some advices related to extraction processes that have steered me toward the aimed direction.

I am also deeply grateful to Ms. Nhu-Trang TRAN-THI for having mentored me in 2015. You indeed introduced me the program “Bourse d'Excellence de l'Ambassade de France au Vietnam” and Prof. Stéphane DANIELE at the University Lyon 1. As in hero-journey stories' motif, the protective figure who provides the adventurer with amulets was you. Thank you very much!

I must thank Mr. Youssouf TRAORE (MORPHOSIS company) for having taken part in this adventure. I really appreciate your sharing practical knowledge in recycling industry, your providing e-wastewater samples, your time and your patience.

I also greatly acknowledge all jury's members, including: Mr. Peter HESEMANN (Reviewer) at Institut Charles Gerhardt Montpellier (ICGM, Montpellier), M. Dominique TREBOUET (Reviewer) at Institut Pluridisciplinaire Hubert CURIEN (IPHC, Strasbourg), Ms. Bénédicte LEBEAU (Examiner) at Institut de Science des Matériaux de Mulhouse (IS2M, Mullhouse), Ms. Anne GIROIR-FENDLER (Examiner) at Institut de recherches sur la catalyse et l'environnement de Lyon (IRCELYON, Villeurbanne) for having taken your valuable time and effort to attend my thesis' defense.

Many thanks are due to the staff of IRCELYON including: Ms. Bernadette JOUGUET – manager of thermal analysis service, Ms. Chantal LORENTZ – manager of Nuclear Magnetic Resonance service, Ms. France SIMONET-BEAUCHESNE and Ms. Laurence BUREL – technical and administrative staff of Microscopy service and especially Ms. Pascale MASCUNAN – manager of Chemical and textural analysis for your prestigious tolerance toward the frequency and the number of my samples. I'd also like to thank Ms. Nadine ESSAYEM – leader of “Chimie durable: du fondamental à l'application” (CDFA team, IRCELYON) and all team's members for having generously allowed me to carry out my thesis, participate in research activities and using equipment from 2015 to 2018.

Many thanks are also due to Ms. Claire BORDES and Ms. Marie HANGOUET for your support to the measurement of surface charge of polypropylene textiles at ISA Institute. I am also grateful to Mr. Dirk HEGEMANN (EMPA Institute, Switzerland), and Mr. Samuel HOUILLIEZ at SAATI company for eagerly supplying polypropylene textile samples.

Special thanks are due to my colleagues: Mr. Alexandre VERCHÈRE – for being really supportive to me, if the introduction and conclusion parts in French of this thesis are appreciated, it's mainly because of you, Ms. Diane BIJOU – for your dynamic spirit and Ms. Lama Omar – for instructing me how to perform BET specific surface area measurements.

Last but not least, I would like to express my love and gratitude toward my family for your encouragement and unceasing consolation. I love you more than words can express. Especially, my loving sister for double-checking the details of my thesis although you had just 2 months remaining before going into labor and zero background in chemistry.

CONTENT

CHAPTER 1.	GENERAL INTRODUCTION.....	1
1.1.	Overview about metal sustainability in high-tech society.....	1
1.2.	Mining production, consumption and future demand of precious metals.....	4
CHAPTER 2.	STATE-OF-ART OF RECYCLING PROCESSES	8
2.1.	Recycling Processes	8
2.1.1.	Definitions, classifications, and compositions of E-waste	8
2.1.2.	Metal recycling rates.....	9
2.1.3.	Metal recovery approaches	10
2.1.3.1.	Informal recycling and formal recycling	10
2.1.3.2.	Separation of metallic and non-metallic fraction.....	10
2.1.3.3.	Metallurgical processes for the extraction of gold and PGM from E-waste	12
2.2.	Adsorbents for treatment of precious metals from water and wastewater	19
2.2.1.	Mechanisms in precious metals adsorption	19
2.2.2.	Biosorbents – carbonaceous adsorbents	20
2.2.2.1.	Cellulose-based and lignin-based materials.....	21
2.2.2.2.	Tannin-based adsorbents.....	21
2.2.2.3.	Chitosan-based adsorbents.....	22
2.2.3.	Polymer-based adsorbents	24
2.2.3.1.	Ion-exchange resins and resins impregnated with ligands.....	24
2.2.3.2.	Functionalized polymers	27
2.2.4.	Hybrids Nanocomposites : Nano-oxides based adsorbents and polymer/Metal oxide	29
2.2.4.1.	Coupling molecule and nanocomposites applications	31
2.2.4.2.	Synthesis of Polymer/Metal Oxide Hybrid Nanocomposites	38
	The outlines of the thesis.....	45

CHAPTER 3.	MATERIALS AND EXPERIMENTAL PROCEDURE	49
3.1.	Materials and chemicals	49
3.2.	Characterization methods	50
3.2.1.	Fourier Transform Infra-Red Spectroscopy (ATR-FTIR + DRIFT).....	50
3.2.2.	X-Ray Diffraction analysis	51
3.2.3.	Thermo gravimetric analysis (TGA)	52
3.2.4.	Brunauer–Emmett–Teller method	53
3.2.5.	Solid-State ³¹ P MAS-NMR Spectroscopy	53
3.2.6.	Scanning Electron Microscopy.....	54
3.2.7.	Elemental Analysis (ICP-OES)	54
3.2.8.	Surface zeta potential measurement of nanosuspensions and textiles.....	55
3.3.	Experimental procedures	55
3.3.1.	Surface modification of zirconia	55
3.3.2.	Deposition of zirconia on the surface of polypropylene and impregnation with ligands	57
3.3.2.1.	Dip coating.....	57
3.3.2.2.	Layer-by-Layer dip-coating method (LbL)	58
3.3.3.	Batch adsorption experiment and adsorption isotherm	59
CHAPTER 4.	HYBRID ZrO ₂ NANOPOWDERS: SYNTHESSES AND APPLICATIONS	61
4.1.	Syntheses of the hybrid ZrO ₂ nanoparticles using different kinds of ligands ...	61
4.2.	Characterization of hybrid zirconia nano-powders:	63
4.2.1.	FT-IR spectroscopy	63
4.2.2.	³¹ P MAS solid-state NMR	68
4.2.3.	Elemental analysis and thermogravimetric analysis method.....	70
4.3.	Synthesis of ZrO ₂ -TOA with different mole ratios of ZrO ₂ to TOA	72
4.4.	Investigation of gold and palladium adsorption capability	74
4.5.	Investigation of adsorption capability of ZrO ₂ -TOA	77

4.5.1.	Adsorption isotherm and capacity of ZrO ₂ -TOA	77
4.5.2.	Effect of contact time.....	80
4.5.3.	Effect of HCl and chloride to the adsorption.....	83
4.5.4.	Stripping investigation.....	86
4.5.5.	Reusability of the ZrO ₂ -TOA	87
4.6.	Two-step surface modification of ZrO ₂	91
4.6.1.	Fourier-Transform Infrared Spectroscopy	93
4.6.2.	Thermogravimetric analysis (TGA)	96
4.6.3.	³¹ P MAS solid-state NMR	97
4.6.4.	BET specific surface area	98
4.6.5.	SEM images.....	99
4.6.6.	Adsorption study of ZrO ₂ -AA-TOA.....	100
4.6.6.1.	Maximum adsorption capacities toward Pd and Au	100
4.6.6.2.	Adsorption kinetics of ZrO ₂ -AA-TOA	102
4.6.6.3.	Reusability of ZrO ₂ -AA-TOA	103
4.6.6.4.	Adsorption of surface modified nano-ZrO ₂ materials toward Pd and Au in the real e-waste effluent.....	104
CHAPTER 5.	DESIGN OF COMPOSITE DEVICE	109
5.1.	Deposition of nano-zirconia coating on the polypropylene with high density of grafting group (single dip coating)	112
5.1.1.	Effect of pH of zirconia nanosuspension to dip coating process.....	113
5.1.2.	Effect of zirconia nanosuspensions concentration.....	114
5.1.3.	Effect of temperature	116
5.1.4.	Investigation into adsorption capability of PP-COO-ZrO ₂ (dip coating) impregnated with thioctic acid	116
5.2.	Deposition of ZrO ₂ on the polypropylene with low density of grafting group (layer-by-layer dip coating method).....	118
5.2.1.	The difference in carboxylic group density	118

5.2.2.	Effect of the type of nanosuspension of zirconia to the coating process..	119
5.2.3.	Effect of the number of layers	121
5.2.4.	Effect of molecular weight of polyacrylic acid	125
5.2.5.	The role of sodium chloride.....	126
5.2.6.	Effect of the ZrO ₂ nanosuspension's concentration	127
5.2.7.	Stability test of LbL coating on the PP-COOH substrate.....	128
5.2.8.	Application of LbL dip-coating to commercial SAATI polypropylene textiles	129
5.2.9.	Investigation of adsorption capability of LbL-made PP-COO-ZrO ₂ impregnated with TOA.....	133
GENERAL CONCLUSIONS & PERSPECTIVES		135
REFERENCES		145

LIST OF FIGURES

Figure 1-1 – Global estimates of end-of-life recycling rates for 60 metals and metalloids by UN.	3
Figure 1-2 – World gold production in 2015 and 2016 (source: USGS)	5
Figure 2-1 – Structural formula of tributyl phosphate (TBP, I) and trialkyl phosphine oxide (TRPO, II)	15
Figure 2-2 – Structural formulas of carbamoylmethylphosphine oxide derivatives (CMPO, III) and malonamide derivatives (IV) and N,N'-dimethyl-N,N'-dialkyltetradecylmalonamide	15
Figure 2-3 – Structural formulas of diglycoamide derivatives and dioxodiamide derivatives	16
Figure 2-4 – Structural formulas of dialkylsulfide (left) and dialkyl disulfide (right)	16
Figure 2-5 – Structural formulas of thiodiglycoamide derivatives (left) and dithiodiglycoamide derivatives (right)	17
Figure 2-6 – Structure of thiacalix[4]arenes derivatives [31].....	18
Figure 2-7 – Structural formulas of synthesized thiacalix[n]arene [32]	18
Figure 2-8 – Proposed major composition of Pt(IV) extracted species by extractant 1	19
Figure 2-9 – The structure of lignin.....	21
Figure 2-10 – The structure of tannin.....	22
Figure 2-11 – The structure of chitosan.....	22
Figure 2-12 – The number of publications on nanotechnology or its applications for environmental remediation [69].	29
Figure 2-13 – Schematic representation of Fe ₃ O ₄ @SiO ₂ -TOA [62].....	32
Figure 2-14 – Schematic representation of Imidazole-SBA-15[70].....	33
Figure 2-15 – Schematic representation of the impact of water on the surface modification of oxide surface using trimethoxysilane [78]	34
Figure 2-16 – The binding modes of carboxylic acids on oxide surfaces.	34
Figure 2-17 – Competition between surface modification and dissolution/precipitation processes using phosphonic acids [78]	35
Figure 2-18 – Schematic illustration of surface modification of phosphonic acids on oxide surface, R' represents the introduced functional group [80].....	36
Figure 2-19 – Illustration Arbuzov reaction.....	37
Figure 2-20 – Illustration of aza-Michael reaction.....	37
Figure 2-21 – The structure of TiO ₄ (EtO) ₁₂ (^t BuPO ₃) (left) and Ti ₁₀ O ₂ (EtO) ₃₂ (AEP) ₂ (AEP = 2-aminoethylphosphonate) [84]	38
Figure 2-22 – Illustration of how individual shortcomings of nanoparticles and polymeric host material can be circumvented by polymer-supported nano particles [86].....	39

Figure 2-23 – Different synthetic strategies in the formation of polymer/inorganic hybrid material [85]	39
Figure 2-24 – Schematic representation of layer-by-layer approach based on zirconia nanosuspension and aqueous polypropylene solution.	43
Figure 2-25 – Schematic illustration of proposed structure of substrate-supported hybrid ZrO ₂ nanoparticles.....	45
Figure 2-26 - The tentative combination between grafting and chelating groups for specifically target metals.....	47
Figure 3-1 – Picture of ATR-FTIR equipment (left) and schematic representation of the measuring principle (right).....	51
Figure 3-2 – Picture of XRD equipment	51
Figure 3-3 – Temperature program used for TGA experiment	52
Figure 3-4 – Picture of TGA equipment.....	52
Figure 3-5 – Picture of Micrometrics ASAP 2020	53
Figure 3-6 – Picture of solid-state NMR equipment	53
Figure 3-7 – Picture of ICP-OES equipment.....	54
Figure 3-8 – Schematic representation of post-modification procedure	56
Figure 3-9 – Schematic representation of two-step surface modification	57
Figure 3-10 – Schematic representation of the deposition and impregnation processes onto surface-modified polypropylene.....	58
Figure 3-11 – Schematic representation of our LbL coating process.....	59
Figure 3-12 – Schematic representation of batch adsorption experiment	60
Figure 4-1. The structures of selected ligands to functionalize the zirconia’s surface.....	62
Figure 4-2 – XRD spectrum of bare zirconia nanoparticle from Sigma Aldrich	63
Figure 4-3 – FT-IR spectra of bare nano-ZrO ₂ , nano-ZrO ₂ modified with TOA and TOA	65
Figure 4-4 – FT-IR spectra of nano-ZrO ₂ , nano-ZrO ₂ modified with DODGA and DODGA	66
Figure 4-5 – FT-IR spectra of bare nano-ZrO ₂ , nano-ZrO ₂ modified PMIDAA and PMIDAA ...	66
Figure 4-6 – FT-IR spectrum of bare nano-ZrO ₂ , nano-ZrO ₂ modified with DEHCPMPA	67
Figure 4-7 – FT-IR spectrum bare nano-ZrO ₂ , nano-ZrO ₂ modified with DOCMPA and DOCMPA	67
Figure 4-8 – (a) ³¹ P NMR spectra of phosphonic ligands, (b) ³¹ P MAS solid-state NMR spectra of zirconia nanoparticles modified with phosphonic ligands, and (c) ³¹ P MAS solid-state NMR spectra of zirconia nanoparticles modified with phosphonic ligands after heating process. (*) spinning side bands.....	69
Figure 4-9 – TGA curves of surface-modified nano-zirconia	71
Figure 4-10 – The effect of mole ratio of ZrO ₂ /TOA to the deposition process	73

Figure 4-11 – Extraction percentage (%) of ligand-functionalized zirconia nanoparticles based on single solution. [Pd] = 10 ppm, [Au] = 10 ppm, V = 20 mL, m _{material} = 50 mg, time = 24 ^h , T° = 25°C	74
Figure 4-12 – A photograph of the location of modified-zirconia particles in the immiscible mixture of water and CH ₂ Cl ₂	76
Figure 4-13 – Au and Pd capacities of ZrO ₂ -TOA as a function of initial concentration	78
Figure 4-14 – Langmuir isotherm for Pd adsorption	79
Figure 4-15 – Langmuir isotherm for Au adsorption	79
Figure 4-16 – The influence of contact time on the Pd and Au adsorption	81
Figure 4-17 – Pseudo-first-order and pseudo-second-order models for Pd adsorption kinetics ...	82
Figure 4-18 – Pseudo-first-order and pseudo-second-order models for Au adsorption kinetics...	82
Figure 4-19 – Impact of HCl concentration on the Au and Pd extraction	84
Figure 4-20 – Schematic representation of the protonation process of sulfur atoms in functional groups	85
Figure 4-21 – Effect of Cl ⁻ concentration to the Pd adsorption	85
Figure 4-22 – Schematic representation of the cleavage of the bond between thioctic acids and ZrO ₂ 's surface	85
Figure 4-23 – The back-extraction (stripping) percentage of Pd and Au using different mixtures of thiourea and hydrochloric. The anterior adsorption was carried out using the dual solution of Au and Pd with the concentration of 10 mg/L/each.	86
Figure 4-24 – Comparison of back-extraction performance between TU + HCl and NaNO ₂	87
Figure 4-25 – Extraction and stripping percentage through adsorption/desorption cycles	88
Figure 4-26 – Extraction performance of ZrO ₂ -TOA through adsorption/desorption cycles in the real effluent	88
Figure 4-27 – Schematic explanation about the loss of TOA on the zirconia's surface after desorption	89
Figure 4-28 – Reusability test of ZrO ₂ -DOCMPA	90
Figure 4-29 – The extraction percentage of metals present in the real effluent (left), and a photo of e-wastewater provided from MORPHOSIS (right)	90
Figure 4-30 – Schematic representation of two-step surface modification of ZrO ₂	92
Figure 4-31 – The mechanism of amide coupling reaction mediated by DCC [116]	93
Figure 4-32 – ATR-FTIR spectra of bare ZrO ₂ , ZrO ₂ -AA, and AA	94
Figure 4-33 – DRIFT spectra of ZrO ₂ -AA, ZrO ₂ -AA-TOA (NHS-TOA), ZrO ₂ -AA-TOA (TOA/DCC) and ZrO ₂ -TOA	95
Figure 4-34 – DRIFT spectra of ZrO ₂ -AA, ZrO ₂ -AA-TOA (NHS-TOA) and ZrO ₂ -AA-TOA (TOA/DCC) after water desorption	96

Figure 4-35 – TGA curves of ZrO ₂ -AA and ZrO ₂ -AA-TOA (NHS-TOA) and ZrO ₂ -AA-TOA (TOA/DCC).....	97
Figure 4-36 – ³¹ P solid-state MAS NMR spectra of ZrO ₂ -AA, ZrO ₂ -AA-TOA and AA	98
Figure 4-37 – SEM images of ZrO ₂ -TOA (a), ZrO ₂ -AA-TOA (NHS-TOA) (b), and ZrO ₂ -AA-TOA (TOA/DCC).....	100
Figure 4-38 – SEM-EDX spectrum of ZrO ₂ -AA-TOA (NHS-TOA).....	100
Figure 4-39 – Oxidation process of thiol group [119].....	101
Figure 4-40 – A)The effect of contact time on adsorption capacity and B) pseudo-second order model of Pd adsorption kinetics of ZrO ₂ -AA-TOA (NHS-TOA)	103
Figure 4-41 – Recyclability of ZrO ₂ -AA-TOA materials for capturing Pd in the single solution at 10 mg/L through 5 cycles of adsorption/desorption.....	104
Figure 4-42 – Comparison of surface-modified ZrO ₂ materials' recyclability toward Pd.....	105
Figure 4-43 – Reusability test of ZrO ₂ -AA-TOA (NHS-TOA) in the effluent diluted 5-fold and spiked with Pd	106
Figure 4-44 – Reusability test of ZrO ₂ -AA-TOA (NHS-TOA) in the effluent diluted 5-fold and spiked with Pd and Au.....	107
Figure 5-1 – Schematic structure of the aimed inorganic/organic material	110
Figure 5-2 – Different approaches to zirconia coating on the polypropylene.....	111
Figure 5-3 – Schematic representation of single dip-coating approach	112
Figure 5-4 – ATR-FITR spectra of carboxylic-modified polypropylene (red), ZrO ₂ -coated bare polypropylene (green), ZrO ₂ -ammonium-modified polypropylene (blue) and ZrO ₂ -coated carboxylic-modified polypropylene (yellow).....	113
Figure 5-5 – ATR-FTIR spectra ZrO ₂ -coated PP-COOH samples using ZrO ₂ nanosuspension with pH 10 and pH 1.....	113
Figure 5-6 – XRD spectra of different ZrO ₂ -coated PP-COOH.....	114
Figure 5-7 – SEM images of different ZrO ₂ -coated PP-COOH.....	115
Figure 5-8 – ATR-FTIR of PP-COOH coated ZrO ₂ at different temperatures	116
Figure 5-9 – Photos of PP-COOH-ZrO ₂ impregnated with TOA before and after Pd adsorption process (left), and PP-COOH-ZrO ₂ textiles from CREAT and EMPA.....	117
Figure 5-10 – FTIR spectra of carboxylic-modified polypropylene samples from EMPA and CREAT.....	118
Figure 5-11 – The content of ZrO ₂ deposited on PP substrate by LbL method using different sources of nanosuspension	119
Figure 5-12 – Surface zeta potential curves of the used nanosuspensions and PAAH	120
Figure 5-13 – Surface zeta potential curves of textiles based on streaming potential measurement	120
Figure 5-14 – TGA curves of PP-COOH coated with 100% ZrO ₂ by LbL method.....	121

Figure 5-15 – ATR-FTIR spectra of bare PP-COOH, PP-COOH coated with 15 layers and 30 layers of (ZrO ₂ /PAAH)	122
Figure 5-16 – Illustration of PP-COOH (EMPA) textiles before (left) and after (right) LbL coating with nano-ZrO ₂ . The change of textile's color from brown to white after LbL process has been indicative of the presence of ZrO ₂ on textile's fibers	122
Figure 5-17 – SEM images of PP-COOH coated with 10, 15, and 30 layers of (ZrO ₂ /PAAH)..	124
Figure 5-18 – TGA curves of PP-COOH samples coated with (ZrO ₂ /PAAH) using PAAH solutions with different M _w	125
Figure 5-19 – Schematic representation of the LbL build-up process [122].....	126
Figure 5-20 – Effect of NaCl in PAAH solution on ZrO ₂ content (% wt.). Conditions: [ZrO ₂] = 1% wt. pH 2.5; [PAAH] = 0.5% wt. pH 2.5 with [NaCl] varied from 0 to 1.5 M	127
Figure 5-21 – Effect of ZrO ₂ nanosuspension's concentration. Conditions: [ZrO ₂] = 1 - 5% wt. pH 2.5; [PAAH] = 0.5% wt. pH 2.5 with [NaCl] = 0 M	128
Figure 5-22 – Stability test of ZrO ₂ on PP substrate	129
Figure 5-23 – SEM images of naked PP substrates 106/26.....	130
Figure 5-24 – SEM images of ZrO ₂ -coated PP substrates 106/26	131
Figure 5-25 – SEM images of ZrO ₂ -coated PP substrates 297/35	132
Figure 5-26 – Reusability test of PP-COOH-ZrO ₂ impregnated with thiocetic acid	133

LIST OF TABLES

Table 1-1. Critical metals for a range of countries [2]	1
Table 1-2. The average quantity of precious metals in typical electronic products (mg/unit)[7] ...	4
Table 1-3. The consumption of precious metals in EEE during 2005-2014 (in tons) (source: USGS)	6
Table 2-1. WEEE categories according to the EU directive on WEEE	8
Table 2-2. Main materials found in electrical and electronic equipment (EEE)	9
Table 2-3. Contemporary mechanical separation processes [10].....	11
Table 2-4. Typical hydrometallurgical processes (leaching processes) of gold from WPCB.....	13
Table 2-5. Examples of biosorbents used for recovering Au and Pd	23
Table 2-6 . Examples of commercial anion-exchangers	25
Table 2-7 . Experimental adsorption capacities toward Au and Pd of different synthesized polymers [67]	28
Table 2-8. Applications of polymer-supported metal oxides hybrid material in heavy removal..	40
Table 3-1. Selected wavelengths in elemental measurements by ICP-OES.....	54
Table 4-1. The fraction of ligand and calculated grafting density of modified zirconia	72
Table 4-2. The adsorption capacity of studied materials.....	80
Table 4-3. Summary of kinetic parameters of Pd and Au adsorption on ZrO ₂ -TOA.....	83
Table 4-4. Specific surface areas of surface-modified ZrO ₂ materials determined by BET method	99
Table 4-5. The maximum adsorption capacities of ZrO ₂ surface-modified via NHS-activated ester of TOA and DCC-mediated TOA-amide coupling	101
Table 5-1. The results of Pd concentration after adsorption after using PP-COO-ZrO ₂ impregnated with TOA for 5 min, 30 min, 2 hrs and 24 hrs.....	117
Table 5-2. The content of ZrO ₂ coated on PP-COOH.....	123
Table 5-3. Specifications of SAATI PP textiles	130

LIST OF ABBREVIATIONS

PCBs: Printed Circuit Boards

ICs: Integrated Circuits

UN: United Nations

OECD: The Organization for Economic Cooperation and Development (OECD)

EOL: End-Of-Life

EOLRR: End-Of-Life Recycling Rate

PCs: Personal Computers

WEEE: Waste Electric and Electronic Equipment

EEE: Electric and Electronic Equipment

WPCB: Waste Printed Circuit Boards

UN: United Nations

PGMs: Platinum Group Metals

PGEs: Platinum Group Elements

USGS: United States Geological Survey

EDTA: Ethylenediaminetetraacetic acid

DTPA: Diethylenetriaminepentaacetic acid

INTRODUCTION

De nos jours, les changements climatiques et l'épuisement des ressources fossiles sont les principales préoccupations des différents gouvernements. Par conséquent et afin de réduire la dépendance aux énergies fossiles, de nouvelles législations nous imposent de trouver des nouvelles technologies capables de réduire notre dépendance aux énergies fossiles. Malheureusement, la résolution d'un problème a créé un autre via l'épuisement des ressources minières nécessaire à la fabrication de ces nouvelles technologies. En effet, toutes ces technologies considérées comme des «technologies à faible émission de carbone», tel que les éoliennes, les voitures électriques et les convertisseurs catalytiques utilisent des métaux rares et précieux.

L'utilisation des appareils électroniques (PC, téléphones portables et appareils de divertissement) a fortement augmenté durant les dernières décennies. En 1994, on estimait qu'environ 20 millions de PC (environ 7 millions de tonnes) étaient devenus obsolètes. En 2004, ce chiffre est passé à plus de 100 millions de PC. Bien qu'il n'existe pas d'estimation précise, l'ONU estime que la quantité mondiale des déchets électroniques produite par an est comprise entre 20 et 50 millions de tonnes. Entre 1997 et 2007, 500 millions d'ordinateurs ont été jetés aux États-Unis et 610 millions d'ordinateurs sont devenus obsolètes au Japon en 2010. Ce flux de déchets s'accélère car la demande de PC augmente et la durée de vie d'un PC diminue rapidement. Une étude plus récente a montré que la quantité totale de déchets électroniques en Inde entre 2007 et 2011 est de 2,5 millions de tonnes, avec un taux de croissance annuel de 7 à 10%.

La composition des déchets électroniques est hétérogène, complexe et dépend du type de produit. De plus, il diffère selon l'année de fabrication du fait que les nouvelles technologies ont été développées progressivement. Dans les déchets électroniques, on estime qu'il existe plus de 30 substances, dont un mélange de métaux ferreux, de verre, de plastique, de métaux de base (cuivre, aluminium, etc.), de métaux lourds (mercure, plomb, chrome, etc.), métaux précieux (or, argent, métaux du groupe du platine) et autres.

Les appareils électroniques usuels (PC, tablette, téléphone portable) sont considérés comme des «mines urbaines» car ils accumulent des concentrations relativement élevées de métaux précieux tels que le cobalt, le gallium, le tantale ou l'indium. Les métaux précieux peuvent

être présents à des concentrations dix fois plus élevées dans les appareils électroniques que dans les minerais dont ils sont issus. En recyclant une tonne d'appareils électroniques, on peut récupérer plus de 300g d'or, d'argent, de palladium et d'autres métaux précieux. À titre d'exemple, on récupère moins 10 grammes d'or dans une tonne de minerai. De plus, la quantité d'énergie requise pour recycler les métaux est beaucoup plus faible que pour l'extraction de métaux des minerais. Par exemple, la production d'une tonne d'aluminium nécessite 4700 tétra-joules et 100000 tonnes de minerai, alors que le recyclage d'une tonne d'aluminium requiert 240 tétra joules pour la même masse de déchet électronique.

Généralement, huit métaux sont classés dans le groupe des métaux précieux y compris l'or, l'argent et les métaux du groupe du platine (Ru, Rh, Pd, Os, Ir, et Pt) compris. Grâce à leurs propriétés physiques et chimiques particulières, notamment leur bonne conductivité électrique, leur point de fusion élevé et leur résistance à la corrosion, ils sont couramment utilisés dans de nombreuses applications industrielles.

La quantité moyenne de métaux précieux dans les produits électroniques typiques (mg/unité)

Métaux précieux	Téléphone portable	Ordinateur	Ecran	Laptop
Ag	261	6378	515	343
Au	26.1	92.7	161	160.8
Pd	11.6	39.9	42	40.2

À l'avenir, le développement technologique garantira l'arrivée des nouvelles substitutions aux métaux précieux. De plus, les ressources en métaux précieux seront sécurisées et maintenues grâce à des innovations de technologie de recyclage et des politiques harmonisées pertinentes pour les déchets électroniques.

L'objectif de mon travail était de développer de nouveaux nano-adsorbants pour l'extraction d'or et de palladium présents dans les lixiviats provenant des procédés de recyclage des déchets électroniques. Ce travail a été réalisé en collaboration avec la société MORPHOSIS située au HARVE. MORPHOSIS, société fondée en 2008, est l'un des leaders de l'extraction et du raffinage de métaux rares et précieux provenant des différents équipements électriques et électroniques usagés.

Le manuscrit est divisé en 5 chapitres et se termine par des conclusions générales, des perspectives. Toutes les références sont rassemblées à la fin du manuscrit.

Le chapitre 1 est une introduction générale qui aborde les différents aspects de l'économie mondiale liés aux recyclages des déchets électroniques.

Le chapitre 2 présente un état des lieux des procédés de recyclage des métaux précieux tels que l'or, le palladium et le platine et donne un aperçu des nano-absorbants déjà existants. Après cet état des lieux, les défis et les objectifs de ce projet seront abordés.

Le chapitre 3 fournit des informations sur les matières premières, les produits chimiques et les procédures expérimentales qui ont été effectuées pour les synthèses et les caractérisations des matériaux.

Le chapitre 4 tente de mieux comprendre la nature de la liaison et les performances de recyclage de différents ligands carboxyliques et phosphoniques à la surface de ZrO_2 . La capacité d'adsorption du matériau nano- ZrO_2 modifié avec un acide thioctique sera largement étudiée. Il est important de noter que les processus de modification de la surface seront réalisés en deux étapes afin d'améliorer la robustesse des liaisons du ligand sur la surface de ZrO_2 .

Le chapitre 5 se concentre sur la conception du nano-revêtement sur les textiles en polypropylène par dip-coating ou par un procédé dit « couche par couche » afin de créer une couche ZrO_2 homogène et robuste.

Enfin, une conclusion générale résume les principaux résultats de ce travail et propose des perspectives pour d'autres travaux.

CHAPTER 1. GENERAL INTRODUCTION

1.1. Overview about metal sustainability in high-tech society

Climate change and peak oils crises have been making headlines with increasing intensity over the past decade. Consequently, solutions are being sought to lessen our dependence on fossil fuel with new legislations and key “buzz phrases” like “low carbon technology” and “low carbon future” driving technological change. Unfortunately, there is a serious problem emerging that new technologies have been developed to tackle one challenge, while we are creating another issue through resource depletion [1]. Many of the new technologies considered as “low carbon technologies”, for instances, wind turbines, electric cars, energy saving light bulbs, fuel cells, and catalytic converters, require rare and precious metals for their production. For most technologies using these metals, substitutive materials neither exist nor replace the functionality of the original material. In some cases, they are also considered critical materials, for example antimony tin oxide as a substitute for indium tin oxide in liquid crystal display. However, according to a report by European Commission, antimony is classified as one of the most critical materials among others (Table 1-1).

Table 1-1. Critical metals for a range of countries [2]

Country or region	Critical metals
Japan	Ni, Mn, Co, W, Mo, V
European Union	Li, Sb, Sc, Be, Co, Cr, Co, Ga, Ge, In, Mg, Nb, REEs, Ta, W, PGMs
The Netherlands	Ag, As, Au, Be, Bi, Cd, Co, Ga, Ge, Hg, In, Li, Mo, Nb, Nd, Ni, Pb, PGMs, REEs, Re, Ru, Sb, Sc, Se, Sn, Sr, Ta, Te, Tl, V, W, Y, Zn, Zr.
China	Sb, Sn, W, Fe, Hg, Al, Zn, V, Mo, REEs.
South Korea	As, Ti, Co, In, Mo, Mn, Ta, Ga, V, W, Li, REEs, PGMs, Si, Zr.
Australia	Ta, No, V, Li, REEs.
Canada	Al, Ag, Au, Fe, Ni, Cu, Pb, Mo.
Germany	Ag, Be, Bi, Co, Cr, Ga, Ge, In, Mg, Nb, PGMs, Re, REEs, Sb, Sn, Ta, W.
France	Au, Co, Cu, Ga, Ge, In, Li, Mg, Ni, Nb, Re, REEs, Se, Ta.
Finland	Ag, Co, Cr, Cu, Fe, Li, Mn, Nb, Ni, PGMs, REEs, Ti, Zn.
United States	Ce, Co, Dy, Eu, Ga, In, La, Li, Nd, Pr, Sm, Tb, Te, Y.

The use of electronic devices has increased in recent decades in proportion to their quantity, such as PCs, mobile phones and entertainment devices that are being disposed of. In 1994, it was estimated that approximately 20 million PCs (about 7 million tons) became obsolete. By 2004, this figure increased to over 100 million PCs [3]. In spite of the lack of an accurate estimate of the global e-waste production, the UN estimates that the global quantity of waste electric and electronics equipment (WEEE) or e-waste is 20-50 million tons per year. Between 1997 and 2007, 500 million computers were discarded in the United States and 610 million computers became obsolete in Japan by the end of 2010. This fast-growing waste stream is accelerating because the global market for PCs is far from plateau and the average lifespan of a PC is decreasing rapidly – for instance, CPUs from 4-6 years in 1997 to 2 years in 2005. A more recent study showed that the total WEEE amount in India between 2007 and 2011 is 2.5 million tons with an annual growth rate of within 7-10 %.

The material composition of e-waste is heterogeneous, complex and dependent on the type of the product. Additionally, it differs according to the year of manufacture due to the fact that the new technologies have been developed progressively. For instance, liquid crystal display (LCD) is replacing cathode ray tubing (CRT) technology. In e-waste, it is estimated that there are over 30 substances including a mixture of ferrous metals, glass, plastics, base metals (copper, aluminum, etc.), toxic heavy metals (mercury, lead, chromium, etc.), precious metals (gold, silver, platinum group metals), and others. Information and telecommunication equipment appliances in particular are considered “urban mines” as they accumulate relatively high concentrations of precious and critical metals such as cobalt, gallium, tantalum, or indium. Precious metals can occur at concentrations more than ten-fold higher in PCBs than in commercially mined minerals. By recycling one ton of scrap information technology (IT) appliances, over 300 g of gold, silver, palladium, and other precious metals can be recovered. The computer motherboards contain around 200-250 g.t⁻¹ of gold and around 80 g.t⁻¹ of palladium; mobile phone handsets carry up to 350 g.t⁻¹ of gold and 130 g.t⁻¹ of palladium; and automotive catalytic converters may contain up to 2000 g.t⁻¹ PGMs in the ceramic catalyst brick, the active part of the converter [4]. This is significantly higher than the gold content in primary ores (on average < 10 g.t⁻¹). Moreover, the amount of energy required for recycling metals is much lower than for mining primary metals from ore. Producing one ton of primary aluminum, for instance, requires 4700 tetra joules per 100000 tons, which is almost 20 times as much as the energy needed to recycle the same quantity from scrap (240 tetra joules per 100000 tons) [5].

Importantly, over 50 % of the e-waste arising fail to enter the recycling chain. Currently, it is estimated that only around 30% of the total e-waste are being collected by the strategy developed by member states of European Union [5]. In other words, metal recycling rates from end-of-life (EOL) high-tech products, in most cases, are very low. As a result, a large number of metals contained in EOL products have been lost to the dumpsites or landfills after single or short use. The EOL recycling rate (EOLRR) of a certain metal is defined as its fraction in discarded products that is reused in such a way to retain its functionality. The EOLRR depends on the collection rate of end-of-life products and the efficiency of the subsequent separation and pre-processing steps [6]. Recycling rates of 60 elements are defined and quantified by UN (Figure 1-1).

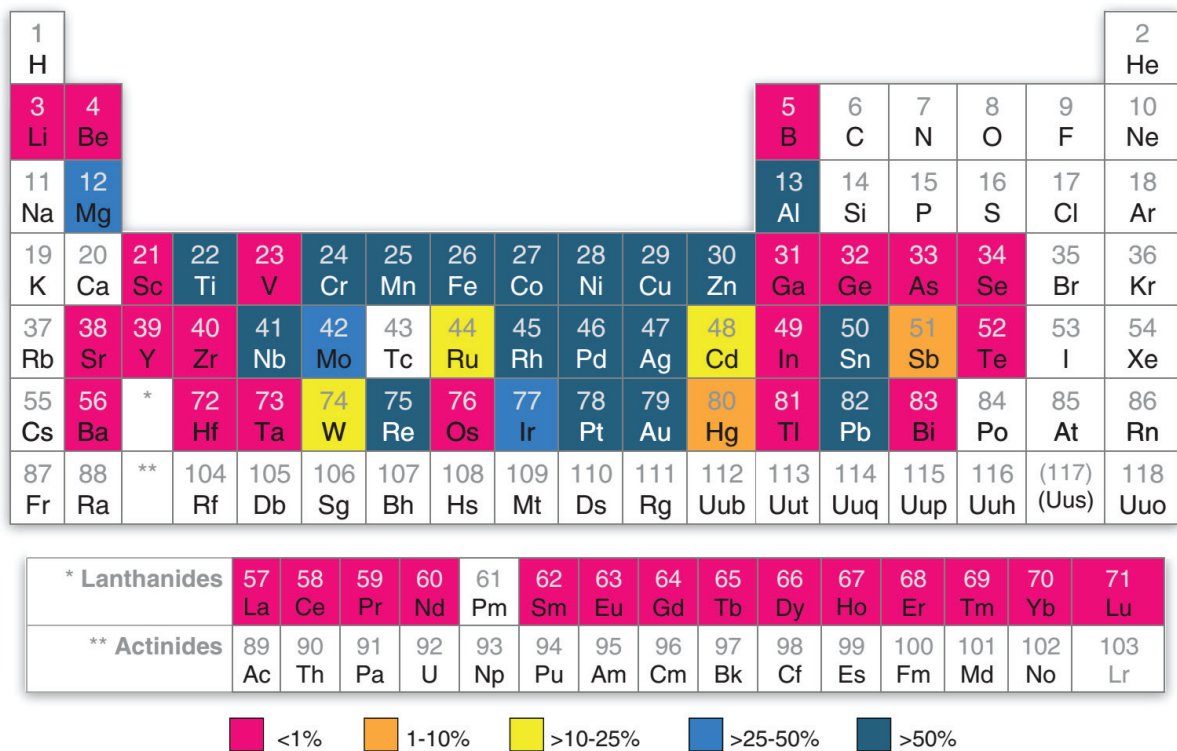


Figure 1-1 – Global estimates of end-of-life recycling rates for 60 metals and metalloids by UN.

Recycling requires an economical compromise between benefits derived from recycling and input of primary resources required for recycling. This has been resulting in concerns about improving recycling efficiency so as to increase metal sustainability. In the article of Christian Hagelucken, the “seven conditions” for effective recycling and their impact within Europe are discussed, including: (i) Technical recyclability, (ii) Accessibility, (iii) Economic viability, (iv) Collection mechanisms, (v) Entry into the recycling chain, (vi) Optimal technical and organizational, and (vii) Sufficient capacity [4].

1.2. Mining production, consumption and future demand of precious metals

Generally, eight metals are categorized into the precious metals group consisting of gold, silver, and the platinum group metals (PGMs). The Platinum Group Metals (PGM, also referred as the PGM's, platinoids, platidises, platinum groups, platinum family, or the platinum group elements – PGE's) comprise of six metallic elements: Ruthenium (Ru), Rhodium (Rh), Palladium (Pd), Osmium (Os), Iridium (Ir) and Platinum (Pt). Thanks to their special physical and chemical properties including good electrical conductivity, high melting point and corrosion resistance, they have been commonly used in many industrial applications. For instances, in the electronics industry, computer hard disk drives manufacturing employs a good amount of precious metals when it comes to increasing the storage capacity. The average quantity of precious metals in typical electronic products (mg per unit) is shown in Table 1-2.

Table 1-2. The average quantity of precious metals in typical electronic products (mg/unit)[7]

Precious metals (mg/unit)	Mobile phone	PC	Flat screen on TV monitor	Laptop
Ag	261	6378	515	343
Au	26.1	92.7	161	160.8
Pd	11.6	39.9	42	40.2

In 2014, 72% of global production of gold from natural mines was represented by the twelve leading countries including China, Australia, United States, Russia, Peru, South Africa, Canada, Mexico, Uzbekistan, Ghana, Colombia, and Brazil. Described in Figure 1-2 is the gold production in the major countries. Currently, supply from secondary sources contributes 28% to the total global production. Gold is predominantly used in EEE for contacts and in ICs which accounts for 6% of global consumption in 2012. Global demand for gold in 2015 was 4124 tons, approximately 20% lower than the record demand of 5087 tons reached in 2013.

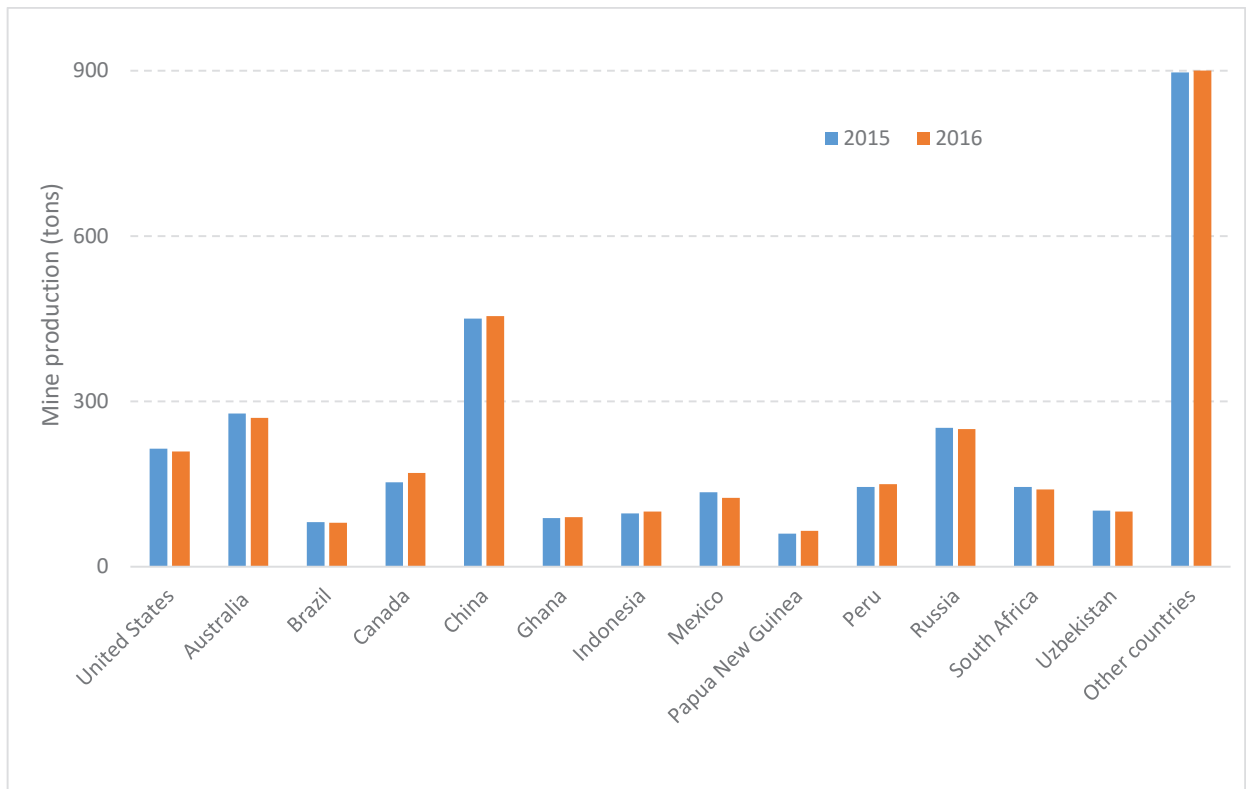


Figure 1-2 – World gold production in 2015 and 2016 (source: USGS)

The major commercial stocks of PGMs are located in only few places – Russia, South Africa, Canada, United States, and Zimbabwe. The PGM supply in United States, Canada, and Russia derives from Cu and Ni mining. Vast PGM stocks were discovered in the Transvaal in South Africa in 1935, leading to this region becoming a producer of the majority of the world’s PGM. In 2014, South Africa produced 94 tons of Platinum (Pt) and 60 tons of Palladium (Pd), which represented 64% and 30% of the world Pt and Pd productions. For other PGMs, South Africa was also the main contributor to global production, which accounts for 78%. Generally, PGMs such as Pt, Pd and Rh have been widely used in auto-catalyst industry and electronics manufacture. For instance, 65% of Pd, 45% of Pt and 84% of Rh were used in auto-catalyst industry.

The skyrocketing increase in precious metals consumption has been recorded over decades since 1980 along with computer technology, especially precious metals. However, albeit the number of electronic appliances is still increasing, the demand for precious metals tends to have been decreasing recently owing to technology advancement (Table 1-3).

Table 1-3. The consumption of precious metals in EEE during 2005-2014 (in tons) (source: USGS)

Year	Gold	Platinum	Palladium
2005	277	11.0	30
2006	302	13.3	33
2007	311	13.2	40
2008	293	7.00	41.2
2009	246	5.90	39.5
2010	327	6.84	43.9
2011	320	7.15	42.9
2012	285	5.13	37.3
2013	279	5.88	38.2
2014	279	5.85	38.8

In the future, the momentum of technology development will guarantee the advent of the new substitutions for the precious metals. Moreover, with the innovations in recycling technology and harmonized policies related to WEEE, the precious metals resources will be secured and sustained.

The aim of the present work was to develop new nanoadsorbents for the extraction of trace of gold and palladium that are present in the leachates coming from recycling processes of WEEE (waste from electrical and electronic equipment) or e-waste. This work has been done in collaboration with company MORPHOSIS located at Le Havre. MORPHOSIS, a French company founded in 2008, is one of the leaders in the extraction and the refining of rare and precious metals mainly originating from the various waste electrical and electronic pieces of equipment. It has developed a unique process to recycle precious metals such as gold, silver, copper and platinoïds (Pt, Pd) from E-waste. This process is the outcome of 4 years of research and several R&D programs which represents a total budget of 1 M€.

The manuscript is divided in 5 chapters and finished with general conclusions, perspectives. All the references are gathered at the end of the manuscript.

Chapter 1 is a general introduction that discusses different aspects about worldwide recycling economy on E-waste.

Chapter 2 presents the state-of-art about recycling processes for precious metal such as gold, palladium and platinum and gives an overview about nanoadsorbents. In the context of this literature review, challenges and objectives of this project are addressed.

Chapter 3 provides information about the raw materials and chemical used in this project and experimental procedures that has been carried out for syntheses and characterizations.

Chapter 4 attempts to gain some insights into the bonding nature and the recycling performances of different carboxylic and phosphonic ligands on ZrO_2 's surface. The adsorption capability of thioctic surface-modified nano- ZrO_2 material toward Pd and Au was extensively investigated. Importantly, two-step surface modification processes were studied as an approach to improve the robustness of ligand bonds onto ZrO_2 surface.

Chapter 5 focuses on the design of the nano-coating on polypropylene textiles through either dip coating or Layer-by-Layer process with the aim to create a homogeneous, rugged and robust ZrO_2 layer.

Finally, a general conclusion summarizes the main results of this work and proposes perspectives for further works.

CHAPTER 2. STATE-OF-ART OF RECYCLING PROCESSES

2.1. Recycling Processes

2.1.1. Definitions, classifications, and compositions of E-waste

There is no standard definition for WEEE (waste from electrical and electronic equipment) or e-waste. This latter includes various forms of electrical and electronic equipment (EEE). According to European WEEE Directive, “electrical and electronic equipment (EEE) which is waste including all components, sub-assemblies and consumables, which are parts of the product at the time of discarding.” Based on description of Basel Action Network, “E-waste encompasses a broad and growing range of electronic devices ranging from large household devices such as refrigerators, air-conditioners, cell phones, personal stereos, and consumer electronics to computers which have been discarded by their users.”[3]

The European WEEE Directives classified WEEE or e-waste into ten categories (Table 2-1) in which categories 1-4 constitute 95% of WEEE generated. The main constituent of WEEE is the printed circuit board (PCB) which contains a large fraction of precious metals. By way of illustration, one metric ton of circuit boards can contain between 80 and 1500 g of gold and between 160 and 210 kg of copper – in other words, the gold amount in PCBs is 40-800 times higher than that in gold ore and the concentration of copper in PCBs is 30-40 times more than that in copper ore mined in the United States.

Table 2-1. WEEE categories according to the EU directive on WEEE

No.	Category	Label
1	Large household appliances	Large HH
2	Small household appliances	Small HH
3	IT and telecommunications equipment	ICT
4	Consumer equipment	CE
5	Lighting equipment	Lighting
6	Electrical & electronic tools (with the exceptions of large-scale stationary industrial tools)	E & E tools
7	Toys, leisure and sport equipment	Toys
8	Medical devices (with the exception of all implanted and infected products)	Medical equipment

9	Monitoring and control instruments	M & C
10	Automatic dispensers	dispensers

Almost all WEEE have printed circuit boards (PCBs). Their amount has been estimated around 3% of all WEEE produced. Moreover, PCBs have been received a great deal of attention due to their valuable portions, especially some precious metals which are classified as scarce or critical material. Yet, their diverse constituents physically and chemically intertwined in such a small platform of PCBs pose a technical challenge for the separation, recovery, and recycling. The heterogeneous mixture of organic, glass fiber, plastics, precious metals as well as heavy metals is shown in the Table 2-2.

Table 2-2. Main materials found in electrical and electronic equipment (EEE)

Material	Ferrous	Non-ferrous	Plastics	Glass	Wood	Other
Percentage (%)	38	28	19	4	1	10

2.1.2. Metal recycling rates

End-of-life recycling rates (EOLRR) of 60 elements were identified and determined by UN in the early 2011 and indicated that: (i) EOLRR values of common base metals are a little above 50%, (ii) the EOLRR value of Pb is around 80%, (iii) specialty elements, including REE are seldom recycled, and (iv) EOLRR values of precious metals (Au, Ag, Pt, Pd, Rh) are various depending on the end-of-life products, for example EOLRR of 80-90% for catalysts in industrial applications, 50-60% in automotive applications, and only 5-10% in electronic applications [8].

The main reason for such a variation is linked to an effective collection system for EOL products. Considering the electronic products, the recycling circumstance becomes worse, for instance EOLRR value for Au, an important constituent of cell and smart phone, is 10-15%, the one for Ru, a necessary part of hard disk is 0-5%, the same as for Pd. These very low EOLRR values indicate that most of EOL electronic product ended up in dumpsites including landfill, incineration wastes, ocean disposal, unregulated dumping, and other repositories (closets and drawers). As aforementioned, the EOLRR values for precious metals in e-wastes would be improved if collection systems for formal recycling of e-wastes in OECD nations were adequate or feasible – that means the choice is based on economics

and convenience, which is balanced by the shareholders. If a collection system is effectively developed and operated, many benefits will be achievable in terms of economic, environmental, public health and safety benefits. These have been driving forces for innovations in e-waste recycling industry whose many issues will be addressed in the following part.

2.1.3. Metal recovery approaches

2.1.3.1. Informal recycling and formal recycling

Informal recycling includes the processes which are employed to recover precious metals without controlling emission of pollutant, including heavy metals and persistent organic pollutants. In some developing countries or non-OECD nations, informal recycling is very popular and refers to unregulated practices or primitive activities to retrieve valuable material, mainly precious metals (Au, Pd, and Pt) and copper. Limited capital, untrained workers, as well as low-technologies extraction and separation are used. Informal recycling processes have been widely employed and become crucial in many developing countries because of economic benefits. The most challenging underlying reason is to find a compromise and cooperation between the stakeholders in searching for viable and effective solutions.

In contrast, with advanced industry in some developed countries, metals in WEEE are recovered through mechanical dismantling and metallurgical refining processes. In these processes, environmental, health problems and energy security are considered in each stages, including controlling the emissions (pollutants and wastes) and optimizing the energy consumption. By using the amount of plastic in the former fractions as energy inputs, it is estimated that 80% of CO₂ emissions are cut down in smelters at Hoboken, Belgium[8]. Nevertheless, the capital cost for the integrated smelter is quite high, generally above US\$1billion, so there are quite a few of companies operating this process all over the world [UMICORE (Belgium), Aurubis (Germany), Boliden (Sweden and Finland), Xstrata (Canada), and DOWA (Japan)].

2.1.3.2. Separation of metallic and non-metallic fraction

Physical processes

In the recycling process, e-wastes undergo three main stages, including collection, preprocessing (mechanical processing or physical processing), and metallurgical processing (chemical processing). Physical processing consists of disassembling (dismantling), grinding, classification, and separation of materials. The separation of materials based on the physical properties includes differences in density, weight, particle size, magnetic properties or electrical properties, which is divided to 2 steps: crushing process and metals enrichment (concentration) process.

The purpose of the crushing process is to separate metals from non-metals in PCB waste. Generally, the crushing process is performed in two steps. In the first step, the boards are shredded by the shearing machine to a size of around 50 x 50 mm, then successively reduced to a size of less than 10 mm and finally ground to a size that permits the release of metals in the second step (< 2 mm) by hammer mills. After grinding, it is important to make a particles size separation (vibrating screen) prior to other separation processes.

Alternating step (concentration step) could be carried out according to gravimetric or density-based separation, magnetic and electrostatic separation. Table 2-3 shows the current separating technologies which fulfill the demands in terms of performance, and environmental protection. To employ the advantages and overcome the downside of each methods, the widely used processes are the combined processes of two or all aforementioned methods. An illustration of an integrated system is the recycling system employed in Shanghai Xinjinqiao Environmental Company Ltd. and Yangzhou Ningda Precious Metal Company Ltd. with the productivity of 5000t of WPCBs per year. Two-step crushing and cyclone air – corona electrostatic separation are utilized, in which the WPCBs are first crushed in the form of particles with the size between 0.6 and 1.2 mm. Not only have these processes been providing the advantages of environmental protection, but there are also some improvements in efficiency and expenses. Thanks to this automatic line, above 95% of metals could be recovered with the purity of about 97.5% of metals [9].

Table 2-3. Contemporary mechanical separation processes [10]

Methods	Description	Main advantages and disadvantages
Magnetic separation	Separation of ferrous metals	Most suitable for separating steel and iron, but not suitable for separating non-ferrous materials.

Eddy current separation	Separation of ferrous and non-ferrous materials	Mainly used to separate non-ferrous materials such as aluminium and copper
Cyclone Air current separation	Separation of light particles from heavy particles	Wind velocity, particle size, particle density, etc. are the critical parameters
Corona electrostatic separation	Separation of metallic particles (size from 0.2 mm to 1 mm) from non-metallic particles	The movement trajectory and collection position of metallic particles are hard to predict and to compute

According to the technological points of view, mechanical processes are necessary to simplify the composition of the wastes and improve the efficiency of the following processes (metallurgical processes). Different techniques have been used in the final step, including pyrometallurgical, hydrometallurgical and biometallurgical.

2.1.3.3. Metallurgical processes for the extraction of gold and PGM from E-waste

Pyrometallurgical processes

Smelting in furnaces, incineration, combustion and pyrolysis are typical e-waste recycling processes. State of the art smelters and refineries can extract valuable metals and isolate hazardous substances efficiently. The liberation of metals is not achieved by leaching, crushing or grinding but by smelting in furnaces at high temperatures. Nevertheless, subsequent steps such as separation and purification employ the same principles of hydrometallurgical approaches. In these processes, metals are sorted based on their chemical and metallurgical properties. Pyrometallurgical processing is done at plants with equipment that was initially developed for the primary metallurgical processing of copper and lead. Currently, industrial processes for recycling metals integrate all aforementioned processes including pyrometallurgical, hydrometallurgical and electrometallurgical processes. Some metals extracting companies are operating the incorporated process consisting of Umicore (Belgium) with integrated smelting and refining facility, Noranda (Quebec, Canada), Rönnskär smelters (Sweden), Kosaka's recycling plant (Japan), the Kayser recycling system (Austria) [11].

Hydrometallurgical Processes

Hydrometallurgical processes consist of two main steps: (i) leaching step using acidic or caustic solutions and (ii) separation and purification processes, such as precipitation, solvent extraction, adsorption and ion-exchange enrichment processes [12]. The Table 2-4 summarizes typical chemical reactions used as leaching step for gold recovery.

Table 2-4. Typical hydrometallurgical processes (leaching processes) of gold from WPCB

Reagent	Typical reaction	Conditions	Efficiency	References
Aqua regia	$2\text{Au} + 11\text{HCl} + 3\text{HNO}_3 \rightarrow 2\text{HAuCl}_4 + 3\text{NOCl} + 6\text{H}_2\text{O}$	Fixed ration of metals to leachant = 1/20 g/mL	98% Ag, 93% Pd, and 97% Au	[13]
Cyanide	$4\text{Au} + 8\text{CN}^- + \text{O}_2 + 2\text{H}_2\text{O} \rightarrow 4[\text{Au}(\text{CN})_2]^- + 4\text{OH}^-$	$[\text{CN}^-] = 4 \text{ g/mL}$, pH = 10.5-11	46.6% Au	[14]
Thiourea	$\text{Au} + \text{CS}(\text{NH}_2)_2 + 2\text{Fe}^{3+} \rightarrow [\text{Au}(\text{CS}(\text{NH}_2)_2)_2]^{2+} + 2\text{Fe}^{2+}$	$[\text{Thiourea}] = 24 \text{ g/L}$, $[\text{Fe}^{3+}] = 0.6\%$,	90% Au, 50% Ag	[15]
Thiosulfate	$4\text{Au} + 8\text{S}_2\text{O}_3^{2-} + \text{O}_2 + 2\text{H}_2\text{O} \rightarrow 4[\text{Au}(\text{S}_2\text{O}_3)_2]^{3-} + 4\text{OH}^-$	Ammonium thiosulfate	$\geq 90\%$ Au	[16]

Because of the high degree of toxicity, leaching processes using cyanide have prompted the needs to find new substitutes. Gold leaching processes with thiourea, thiosulfate, and halide have been studied. In a study of Jing-Ying et al., the solution containing 24 g/L of thiourea and 0.6% of Fe^{3+} in the recovery of gold and silver from the PCBs of mobile phones were used to obtain leaching rates of 90% for gold and 50% for silver [15]. The high concentration of copper found in PCBs significantly affects the dissolution of gold. Therefore, a pretreatment with sulfuric acid and hydrogen peroxide to recover the copper beforehand is often used. However, there are some drawbacks using the leaching processes with thiourea: (i) thiourea is more expensive than cyanide; (ii) consumption is higher because thiourea is oxidized in solution.

Halide leaching especially chlorine/chloride leaching has proved to be well-established route for dissolution of gold in acidic medium. Nevertheless, the handling of chlorine gas and requirement of special reactor hinders its application in the full-scale process. Xu et al. [9] attempted the iodide leaching of gold from waste PCBs and achieved 95% gold recovery. Iodine leaching is considered to be non-toxic, non-corrosive and very selective

toward gold as gold – iodide complex is the most stable compound in gold – halide complexes.

With a raising level of concern about toxicity of the conventional cyanide leaching stage, thiosulfate leaching has been developed as an less-toxic and cost-efficient alternative, that Au(0) is converted to $[\text{Au}(\text{S}_2\text{O}_3)_2]^-$ in the presence of additional reagents such as ammonium/ammonia and oxidation catalyst (Cu^{2+}) [15].

The reduction-precipitation with metal hydrides has been used to reduce gold and silver from the leachate at a commercial scale. The most used metal hydride reductant is sodium borohydride. The recovery of gold from solutions of thiourea, thiosulfate or thiocyanate using a solution containing 12 % of NaBH_4 and 40 % of NaOH was successfully carried out. The results showed that gold could be reduced at ambient temperature either in very diluted or more concentrated solution [14].

Solvent extraction has been successfully applied to recover some metals after leaching processes. Fray and Park used toluene, followed by precipitation using dodecaethiol and sodium borohydride to selectively recover the gold leachate from PCBs using aqua regia solution[13]. Kinoshita et al. used the commercial solvent LIX[®]984 (a 1:1 mixture of 5-dodecylsalicylaldoxime and 2-hydroxy-5-nonylacetoophenone oxim in a high flash point hydrocarbon diluent) in the selective extraction of copper in leachate containing copper, nitric acid, and nickel impurities[17]. The commercial solvent LIX[®]79 (cyanide-based solvent) can be used in the extraction of gold in alkaline solutions containing cyanide, while Cyanex 921 (tri-n-octylphosphine oxide extractant) can be used for all pH ranges.

Finally, in the recovery of gold and PGMs, some organophosphorus derivatives, guanidine derivatives and mixtures of amines-organophosphorus derivatives products have been studied.

Organophosphorus class of extractants has been widely studied and used for removal of Pd(II). The extractability increased in the following order: organophosphate < organophosphonate < organophosphine oxide. Tributyl phosphate (TBP) (Figure 2-1, I) can extract Pd quantitatively from 0.1-1.0 M HNO_3 with maximum distribution (D_{Pd}) in the acidity range of 0.4 M to 0.8 M; however, no Pd is extracted when nitric acid

concentration exceeded 4.0 M and distribution of Pd was low in the range of 0.6 – 1.0. Co-extraction of other actinides and fission products became unavoidable. Also, the extraction was highly suppressed by increase in the nitric acid concentration regardless of the higher extractability of trialkyl phosphine oxide TRPO (R = butyl, isoamyl, or octyl).

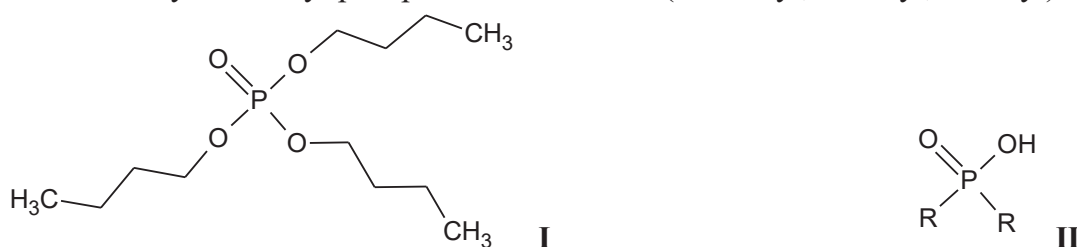


Figure 2-1 – Structural formula of tributyl phosphate (TBP, I) and trialkyl phosphine oxide (TRPO, II)

To improve performance and distribution of Pd(II) extraction, some bidentate and tridentate ligands have been used and showed effective Pd extraction, namely, alkyl(phenyl)-N,N-diisobutylcarbamoylmethylphosphine oxide (CMPO-1), and diphenyl-N,N-diisobutylcarbamoylmethylphosphine oxide (CMPO-2), malonamide [18-21], dyglycoamide [22, 23] and dioxodiamide (Figure 2-2).

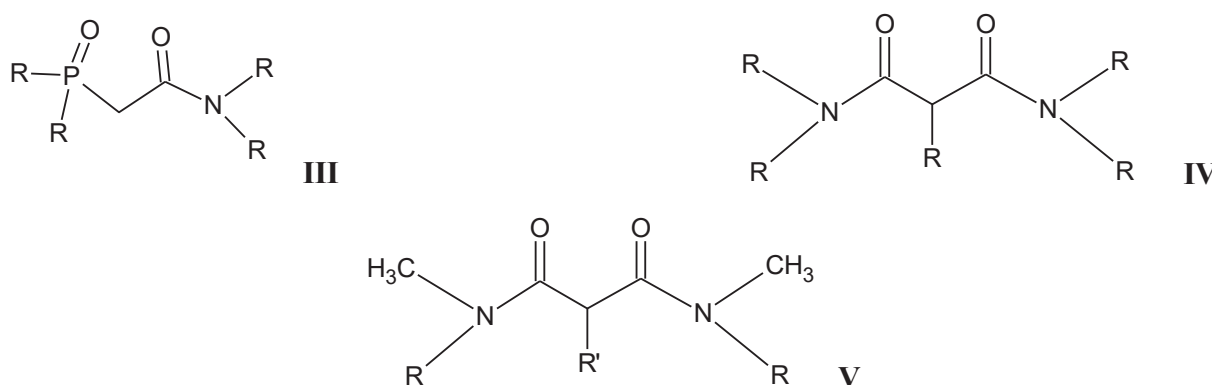


Figure 2-2 – Structural formulas of carbamoylmethylphosphine oxide derivatives (CMPO, III) and malonamide derivatives (IV) and N,N'-dimethyl-N,N'-dialkyltetradecylmalonamide

The research group of Ana Paula Paiva et al. has carried out many works related to the development of amide derivatives for the solvent extraction of PGMs from HCl solutions, particularly N,N'-tetrasubstituted malonamides. The structures of extractants synthesized and investigated by this group are shown in Figure 2-2. The capability of N,N'-dimethyl-N,N'-diphenyltetradecylmalonamide to extract Pt and Rh and mutual separation of Pd, Pt, and Rh have been extensively investigated [19, 21, 24, 25].

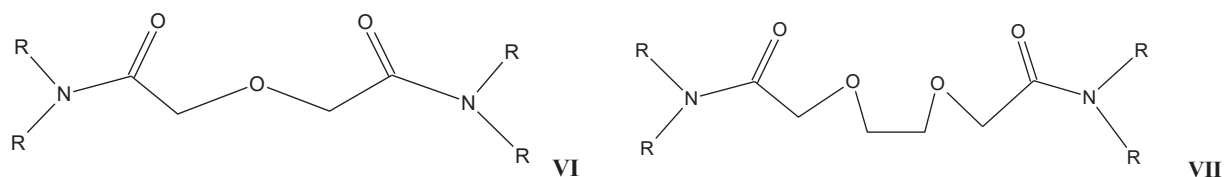


Figure 2-3 – Structural formulas of diglycoamide derivatives and dioxodiamide derivatives

Precious metals, such as Pd and Au are categorized in the soft acids group based on HSAB theory. They will accordingly form stronger coordinate bonds to ligands bearing soft donor atoms like “N” or “S”. Following are the typical extractants/ adsorbent developed for mutual separation of precious metals.

Dialkyl sulfide derivatives have then appeared to be very effective in terms of high distribution ratios for Pd(II) [26]. However, their uses are limited due to very slow adsorption kinetics and instability in nitric acid medium.



Figure 2-4 – Structural formulas of dialkylsulfide (left) and dialkyl disulfide (right)

Recently, ligands such as thiodiglycoamides and dithiodiglycoamides have been recognized as one of the most promising extractants for Pd, Au, and Pt removal (Figure 2-4). Paiva, A. P. et al synthesized N,N'-dimethyl-N,N'-dicyclohexylthiodiglycoamide and applied it for solvent extraction of Pt(IV) and Pd(II) from concentrated hydrochloric acid media [27]. It was found that Pd(II) and Pt(IV) at the concentrations of 102 and 85 mg/L were efficiently extracted from 8 M HCl feed aqueous solution. By using subsequent a 1 M HCl solution and a mixture of 0.1 M thiourea and 1 M HCl, Pt(IV) and Pd(II) could be mutually separated. Compared to thiodiglycoamides derivatives, a novel multidentate ligand, namely, tetra-(2-ethylhexyl)-dithiodiglycoamide (DTDGA) was believed to separate Pd more efficiently thanks to the higher number of “S” donor sites [28, 29]. Furthermore, this ligand was impregnated in Amberlite XAD-16 resin beads and evaluated for the gold separation from electronic waste solutions [30]. The kinetics of adsorption occurred rapidly and quantitatively in approximately 180 min, which followed the pseudo-second order model. The maximum experimental adsorption capacity was found to be 35 mg/g. The adsorption data demonstrated to fit well the Langmuir isotherm model.

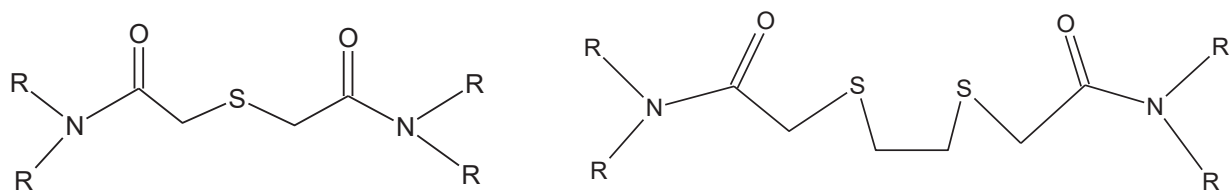


Figure 2-5 – Structural formulas of thiodiglycoamide derivatives (left) and dithiodiglycoamide derivatives (right)

Compared to calix[n]arenes, thiacalix[n]arenes have also received increasing attention due to bridging sulfur moieties, and hence they form complexes with a wide range of metal ions. Thiacalix[n]arenes ($n = 4, 6$ and 8) are composed of phenol rings linked with sulfur sites and can be modified to create upper and lower-rim functionalized derivatives that increase intermolecular interactions with various guest species. Functionalization of the upper and lower rims of thiacalix[n]arenes with heteroatoms (O, N, S, P, etc.) leads to several-fold increase in the extraction properties.

C. Fontàs et al. tested functionalized thiacalix[4]arenes as extractants for Au, Pd and Pt [31]. Four thiacalix[4]arenes were selected including p-tert-butyl-thiacalix[4]arenes with amide (1) and ester (2) group, p-tert-butyl-thiacalix[4]arenes (3) and thiacalix[4]arenes (4) (Figure 2-6). It was found that derivative 1 bearing amide group showed highest extraction capability and selectivity toward Au (in the order: Au > Pd > Pt) via ion exchange mechanism, whereas derivative 4 selectively extracted Pd through complexation mechanism. In all cases, a solution of 0.5 M thiourea in 1 M HCl effectively eluted extracted metals. In this study, it was observed that impregnated commercial adsorbents showed remarkably enhanced adsorption toward Au, Pd and Pt.

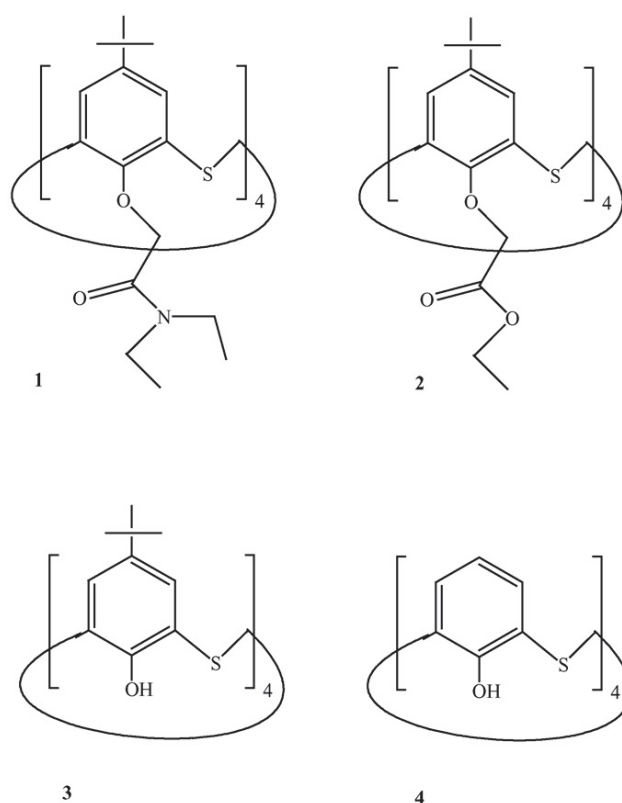


Figure 2-6 – Structure of thiacalix[4]arenes derivatives [31]

A series of functionalized thiacalix[n]arenes were synthesised by a Japanese research group led by Prof. Fumio Hamada to recover Pt(IV), Pd(II), and Rh(III) ions from a spent automotive catalyst residue using liquid-liquid extraction. Authors have synthesized and compared different thiacalix[n]arene derivatives (Figure 2-7) and the extractant **1** named *p*-diethylaminomethylthiacalix[4]arene has shown a remarkable high affinity and selectivity for Pt(IV) ions [32]. The extraction of Pt(IV) ions from HCl solutions was mainly governed by an ion-pair mechanism (Figure 2-8) and partially supported via coordination mechanism. Almost all the other metal ions in leachate were not extracted; however, Pd(II) was still be co-extracted with Pt(IV).

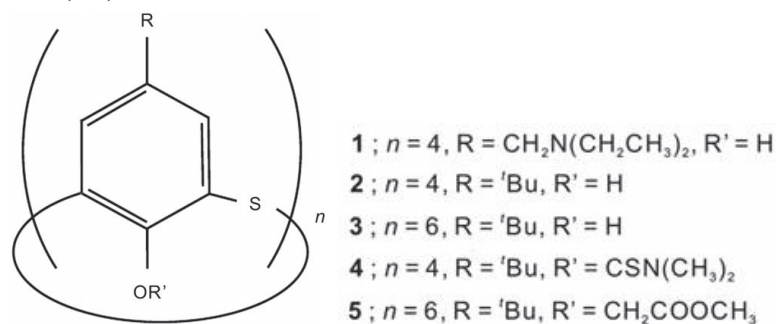


Figure 2-7 – Structural formulas of synthesized thiacalix[n]arene [32]

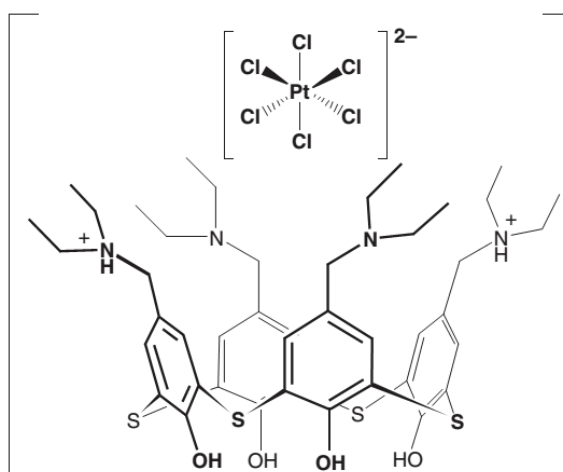


Figure 2-8 – Proposed major composition of Pt(IV) extracted species by extractant I

2.2. Adsorbents for treatment of precious metals from water and wastewater

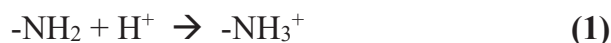
Various technologies such as chemical precipitation, flotation, ion exchange, electrochemical processes, solvent extraction, membrane technologies, and adsorption have been used to extract metals from water and wastewater. Each of methods has its inherent advantages and limitations.

Among metal treatment methods, adsorption has emerged as an attractive method due to many its advantages such as cost-effectiveness, high performance and ease of use. The driving force of this method is based on mass transfer and physical/chemical interactions between solid and liquid phase. In turn, these processes are affected mainly by properties of solid phase (adsorbent) including specific surface area, and reactive sites.

2.2.1. Mechanisms in precious metals adsorption

Many types of interactions have been suggested including physisorption, surface complexation, ion exchange, electrostatic interaction, and hard/soft acid-base interaction (HSAB) [33].

With respect to amine-functionalized adsorbents, the mechanism for the sorption of metal ions can be expressed by the following reactions:



At $\text{pH} < \text{pK}_a(-\text{NH}_3^+)$, the reactions (1) and (2) may occur simultaneously. However, the reaction (1) is dominant, so only a few active sites are available for the adsorption of metals. Additionally, the electrostatic repulsion between M^{n+} and the positive charged nanoparticles increases with the formation of more $-\text{NH}_3^+$, hence the adsorption capacity decreases.

With the increase of pH, the concentration of H^+ diminishes and the reaction (1) shifts to left, the number of $-\text{NH}_2$ sites increases and favor the complexation reaction (2). Albeit OH^- ions in the solution compete with M^{n+} for $-\text{NH}_2$ sites [reactions (2) and (3)] at pH values beyond $\text{pK}_a(-\text{NH}_3^+)$, the adsorption capacity still increases owing to the electrostatic attraction between M^{n+} and $-\text{NH}_2\text{OH}^-$ sites [reaction (4)].

One of the most used interaction in metal adsorption processes was based on Lewis Acid-Base ones (following the HSAB or Pearson concept). In the case of thiol-functionalized nanoparticles, the adsorption of metal ions underwent two types of interactions including favorable complexation according to Pearson's hard/soft acid-base theory (primary) and electrostatic interaction (secondary). Based on Pearson's theory, soft metal ions interacts with soft bases which are ligands carrying S, N, P atoms; conversely, hard metal ions strongly bond to hard bases which are ligands bearing O, halogen atoms.

Many factors contribute to the efficiency and selectivity, such as the type and concentration of ligands on the substrate, the nature of substrate, pH of solution, and the presence of competing ion. Furthermore, when it comes to adsorption selectivity toward metals with the same physical/chemical properties (lanthanides or actinides), the density (steric hindrance) [34] conformation (the freedom of movement) [35] of immobilized ligands on a surface are of crucial importance.

2.2.2. Biosorbents – carbonaceous adsorbents

General speaking, biosorption has been a promising process in various applications relevant to metal removal thanks to its abundant availability and eco-friendliness. As a result of striving toward sustainable development, biosorption has been gaining tremendous attention. A variety of biosorbents have been developed and studied in recovering precious metals, especially gold and palladium. In the review of Nilanjana Das, different biomaterials were introduced ranging from biomass (algae, fungi, bacteria...) to biopolymers and biowaste materials [36].

2.2.2.1. Cellulose-based and lignin-based materials

Algae, fungi, bacteria, or yeast... are classified as cellulose-based materials that are considered as a matrix of cellulose, lignin, hemicellulose and amino sugars. Therefore, the abundance of hydroxyl groups (-OH) or O-containing sites in their structure is responsible for capturing metal ions.

The adsorption capabilities toward Au of different species of microorganisms were screened including 8 bacteria, 9 actinomycetes, 8 fungi and 5 yeasts. Among them, Escherichia Coli and Pseudomonas maltophilia were the bacterial strains that have higher maximal adsorption capacities toward Au than do actinomycetes, fungi, and yeasts [37].

Lignin naturally occurs in wood accounting for 10-30% of wood's structure. Described in the Figure 2-9 is the structure of lignin that consists of dissimilar repeating units with different functional groups such as hydroxyl, ether and carbonyl. It has been found that lignophenol, a product of lignin and phenol, exhibits the high selectivity toward Au(III) regardless of whether other metals coexist in the solution or not [38, 39].

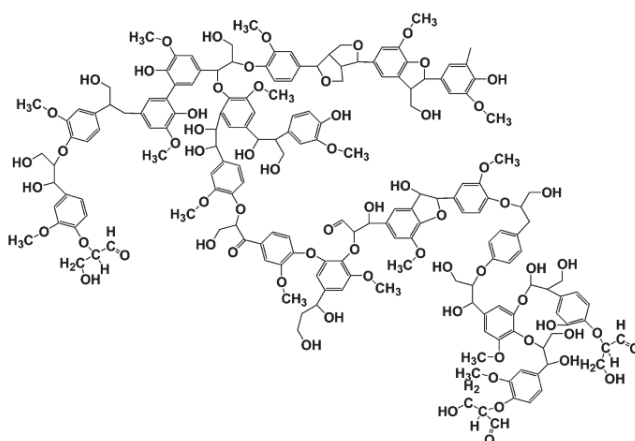


Figure 2-9 – The structure of lignin

2.2.2.2. Tannin-based adsorbents

The pursuit of K. Inoue et al. in tannin-based adsorbents deriving from persimmon extract is illustrated as a representative of studies about tannin-based biosorbents[40-44]. It has been realized that persimmon extract is rich in tannin (Figure 2-10) and is known to contain several polyphenols such as catechol, tannic acid, gallic acid, pyrogallol...In terms of chloro complex of gold, the mechanism of the adsorption-reduction process has been proposed as follows:

- (i) Interaction between AuCl_4^- and positively charged sites on the biosorbents' surface.
- (ii) Reduction of AuCl_4^- to Au (0) by hydroxyl groups of polyphenolic subunits in the biosorbents' structure.
- (iii) Aggregation of nano-gold particles to bigger to form the bigger gold aggregates

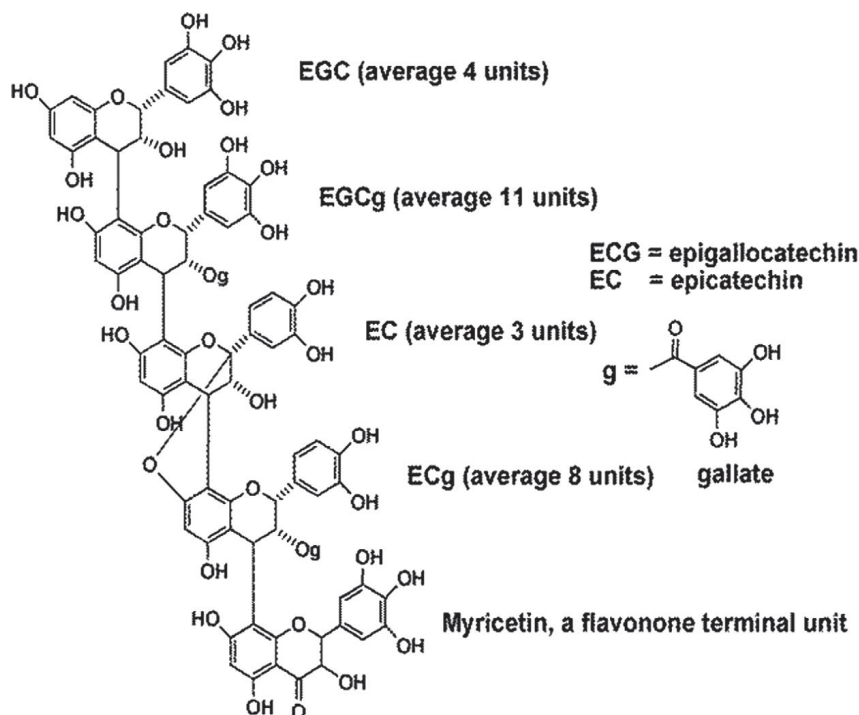


Figure 2-10 – The structure of tannin

2.2.2.3. Chitosan-based adsorbents

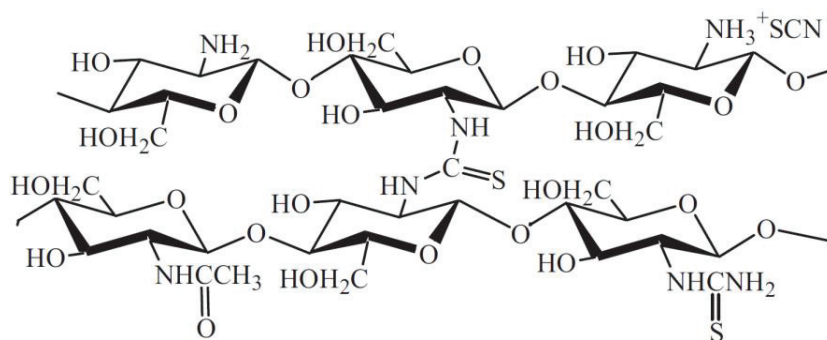


Figure 2-11 – The structure of chitosan

Chitosan is a linear polysaccharide composed of randomly distributed β -(1-4)-linked D-glucosamine (deacetylated unit) and N-acetyl-D-glucosamine (acetylated unit). Thanks to its hydrophilicity and abundance of $-\text{NH}_2$ groups, this kind of aminopolysaccharide has

been extensively studied in the applications pertaining to heavy metals removal. Moreover, the adsorption capacity and selectivity toward target metals of chitosan can be tuned by modifying the amino headgroups. For instance, thiocarbamoyl chitosan – a chitosan sulfur derivatives – has been synthesized via reaction in eutectic two-component system of ammonium thiocyanate-thiourea. The adsorption test showed a correlation between substitution degree and adsorption capacities toward Au and Pd [45].

Table 2-5. Examples of biosorbents used for recovering Au and Pd

Adsorbents	Adsorption capacity (mg/g)		References
	Au	Pd	
Dealginated seaweed waste	78.89	-	[46]
Fungi Cladosporium cladosporioides 1 & 2	94.2 (Strain 1, pH 4); 104.3 (Strain 2, pH 4)	-	[47]
Bacteria	5.55 (Spirulina platensis, pH 4), 6.00 (Streptomyces erythraeus, pH 4) , 5.55 (Saccharomyces cerevisiae, pH 4)	-	[48]
Desulfovibrio desulfuricans	-	190 (pH 3)	[49]
BTU-modified PT (bisthiourea-modified persimmon tannin)	1020	192	[41]
TEPA-modified PT (tetraethylenepentamine-modified persimmon tannin)	1166	187	[40]
Sulfuric acid cross-linked PT gel	1517	-	[43]
Aminated lignin derivatives: (from wood powder)	607 (EA-lignin); 384 (PA-lignin)	57 (EA-lignin); 40 (PA-lignin)	[39]
Pine (Pinus Sylvestris) sawdust-based biosorbent modified with thiourea groups	79	181	[50]
Moss (Racomitrium lanuginosum) biomass	-	37.2 (pH 5)	[51]
Glutaraldehyde-crosslinked chitosan	-	180	[52]

Of the aforementioned biosorbents, biosorbents originating from cellulose-based materials appears to be versatile when it comes to its diversity, yet the susceptibility of these materials to the harsh conditions of effluent (low pH, high total dissolution solid content...) has been of main concern. In other words, most reviewed studies observed the optimal adsorption capability in the pH range of 3-5. Notwithstanding the high selectivity and adsorption capacities toward Pd and Au, the reduction of AuCl_4^- to $\text{Au}(0)$ was observed in all studies when lignin and tannin-derivatives were employed. The main driving force of the reduction process stems from the abundant presence of hydroxyl groups in their structure; hence the regeneration of the biosorbents and metals recovery should be carefully taken into consideration regarding their reusability in the real-life applications.

The superiority in adsorption capacity of biosorbents in comparison with other types of adsorbents resulted from a combination of adsorption-reduction that leads to cycles of “Au(III) adsorption-Au(III) reduction-Au(0) release”[53].

2.2.3. Polymer-based adsorbents

2.2.3.1. Ion-exchange resins and resins impregnated with ligands

Basically, when it comes to adsorption processes based on electrostatic attraction, the choice of the type of ion exchanger is predicated on existing species of target metals. In turn, the metal species existing in the solution are dependent on recovering processes which are either aqueous hydrochloric acid system (HCl or Cl_2/HCl) or aqueous nitric acid system (aqua regia).

In the solutions containing $>0.1\text{M}$ HCl or high HNO_3 concentration ($>1\text{M}$), anionic complexes of Au and Pd, such as AuCl_4^- , PdCl_4^{2-} , $[\text{Pd}(\text{H}_2\text{O})(\text{NO}_3)_3]^-$ or $[\text{Pd}(\text{NO}_3)_3]^-$, are the predominant forms, so basic anion exchange resins bearing positively charged sites have been employed. Anion exchangers are categorized into two main types including weakly basic anion and strongly basic anion exchangers. The fundamental difference between aforementioned anion-exchangers is based on the formation of positively charged site as a function of pH. Strongly basic anion-exchangers tend to be readily protonated or easily positively charged; in either case, positive charges on the surface are present regardless of pH. In the meantime, weak basic anion-exchangers are limited to form positive charges depending on the pH of solution, especially they act as anion-exchangers at relatively high

acidic conditions. Table 2-6 exemplifies some applications of commercial anion exchangers in capturing Au and Pd from effluents.

Table 2-6. Examples of commercial anion-exchangers

Adsorbent	Description	Adsorption (mg/g)		Reference
		Pd	Au	
Amberlyst A21	Weakly basic anion-exchanger with tertiary amine group $-N(CH_3)_2$ on polystyrene skeleton	9.12 – 9.99	-	[54]
Amberlyst A29	Strongly basic anion-exchanger type 2 with quaternary $-N^+(CH_3)_2C_2H_4OH$ on a styrene divinylbenzene skeleton	7.86 – 9.67	-	
Varion ADAM	Weakly basic anion-exchanger with tertiary amine group $-N(CH_3)_2$ on polyacrylate skeleton	9.86	-	[55]
Varion ATM	Strongly basic anion-exchanger type 1 with quaternary $-N^+(CH_3)_3$ on a styrene divinylbenzene skeleton	9.52	-	
Varion ADM	Strongly basic anion-exchanger type 2 with quaternary $-N^+(CH_3)_2C_2H_4OH$ on a styrene divinylbenzene skeleton	9.47	-	
Amberlite XAD-7HP	Macroreticular polyacrylate resin	-	147	[56]
Bonlite BA304	Strongly basic anion-exchanger type 1 with	-	123	

	quaternary -N ⁺ (CH ₃) ₃ on a styrene divinylbenzene skeleton			
Purolite A-500	Strongly basic anion- exchanger type 1 with quaternary -N ⁺ (CH ₃) ₃ on a styrene divinylbenzene skeleton	-	78	

Ion exchange resins can be used in the recovery of gold from leaching solutions. Such commercial resins as Dowex G51, Dowex 21 K, and Amberlite IRA-410 have been tested with success in the recovery of gold from thiosulfate solutions. These resins are gel-type with a polystyrene divinylbenzene matrix, with quaternary ammonium in their functional groups [14].

The use of commercially available anion-exchange resins for separation and removal of Pd(II), Pt(IV) and Rh(III) has been thoroughly conducted [57, 58]. Generally, PGMs form anion species in acidic solutions permitting their adsorption via an ion-exchange and coordinative mechanism based on HSAB theory.

In a research of S. H. Lee et al. [59], commercially strongly basic anion exchangers, such as IRN-78 and Dowex 1x8 were used to separate Pd (II) and Ru (III) in radioactive high-level liquid waste. Dowex 1x8 with the ionic group of quaternary methyl ammonium showed a higher capacity than IRN-78 containing amine group. Pd (II) could be easily eluted by a mixture of 0.5 M thiourea solution and 0.1 M nitric acid, while Ru (III) was effectively eluted using a 6 M HCl solution. On the other hand, various ion exchange resins including AR-01, Dowex 1x8, IRA-93ZU and Dowex 50 were investigated in terms of adsorption capability toward Pd(II) and Rh(III) in high-level low radioactive liquid waste by the same authors [60]. They came to realization that (i) Dowex with -SO₃H group showed significantly strong Rh(III) adsorption at dilute nitric concentration ranges below 0.5M; (ii) Dowex 1x8 with quaternary methyl ammonium group (-CH₂(CH₃)₃ N⁺) had a higher Pd(II) adsorption capacity than that of IRA-93ZU with amine group (-N(CH₃)₂OH); AR-01 with benzimidazole group showed significantly strong Pd(II) adsorption.

In a study relevant to Pd(II) recovery in the leachate of automotive catalysts, p-tert-butylthiacalix[4/6]arenes and their thiocarbamoyl-modified derivatives were impregnated into Amberlite XAD-7 resin[61]. Authors have demonstrated that thiacalixarenes derivatives bearing thiocarbamoyl (-OC(=S)N(CH₃)₂) displayed an enhance Pd(II) extraction via coordination between PdCl₄²⁻ and “S” sites of thiocarbamoyl. XAD-7 resins immobilized with thiacalixarenes derivatives captured 99% of Pd(II) ions from automotive catalysts leachate containing Rh, Pd, Pt, Zr, Ce, Ba, Al, La and Y in 0.1 M HCl media. Furthermore, the desorption for Pd (II) ions from the thiocarbamoyl derivatives immobilized resins was exceeded 96% when a mixture of 0.1 M thiourea solution and with 1 M HCl solution was used as a stripping agent and their sorption capacity was still high after five sorption cycles.

Furthermore, the adsorption performance (adsorption capacity, selectivity, applicability) toward Pd or Au could be tailored or improved by ligand impregnation into the polymer network. A series of studies based on this process were conducted in which different macromolecules deriving from thiacalixarenes were synthesized and impregnated into the XAD-7 resin and the resultant materials were applied to Pd recovery from leach liquors of automotive catalysts. It was found that all materials showed a profound augmentation in adsorption capacity compared to bare XAD-7 and the recyclability [61-63]. R. Ruhela et al. in the same direction synthesized a novel multidentate ligand N, N, N', N'-tetra(2-ethylhexyl)dithiodiglycoamide (DTDGA) and impregnated this ligand in XAD-16. The resultant material showed a high selectivity toward Au in a simulated electronic waste solution containing different metal ions [30].

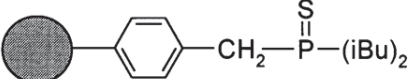
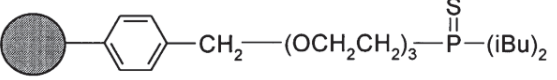
2.2.3.2. Functionalized polymers

Another approach to increase selectivity of resins is to modify or graft functional groups bearing electron-donating atoms such as S or N on the backbone of polymer. By way of illustration, J. M. Sánchez et al. have synthesized a collection of polymers based on grafting the moiety bearing the diisobutyl phosphine sulfide headgroups and/or spacer arms containing S/O divinylbenzene polystyrene backbone. Authors have demonstrated that polymers carrying S or O atoms in the spacer arms increased the hydrophilicity of polymers, and hence impart the improved adsorption capacity toward Au and Pd. The adsorption capabilities of polymers with spacer arms containing O and S atoms were tested following

batch and column modes and it was found that polymer with S atoms in spacer arm possesses the poorer separation in the column mode albeit it has higher adsorption toward Au and Pd than polymer with O atoms in spacer arm [64]. Both polymers are highly selective toward Pd and Au in the matrix of HCl containing different metals (Fe, Cu, Ni, Zn); however, the susceptibility of phosphine sulfide group and S sites in the spacer arm to oxidation should be taken into consideration. In order to circumvent conditions in which Au or Pd are present in the effluents with high concentration of nitric acid, a series of products, based on the macroporous backbone of polyacrylic and phosphine oxide (P=O) coordinating functional groups, has been commercialized by Italmatch-Magpie [65, 66]. MPX-310, one of those products has shown improved stability in harsh conditions with effluents prepared from the dissolution of mixed metals in aqua regia. In this study, the adsorption performance toward Pd, Pt, and Rh of MPX-310, of Lewatit Monoplus TP-124 and of Dowex Marathon WBA were compared and MPX-310 displayed the highest selectivity and adsorption capacity; for instance, MPX-310 was able to capture 100-110 mg PGMs/kg and 5-7 g Cu/kg, whereas Dowex reached about 70 mg PGMs/kg and 25 g Cu/kg. TP-124 adsorbent (S-containing adsorbent) has shown lower selectivity in simple solutions and poor compatibility with the simulated solution with high oxidizing condition (abundant nitrate and copper ions).

Development of polymers based on triisobutyl phosphine sulfide (TIPS) were conducted in order to investigate the effect of spacer arms between polymer matrix and the functional group on the adsorption process of resulting polymers [67, 68]. According their findings, these polymers were selective toward Pd and Au compared to other noble metals (Pt, Rh and Ir) and base metals (Fe, Cu, Ni, and Zn) metals. Moreover, authors have observed a significant improvement with respect to adsorption capacity and selectivity with polymers containing ethylene sulfide or/and ethylene oxide.

Table 2-7. Experimental adsorption capacities toward Au and Pd of different synthesized polymers [67]

Polymer	Structure	Capacity (mmol/g)	
		Au	Pd
1		0.40	0.11
2		2.82	0.51

3		6.50	0.72
---	--	------	------

This surface functionalization concept has been widely used with nano-oxide supports to achieve more stable and more efficient hybrid (Organic-Inorganic) nanoabsorbents.

2.2.4. Hybrids Nanocomposites : Nano-oxides based adsorbents and polymer/Metal oxide

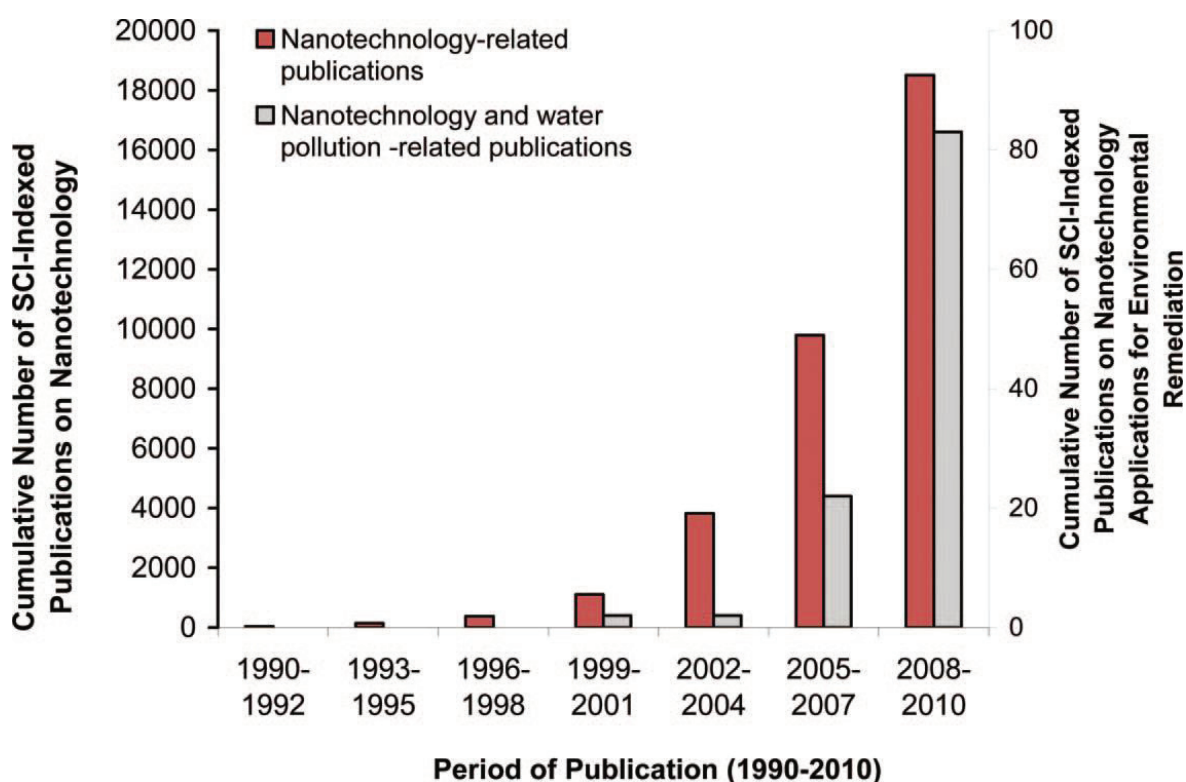


Figure 2-12 – The number of publications on nanotechnology or its applications for environmental remediation [69].

In water treatment technologies based on adsorption, two intrinsic concerns are technical capability and cost-effectiveness. From technological point of view, the adsorption process must be able to capture the target adsorbates rapidly, while the capital investment (cost of adsorbent, system construction...) operational cost (chemicals, labor) and maintenance expense (regeneration, reusability of the adsorbent) are the prioritized considerations in terms of economical points of view. With respect to adsorption efficiency, specific surface area and reactive sites of the adsorbent play important roles. Activated carbon has been commonly employed in heavy metals removal, but its increasing price has been restricting

its applicability. The search for alternatives which are abundant and inexpensive has been of crucial interest, hence the adsorbents based on natural source such as fruit peels, agricultural waste as well as carbonaceous material (seeds, woods, eucalyptus bark...) have been studied and their adsorption capability has been confirmed but the industrial applicability is still limited. Since 1990, the researches and manipulation of materials and systems at nanoscale (less than 100nm) have increased exponentially in terms of quantity; mainly driven by their uses in water pollution treatment as shown in the Figure 2-12.

Owing to their nanoscale, materials express some superior characteristics in comparison to the bulk counterparts, for instances, the large surface to volume ratio, high reactive sites (high surface energy). This increasing number of atoms or excess of energy at the surface led to thermodynamic metastability of the system that could be reduced by surface adsorption (that was the strategy of plenty of publications for water pollutant remediation). Moreover, surface modifications of nanoparticles have been employed to overcome agglomeration/aggregation and to improve their dispersibility/compatibility in different matrixes. This surface-modification process can be carried out via physical (physisorption through weak interactions including hydrogen bonding, van der Waals, $\pi - \pi$ or weak electrostatic interactions) or chemical routes (chemisorption through strong ionocovalent or coordinative bonds). A drawback of physical modification is that the resultant bonds are more labile [70].

Then, if organic complexants can be effectively attached onto the surface of nanoparticles, capacity and selectivity toward specific target adsorbates can be tuned. Among nanoadsorbents, nano metal-oxide supports have attracted much interest thanks to commercial availability, ease of synthesis or modification and regeneration and reusability.

Therefore, the following sections will be dedicated to reviewing applications of metal-oxide nanocomposites in precious metal (Au and Pd) adsorption. Three classes of molecules have been commonly used as surface coupling agent : organosilanes, carboxylates and more recently organophosphorus derivatives.

2.2.4.1. Coupling molecule and nanocomposites applications

Organosilane chemistry is powerful to anchor functional groups on the surface of nanoparticles. There are organosilicon compounds that have two different functional groups. The general formula for a silane coupling agent typically show two classes of functionality is $\mathbf{X}-(\text{CH}_2)_n-\text{Si}-\mathbf{R}_3$. The \mathbf{X} group represents the functional organic groups that can be modified to attach the desired functional groups, for instances, amino ($-\text{NH}_2$), mercapto ($-\text{SH}$) and etc. In contrast, the \mathbf{R} group represents hydrolyzable groups such as alkoxy or chloro ones that react with $-\text{OH}$ groups on the metal oxide surface through a condensation reaction.

Thanks to its magnetic property, magnetite (Fe_3O_4)-based adsorbents has also become attractive with regard to the simplicity of synthetic procedure and the ease of liquid-solid adsorption operation in which the separation usually is conducted by application of external magnet instead of centrifugation or filtration. Magnetite can be easily oxidized to maghemite ($\gamma\text{-Fe}_2\text{O}_3$) with the standard redox potential of 0.444V (vs. SHE) that is lower than that of $\text{AuCl}_4^-/\text{Au}$ (1.002V vs. SHE). Therefore, magnetite could be used as an reactive adsorbent that reduces AuCl_4^- to Au^0 [71]. Nevertheless, from the recovery point of view, most of the processes aimed at separating the target metals to end up in the form of concentrated solution or purified metals, regenerating and reusing the used adsorbent. An approach to tune the redox activity of magnetite nanoparticles and to improve the chemical resistance of magnetite nanoparticles to gold extraction is to elaborate $\text{Fe}_3\text{O}_4\text{-SiO}_2$ core-shell structures from which the surface SiO_2 coating will be modified with specific organosilane to impart the selectivity toward target metals.

A very recent publication that was published during our study by M. Shamsuddin et al. has demonstrated this strategy by synthesizing thioctic acid functionalized silica coated magnetite nanoparticles for capturing Au(III) ions [72]. In this study, authors created a layer of SiO_2 on the magnetite particles through codensation reaction with tetraethylorthosilicate (TEOS), then the surface modification of $\text{Fe}_3\text{O}_4@\text{SiO}_2$ with thioctic acid proceeded via two steps: (i) grafting $-\text{NH}_2$ functional groups to the $\text{Fe}_3\text{O}_4@\text{SiO}_2$ and (ii) amide coupling with thioctic acid in the presence of $\text{N,N}'$ -dicyclohexylcarbodiimide (DCC) and N -hydroxysuccinimide (NHS). With regard to gold adsorption, they found that the maximum adsorption capacity of resultant material was 222 mg/g (pH 5, 25°C) and the as-synthesized

material can be reusable through 5 cycles of adsorption/desorption demonstrated despite a slight reduction in adsorption capacity.

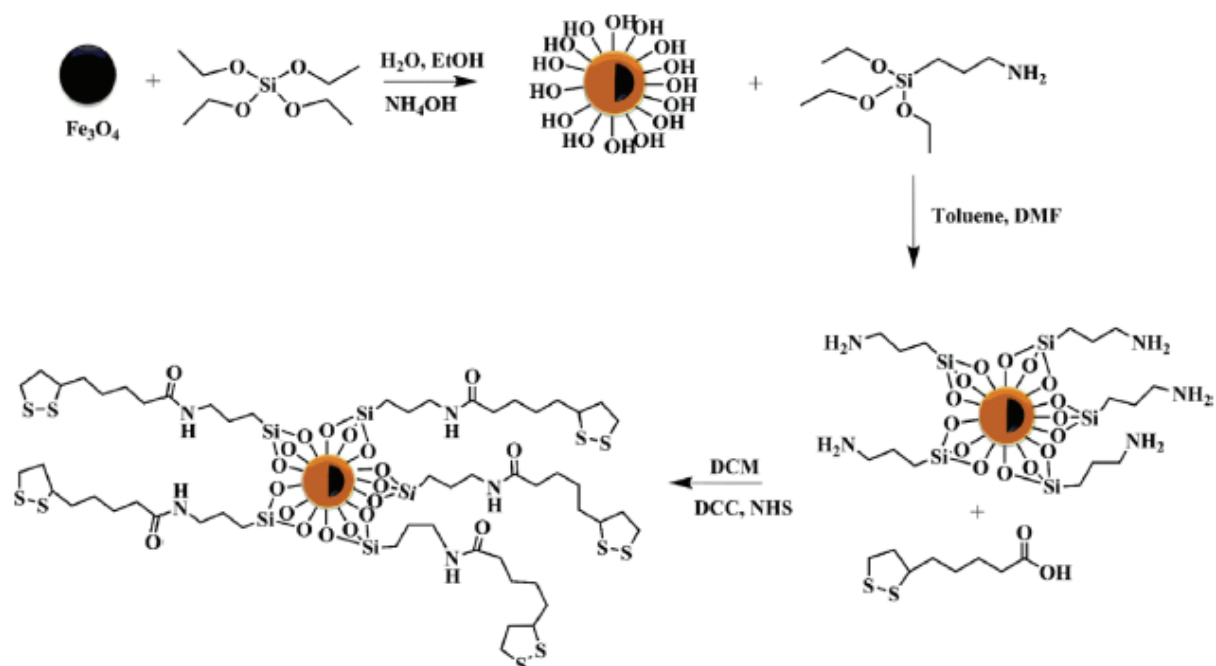


Figure 2-13 – Schematic representation of Fe₃O₄@SiO₂-TOA [62]

Furthermore, R. Roto et al. have demonstrated that the SiO₂ coating layer could protect the Fe₃O₄ from being dissolved by HCl, and could avoid agglomeration of Fe₃O₄ nanoparticles [73]. According to this study, SiO₂ was coated on the surface of Fe₃O₄ nanoparticles through the hydrolysis of Na₂SiO₃ under acid condition [74]. The thiol functional groups (-SH) were introduced to Fe₃O₄@SiO₂'s surface by silanization reaction between -Si-OH and 3-mercaptopropyltrimethoxysilane (3-MPTS). It was found that the adsorption of Fe₃O₄@SiO₂-SH toward [AuCl₄]⁻ followed the Langmuir isotherm model with the maximum adsorption capacity of 115 mg/g at pH 3.

Surface modified mesoporous silicas (such as SBA-15, MCM41, ...) have also been used as nanostructured support for extracting precious metals such as gold, platinum, palladium from wastewater. J. Yi et al. have demonstrated that the modification of SBA-15 surface with imidazole functional groups led to high adsorption selectivity toward Pd and Pt in the presence of excess Ni²⁺, Cu²⁺ and Cd²⁺ (Figure 2-14) [75]; for instance, the selectivity coefficients of this material ranges from 3.8x10² – 6.6x10² for Pt²⁺ and 9.7x10² – 1.8x10³ for Pd²⁺ in solutions containing 1mM Pt²⁺ or Pd²⁺, 10 mM Ni²⁺, 10 mM Cd²⁺, and 10 mM Cu²⁺. The decrease in the BET surface area, pore diameter, and pore volume was observed

after surface modification (from 712 m²/g for SBA-15 to 161 m²/g for Imidazole-SBA-15). The mesoporous structure remained intact, as proven by the similar patterns of N₂ adsorption/desorption isotherms.

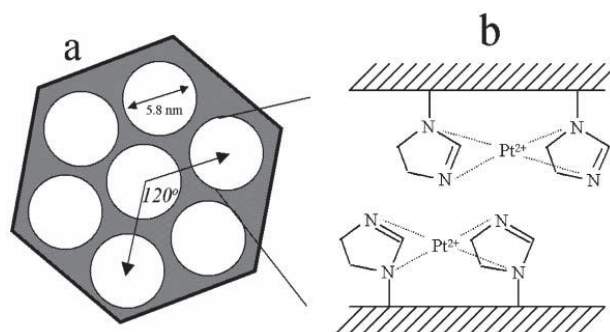


Figure 2-14 – Schematic representation of Imidazole-SBA-15[70]

Surface modification of MCM-41 by aminopropyl (-C₃H₆NH₂) moiety was made through the condensation between 3-aminopropyltrimethoxysilane (APTS) and hydroxyl groups of MCM-41 [76]. Despite the reduction in BET surface area from 1140 m²/g to 750 m²/g, the adsorption Pd and Au behaviors of the final material dependent on the pH of the solution. The Pd and Au adsorption processes were subsequently carried out at pH 1 and at pH 2.5 with the presence of competing metals (Cu, Ni, Co and Zn) and desorptions were conducted in between using HCl 5M. These findings, including pH dependence of adsorption capacities toward Pd and Au and utilization of HCl for recovering the target metals demonstrated that the electrostatic attraction plays the key role in the adsorption process of NH₂-modified MCM-41.

However, in the case of organosilane coupling molecules, the quality of surface modification (to obtain a monolayer for instance) is very sensitive to the amount of water in the solvent or adsorbed on the surface of the oxide that can induce homo-condensation reactions between Si-OH groups to end Si-O-Si bonds (Figure 2-15).

Carboxylate-based ligands have been also tremendously used for modifying the surface of metal oxide nanoparticles. Adsorption can occur through physisorption or chemisorption and the surface binding modes could be size-dependent. Generally, physisorption decreases, as the size of nanoparticles gets smaller, whereas the proportion of the chemisorption forms increase. In other words, carboxylic acid groups are capable of

binding to the oxide surface through “outer-sphere adsorption complexes” and “inner-sphere adsorption complexes” (Figure 2-16). In inner-sphere adsorption complexes, there are three common carboxylate coordination modes: mono or unidentate metal-ester coordination **(d)**, bridging bidentate **(e)**, and chelating bidentate **(f)**, whereas the interactions of carboxylic groups and metal oxide surface via hydrogen bonding are classified to outer-sphere adsorption complexes **(b, c)**. In addition, adsorption may occur through an Lewis acid-base reaction between the conjugated base (RCOO^-) and the acid sites at the surface (M^+) **(a)** [77].

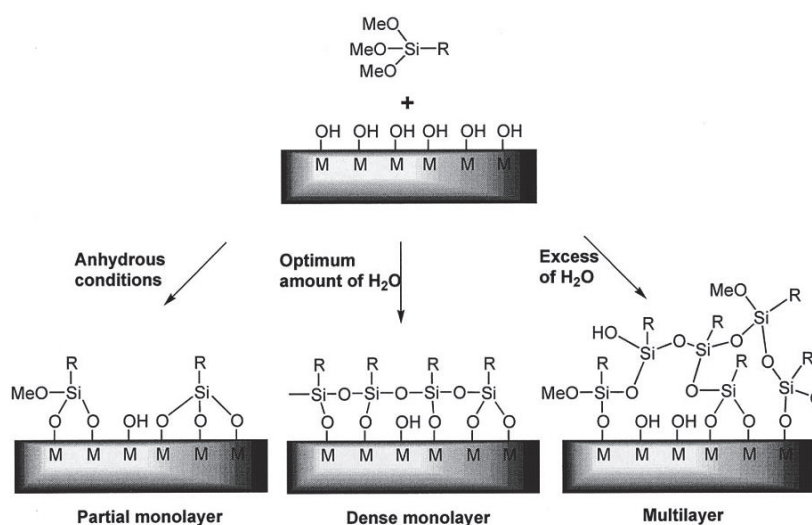


Figure 2-15 – Schematic representation of the impact of water on the surface modification of oxide surface using trimethoxysilane [78]

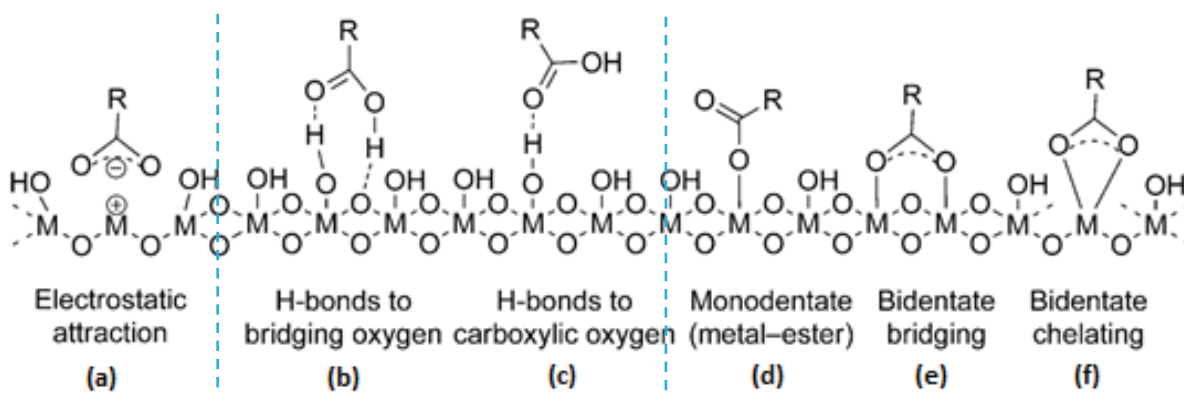


Figure 2-16 – The binding modes of carboxylic acids on oxide surfaces.

Very few studies have been conducted in order to apply the carboxylate-surface modified nano-oxides in the heavy metals removal generally and PGMs recovery particularly. In a study of Md. Rabiul Awwal et al., 3-(((5-ethoxybenzenethiol)imino)methyl)-salicylic acid ligand bearing hydroxyl and carboxylic as grafting groups was immobilized onto mesoporous silica monoliths substrate. The resultant material showed a high adsorption capacity and selectivity toward Pd (164.2 mg/g at pH 3) and the reusability through 10 cycles adsorption/desorption [79].

Recently, and in particular thanks to the work of Dr André VIOUX and Dr Hubert MUTIN, organophosphorus acids (PAs) have emerged as a fascinating class of coupling agents for the surface functionalization of nanoparticles. The main advantages compared to the organosilane and the carboxylate ligands are (i) the elaboration of monolayer since only hetero-condensation is possible (homo-condensation to give P-O-P is not favorable) (ii) the high hydrolytic stability of the P-O-M ($M \neq \text{Si}$) due to multiple bonding mode (mono-, bi- and tridentate) [78]. A dissolution-precipitation process may compete with surface modification depending on the reaction conditions and chemical stability of the oxide.

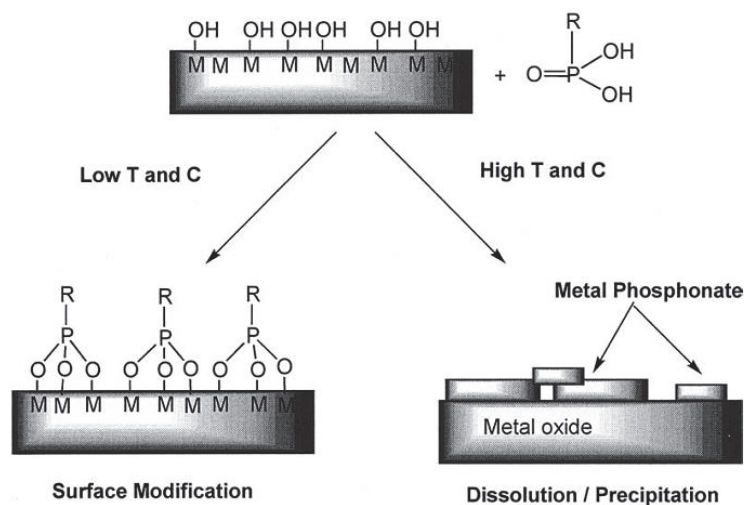


Figure 2-17 – Competition between surface modification and dissolution/precipitation processes using phosphonic acids [78]

PAs bind to a wide range of metal oxide surfaces by formation of M-O-P bonds, resulting from the condensation of P-OH groups with surface hydroxyl groups and the coordination of P=O groups to M atoms (Figure 2-18); however, PAs cannot be used to modify silica surfaces in aqueous medium due to the low hydrolytic stability of Si-O-P bond. In self-assembled monolayers formed by the reaction of carboxydodecyl-phosphonic acid with a

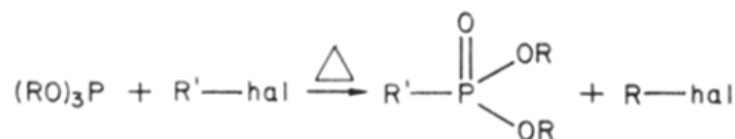


Figure 2-19 – Illustration Arbuzov reaction

In our group, the aza-Michael reaction of amines to diethyl vinylphosphonate followed by hydrolysis was employed to form the carbon-nitrogen, focussing on aromatic amines towards 2-(arylamino)ethylphosphonic compounds [83].

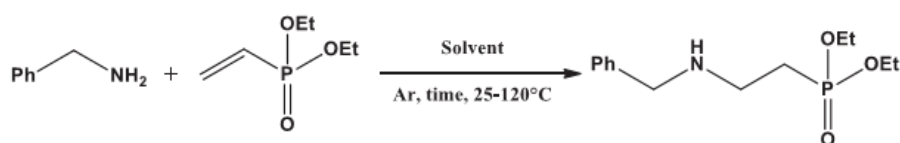


Figure 2-20 – Illustration of aza-Michael reaction

Gulaim A. Seisenbaeva et al. obtained the insight into the molecular aspects of ligand grafting of hybrid organic-inorganic adsorbents bearing phosphonate ligand monolayers as active functions. Using single crystal X-ray method to investigate the ligand-functionalized titanium alkoxide model complexes, they elucidated the tripodal vertical fashion of the attachment onto the surface of TiO₂. Illustrated in Figure 2-21 are the molecular structures of the model compounds which elucidate that phosphonic ligands are bonded via three Ti-(μ-O)-P bridges to three Titanium atoms Ti(2), Ti(3), Ti(4).

Imino-bis-methylphosphonic acid (IMPA, NH(CH₂PO₃H₂)₂) and aminoethylphosphonic acid (AEPA, H₂NC₂H₄PO₃H₂) were selected to modify the surface of TiO₂ nanorods. The final hybrid adsorbents have high capacities toward adsorption of Rare Earth Element (REE) cations, such as Dy³⁺ (39 mg/g), Nd³⁺ (30.3 mg/g), Y³⁺ (16 mg/g) and La³⁺ (31.95 mg/g), but adsorption processes occurred relatively slowly. A possible option for application of the such materials could be in water remediation with long contact times in sedimentation baths [84].

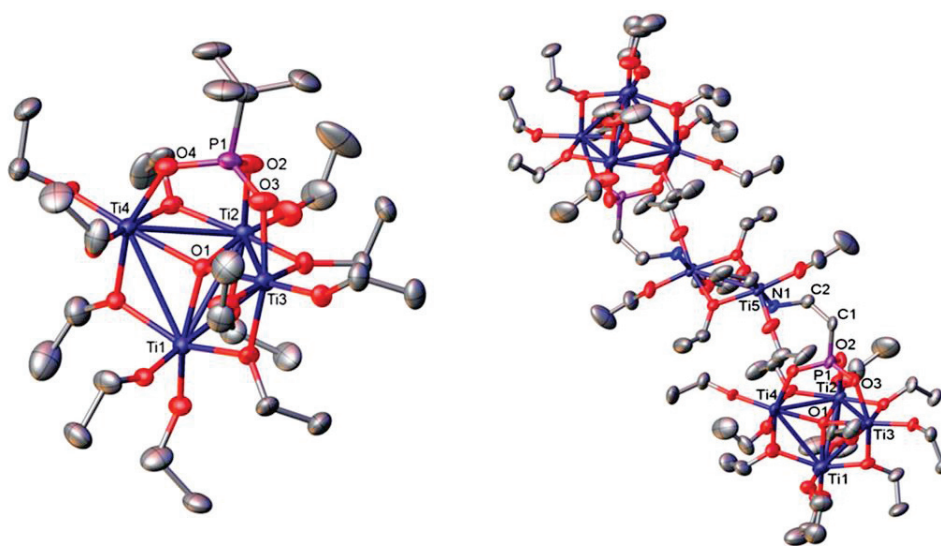


Figure 2-21 – The structure of $\text{TiO}_4(\text{EtO})_{12}(\text{t-BuPO}_3)$ (left) and $\text{Ti}_{10}\text{O}_2(\text{EtO})_{32}(\text{AEP})_2$ ($\text{AEP} = 2\text{-aminoethylphosphonate}$) [84]

2.2.4.2. Synthesis of Polymer/Metal Oxide Hybrid Nanocomposites

The role of Polymer/Metal Oxide Hybrid Nanocomposites

When it comes to real-life or industrial applications, the difficulty in collecting nanoscale metal oxide nanoparticles and the problems pertaining to their dispersion in liquid phase have been observed. On the other hand, in fixed-bed column operation, they exhibit high pressure drop because of aggregation between nanoparticles. Besides, their tendency to aggregate reduces their high surface area to volume ratio. Therefore, dispersing nanoparticles on a polymer supports is an approach to alleviating the drawbacks and hence to endow the resultant material with synergistic properties (Figure 2-22).

According to R. Muñoz-Espí et al., four possible strategies in the synthesis of inorganic/organic hybrid materials are distinguished [85]:

- (i) Strategies in which both inorganic and polymer components are synthesized ex-situ, and the hybrid material is formed by their mechanical combination. Two cases can be differentiated: (i) polymer chains are attached to inorganic particles and (ii) polymer particles and inorganic nanoparticles are mixed together. In both cases, the attachment can be noncovalent and covalent **(i)**.
- (ii) Strategies in which the inorganic nanoparticles are formed ex-situ and, afterwards, the polymerization of the organic component takes place in its presence (in-situ) **(ii)**.

- (iii) Strategies in which the polymer or the polymer particles are formed ex-situ and the precipitation/crystallization of the inorganic component takes place in-situ (iii).
- (iv) Strategies in which both polymer and inorganic components are simultaneously formed in-situ (iv).

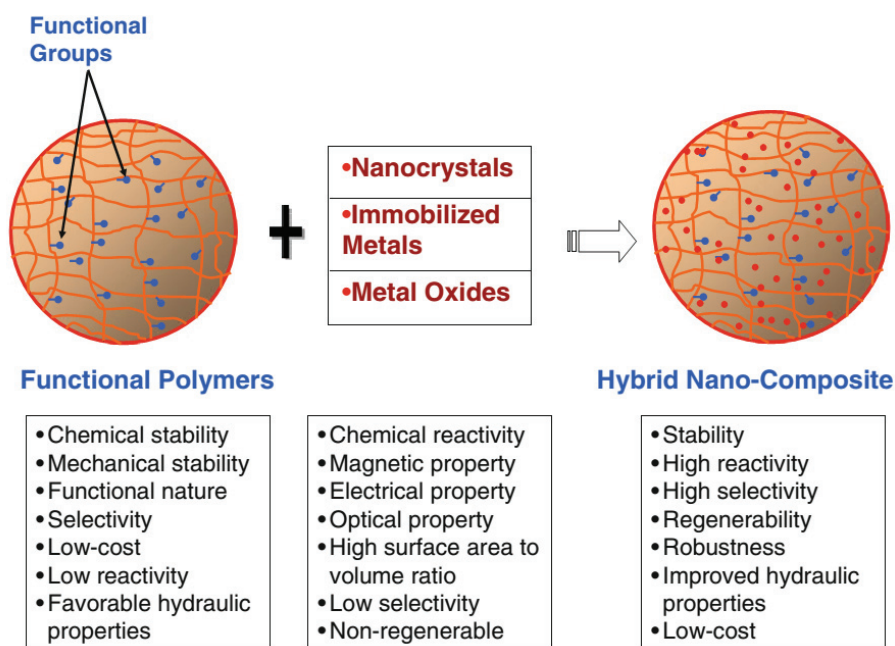


Figure 2-22 – Illustration of how individual shortcomings of nanoparticles and polymeric host material can be circumvented by polymer-supported nano particles [86]

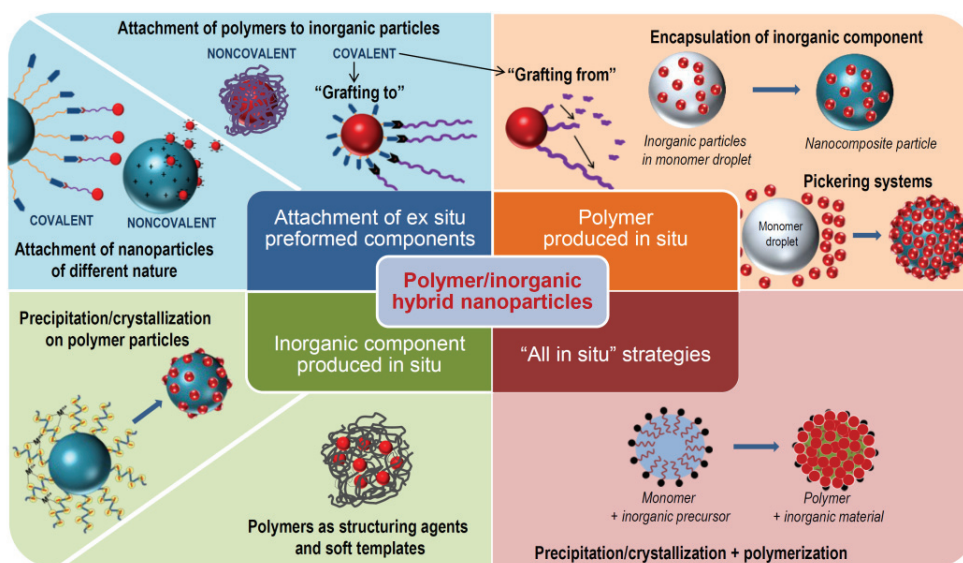


Figure 2-23 – Different synthetic strategies in the formation of polymer/inorganic hybrid material [85]

Regarding the polymer-supported metal oxides hybrid materials for applications of metals uptake, several examples collected and listed in Table 2-8 provide some information about synthetic route, target metals.

Table 2-8. Applications of polymer-supported metal oxides hybrid material in heavy removal

Adsorbent (Strategy)	Brief process of synthesis	Target metals	References
Chitosan-coated bentonite beads (i)	Bentonite was added to a solution of chitosan in 5% (v/v) HCl, then the mixture was mixed in 3 ^h and finally precipitation of chitosan onto the bentonite surface was carried out to add dropwise NaOH 1N.	Cu(II)	[87]
Silicagel gel microspheres encapsulated by imidazole functionalized polystyrene (ii)	Silica gel was modified with vinyl triethosilane (SG-C=C). Polymerization and encapsulation were carried out to obtain the silicagel surface-functionalized with salicylic acid (core-shell structure)	Cr(III), Mn(II), Fe(III), Ni(II), Cu(II), Zn(II), Hg(II), Pb(II), Pd(II), Pt(II), Ag(I), and Au(III)	[88]
Polyacrylamide-grafted iron(III) oxide (ii)	Hydrous iron (III) oxide was immersed in aqueous solution of N,N'-methylenebisacrylamide and potassium peroxydisulphate, then acrylamide was added and grafting was performed at 70°C.	Pb(II), Hg(II), and Cd(II).	[89]
Polypyrrole/maghemite and polyaniline/maghemite magnetic nanocomposites (ii)	γ -Fe ₂ O ₃ was mixed with sodium dodecyl sulfate and monomer (pyrrole or aniline) and then the mixture was stirred for 15 min and initiator (FeCl ₃ or (NH ₄) ₂ S ₂ O ₈) was added. The polymerization reaction was allowed to occur for 24 ^h at room temperature.	Cr(VI) and Cu(II)	[90]

<p>Polymer-supported magnetite (Fe₃O₄) nanoparticles (iii)</p>	<p>Cation exchange resin (gel or macroporous type) were loaded with Fe²⁺ ions at acidic pH under N₂ at 60°C.</p> <p>Slow oxidation at pH 10 by addition of 5% NaCl and 0.5% NaOH with bubbling of air with volume concentration of O₂ in 0.1-1% range.</p> <p>Rinsing and drying after washing with alcohol.</p>	<p>As(V), As(III)</p>	<p>[91]</p>
<p>Cation exchange resin-supported hydrous ZrO₂ nanoparticles (iii)</p>	<p>Cation exchanger D-001 was soaked in the solution of ZrOCl₂ (25% C₂H₅OH), then the mixture was stirred for 24h.</p> <p>Zr(IV)-preloaded D-001 beads were filtered, desiccated under ambient temperature, transferred to a binary NaOH-NaCl solution and stirred for 12 hrs.</p> <p>D-001 beads containing Zr(OH)₄ were dried at 60°C for 12 hrs.</p>	<p>Pb(II), Cd(II)</p>	<p>[92]</p>
<p>EDTA-modified chitosan-silica hybrid materials (iii)</p>	<p>Reacting chitosan with tetraethylorthosilicate. The resulting hybrid material was functionalized with EDTA by reacting with EDTA anhydride.</p>	<p>Co(II), Ni(II), Cd(II), and Pb(II)</p>	<p>[93]</p>
<p>Organic – inorganic interpenetrated hybrids based on cationic polymer and hydrous zirconium oxide (iv)</p>	<p>The synthesis of the hybrid consists of two stages: (i) radical copolymerization between 4-(vinylbenzyl)trimethylammonium chloride (CIVBTA) and [3-(methacryloyloxy)propyl]trimethoxysilane; (ii) sol-gel reaction that involves the hydrolysis of tetrabutoxi zirconium (TBZr).</p>	<p>As(V), As(III)</p>	<p>[94]</p>

The main difficulty in the ex-situ mixing process or blending is to tailor the homogeneity of the fillers in the polymer matrix because of the tendency of nanoparticles to aggregate.

Therefore, in-situ syntheses have been emerging as a promising alternative in which the preformed polymer phase acts as a micro-reactor and metal and metal oxide nanoparticles are generated inside the polymer phase from a precursor. Through simple precipitation or sol-gel reactions, size of nanoparticles are controlled, thereby, the well-dispersion of nanoparticles in polymer is achievable. Among all the aforementioned synthetic strategies, “all in-situ” method remains an uncharted field not simply because it can simplify the synthesis, but also because it does probably allow to manipulate the reaction at the atomic or molecular scale [85]. When it comes to eco-friendliness as well as sustainable development, the employment of bio-polymer should be further investigated with the aim to extend applicability at industrial scale.

Grafting nanoparticles on a support such as polymeric textiles like commercial polypropylene is not trivial and reports are rather scarce. Carbon textiles after surface modification process via heat treatment process has shown adsorption capability toward formaldehyde in the indoor air and the authors believe that the robustness of the resultant material which is based on coating the surface-modified mesoporous silica on carbon textiles will be markedly enhanced [95, 96]. One possible strategy that we have explored in this thesis was the layer by layer (LbL) method.

The concept of layer-by-layer (LbL) deposition was developed in the 1990s by G. Decher. It starts with buildup of ultrathin multiplayer films by a self-assembly process by consecutively alternate adsorption of anionic and cationic polyelectrolytes on charged surfaces [97]. The driving force to construct multilayers on a support is mainly based on electrostatic attraction which involves alternate exposing a charged substrate to two aqueous solutions of polyelectrolytes (PEs) with opposite charges; subsequently, the initial charge of substrate is reversed or “overcharged”. Rinsing with water is a necessary step to remove unbound, loosely attached PEs. After one cycle of soaking-washing-soaking, a paired layer or a bilayer is formed and multilayer thin film can be obtained by repeating this cycle (Figure 2-24). Furthermore, various building modes between components that construct the layer can be exploited including the hydrogen bonding [98], hydrophobic interactions, van de Waals forces.

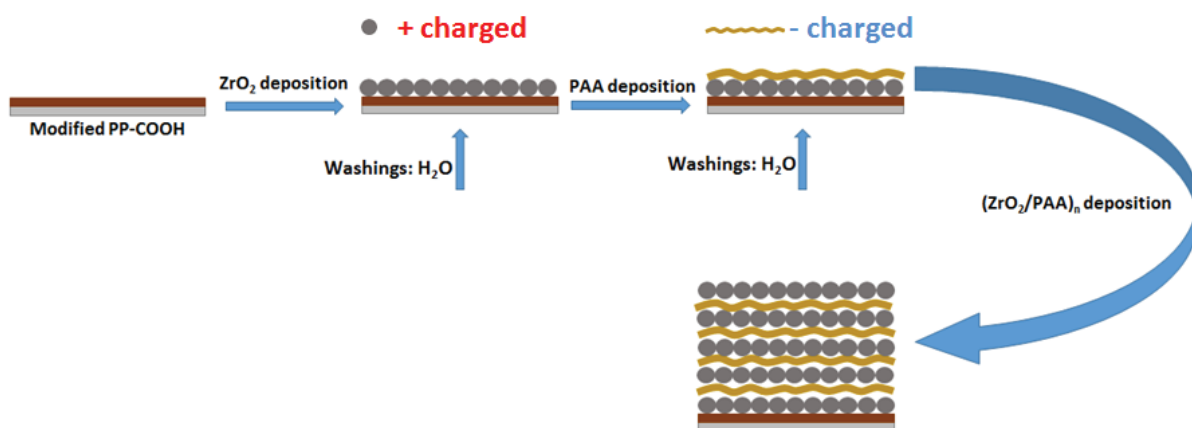


Figure 2-24 – Schematic representation of layer-by-layer approach based on zirconia nanosuspension and aqueous polypropylene solution.

As compared to other coating methods, LbL deposition offers some superior characteristics, including (i) ease of coating process with respect to equipment and procedure, (ii) flexibility in terms of a wide range of PEs (polymers, nanosuspensions...) and substrates, and (iii) eco-friendliness and sustainability when it comes to limiting used chemicals, and reducing energy consumption. Recently, LbL coating method has been attracting more attentions in the separation membrane design field in which the requirements of real application about a membrane being able to operate at high flux with high selectivity. Currently, to fulfill the above needs, reseach is focused on the preparation of defect-free membranes and LbL appears to be attractive coating method in order to control and tune the desired composition and properties.

Numerous studies have been done with the aim to get insights into the mechanism of the LbL coating process. It is realized that the formation, structure and stability of layers can be controlled by adjusting some basic parameters of PEs'solutions, for instance, ionic strength (screening effect), pH. Either of them has been of particular insterests in order to tune the properties of layer (thickness, roughness, porosity, hydrophilicity, and swellability). With respect to the effect of ionic strength, many publications reach unanimous explanations on the effect of salt concentration to the thickness and conformation of layers which are based on the screening effect of salt's ions. At low salt concentration, the PE chains are more expanded because of the electrostatic repulsion between charged sites on the PE chains, and the charges of layer are not affected by the counter-ions in the medium; hence the layers of PE chains are deposited mainly by charge overcompensation that results in a thin but stable layer on the substrate. In contrast, at high

salt concentration, counter-ions of medium can pair with charged sites of PE chains; in other words, PE chains are “screened” by electrolyte ions [99]. The screening effect reduces the charge density of PEs, so PE chains tend to be coiled and loopy; as a result, layer of PEs will be thicker due to higher amount needed for charge overcompensation and the loops and tails structure of PEs. The pH of medium is another important parameter during LbL coating due to the fact that dissociation of PE is able to be tailored by changing pH. As such, the charge density of PEs can be controlled to obtain the desired properties of coating layer.

Interestingly, even if PEs chains are screened or charge-compensated completely, the increase in PEs’ amount on the substrate still happens. Therefore, it has been believed that apart from the electrostatic repulsion, layers might be built up according to non-electrostatic interactions or hydrophobic interactions [100]. In order to prepare polyelectrolyte multilayer coating, three approaches have been developed consisting of dip-coating, spray-coating and spin-coating. It has been observed that dip-coating technique can offer a thicker, denser, smoother multilayer coating compared to others, but the deposition process is tedious and laborious. Although some automatic dip-coating systems have been studied and commercialized, scalability of the dip-coating process for the large substrate is the main limitation [101].

The outlines of the thesis

In the literature context, the objective of our collaborative project called SPONGE between the Institut de Recherches sur la Catalyse et l'Environnement de Lyon (IRCELYON, UMR5256), the Institut de Chimie Séparative de Marcoule (ICSM, UMR 5257) and the companies LOTUS SYNTHESIS (Villeurbanne) and MORPHOSIS (Le Havre) was to develop novel hybrid nano-sorbents for efficient recovery of trace of precious metals (Au, Pd, Pt) from e-wastewater leachates.

The basic principle of our project was to graft a functionalized nanostructured metal oxide layer on external surface of non-woven textile fibers with the aim to obtain a hybrid material with synergistic properties of nanoparticles and textile substrate (Figure 2-25). First, the chelating functional groups immobilized on the nanostructured metal oxide should offer the adsorption selectivity toward target metal ions to the resultant material. Second, the large surface area to volume of nano-metal oxide should improve the adsorption kinetics and capacity. Third, the textile substrate should lead to the homogeneous dispersion of nanostructured metal oxides; on the other hand, thanks to its interconnected voids between fibers, the resultant hybrid nano-material should possess better hydraulic properties, such as higher tolerance of large flux, which are required in flow-through adsorption technique in industry.

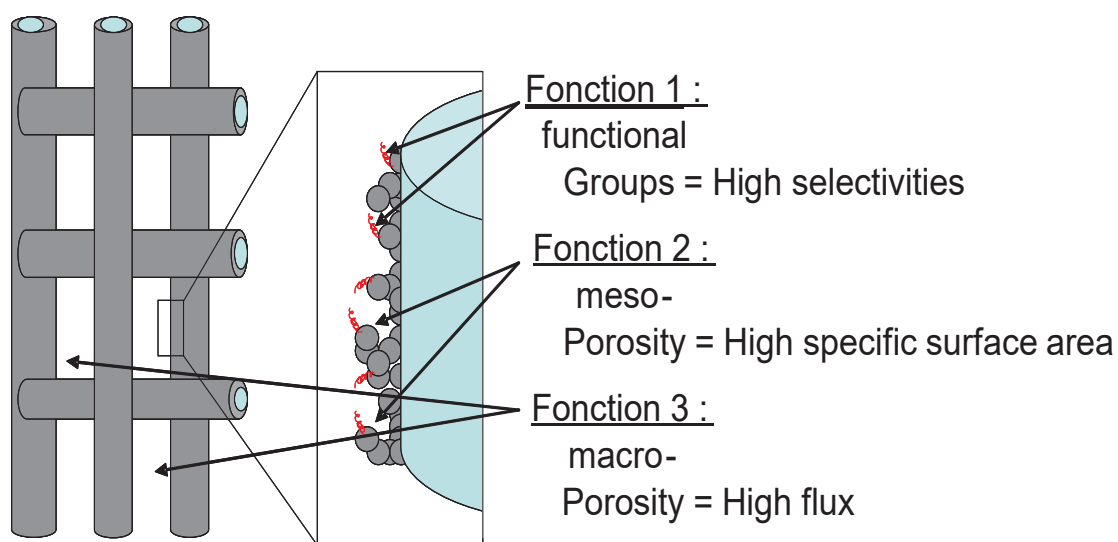


Figure 2-25 – Schematic illustration of proposed structure of substrate-supported hybrid ZrO_2 nanoparticles

One of the main scientific challenges of this study will be to understand the relationship between the final properties and the surface structure governed by the interaction between the textile substrate and the hybrid metal oxide layer deposited on it. Therefore, the study will be concentrated on the optimization of the textile surface functionalization by an hybrid oxide layer. Eco-friendly approach will be also taken into account all aspects of the whole synthetic pathway among them the prevention of wastes, the energy consumption, the atom efficiency, the use of benign solvents and the decrease of the required steps and time of a synthetic pathway, in respect with sustainable development guidelines.

The ultimate goal of this thesis was to synthesize a hybrid nanomaterial which can achieve (i) high adsorption capacity toward Pd, Au, (ii) fast adsorption rate and (iii) reusability. The study will be focused on nano-ZrO₂ which demonstrates high insolubility in most acids, alkalis and that could be supplied by our partner LOTUS SYNTHESIS in stable aqueous suspension.

Based on the requirements, the thesis was organized into three level of activities :

WP1 Preparation : synthesis of surface-modified ZrO₂ nanoparticles with ligands and screening of their Au and Pd extraction performances

WP2 Processing: deposit of an hybrid nano-coating onto modified-surface textile fibers (polypropylene) in order to elaborate multifunctional and hierarchical (molecule/nano-coating/fabric) nano-composites

WP3 Properties: in-depth characterization and evaluation of the properties of hybrid textile, namely the analysis of water containing cationic derivatives from simulated and real e-wastewaters.

WP1: Preparation of hybrid ZrO₂ nanoparticles and Au and Pd extraction performances

The first aim of WP1 was to be synthesize and to characterize new hybrid ZrO₂ nanoparticles through a list of ligands proposed by the partner ICSM. Surface modification will be tailored using carboxylate, phosphonate derivatives or enediol ones (Figure 2-26),

which have already demonstrated good extraction performance to critical metals (PGM, Ln, Ga, Ge ...). All hybrid nanomaterials will then be tested in terms of their capacity, their efficacy (coefficient distribution), their affinity (selectivity) and their regeneration/reusability. Classical studies towards physical and chemical parameters which influence the separation (initial concentration, contact time, HCl/Cl⁻ concentration, stripping agents) will be carried out in order to select the more efficient ZrO₂-ligand assembly. ICP-MS or ICP-OES will be used to determine the metals concentrations.

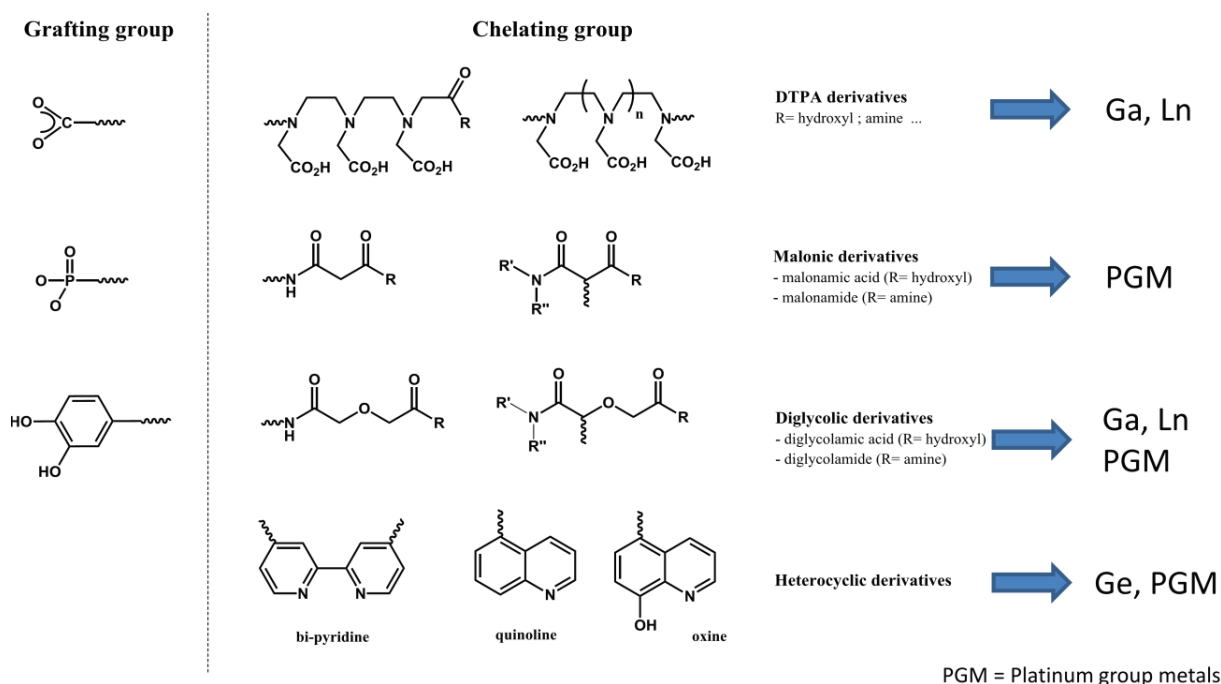


Figure 2-26 - The tentative combination between grafting and chelating groups for specifically target metals.

WP2: Processing of hybrid ZrO₂ nano-coatings onto textiles

The first aim of WP2 was to select an appropriate modified-surface polypropylene textile with carboxylic acid functions that can further react either with O-containing molecular precursors such as oxide nano-suspensions. Non-woven fabric will be preferable to resist to coating treatments without any loss of their mechanical properties. Depending on the selected hybrid nanomaterials in WP1, the aim of WP2 will be the processing of hybrid ZrO₂ thin films (thicknesses between 100-500 nm), starting from ZrO₂ nano-suspensions, on surface textile fibers containing carboxylic acid functions. LOTUS SYNTHESIS will supply aqueous batches of ZrO₂ nano-suspensions of different concentrations (5-40g.L⁻¹)

and aggregate sizes (30-250 nm) in order to check the impact of such factors onto the performances of the nano-coating. The results, together with detailed microstructural characterizations will be used to improve the understanding of selectivity and performances of selected nano-composite materials.

WP3: Properties in metal ions removal in simulated and real e-wastewater.

Throughout different activities, the adsorption capabilities of resultant materials (nanopowder and surface-modified PP textile) will be tested toward target metal ions. The adsorption capacity, kinetics, selectivity, the influences of experimental conditions ([HCl], [Cl⁻], stripping agents) and regeneration/reusability will be carried out in batch adsorption mode.

MORPHOSIS will provide real wastewater solutions originating from their recycling process and the adsorption capabilities of the resulting materials will be checked in terms of capacity and selectivity.

Our aspiration was to reach benchmarking activities and industrial implementation. In other words, prototype of the material was expected to be developed and investigated at the pilot or industrial scale.

CHAPTER 3. MATERIALS AND EXPERIMENTAL PROCEDURE

3.1. Materials and chemicals

DL-Thioctic acid (TOA) (> 98%, $C_8H_{14}O_2S_2$, $M_w = 206.32$ g/mol) and Alendronic Acid (AA) (> 98%, $C_4H_{13}NO_7P_2$, $M_w = 249.1$ g/mol) were purchased from ACROS OrganicsTM and Sigma Aldrich, respectively, and used as received. N-hydroxysuccinimide NHS-activated ester of TOA and others ligands including dioctyldiglycoamide (DODGA), thioctic acid (TOA), (N,N)-bis(2-ethylhexyl)carbamoymethylphosphonic acid (DEHCOMPA), (N,N)-dioctylcarbamoymethylphosphonic acid, phosphonmethylimino diacetic acid (PMIDAA) were synthesized and provided by Institut de Chimie Séparative de Marcoule (ICSM).

Standard solutions of Pd ($9373 \text{ mg kg}^{-1} \pm 20 \text{ mg kg}^{-1}$ in 10% HCl, TraceCERT[®]) and Au ($975 \text{ mg kg}^{-1} \pm 2 \text{ mg kg}^{-1}$ in 5% HCl, TraceCERT[®]) were purchased from Sigma-Aldrich. Ethanol (C_2H_5OH , ACS reagent, 100%) and hydrochloric acid (HCl, ACS reagent, fuming, $\geq 37\%$) was purchased from Sigma-Aldrich.

All solutions were prepared using 18 M Ω .cm water that is produced from VEOLIA company based on AQUADEM system. In this system, the feeding water is passed through different adsorbents including inert adsorbent (filter), active carbon, cationic and anionic exchangers. Resistivity of deionized water is monitor by a LED meter.

Sodium chloride (ACS reagent) was purchased from Carlo Erba. All chemicals were of analytical grade and used without further purification.

Zirconia nanosuspensions were purchased from Sigma Aldrich or given from Lotus synthesis company (Villeurbanne, Fr):

Supplier/Code	Concentration	pH	Nanoparticles (nm)
Lotus Synthesis/AFR-9-009-62	30 wt. % in H ₂ O	11-12	~ 10
Lotus Synthesis /AFR-9-062-14.2	12 wt. % in H ₂ O	1	~ 10
Sigma Aldrich/.CAS number: 1314-23-4	10 wt. % in H ₂ O	4-5	< 100

Polyacrylic acid solutions were purchased from Sigma Aldrich or given from Coatex company (Genay, Fr):

Supplier/Code	Concentration	Supplier	CAS number
PAAH $M_w \sim 2000$	50 wt. % in H ₂ O	Sigma Aldrich	9003-01-04
PAAH $M_w \sim 5000$	50 wt. % in H ₂ O	Coatex (Arkema group)	
PAAH $M_w \sim 100000$	35 wt. % in H ₂ O	Sigma Aldrich	
PAAH $M_w \sim 240000$	25 wt. % in H ₂ O	Sigma Aldrich	

Polypropylene substrates were obtained from CREAT, EMPA and SAATI companies:

Polypropylene/Supplier	Functional group	Capacity (meq/g)	Specific area (m ² /g)	Thickness (mm)
PP-bare/CREAT	No	-	-	3
PP-Am/CREAT	Ammonium	1.4	700	2
PP-COOH/CREAT	Carboxylic	2.7	700	3
PP-COOH/EMPA	Carboxylic	-	50	0.2
PP-COOH 106/26/SAATI**	Carboxylic	-	-	0.195
PP-COOH 297/35/SAATI**	Carboxylic	-	-	0.420

*CREAT: Chargeurs Recherches Études Applications Textiles

**Carboxylic surface-functionalized by EMPA using CO₂/CH₄ plasma process.

3.2. Characterization methods

3.2.1. Fourier Transform Infra-Red Spectroscopy (ATR-FTIR + DRIFT)

Surface-modified polypropylene and zirconia-coated polypropylene were characterized using attenuated total reflection ATR-FTIR on Thermo scientific system (model Nicolet Avatar 380) equipped with Diamond crystal (working range: 30000 – 200 cm⁻¹). Essentially, ATR is a technique to collect the absorption data from samples and its principle is based on the changes in intensity of infra-red beam when the beam is totally internally reflected while travelling between two media with different indices. The internal reflectance creates an evanescent wave which protrudes from the crystal's surface into samples (Figure 3-1) only a few microns (0.5 – 2 μm) and is attenuated by the energy absorption of the samples. The partially absorbed infra-red beam will be directed to the detector. Thanks to this technique, detecting the changes of functional groups and the

presence of zirconia on textiles would be less complicated with respect to sample preparation, and time of analysis.

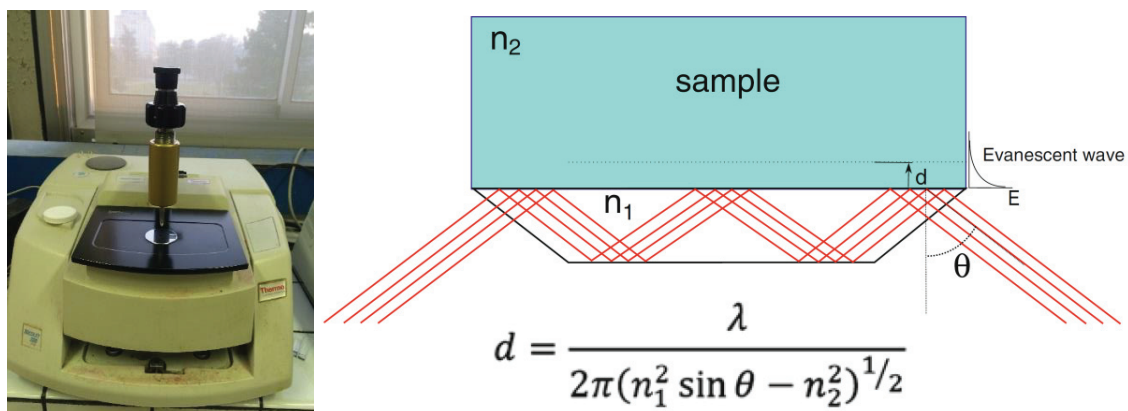


Figure 3-1 – Picture of ATR-FTIR equipment (left) and schematic representation of the measuring principle (right)

Diffuse reflectance (DRIFT) FTIR on Nicolet 6700 was deployed that IR beams are directed in sample cup containing sample particles and/or transparent mixture (KBr). In principle, IR beams interact with sample particles in two ways: (i) being reflected off the surface without absorption (specular reflection) and (ii) penetrating and interacting with the sample (diffuse reflection). Among them, diffuse reflection offers some spectral information that can be retrieved by DRIFT accessory. It has been realized that DRIFT can increase the resolution of spectra by reducing the signals from water bands [102, 103].

3.2.2. X-Ray Diffraction analysis

Identifying phases of ZrO₂ powder and detecting the presence of ZrO₂ on the polymer network were carried out on the XRD system Bruker D8 Advance 25 using radiation source Cu K alpha 1+2 1.54184 Å at a 2θ scan rate of 0.02°/point and step time of 0.5s. The obtained XRD spectra reveal different polymorphs of ZrO₂ in powder or coated on the polymer network.



Figure 3-2 – Picture of XRD equipment

3.2.3. Thermo gravimetric analysis (TGA)

The presence of organic ligands and the determination of ZrO_2 's content on the polypropylene are carried out using TGA/DSC 1 STAR^e system from Mettler Toledo. Samples are placed in crucibles alumina 70 μ L and measurements are automatically operated. The change in weight is recorded in air as it is heated according to the following temperature program:

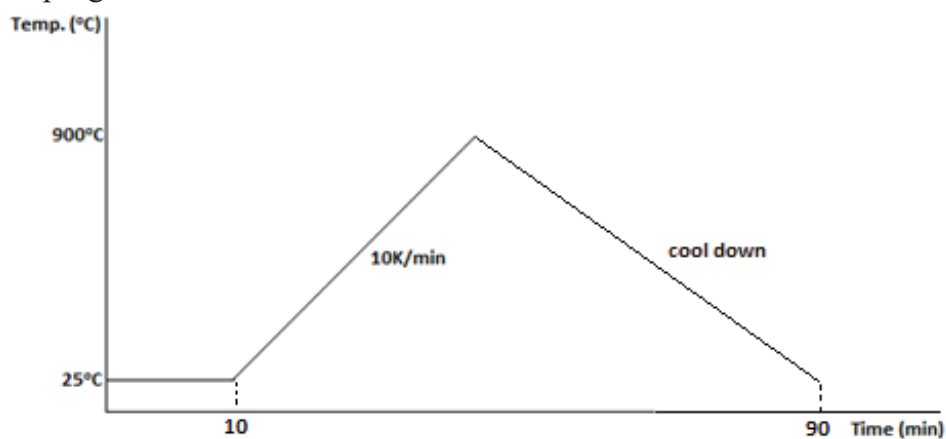


Figure 3-3 – Temperature program used for TGA experiment



Figure 3-4 – Picture of TGA equipment

3.2.4. Brunauer–Emmett–Teller method

Specific areas of surface-modified nano-ZrO₂ materials were determined using the Micrometrics ASAP 2020 system based on the BET method. Prior to measurements, materials were desorped at 150°C (423K) in 3^h. Nitrogen (N₂) gas was used as adsorptive gas and relative pressure (P/P_o) was varied from 0.013 to 0.25.



Figure 3-5 – Picture of Micrometrics ASAP 2020

3.2.5. Solid-State ³¹P MAS-NMR Spectroscopy

AVANCE III 500WB NMR system (500 MHz) with MAS technique (spinning rate of 10 KHz using a 4 mm triple H/X/Y probe) was used to obtain the solid-state ³¹P NMR spectra of zirconia modified with phosphonic acid derivatives. Importantly, the species of different compounds containing phosphorus on the surface of material and binding modes of ligands bearing phosphorus could be identified. The ³¹P chemical shifts were obtained using H₃PO₄ 85% wt. as a reference.



Figure 3-6 – Picture of solid-state NMR equipment

3.2.6. Scanning Electron Microscopy

Morphology of the ZrO₂ coating layer is assessed based on images obtained from scanning electron microscope ESEM-FEG FEI XL30, a platform in CLYM (Centre Lyonnais de Microscopie) located at INSA-Lyon.

3.2.7. Elemental Analysis (ICP-OES)

Elemental analyses determining the concentrations of Pd, Au, Cu, Ni, and Fe and analyzing the content of zirconium and phosphorus on polypropylene are conducted based on the ICP-OES system ACTIVA from HORIBA located at IRCELyon. In regard to liquid samples, direct determination is carried out at suitable emission lines (Table 3-1). With respect to solid samples comprising modified-zirconia powder and polypropylene textiles, samples are prepared by heating at 250 – 300°C in the mixture of H₂SO₄ and HNO₃ (for powder) and H₂SO₄, HNO₃ and HF (for textiles) until the white fume of SO₃ starts to appear, dilute with water and evaporate until dryness. Eventually, the residue is dissolved in HNO₃ 1%.

Table 3-1. Selected wavelengths in elemental measurements by ICP-OES

Element	Wavelength (nm)
Pd	340.46, 324.27
Au	242.79, 267.27
Cu	224.70, 327.39
Ni	221.65, 230.30, 231.60
Fe	240.49, 259.94



Figure 3-7 – Picture of ICP-OES equipment

3.2.8. Surface zeta potential measurement of nanosuspensions and textiles

Zeta potential measurement and streaming potential technique were used to acquire information about surface charges of nanoparticles in suspensions and textiles. With respect to zeta potential of nanoparticles, all nanosuspensions used in this study were diluted to the concentration of 0.1 % wt., NaCl was added to ensure the conductive matrix of samples at the concentration of 10^{-3} M, the measurement was conducted on Zetasizer Nano ZS with an auto-titration unit adjusting pH of nanosuspensions from 2-10.

In terms of streaming potential technique, swatches of pristine polypropylene and carboxylic-surface modified polypropylene were mounted on sample holder. For each type of samples, 2 swatches were needed in sample holder to create the streaming channel so that a tangential flow of an electrolyte (NaCl 10^{-3} M solution, pH 2-5.5) passes through across a solid surface and the streaming potential will arise.

3.3. Experimental procedures

3.3.1. Surface modification of zirconia

Brønsted acid-base reactions were selected to immobilize the ligands on the surface of zirconia nanoparticles consisting of 3 steps. In a typical experiment (Figure 3-8), 6 mL of aqueous 10% wt. ZrO_2 nanosuspension (5 mmol of ZrO_2), at pH 4-5 were added to a 10 mL round-bottom flask. A solution containing 0.1 mmol of each ligand dissolved in ethanol or water (for dissolving phosphomethyliminodiacetic acid – PMIDAA) was added dropwise to the nanosuspension and the mixture was stirred for 24 hrs at 25°C. The mole ratio of ZrO_2 to ligand was maintained at 50/1. The solid phase was separated by centrifugation for 10 min at 10000 rpm. The supernatant was decanted and the solid phase was dispersed in 20 mL of water, sonicated before separated by centrifugation. The washing procedure was repeated twice more with water and three times with ethanol. Finally, the hybrid zirconia powder was dried at 70°C for 24 hrs, and then ground by pestle and mortar to disaggregate. According to this procedure, we were able to recover about 90% of modified zirconia; in other words, about 0.54 g of modified zirconia was obtained with initial amount of aqueous 10% wt. ZrO_2 nanosuspension of 6 mL. On the other hand, the deposition yield of ligands will be discussed in section 4.2.3.

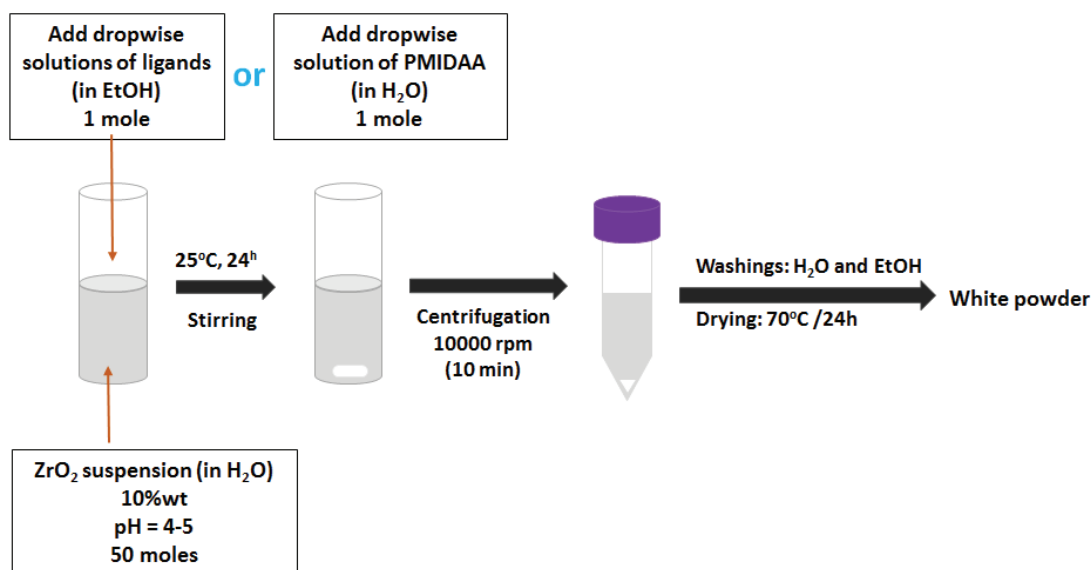


Figure 3-8 – Schematic representation of post-modification procedure

A two-step surface modification of zirconia nanoparticles was also developed during this study (Figure 3-9) :

1st step - surface functionalization with alendronic acid (AA): add 8 g of aqueous 10% wt. ZrO_2 nanosuspension (0.8 g of ZrO_2) and 10 mL of AA solution 10^{-1} M in a 100mL round-bottom flask, then stir under reflux for 4 hrs. The medium was separated and washed with water (3 x 10 mL) and the powder (denoted $\text{ZrO}_2\text{-AA}$) was dried for 24 hrs at 80°C .

2nd step - covalently grafting with TOA moiety using NHS-activated ester of TOA: weigh 0.20 g of $\text{ZrO}_2\text{-AA}$ in a round-bottom flask and add 2 mL of a solution of NHS-activated TOA in DMF 0.2 M reagent to $\text{ZrO}_2\text{-AA}$, then stir the mixture for 24 hrs at 25°C , separate the powder by centrifugation and wash 3 times with DMF (3x15 mL) and 3 times with $\text{C}_2\text{H}_5\text{OH}$ (3x15 mL) and eventually dry the powder at 80°C in 24 hrs.

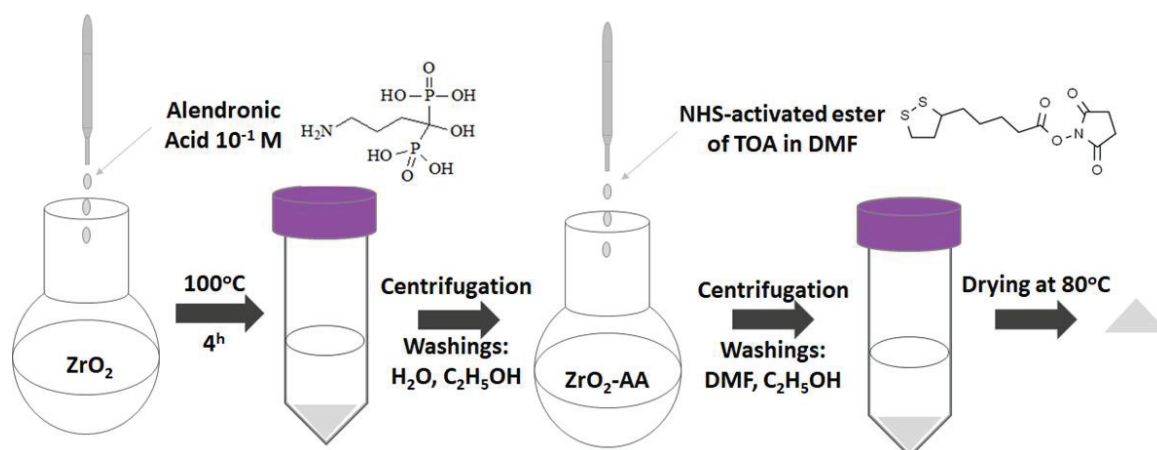


Figure 3-9 – Schematic representation of two-step surface modification

3.3.2. Deposition of zirconia on the surface of polypropylene and impregnation with ligands

3.3.2.1. Dip coating

Dip coating was applied for modified polypropylene substrate having high density of carboxylic groups (Figure 3-10). Typically, pieces of PP-COOH with the size of 1 cm x 1 cm were immersed into zirconia nanosuspension with the concentration of 10% wt. at pH 10-11 (Lotus Synthesis) for 2 hrs at 25°C. PP-COOH pieces were then taken out, washed three times with water (3 x 5 mL) and three times with ethanol (3 x 5 mL) and then dried for 4 hrs at 105-110 °C. After, zirconia coated polypropylene substrates were modified with suitable ligand by soaking polypropylene pieces in the solutions of a defined ligand at the concentration of 10⁻² M for 24 hrs at 25°C, especially 20 mL of this solution were used for 5 pieces of polypropylene. Finally, 1 cm x 1 cm PP pieces were washed and dried for 24 hrs at 105-110°C.

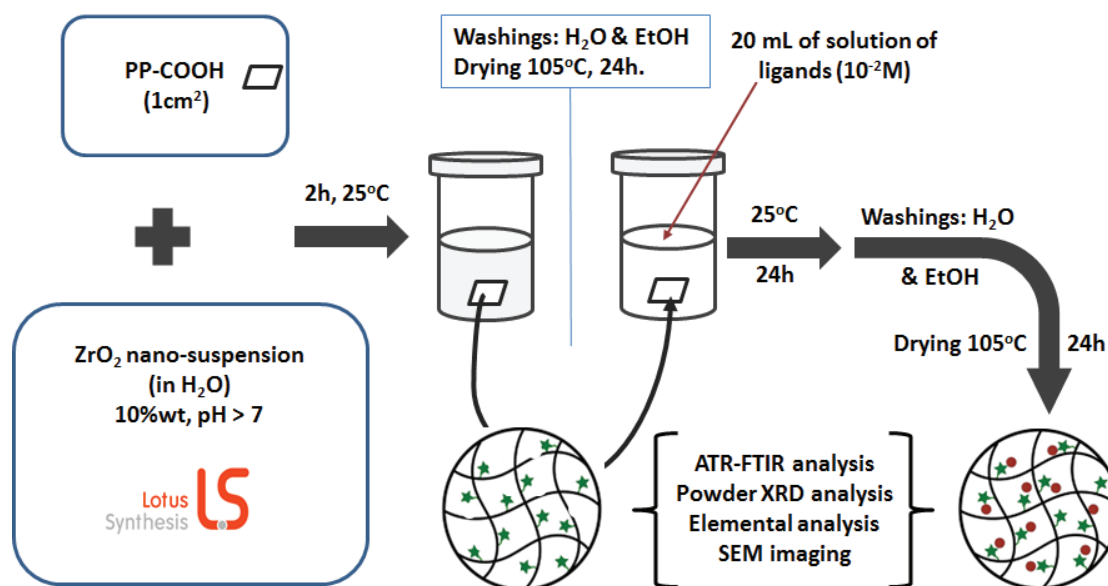


Figure 3-10 – Schematic representation of the deposition and impregnation processes onto surface-modified polypropylene

3.3.2.2. Layer-by-Layer dip-coating method (LbL)

All ZrO₂ nanosuspensions were expected to be positively charged at pH 2.5, so they were diluted to 1% wt and adjusted to pH 2.5. In the meantime, an electrolyte was needed with a role as a “glue” to attach all layers of zirconia nanoparticles together, thus polyacrylic acid (PAA), a polymer with pK_a in the range of 4.5-4.75, was chosen.

In this study, three types of PAA with different molecular weights consisting of 2500, 5000, 100000, and 240000 Da were selected. They were prepared by adding defined amount of PAA to certain quantity of water, dissolving by sonication and adjusting the pH to 2.5. Based on estimation, the fraction of PAA⁻ was around 1% wt. of the initial concentration of PAA, and it makes the whole chain of PAA charge negatively. Below is the schematic representation of our LbL method, along with specific conditions.

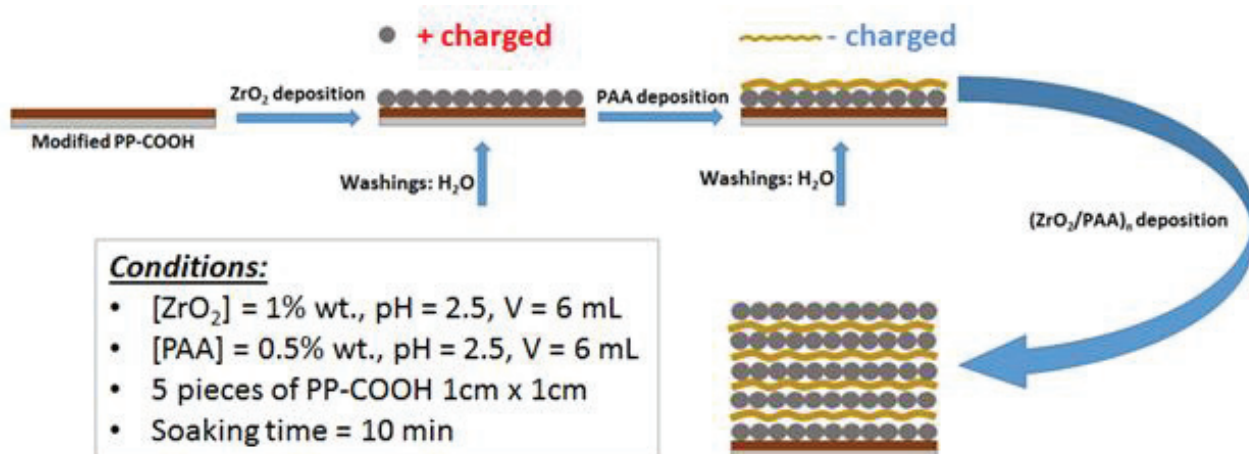


Figure 3-11 – Schematic representation of our LbL coating process

100%-ZrO₂ LbL coating layer

With the aim to create 100% nano-ZrO₂ coating layer on PP-COOH textiles, ZrO₂ nanosuspensions with pH 1 and pH 10 from Lotus Synthesis were employed. They were diluted to the concentration of 1% wt. by deionized water, their pHs were adjusted to 6 and layer-by-layer coating process was carried out as illustrated in Figure 3-11.

3.3.3. Batch adsorption experiment and adsorption isotherm

Batch adsorption experiments were used to assess and compare adsorption capability of each surface-modified zirconia samples. Moreover, this method was also employed to investigate the effect of parameters to the adsorption process of thioctic acid-modified zirconia such as time contact, the effect of HCl, stripping process and so on. The experiment was carried out by adding a fixed amount of adsorbent (m) into a definite volume (V) of a solution containing Pd or/and Au with a defined initial concentration (C_i), then stirring the mixture in a determined period of time (t). Finally, the supernatant solution was separated by centrifuging at 8000 rpm and the final concentrations of Pd or/and Au (C_f) in solution were determined by ICP-OES technique (Figure 3-12).

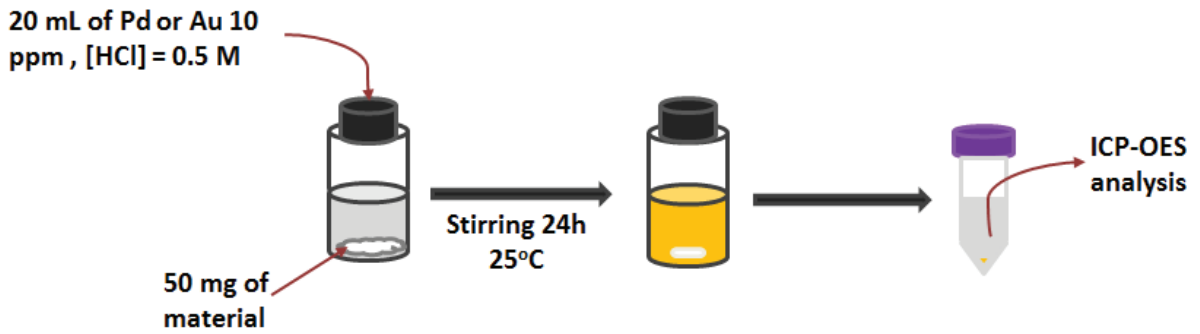


Figure 3-12 – Schematic representation of batch adsorption experiment

The adsorption or extraction percentages E (%) toward Pd or/and Au were calculated as follows:

$$E (\%) = \frac{(C_f - C_i)}{C_i} \times 100\%$$

Similarly, batch experiments were carried out to study the adsorption capacities toward Pd and Au and adsorption isotherm of Pd and Au, but a series of batch experiments was conducted in which initial concentrations of Pd or Au were varied in the range 5-300 mg/L. The equilibrium adsorption capacity q (mg/g) was calculated according to the following formula:

$$q \left(\frac{mg}{g} \right) = \frac{(C_f - C_i) \times V}{m}$$

For stripping and recyclability investigations, ZrO_2 -TOA and ZrO_2 -AA-TOA nanomaterials (50 mg) were put in contact as described previously with 20 mL of an aqueous solution of Pd at 10 ppm, and then recovered by centrifugation and washed with water. The final solids were then stripped by a 10mL mixture of thiourea 0.1-0.2 M and HCl 0.5 M for 4 hrs. After, the ZrO_2 -materials were washed twice with 15 mL of water and reused in a further adsorption step.

CHAPTER 4. HYBRID ZrO₂ NANOPOWDERS: SYNTHESES AND APPLICATIONS

Introduction

The objectives of this task were to modify the ZrO₂ nanoparticles' surface by organic complexants and assess their adsorption capability and selectivity toward palladium (Pd) and gold (Au). Moreover, the relationship between structure of ligands and extractability was interpreted.

The development of hybrid nanoparticles is discussed in relation to the following aspects:

- Syntheses of the ZrO₂ hybrid nanoparticles.
- Characterizations of the as-synthesized hybrid nanoparticles by using FT-IR (ATR & DRIFT), TGA, ³¹P solid state NMR and elemental analysis (Zr, P) and SEM.
- Investigation (screening) of Pd and Au adsorptions to select the best capturing ligands with the highest capacity and selectivity.
- Investigation of the adsorption capability of thioctic acid-surface modified nano-ZrO₂ material.
- Development of two-step surface modification processes to reinforce the strength of bond between ligand and ZrO₂'s surface

4.1. Syntheses of the hybrid ZrO₂ nanoparticles using different kinds of ligands

The ligands selected contain two important features:

- (i) A grafting group based on carboxylate (-CO₂), or phosphonate (-PO₃) ligands which is capable of binding to metal oxide's surface and not being washed out during application set-up (extraction, desorption/regeneration, and reuse).

- (ii) A trapping group which plays as capturing functional group toward target metals. By tailoring this group, the adsorption capability of the hybrid material could be tuned to selectively extract one or a group of metals over a mixture.

In collaboration with ICSM, five ligands were designed and provided which contain two types of grafting group, including carboxylate and phosphonate, and carbamoyl and diglycolic derivatives as trapping groups. Described in the Figure 4-1 are the specific structures of five ligands. Among them, thioctic acid is commercially available and predicted to efficiently adsorb “soft” metals (Hg, Au, Pd...) thanks to soft “S” sites.

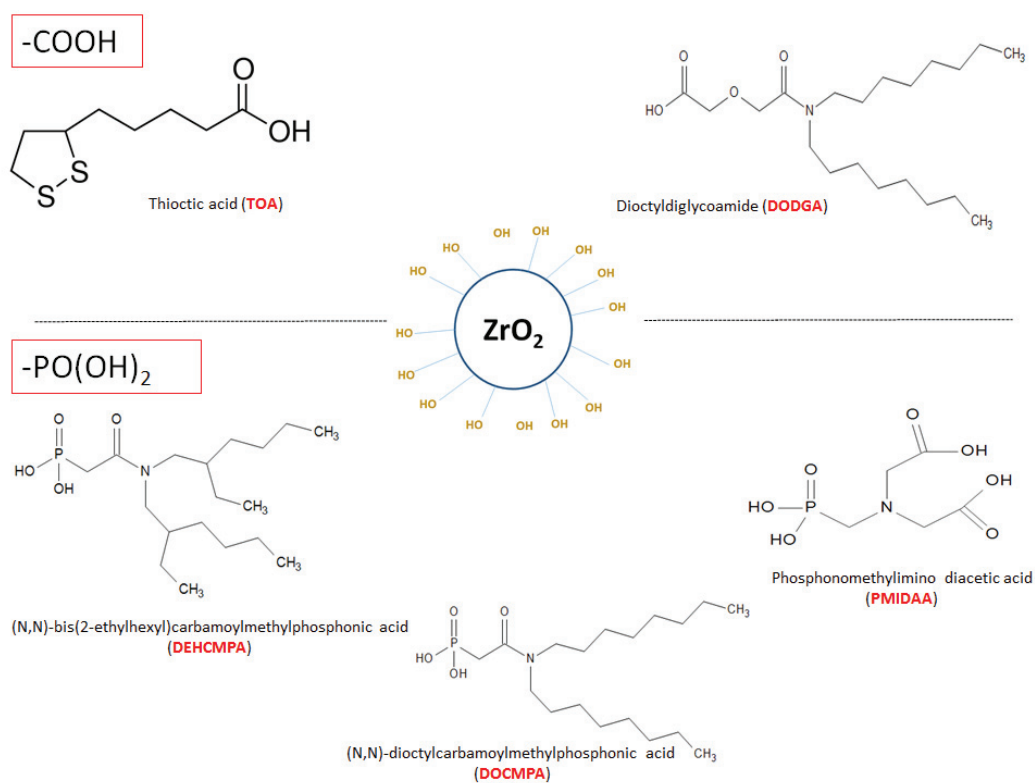


Figure 4-1. The structures of selected ligands to functionalize the zirconia's surface

As described in section 3.3.1, Hybrid nano- ZrO_2 materials were obtained by post-surface modification in which the mole ratio of ZrO_2 to ligand was kept at 50/1.

The powder XRD spectrum of commercial zirconia (from Sigma Aldrich) showed that two phases were simultaneously present, namely, tetragonal (~58%) and monoclinic (~42%).

Using the Rietveld analysis (structure profile refinement), the particle size of zirconia was estimated at around 15 nm.

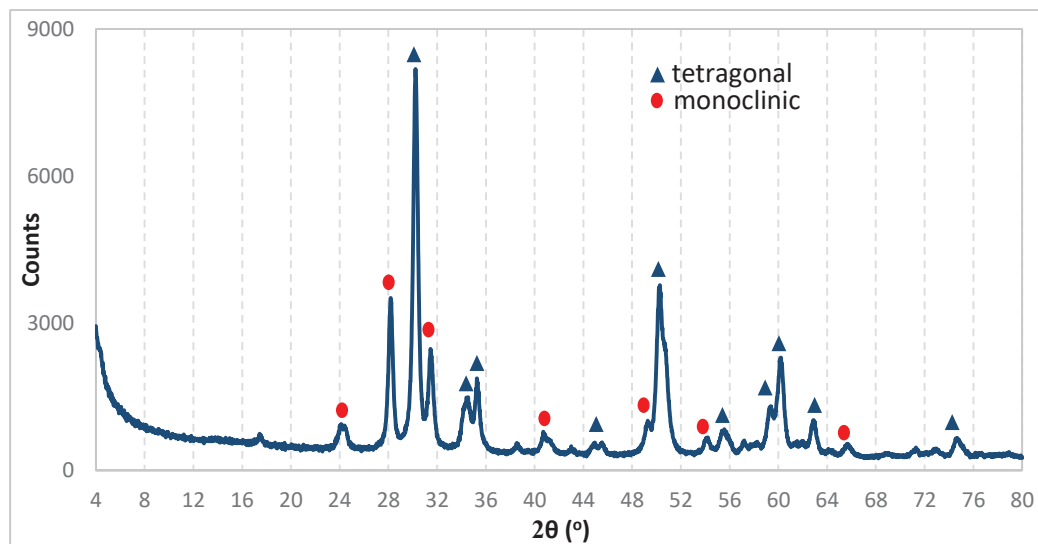


Figure 4-2 – XRD spectrum of bare zirconia nanoparticle from Sigma Aldrich

4.2. Characterization of hybrid zirconia nano-powders:

All surface-modified zirconia nano-powders are characterized by using various methods, namely FTIR, TGA, XRD, BET, solid state ^{31}P MAS NMR and elemental analysis (Zr, P) to identify the content of ligands on the surface of zirconia and to get insights into the binding modes or interaction between ligands and the surface of zirconia. FT-IR is used for determining the presence of organic complexants on zirconia's surface. With respect to phosphonate ligands modified nano- ZrO_2 , solid state ^{31}P NMR is employed to study the bonding mode of phosphonic groups. Finally, with the help of elemental analysis (ICP-OES), the exact ratio Zr/P of phosphonic acid-modified zirconia is determined to consolidate the estimated content from thermogravimetric analysis (TGA).

4.2.1. FT-IR spectroscopy

In the spectrum of nano- ZrO_2 modified with thioctic acid (ZrO_2 -TOA) (Figure 4-3), only two bands associated with methylene stretching bands are present because the TOA's molecular structure is just built up by methylene ($-\text{CH}_2$) chains, carboxylic group and

disulfide group. New bands occur at 1559 cm^{-1} and 1435 cm^{-1} resulting from asymmetric and symmetric stretching of CO_2^- , respectively. The value of band separation $\Delta\nu[\nu_{\text{as}(\text{CO})} - \nu_{\text{s}(\text{CO})}]$ can be used to understand the modes of coordination of carboxylic group. With the value of 124 cm^{-1} , bidentate bridging/chelating coordination is favored. The disappearance of deformation band of Zr-OH at 1395 cm^{-1} in all FTIR spectra of modified-zirconia is most likely to be the result of the interaction between hydroxyl group of zirconia and grafting groups of ligands. The spectrum of nano-ZrO₂ modified with dioctyldiglycoamide (DODGA) in Figure 4-4 shows the similar patterns as that of ZrO₂-TOA, including the stretching band of C-H bonds ($2850 - 2960\text{ cm}^{-1}$), the appearance of new bands ($\nu_{\text{as}(\text{CO})}$: 1587 cm^{-1} and $\nu_{\text{s}(\text{CO})}$: 1421 cm^{-1}), and the broad band below 500 cm^{-1} .

In regard to zirconia powders modified with carbamoyl phosphonic acid derivatives, namely (N,N)-bis (2-ethylhexyl)carbamoylmethylphosphonic acid (DEHCPMPA) and dioctylcarbamoylmethylphosphonic acid (DOCMPA), their spectra indicate new bands between 2800 cm^{-1} and 3000 cm^{-1} . These vibrations correspond to stretching of C-H bonds with methylene-symmetric and methylene-asymmetric stretching modes located at 2857 cm^{-1} and 2924 cm^{-1} , respectively and methyl-asymmetric stretching mode at 2960 cm^{-1} (Figure 4-6 and Figure 4-7).

In the case of phosphonomethylimino diacetic acid ligand which contains one phosphonic group and two carboxylic groups, one of the features highlighted in its spectrum is the band at around 1635 cm^{-1} . As compared to the bare ZrO₂'s spectrum, the intensity at this wavenumber in the spectrum of ZrO₂-PMIDAA is higher as a consequence of carboxylic groups on the surface of zirconia. In the other words, the phosphonic group of PMIDAA shows a preferential affinity for zirconia producing pendent carboxylic groups.

The spectra of ligands having phosphonic groups, namely DEHCPMPA, DOCMPA and PMIDAA indicate the typical bands of P-O vibrations in the $900\text{-}1200\text{ cm}^{-1}$ range. Despite the broadness and complexity of this region, it is noteworthy that observed changes are likely to be interpreted. In general, the bands centered at $\sim 1200\text{ cm}^{-1}$ and 950 cm^{-1}

respectively correspond to P=O stretching and P-O stretching vibrations in the spectra of phosphonic ligands. However, these bands disappear and a broad band arises in the spectra of zirconia modified with DEHCPA, DOCMPA and PMIDAA.

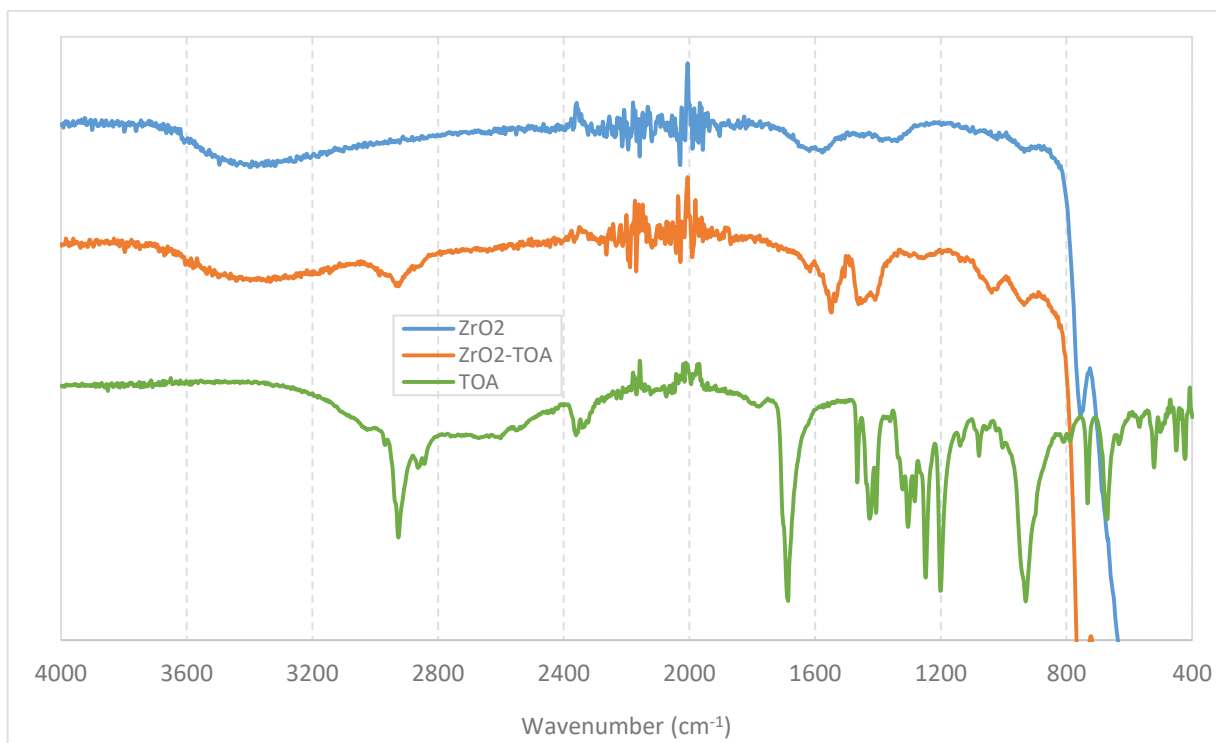


Figure 4-3 – FT-IR spectra of bare nano-ZrO₂, nano-ZrO₂ modified with TOA and TOA

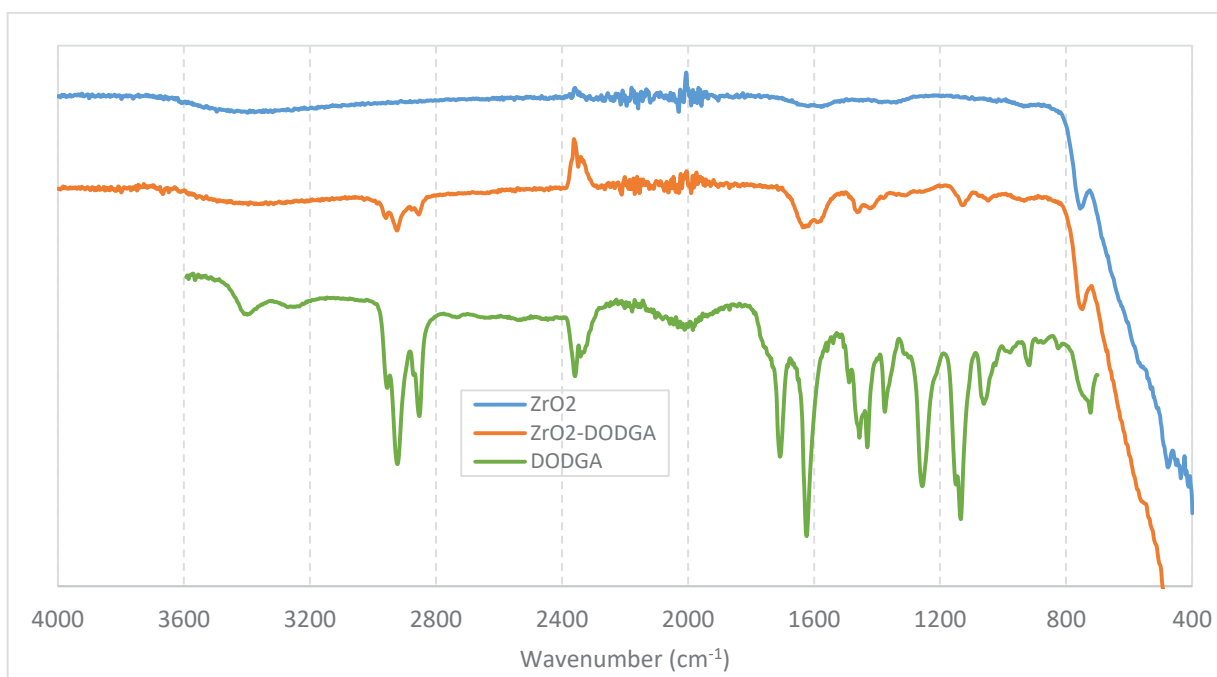


Figure 4-4 – FT-IR spectra of nano-ZrO₂, nano-ZrO₂ modified with DODGA and DODGA

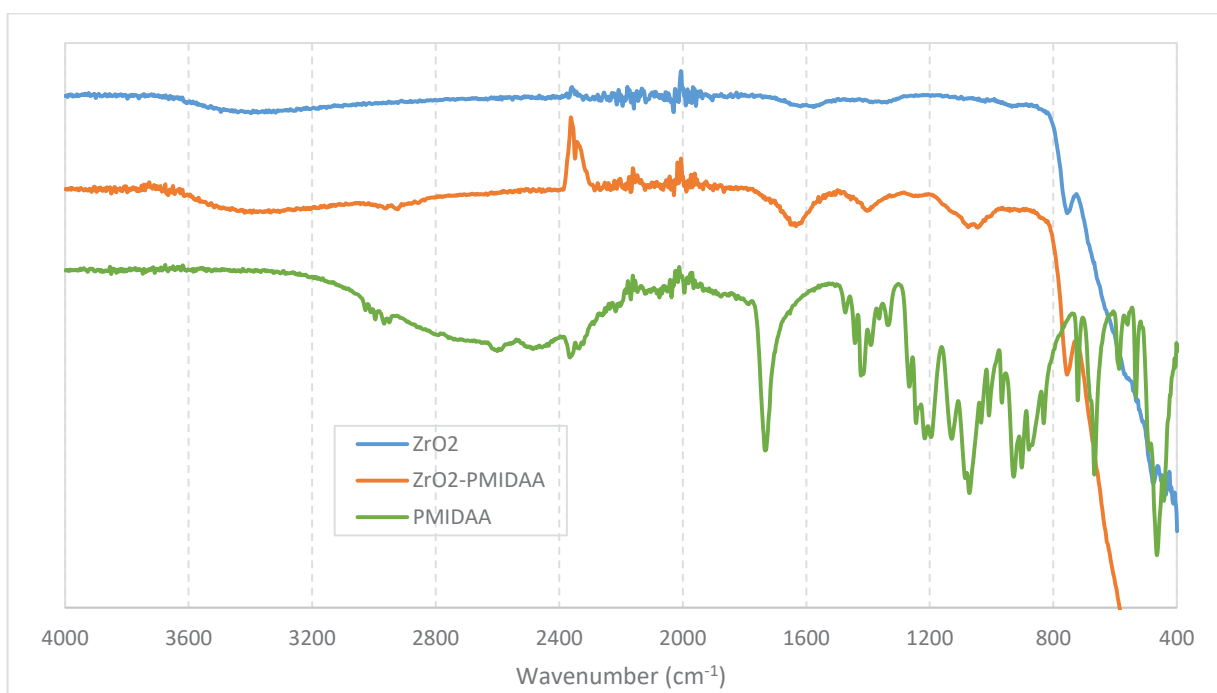


Figure 4-5 – FT-IR spectra of bare nano-ZrO₂, nano-ZrO₂ modified PMIDAA and PMIDAA

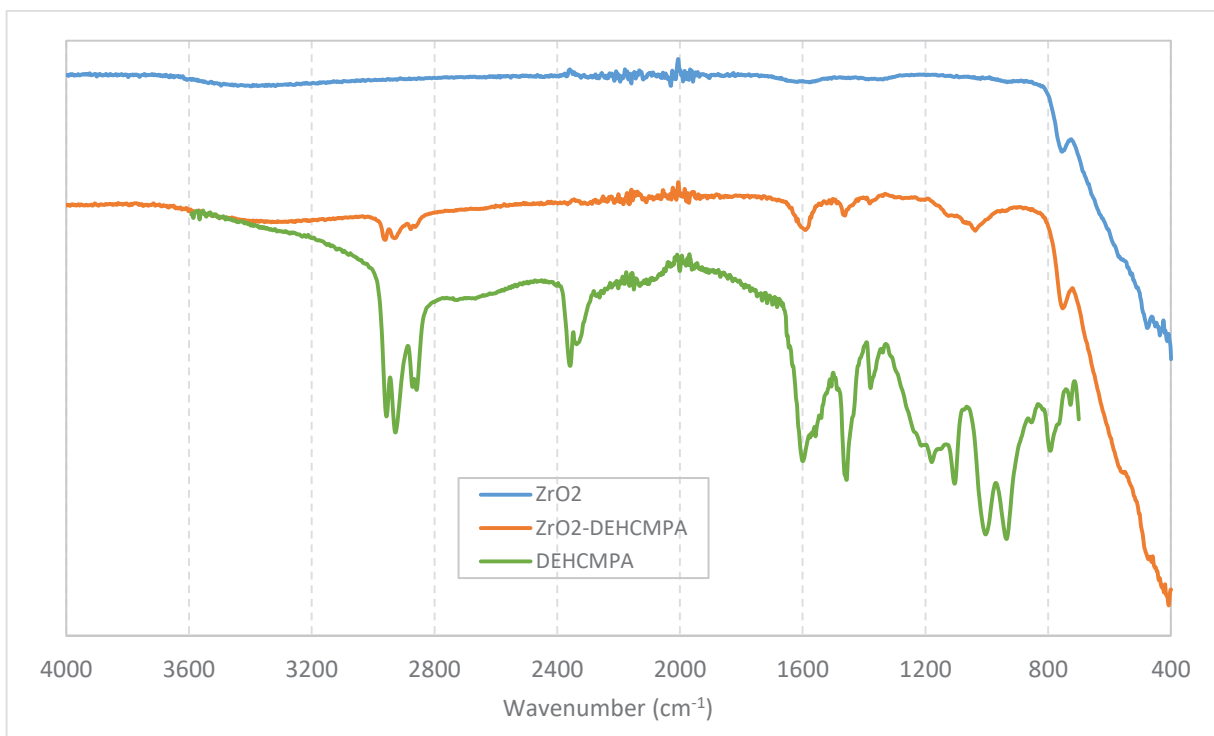


Figure 4-6 – FT-IR spectrum of bare nano-ZrO₂, nano-ZrO₂ modified with DEHCPMA

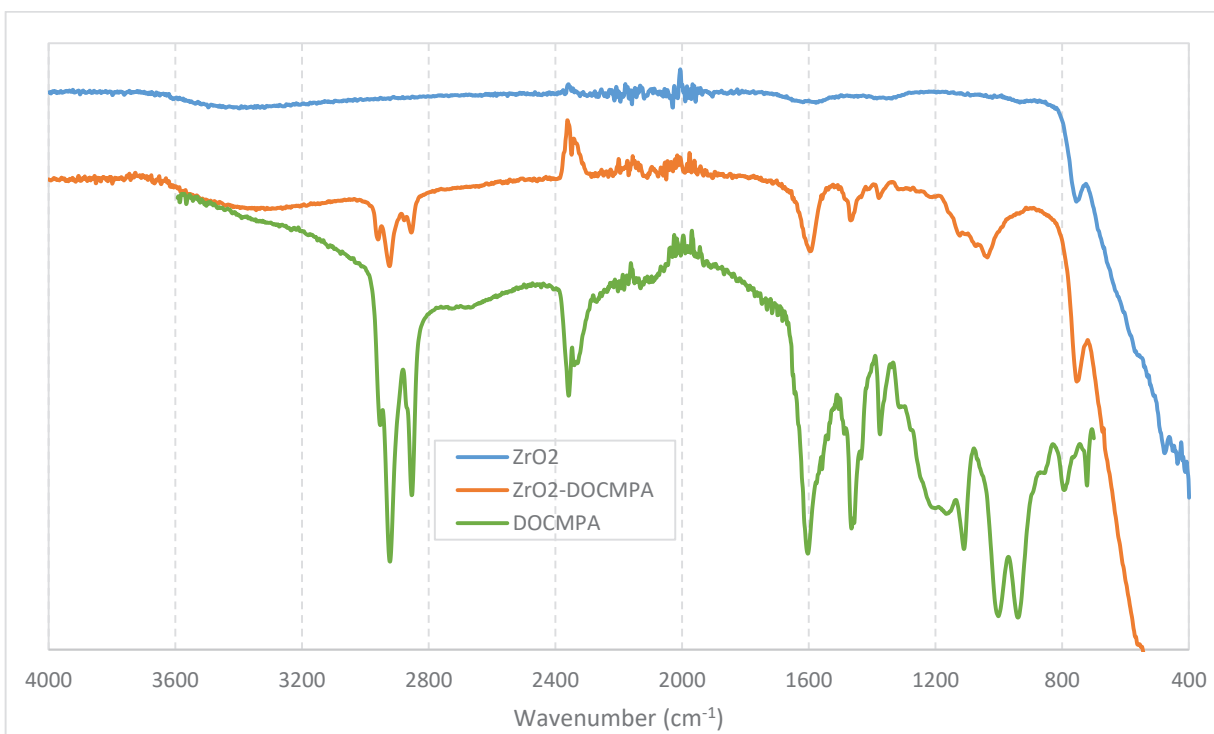


Figure 4-7 – FT-IR spectrum bare nano-ZrO₂, nano-ZrO₂ modified with DOCMPA and DOCMPA

4.2.2. ^{31}P MAS solid-state NMR

As commonly used in the studies of phosphonate-based organic-inorganic hybrid material, ^{31}P solid-state NMR can be carried out to differentiate different phosphorus species on the surface of zirconia and to give some information about bonding modes of phosphonic ligand. Nonetheless, acquiring the exact bonding modes of phosphonic species require a more direct method to provide an unambiguous information. So far, ^{17}O solid state NMR has been utilized to come to the conclusions about predominant bonding mode (monodentate, bidentate or tridentate) or species (physisorbed, chemisorbed and bulk metal phosphonate) [104, 105].

One of the typical features considered as the evidence of chemical bonding of phosphonate ligands is the broadness or the width of resonance signals. Due to bonding process of phosphonic ligands to the Zr-OH surface groups, the conformation of ligands and environment surrounding P atoms is neither well-defined nor uniform[106]. MAS technique in solid-state NMR, thus, is not likely to average out these effects and the resonance signals become broader. As a consequence, the solid-state NMR spectra of modified-ZrO₂ show broad resonances corresponding to the isotropic peaks range from 0 to 35 ppm (Figure 4-8 (b)), accompanying the spinning sidebands. In contrast, all the NMR spectra of phosphonic ligands display a very sharp peaks located at 6.70 ppm for ZrO₂-PMIDAA, 18.31 ppm for ZrO₂-DOCMPA, and 19.21 ppm for ZrO₂-DEHCPA, respectively (Figure 4-8 (a)).

Not only does the bonding modes of phosphonic species on the zirconia's surface broaden the NMR resonance, but they also cause the resonance peaks to shift; hence, the information about species on the surface of ZrO₂ (physisorbed or metal phosphonate species) can be interpreted. In general, the upfield shift of the NMR peak will be the prevailing situation with respect to modification of nano-oxides with phosphonic acid[107]. Moreover, the magnitude of upfield shift will give the preliminary information related to the bonding modes of phosphonic species. In other words, the more shifted the resonance peak is, the higher bonding strength of the phosphonic ligands to the surface of zirconia is, and the more various the bonds are (monodentate, bidentate or tridentate).

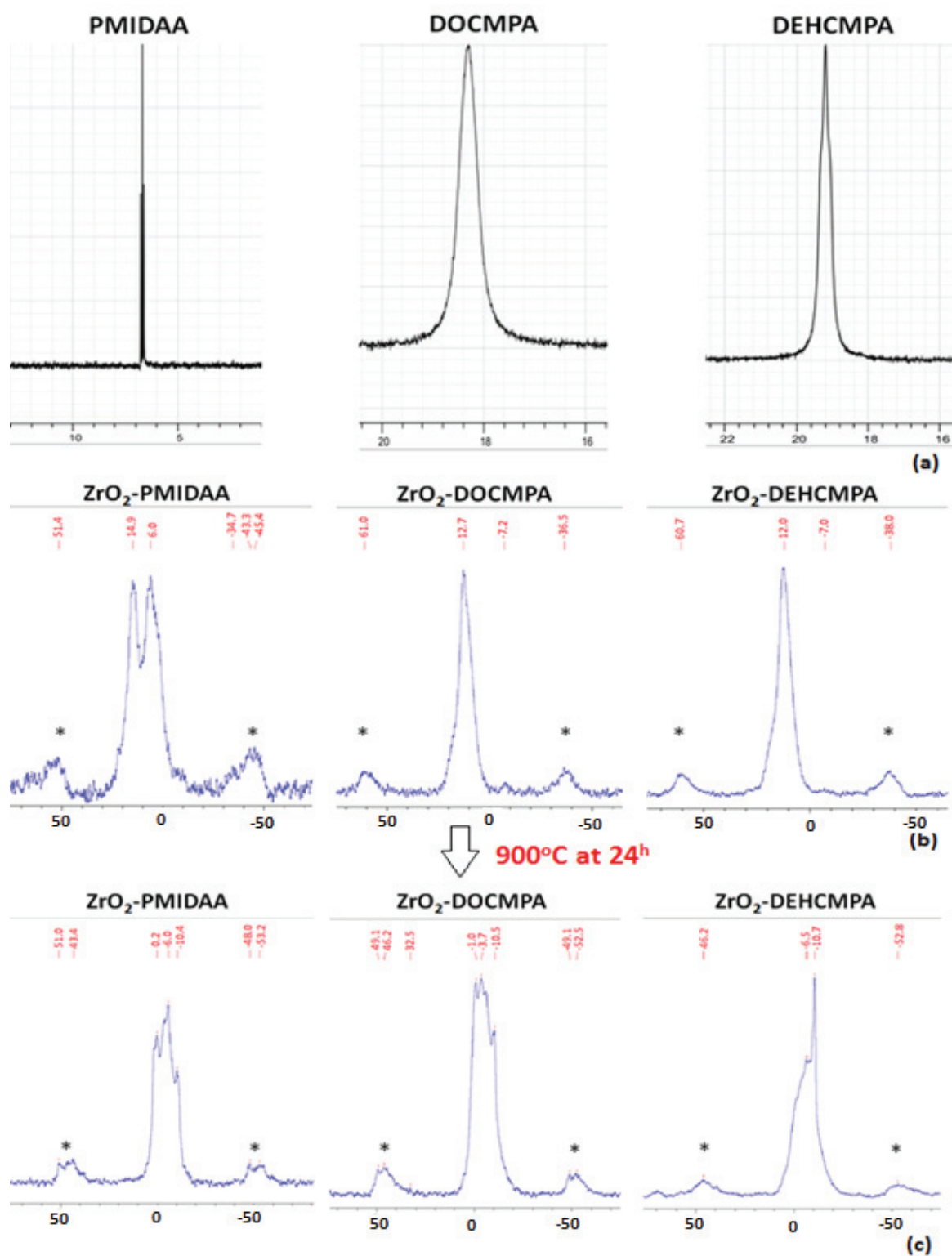


Figure 4-8 – (a) ^{31}P NMR spectra of phosphonic ligands, (b) ^{31}P MAS solid-state NMR spectra of zirconia nanoparticles modified with phosphonic ligands, and (c) ^{31}P MAS solid-state NMR spectra of zirconia nanoparticles modified with phosphonic ligands after heating process. (*) spinning side bands

As illustrated in the NMR spectra of modified zirconia and free phosphonic acid, the isotropic peaks of DEHCMPA and DOCMPA shift upfield by 6.3-6.5 ppm suggesting the monodentate bonding mode would be the predominant, while the negligible upfield shift of PMIDAA modified zirconia results from the weak interaction between PMIDAA and zirconia's surface. According to a study using DFT computations[108] about interaction between dye molecules and TiO₂'s surface through anchoring groups such as carboxylic and phosphonic, monodentate bonding mode is predominant adsorption approach on the surface of titania involving the coordination of P=O group and two hydrogen bonding of two remaining P-OH groups. Noticeably, the absence of sharp peaks arising from free ligands indicates that the excess of ligands is removed during washing step. The presence of metal phosphonate is also eliminated because the absence of sharp peaks regularly located at further upfield chemical shift (~7ppm[106]). The dissolution-precipitation process may be excluded due to the mild reaction condition (low concentration of phosphonic ligands, ambient temperature). Previously reported, the harsher and more aggressive reaction conditions, for instance, high concentration of phosphonic acid, high temperature and extending reaction time led to significant formation of metal phosphonate species[106, 109]. With respect to the discrepancies in mole ratios Zr/P between the results obtained from TGA and Elemental Analysis, the spectra of solid-state ³¹P NMR of phosphonic derivatives-modified zirconia (Figure 4-8 (c)) after heated at 900°C for 24h show a similar all chemical shifts upfield toward the same range of phosphates chemical shift range because phosphonic ligands on the surface of ZrO₂ are oxidized and transformed into phosphates after heating process.

4.2.3. Elemental analysis and thermogravimetric analysis method

TGA in air has been widely employed to detect the presence of ligand on the surface of nanoparticles after post-modification and determine the grafting densities of self-assembled monolayer (SAM). The grafting density could be calculated as follows:

$$GD(\text{molecule}/\text{nm}^2) = \frac{F_L \times N_A}{S \times M} \times 10^{18}$$

Where F_L is the fraction of ligand on the surface of zirconia (%wt.), N_A is Avogadro number, S is specific area of zirconia (m²/g), and M is the molecular of ligand (g/mol). In

the above equation, S is directly measured by BET method or indirectly determined which is based on the density ($d = 5.89 \text{ g/mL}$) and the particle radius of zirconia ($r, \text{ nm}$) (obtained by SEM imaging technique or estimated by XRD technique).

Assuming the shape of zirconia particle is spherical, the specific surface is approximated as follows:

$$S \left(\frac{\text{m}^2}{\text{g}} \right) = \frac{3}{d \times r} \times 10^3$$

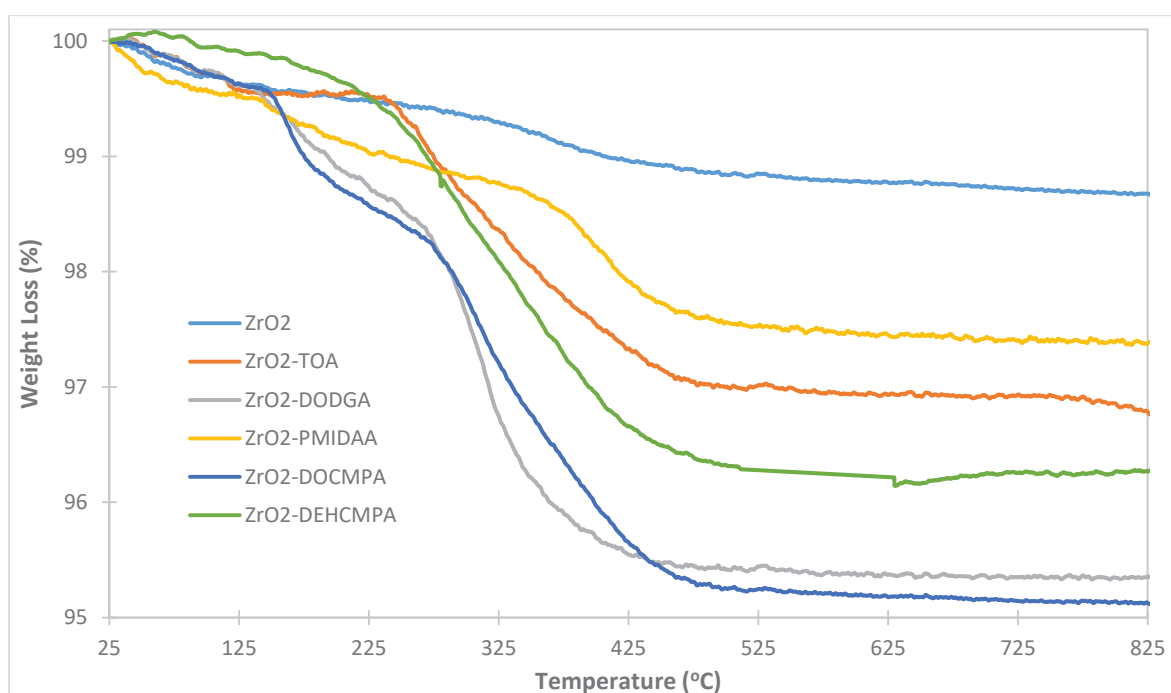


Figure 4-9 – TGA curves of surface-modified nano-zirconia

According to the Figure 4-9, all TGA curves show significant weight losses between 200°C and 800°C which represent the decomposition of ligands on the surface of zirconia. The estimated fraction and surface coverage (grafting density) are given in the Table 4-1.

Table 4-1. The fraction of ligand and calculated grafting density of modified zirconia

	FL (%) TGA	Grafting Density (L/nm ²)	FL (%) ICP-OES	Grafting Density (L/nm ²)
ZrO ₂ -TOA	2.67	1.14	-	-
ZrO ₂ -DODGA	3.56	0.88	-	-
ZrO ₂ -PMIDAA	1.76	0.69	2.23	0.87
ZrO ₂ -DOCMPA	3.60	0.88	5.45	1.33
ZrO ₂ -DEHCMPA	3.40	0.83	-	-

The reliability of the amount of phosphonic ligands is confirmed by using ICP-OES method to determine the phosphorus content of the modified-zirconia. Of three types of phosphonic acid – modified zirconia, two are selected for P analysis, including ZrO₂-PMIDAA and ZrO₂-DOCMPA (because DOCMPA and DEHCMPA have similar molecular structures and properties). Table 4-1 indicates the discrepancies between the values obtained by two methods result from the formation of phosphate species during thermal processes in TGA method as proven by ³¹P solid-state NMR method. As such, the weight losses corresponding to the amount of phosphonic acid ligands reflect a lower value than those of ICP-OES.

In conclusion, the presence of ligands on the surface of zirconia and their bonding modes are elucidated by the combination of various characterization methods including FT-IR, TGA, ³¹P solid-state NMR and ICP-OES. The chemisorption of ligands is the main interaction driven by the condensation between C-OH/P-OH groups and the surface Zr-OH groups and the coordination between carbonyl C=O/ phosphoryl P=O and surface ZrO₂.

4.3. Synthesis of ZrO₂-TOA with different mole ratios of ZrO₂ to TOA

The mole ratio of ZrO₂ to TOA was studied to obtain the insights into the bonding process as well as to find out the best ligand ratio for the modification process. The higher the amount of TOA on the zirconia's surface is, the better the adsorption of ZrO₂-TOA is. All parameters were remained as the procedure in section 3.3.1, but the ZrO₂/TOA mole ratios were changed as follows: 100, 61, 50, 30.5, 15.7, and 5.

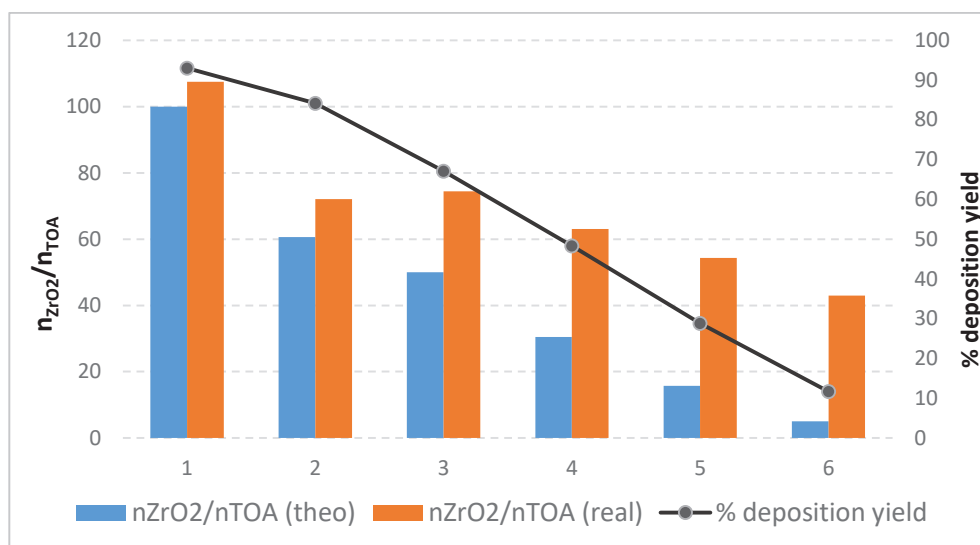


Figure 4-10 – The effect of mole ratio of ZrO₂/TOA to the deposition process

Figure 4-10 depicts three sets of data, namely theoretical mole ratio of ZrO₂/TOA, real mole ratio and TOA deposition yield. Apparently, the deposition yield illustrates the downward tendency while the ZrO₂/TOA mole ratio decreases, or higher amount of TOA is used during modification. Furthermore, the fairly decrease in the deposition yield from 93% to 84.2% was observed corresponding to the diminution in the mole ratio of ZrO₂/TOA from 100 to 61. The constantly downward trend in mole ratio of ZrO₂/TOA leads to the drastical and continuous drop in the deposition performance from 67.2 to 11.7%. Regarding the bar graphs, the theoretical and real mole ratios nearly match each other at the mole ratio of 100, meanwhile the deposition yield reaches quantitatively (~100%) at this ratio. Accompanying the falling-off of deposition yield, the discrepancies between theoretical and real ZrO₂/TOA mole ratio become more and more obvious. Particularly, the real ZrO₂/TOA mole ratio tends to steadily fluctuate when theoretical ZrO₂/TOA mole ratio is changed from 61 to 30.5.

Assuming the covalent grafting between carboxylic groups of TOA and the zirconia's surface, all active sites on the zirconia's surface are accessible for interaction at the high ZrO₂/TOA mole ratio (100, 61). However, the more the quantity of TOA during modification is, the less available the active sites on the zirconia's surface are. It is most

likely that the ZrO₂/TOA mole ratios ranging from 50 to 60 (~2.2 μmol TOA/1m²/1g ZrO₂-TOA; S_{BET}(TOA) = 50.7 m²/g) lead to the complete coverage of TOA on the zirconia's surface. On the other hand, the slightly extensive increase in the amount of TOA might results from Van Der Waals interaction between the formerly adsorbed TOA molecules on the surface and latter TOA molecules.

4.4. Investigation of gold and palladium adsorption capability

Batch adsorption experiments were conducted by mixing 50 mg of a hybrid nanopowder in a 100-mL glass bottle containing 20 mL of an aqueous solution of 10 ppm Pd or Au in 0.5 M HCl medium. The mixture was stirred by magnetic stirrer for 24^h at 25°C. The separation was carried out by centrifugation, then supernatant solution was carefully transferred to a 10-mL vial. The remaining concentration of Pd or Au was analyzed using ICP-OES. The percentage metal adsorption was calculated as follows:

$$E(\%) = \frac{C_o - C}{C_o} \times 100$$

Where C_o (ppm) and C (ppm) are the metal concentration in solutions before and after adsorption, respectively.

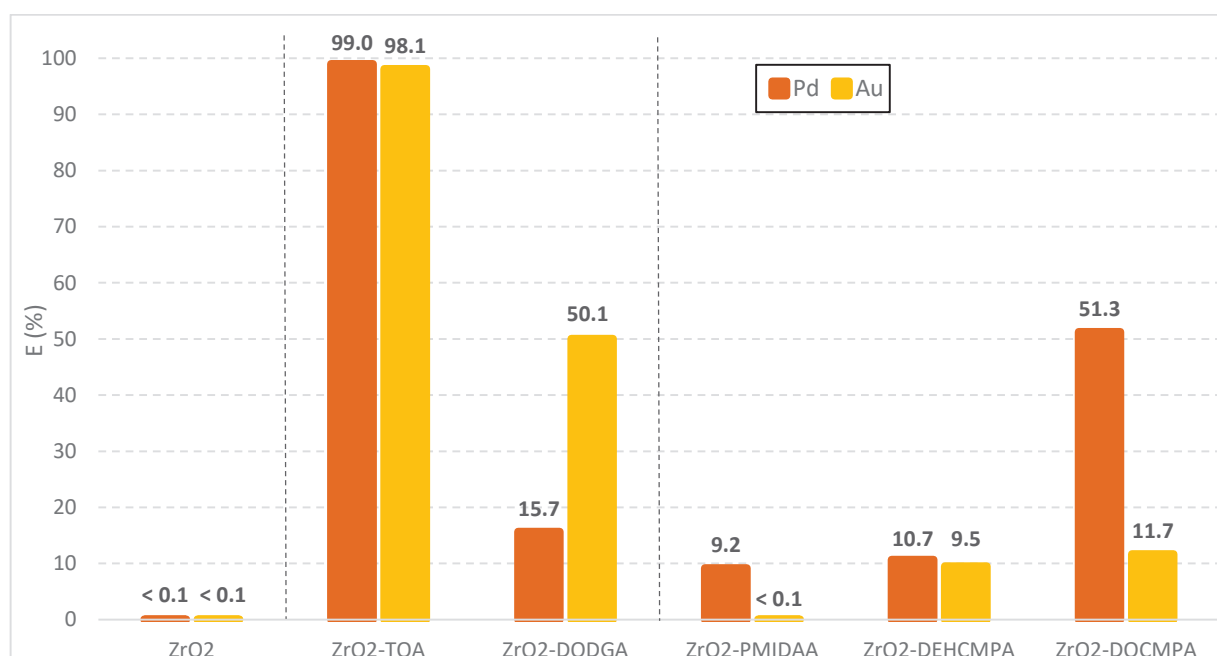


Figure 4-11 – Extraction percentage (%) of ligand-functionalized zirconia nanoparticles based on single solution. [Pd] = 10 ppm, [Au] = 10 ppm, V = 20 mL, m_{material} = 50 mg, time = 24^h, T^o = 25°C

Figure 4-11 provides information about Au and Pd adsorption performance (adsorption capability, selectivity) of all hybrid nano-ZrO₂ as well as demonstrates the dependence of the selectivity on the type of ligands bonded to ZrO₂'s surface.

Firstly, all modified zirconia nanoparticles indicate higher adsorption performance than bare zirconia. None of Au and Pd cations are extracted by bare zirconia, while modified zirconia nanoparticles show a significant increase of Au or Pd adsorption, especially zirconia nanoparticles modified with thioctic acid having Au and Pd adsorption percentages of nearly 100%. With regard to Pd adsorption, the adsorption percentage of all modified zirconia ranges from 9.2% (ZrO₂-PMIDAA) to about 100% (ZrO₂-TOA). Meanwhile, 4 out of 5 modified zirconia, namely ZrO₂-TOA, ZrO₂-DODGA, ZrO₂-DOCMPA and ZrO₂-DEHCOMPA are able to adsorb Au.

Secondly, adsorption selectivity based on single solution between Au and Pd of all modified zirconia nanoparticles can be assessed and compared from the graph. Three hybrid nanoparticles clearly seem to be able to capture Pd and Au selectively, including ZrO₂-DODGA, ZrO₂-PMIDAA, and ZrO₂-DOCMPA. Interestingly, ZrO₂-DODGA favors Au adsorption rather than Pd extraction, yet ZrO₂-PMIDAA is not likely to adsorb Au. In the case of ZrO₂-TOA, it's necessary to carry out further experiments to gain more precise information on its selectivity because all adsorption sites of ZrO₂-TOA are available to quantitatively extract Au and Pd at the selected concentration in this experiment.

Generally, solid-liquid extraction includes two key processes: the diffusion of target species into the solid phase and the reaction between functional groups of the solid phase and aimed adsorbates. Accordingly, the capacity and selectivity of adsorbent can be tailored and modified to fulfill various demands. In the series of ligands in this work, nano-ZrO₂ modified with thioctic acid (ZrO₂-TOA) is expected to effectively adsorb Au and Pd thanks to sulfur atoms in the molecular structure. According to HSAB (hard-soft acid-base), entities (molecules or adsorbent) containing sulfur donor atoms strongly interact with soft acids such as gold and palladium.

On the other hand, one of effects which is cannot be ruled out is the impact of mass transfer or diffusion of metals to/into the solid phase. Due to ligand's property, the surface of modified zirconia will be more hydrophobic compared to the bare zirconia after modification, hence, the modified zirconia will hinder the accessibility of gold and palladium. Among the ligands selected to modify zirconia nanoparticles, DODGA, DOCMPA and DEHCMPA make the zirconia nanoparticles' surface become hydrophobic. Consequently, modified zirconia nanoparticles are hardly dispersed in the aqueous medium by stirring, resulting in the inefficient Au and Pd adsorption. The phase transfer experiment is carried out to demonstrate the impact of modification of zirconia's surface on the hydrophobicity/hydrophilicity of the nanoparticles. Briefly, the dry modified-zirconia nanoparticles are simply dispersed in water, the defined amount of CH_2Cl_2 solvent is added to the nanosuspension and then mixture is mixed and held still for 24^h. As shown in the Figure 4-12, two out three types of zirconia modified with phosphonic ligands and zirconia modified with DODGA are completely transferred from the upper aqueous phase to the lower organic phase, whereas ZrO_2 -PMIDAA nanoparticles still remains in the aqueous phase. On the other hand, the phase transfer of ZrO_2 -TOA is partial.

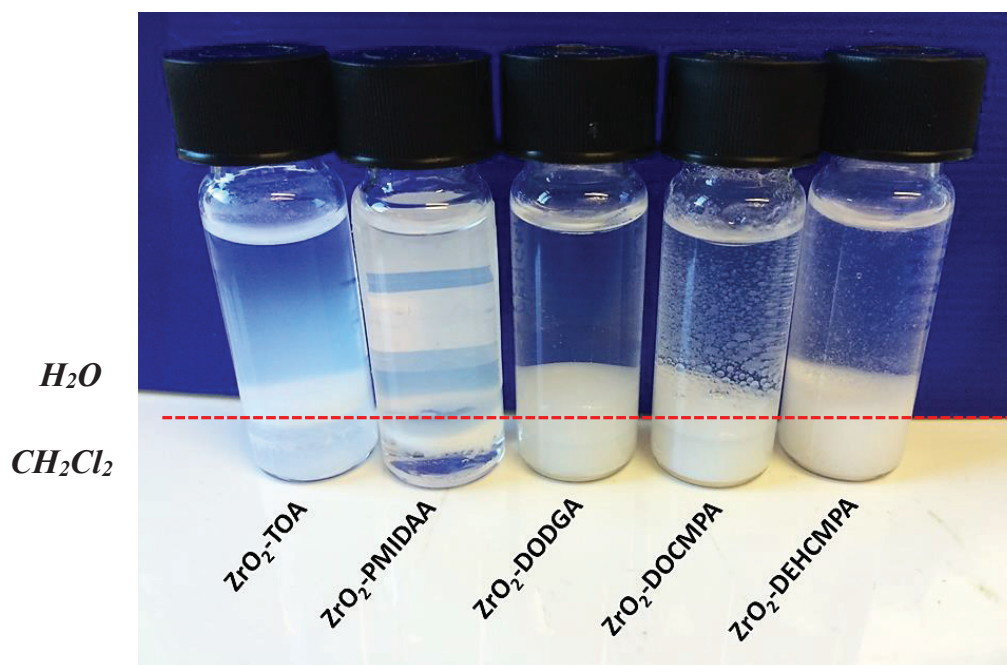


Figure 4-12 – A photograph of the location of modified-zirconia particles in the immiscible mixture of water and CH_2Cl_2

4.5. Investigation of adsorption capability of ZrO₂-TOA

Preliminary tests on adsorption capability of hybrid zirconia nanoparticles in the above section 4.4 have demonstrated that zirconia modified with thioctic acid (ZrO₂-TOA) emerges as a potential adsorbent for Au and Pd adsorptions. With the aim to extensively understand adsorption characteristics and application capability of ZrO₂-TOA, the following aspects were studied including:

- Adsorption characteristics of ZrO₂-TOA: adsorption capacity, the contact time, the impact of HCl and Cl⁻ concentrations, the study of adsorption mechanism through experimental methods and calculation.
- Investigation of stripping/desorption of Au and Pd out of ZrO₂-TOA.
- Application and reusability of ZrO₂-TOA.

4.5.1. Adsorption isotherm and capacity of ZrO₂-TOA

In adsorption studies, determining the adsorption capacity or loading capacity is crucial step to describe the characteristic of adsorbent. Basically, the adsorption capacity is defined as the maximum amount of adsorbate captured by 1g of adsorbent at equilibrium state. Besides, adsorption capacity is considered as an important parameter in order to assess and compare the adsorption performance among the adsorbents toward the certain target adsorbates. In this experiment, the adsorption capacity of ZrO₂-TOA was investigated by stirring 20 mL of the single solution (contains only Pd or Au) with the increasing initial concentration in the range of 5 mg/L to 300 mg/L. The constant agitation was carried out by magnetic stirrer for 24^h at 25°C.

According to the Figure 4-13, Pd and Au data reflect a similar trend: (i) rapid increase in the range of low concentration (0 – 20 mg/L) which is a linear correlation between capacity and initial concentration and (ii) non-proportionally rising relationship at the higher initial concentrations which tends to level-off in the range of more than 100 mg/L. A plausible reason for this tendency stems from fact that at low concentrations all active sites on the zirconia's surface are sufficient for the adsorption process; however, at high concentrations the occupation of former Pd and Au ions limits the accessibility of the zirconia's surface and adsorption of more Pd and Au ions. The maximum experimental adsorption capacity was determined to be 6.3 and 43 mg/g for Pd and Au, respectively.

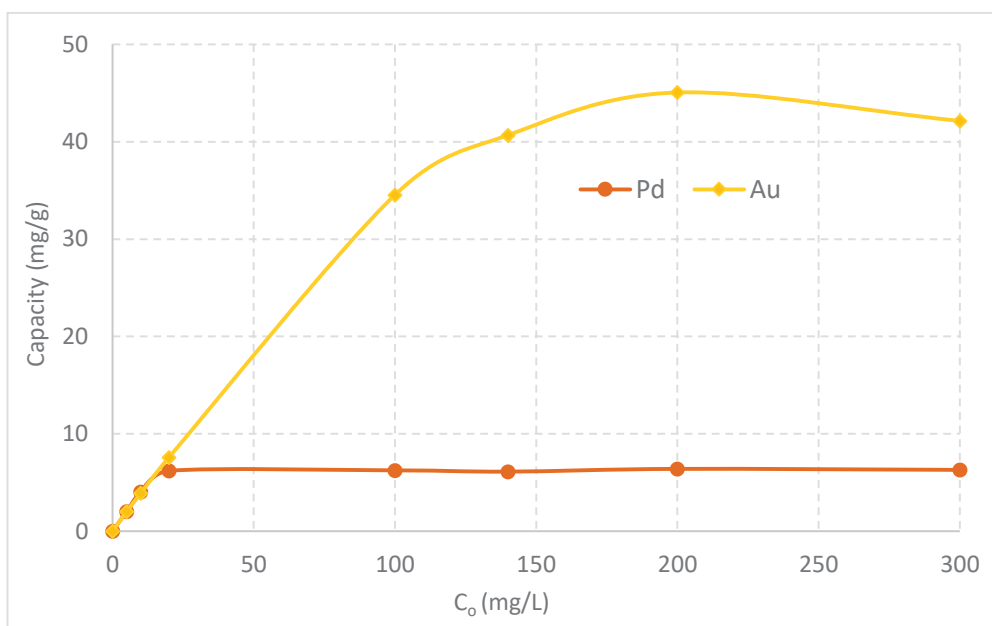


Figure 4-13 – Au and Pd capacities of ZrO_2 -TOA as a function of initial concentration

Interestingly, when taking into consideration the mole ratio of TOA-M (M = Au or Pd), we obtained the mole ratios of 1.83 for TOA/Pd and 0.5 for TOA/Au. That means it's very likely that 2 molecules of TOA were necessary to coordinate 1 Pd ion, while 1 molecule of TOA could form two coordinate covalent bonds to 2 Au ions. Therefore, noting that the major species of Pd(IV), and Au(III) in the acidic solution containing beyond 0.1M are chloro anionic species $PdCl_4^{2-}$, and $AuCl_4^-$ [41, 110], the reaction can be presented as follows:



In-depth investigation of adsorption behavior of Au and Pd ions and ZrO_2 -TOA's surface properties was conducted by applying adsorption data to Langmuir adsorption isotherm model. According to this model, the surface of adsorbent is assumed to be homogeneous in terms of adsorption energy and adsorbates would form monolayer on the adsorbent's surface. In other words, active sites on the surface of adsorbent are supposed to be finite and identical and the interaction between adsorbates is believed to be absent. The mathematical formula of this theory is expressed as follows:

$$q_e = q_{max} \left(\frac{bC_e}{1 + bC_e} \right)$$

Where b (L/mg) is the Langmuir equilibrium constant, q_{\max} (mg/g) is the maximum adsorption capacity, C_e (mg/L) is the equilibrium concentration, and q_e (mg/g) is the equilibrium capacity. In reality, the linear form of the Langmuir model is often used to determine b and q_{\max} :

$$\frac{C_e}{q_e} = \frac{1}{q_{\max}b} + \frac{C_e}{q_{\max}}$$

Or

$$\frac{1}{q_e} = \frac{1}{q_{\max}b} \frac{1}{C_e} + \frac{1}{q_{\max}}$$

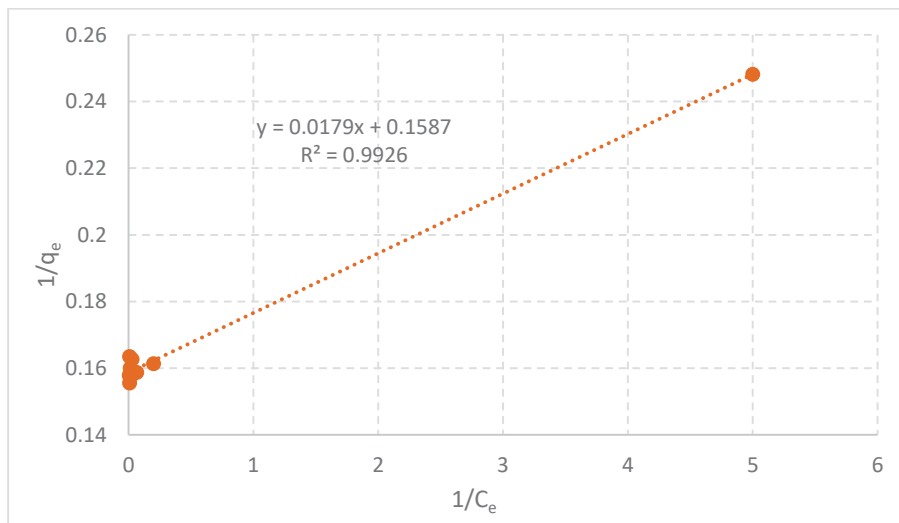


Figure 4-14 – Langmuir isotherm for Pd adsorption

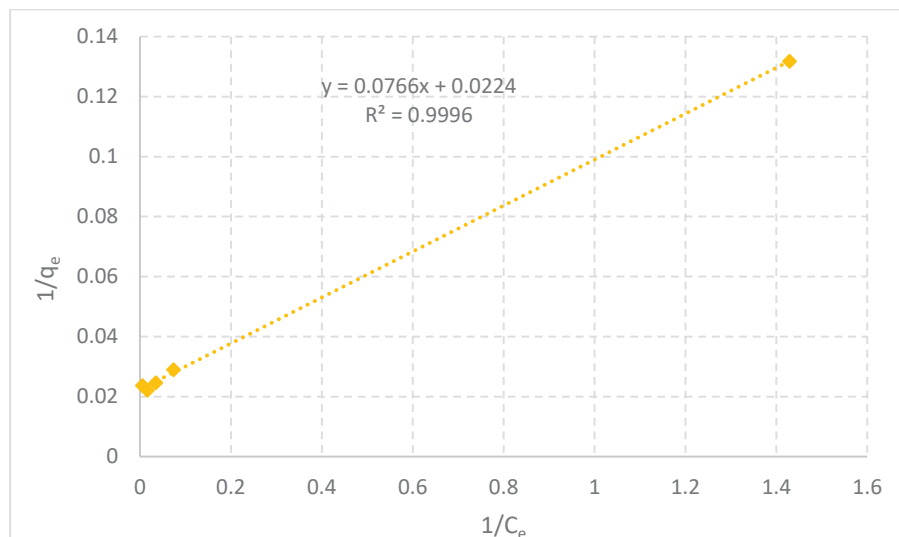


Figure 4-15 – Langmuir isotherm for Au adsorption

According to the adsorption data of Pd and Au, the linear plots were constructed and the conformity to the Langmuir model was assessed through correlation coefficients (R) which were found to be 0.993 for Pd (Figure 4-14) and 0.999 for Au (Figure 4-15), respectively. The maximum Pd and Au capacities calculated from the plots were 6.3 mg/g and 44.6 mg/g, respectively. A good agreement between the experimental and calculated capacities consolidates the suitability of the Langmuir model. Besides, in relation to some published studies which have the same objectives, the adsorption performance of ZrO₂-TOA is compared with that of other materials (Table 4-2) which shows comparable capabilities in Pd and Au adsorptions.

Table 4-2. The adsorption capacity of studied materials

Used adsorbents	Target metals	Capacity (mg/g)		References
		Au	Pd	
Phosphine sulphide-type chelating polymers	Au, Pd	78.8 (polymer 1) 78.8 (polymer 2)	11.7 (polymer 1) 7.4 (polymer 2)	[67]
Diaion WA21J	Pd	-	4.84	[111]
DTDGA-impregnated XAD-16 Beads*	Au	35	-	[30]
Amberlite XAD-16 Functionalized with 2-Acetyl Amide group	Pd	-	9	[112]
Thioctic acid functionalized silica coated magnetite nanoparticles	Au	38	-	[72]
This study	Au, Pd	44.6	6.3	-

4.5.2. Effect of contact time

To understand the adsorption/desorption process was to obtain insights into its thermodynamics and kinetics aspects and hence the overall process can be controlled. If building the adsorption isotherm thermodynamically unveils some information about the equilibrium state of the adsorption process, the study of adsorption kinetics provides some insights into the progress of adsorption process. In this experiment, the adsorption capacities of ZrO₂-TOA were examined from 15 to 480 mins.

The kinetics of adsorption process strongly depends on operating conditions, such as initial concentration, pH, temperature and stirring rate. Generally, the higher the initial concentration is, the longer the time required is to reach equilibrium. Pseudo-first-order and pseudo-second-order models have been commonly employed to shed the light on the adsorption process; among them, pseudo-second-order often better describes the

mechanism of the adsorption in which the adsorption process is mainly driven by chemical reaction. The prefix “pseudo” has been used to distinguish the rate expressions based on capacity values from those based on the concentration values [113]

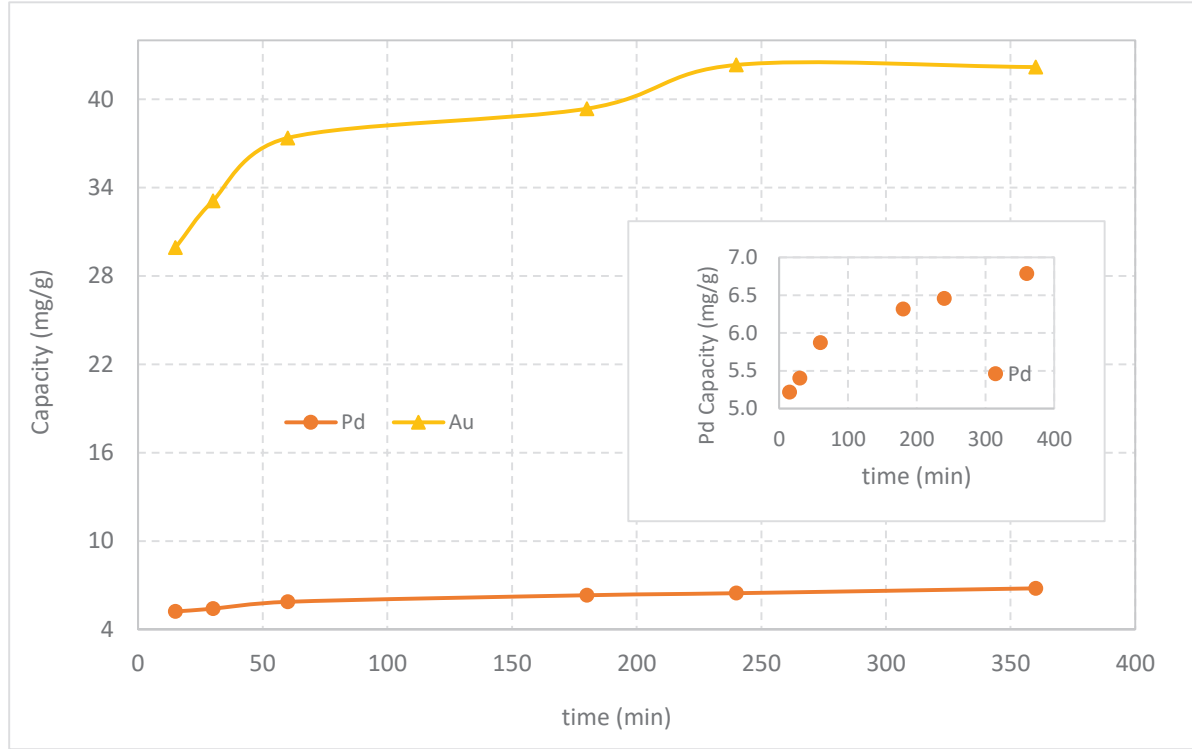


Figure 4-16 – The influence of contact time on the Pd and Au adsorption

According to Largegren, the pseudo-first-order model is described as a differential equation:

$$\frac{dq}{dt} = k_1(q_e - q_t)$$

where q_e and q_t are adsorption capacities (mg/g) at equilibrium and at any time t , respectively and k_1 is the rate constant of pseudo-first-order adsorption model (min^{-1}).

Normally, the equation is integrated and the boundary conditions are applied: $t_0 = 0, q_0 = 0$ and $t_t = t, q_t(\text{equilibrium}) = q_e$ so as to obtain the following equation:

$$\log(q_e - q_t) = \log q_e - \frac{k_1}{2.303} t$$

As a rule of thumb, the plot of $\log(q_e - q_t)$ against t is conducted and the fit of this model is validated by R^2 (coefficient of determination) value. The pseudo-second-order model is expressed by the following equation:

$$\frac{dq}{dt} = k_2(q_e - q_t)^2$$

where k_2 is the pseudo-second-order rate constant ($\text{g mg}^{-1} \text{min}^{-1}$). After integrating and applying the boundary conditions, the following equation is often used to describe the pseudo-second-order adsorption kinetics:

$$\frac{t}{q_t} = \frac{1}{k_2 q_e^2} + \frac{1}{q_e} t$$

Similar to pseudo-first-order model, t/q_t is plotted against t and R^2 value is the parameter to assess the suitability of the model.

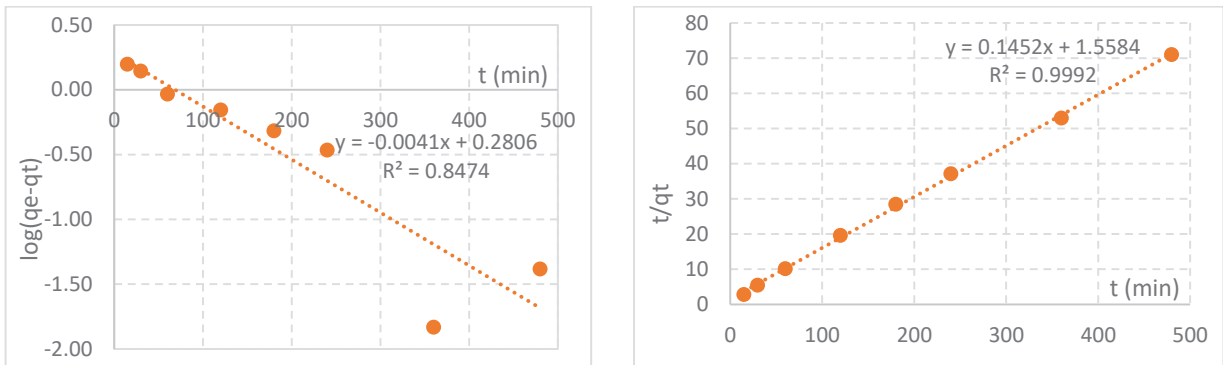


Figure 4-17 – Pseudo-first-order and pseudo-second-order models for Pd adsorption kinetics

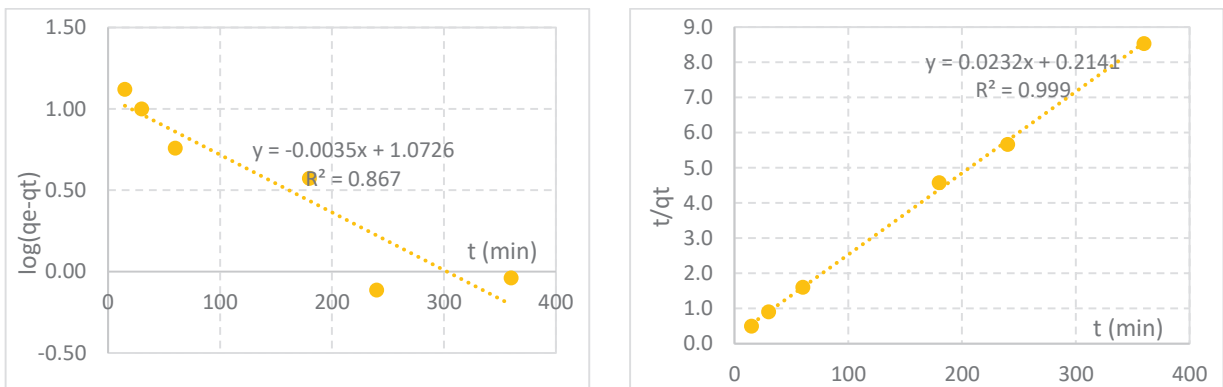


Figure 4-18 – Pseudo-first-order and pseudo-second-order models for Au adsorption kinetics

Presented in the Table 4-3 is the summary of some crucial parameters associated with pseudo-first-order and pseudo-second-order adsorption kinetics models for Pd and Au. Of two models, the pseudo-second-order adsorption kinetics model is the most fitted approach to describe the adsorption process as a function of time with the determination coefficient of larger than 0.999. In the solid-liquid adsorption process, three stages are supposedly involved: (i) external mass diffusion, (ii) intraparticle (pore) diffusion and (iii) interaction

step [114]. During the adsorption process, agitation has been employed to accelerate the external mass transfer, so intraparticle diffusion and chemical reaction become the rate-controlling steps. When it comes to the chemical interaction between ZrO₂-TOA and [PdCl₄]²⁻ or [AuCl₄]⁻, the HSAB Pearson's theory that is predicated on the favorable coordination between target metals and sulfur sites on ZrO₂'s surface is a plausible rationale for the fit of pseudo-second model. Essentially, the principle of pseudo-first and pseudo-second models are based on a general differential equation [115], but the magnitude of concentration relative to the capturing sites on the adsorbent decides which model best describes the adsorption process. In other words, the adsorption process follows the pseudo-second model at the low range of initial concentration (ppm-ppb) and follows the pseudo-first model at the high range of initial concentration.

Table 4-3. Summary of kinetic parameters of Pd and Au adsorption on ZrO₂-TOA

Model	Pd	Au
Pseudo-first-order		
k ₁ (min ⁻¹)	0.00178	0.00152
q _e (mg g ⁻¹)	1.9	12.8
R ²	0.8474	0.8670
Pseudo-second-order		
k ₂ (g mg ⁻¹ min ⁻¹)	0.0218	0.000538
q _e (mg g ⁻¹)	6.9	43.1
R ²	0.9992	0.9990

Observing the curves in Figure 4-16, we will maintain the minimum contact time of 180 mins for the following experiments.

4.5.3. Effect of HCl and chloride to the adsorption

Effluents from the recycling factories and refineries often contain various acids (HNO₃, HCl) in high concentration due to mandatory utilization of acids for dissolving and separating stages. One of the main components is hydrochloric acid (HCl), so the effect of HCl to the adsorption was carried out. The impact of chloride concentration was conducted as well with the aim to understand the driving force governing the chelating process. In this experiment, extraction percentage of a single solution Pd/Au 10 ppm was monitored when the concentration of HCl was varied from 0.08-6 M. All remaining parameters for the

adsorption were similar to those of previous experiments, including 50 mg of ZrO₂-TOA, and 180 mins of stirring.

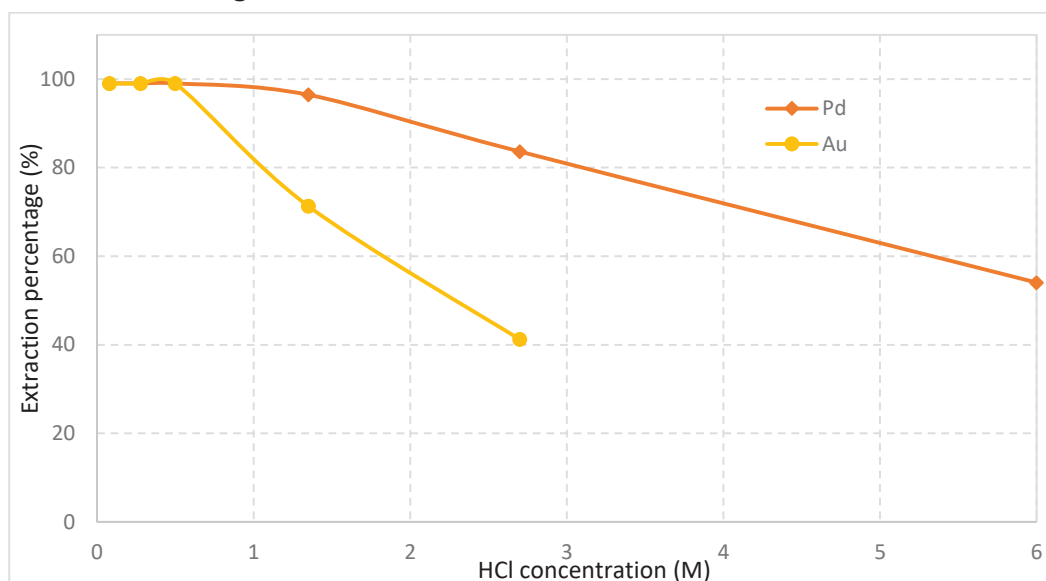


Figure 4-19 – Impact of HCl concentration on the Au and Pd extraction

The data in Figure 4-19 illustrate a declining tendency in the extraction percentage for Au and Pd adsorption when HCl concentration exceeds 1M. At low HCl concentration (< 1M), quantitative adsorption was obtained, while at higher concentration the extraction percentage constantly decreased. The extraction percentage of Pd dropped to 83 % while HCl concentration reached 2.7M and the further decrease in HCl concentration to 6M led to a fall in extraction percentage to 54 %. In the meantime, gold adsorption experiences a decrease at higher extent, especially, the extraction percentage dropped to 41 % when HCl concentration got to 2.7M. Therefore, the concentration of acid in the real e-wastewater should be paid close attention, dilution and pH adjustment particularly may be employed.

A plausible explanation for this phenomenon is that the adsorption is likely to be inhibited due to (i) the shifting of the equilibrium to the left due to the elevated concentration of Cl⁻ which favors the tetrachloro complexes of Au and Pd (according to the reactions **1** and **2**) or (ii) the protonation of sulfur sites when concentration of H⁺ ion is higher than 1M which hinders the complexation of Au and Pd species in the solution to TOA on the ZrO₂'s surface[67] (Figure 4-20). Therefore, the effect of Cl⁻ was individually investigated by designing adsorption experiments in which solutions of Pd 10 mg/L were prepared in the matrices with constant H⁺ concentration at 0.5M and varied Cl⁻ concentration from 0.6 – 4M.

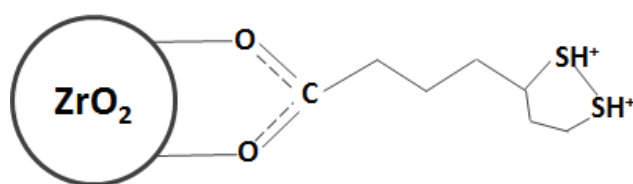


Figure 4-20 – Schematic representation of the protonation process of sulfur atoms in functional groups

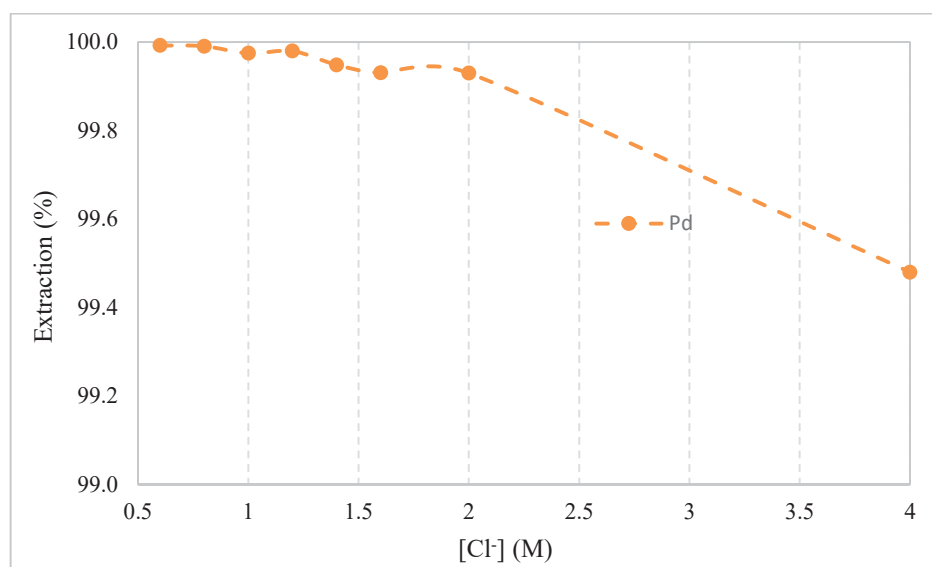


Figure 4-21 – Effect of Cl⁻ concentration to the Pd adsorption

Figure 4-21 shows the poor effect of chloride content on the adsorption process, namely that the extraction percentage is over 99% in the investigated Cl⁻ concentration range of 0.6 – 4M. In other words, the protonation of sulfur sites could be of crucial influence, yet the hydrolysis of Zr-O-C bonds by H⁺ can not be ruled out which leads to the cleavage between thioctic acid and hydroxyl sites on the zirconia's surface (Figure 4-22).

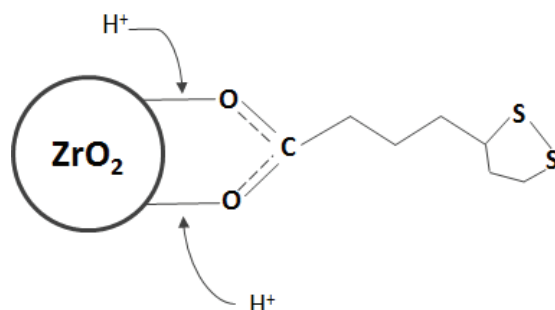


Figure 4-22 – Schematic representation of the cleavage of the bond between thioctic acids and ZrO₂'s surface

4.5.4. Stripping investigation

The rudiments of recycling practices are separating, purifying and recovering the target adsorbates. Stripping or back-extraction process is particularly used to recover the target metals in the recycling processes using liquid-liquid or solid-liquid extraction techniques.

In our experiment, Au and Pd adsorbed onto ZrO_2 -TOA were back-extracted based on different combinations between thiourea and hydrochloric acid. Additionally, sodium nitrite was used as a stripping agent with the aim to selectively back extract Pd.

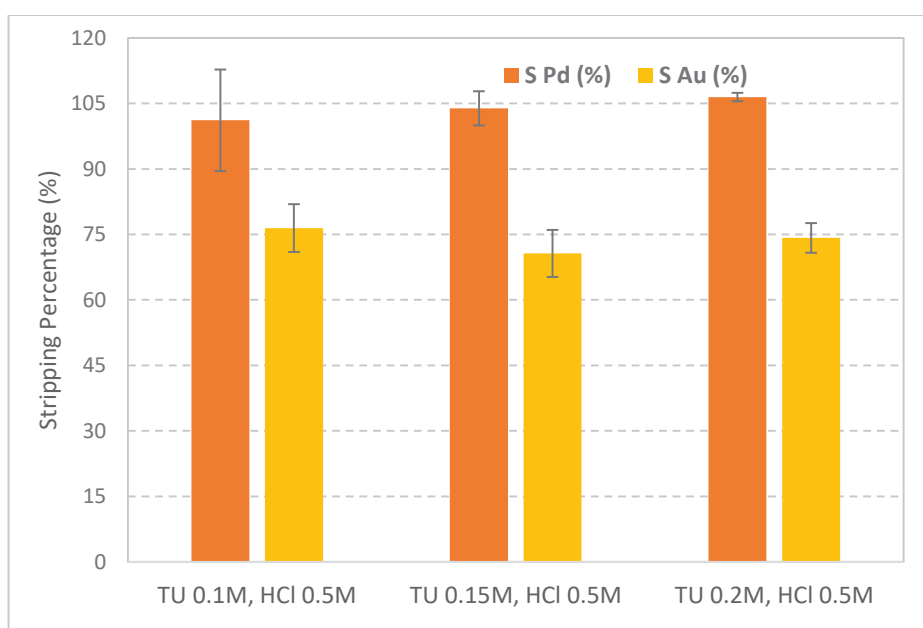


Figure 4-23 – The back-extraction (stripping) percentage of Pd and Au using different mixtures of thiourea and hydrochloric. The anterior adsorption was carried out using the dual solution of Au and Pd with the concentration of 10 mg/L/each.

Figure 4-23 shows the stripping percentage of Pd and Au obtained by using different mixtures of thiourea (TU) and hydrochloric acid (HCl), including (i) TU 0.1M, HCl 0.5M, (ii) TU 0.15M, HCl 0.5M, and (iii) TU 0.2M, HCl 0.5M. As can be seen in Figure 4-23, it is clear that all mixtures of TU and HCl well-suit the Pd stripping process in which nearly 100% of Pd is recovered, whereas the back-extraction of gold is less quantitative with the highest stripping percentage of about 75% using TU and HCl. When it comes to repeatability, using TU 0.2M and HCl 0.5M indicates the highest rate of repeatability compared to mixtures of TU 0.15M and HCl 0.5M and TU 0.1M and HCl 0.5M. In other words, the mixture of TU 0.2M and HCl 0.5M is the best compromise to ensure the stability of the stripping process.

In addition, a back-extraction experiment using sodium nitrite at pH 5 was conducted for selectively recovering Pd without co-extracting Au. The results shown in Figure 4-24 proved that sodium nitrite at pH 5 was not an efficient for Pd back-extraction.

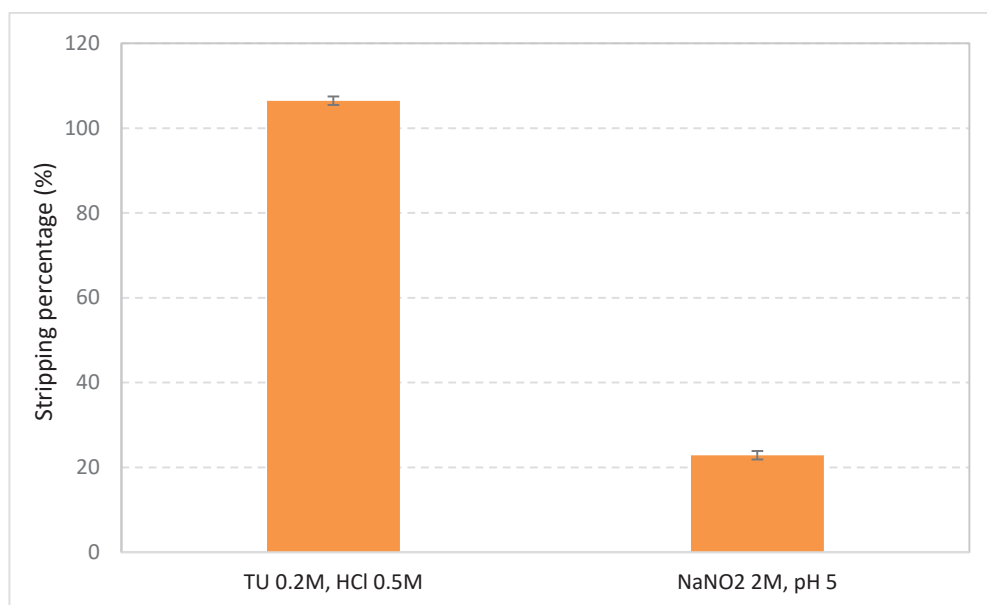


Figure 4-24 – Comparison of back-extraction performance between TU + HCl and NaNO₂.

4.5.5. Reusability of the ZrO₂-TOA

In respect of cost-effectiveness, an adsorbent used in recycling applications should be a consequence of ease of synthesis as well as a material with reusability. Therefore, the regeneration and reusability of hybrid nano-powder of ZrO₂-TOA were tested by repeatedly adsorbing/desorbing Pd up to four times in “model” medium of standard solution (20 mL of Pd 10 mg/L) and real effluent (20 mL, after five-fold diluting pH adjusting to pH 1) from the MORPHOSIS company.

From the earlier experiments, all parameters related to adsorption include $m_{\text{ZrO}_2\text{-TOA}} = 50$ mg, contact time = 180 mins. Regarding desorption process, the mixture of thiourea 0.2M and HCl 0.5 M was stirred with Pd-adsorbed powder of ZrO₂-TOA in 180 mins. The ZrO₂-TOA powder was washed with water and reused for consecutive adsorptions.

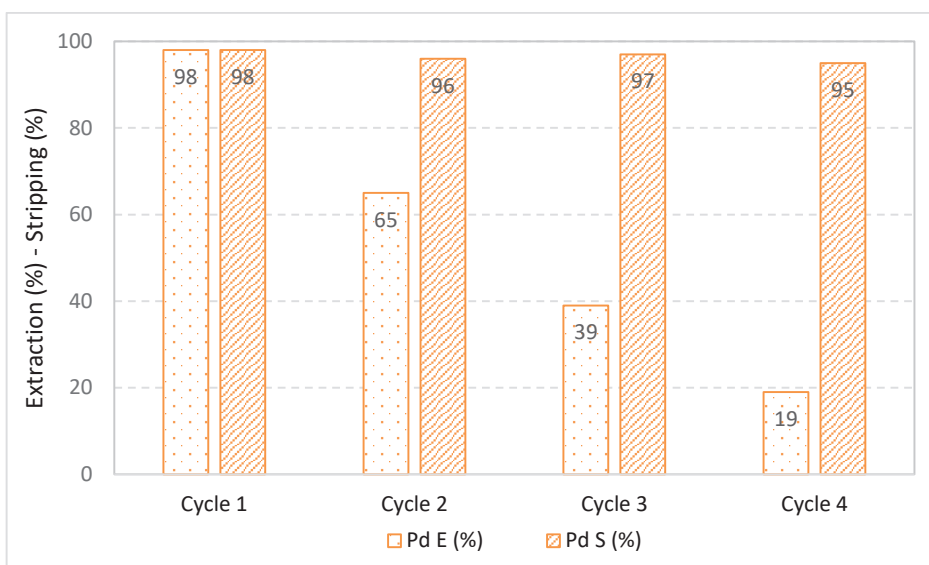


Figure 4-25 – Extraction and stripping percentage through adsorption/desorption cycles

As illustrated in the Figure 4-25, the adsorption capability of ZrO_2 -TOA decreased after each adsorption/desorption cycle although adsorption was carried out in the “model” matrix. In the second adsorption experiment, ZrO_2 -TOA was just able to capture 65% of Pd, to the greater extent, the adsorption capability of ZrO_2 -TOA fell to 19% of Pd. In contrast, a quantitative desorption percentage using TU 0.2 and HCl 0.5M was obtained for four successive adsorption/desorption cycles.

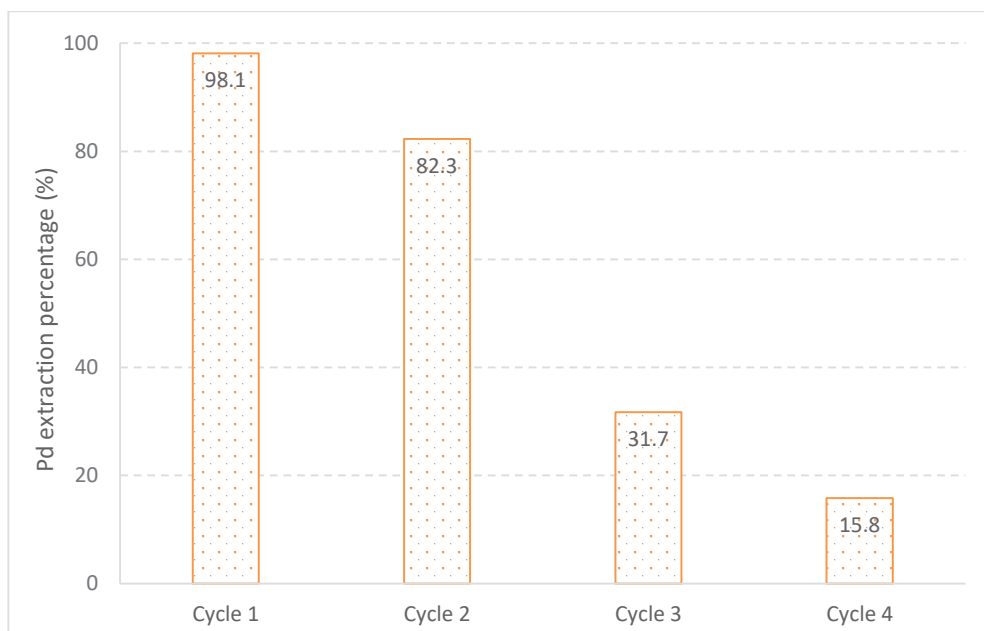


Figure 4-26 – Extraction performance of ZrO_2 -TOA through adsorption/desorption cycles in the real effluent

Similarly, a declining tendency was recorded for four successive adsorption/desorption cycles in the real effluent. These observations lead to possible explanation about the loss of thioctic acid on the surface after each cycles as described in the Figure 4-27 which consolidates the results obtained in the investigation of the HCl effect.

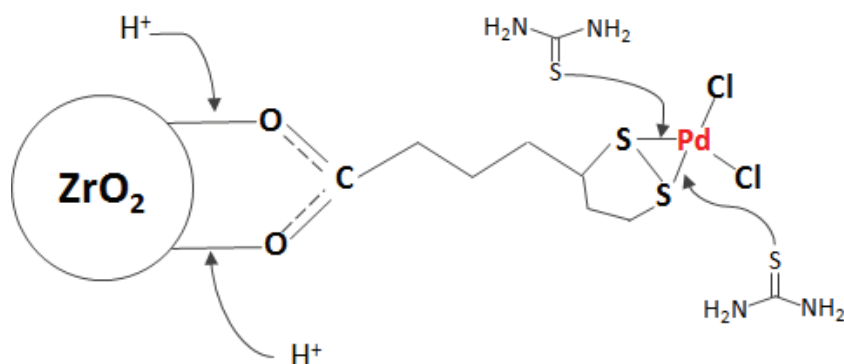


Figure 4-27 – Schematic explanation about the loss of TOA on the zirconia's surface after desorption

In an attempt to reinforce the above assumption, nano-ZrO₂ material modified with DOCMPA was used as the adsorbent in the reusability test. DOCMPA is a ligand bearing phosphonic groups (-PO(OH)₂) as the grafting groups to the ZrO₂'s surface that has been believed that the resultant modified nano-ZrO₂ materials have higher tolerance and resistance toward hydrolysis. As seen in Figure 4-28, the resuability of ZrO₂-DOCMPA was far better than that of ZrO₂-TOA. The data demonstrated that despite the low adsorption capability toward Au and Pd, the steady trend of adsorption percentages of ZrO₂-DOCMPA strengthens the assumption about stability of Zr-O-P bond compared to Zr-O-C. Consequently, it is suggested that TOA moiety be grafted to ZrO₂'s surface via “linker” phosphonic groups anchoring to bare ZrO₂'s surface.

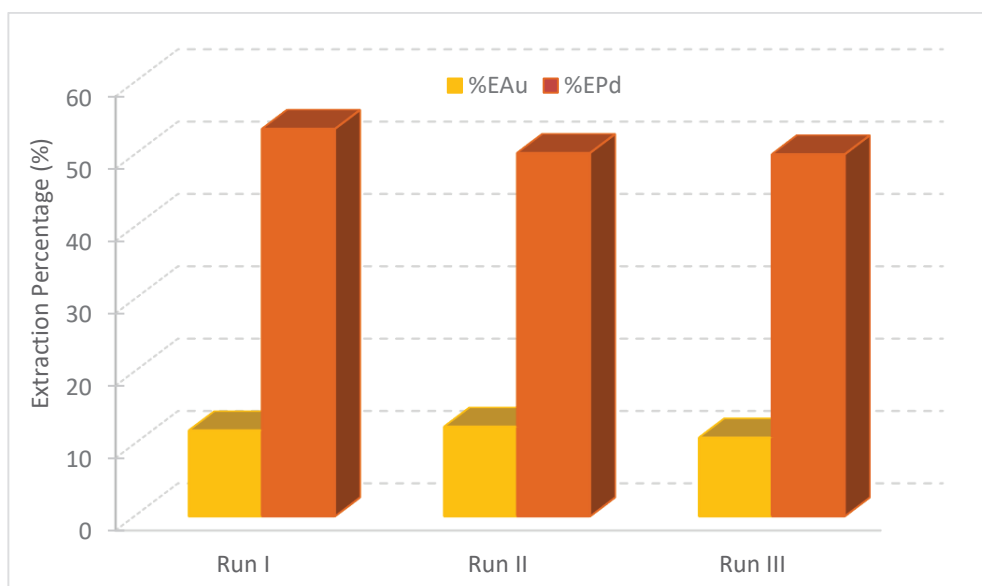


Figure 4-28 – Reusability test of ZrO_2 -DOCPA

Interestingly, when it comes to selectivity of ZrO_2 -TOA toward Pd in the real effluent, Pd was quantitatively extracted despite its trace concentration in the real effluent (1.58 mg/L). On the contrary, Cu, Ni, and Fe were badly-extracted by ZrO_2 -TOA with the extraction percentage of 0.01-0.07 % notwithstanding the major presence of these metals in the initial effluent, namely 1320 mg Cu/L, 3940 mg Ni/L, and 1460 mg Fe/L, respectively.

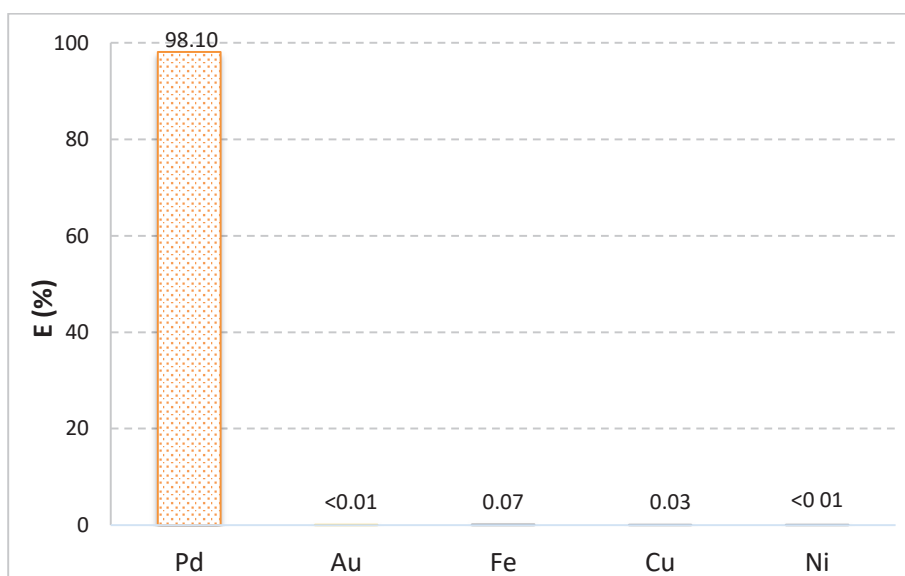


Figure 4-29 – The extraction percentage of metals present in the real effluent (left), and a photo of e-wastewater provided from MORPHOSIS (right)

Summary about the adsorption capability of ZrO₂-TOA toward Pd and Au

The results from in-depth experiments on the adsorption and desorption processes of thioctic surface-modified nano-zirconia (ZrO₂-TOA) have demonstrated that this hybrid nanomaterial showed higher selectivity toward Au (43 mg/g) compared to Pd (6 mg/g) following the Langmuir adsorption isotherm. The adsorption process has turned out to be driven by coordinative interaction between sulfur sites and target metals and following the pseudo-second-order adsorption kinetics; however, in high concentration of HCl (>1M), the adsorption was limited probably owing to the effect of H⁺ on the bonding strength of carboxylic group to ZrO₂'s surface. The effect of Cl⁻ is eliminated because of the quantitative adsorption toward Pd in the wide range of Cl⁻ from 0.6 – 4 M. With respect to desorption process, a mixture of thiourea 0.2 M and HCl 0.5 M has ensured an efficient and reproducible desorption. Importantly, ZrO₂-TOA nanomaterial has shown its limitations in terms of reusability and regeneration because the bonds between TOA and ZrO₂'s surface were cleaved through hydrolysis by acidic components of sample's matrix.

The main drawback of ZrO₂-TOA in reusability of Pd and Au adsorption process has motivated the study to search for an alternative for surface modification through carboxylic grafting group. Either a ligand bearing phosphonic group and disulfide capturing group or a surface modification process that improves the bonding strength of ligand on ZrO₂'s surface would be the vital strategy in order to endow the resultant material with reusability.

4.6. Two-step surface modification of ZrO₂

Surface modified nano-zirconia materials, particularly phosphonate-modified zirconia has not been used as an adsorbent in capturing Pd and Au in the electronic wastewater. In this part, we will discuss some insights into the effect of grafting groups on the bonding mode and stability of resultant materials. In other words, ZrO₂ nanoparticles will be modified via a two-step functionalization process comprising (i) surface modification with alendronic acid (AA) and (ii) covalent grafting of AA with TOA moiety through amide coupling reaction (Figure 4-30). The amide coupling reaction was conducted using either TOA activated by N,N-dicyclohexylcarbodiimide (DCC) (pathway 1) or N-hydroxysuccinimide activated ester of TOA (pathway 2).

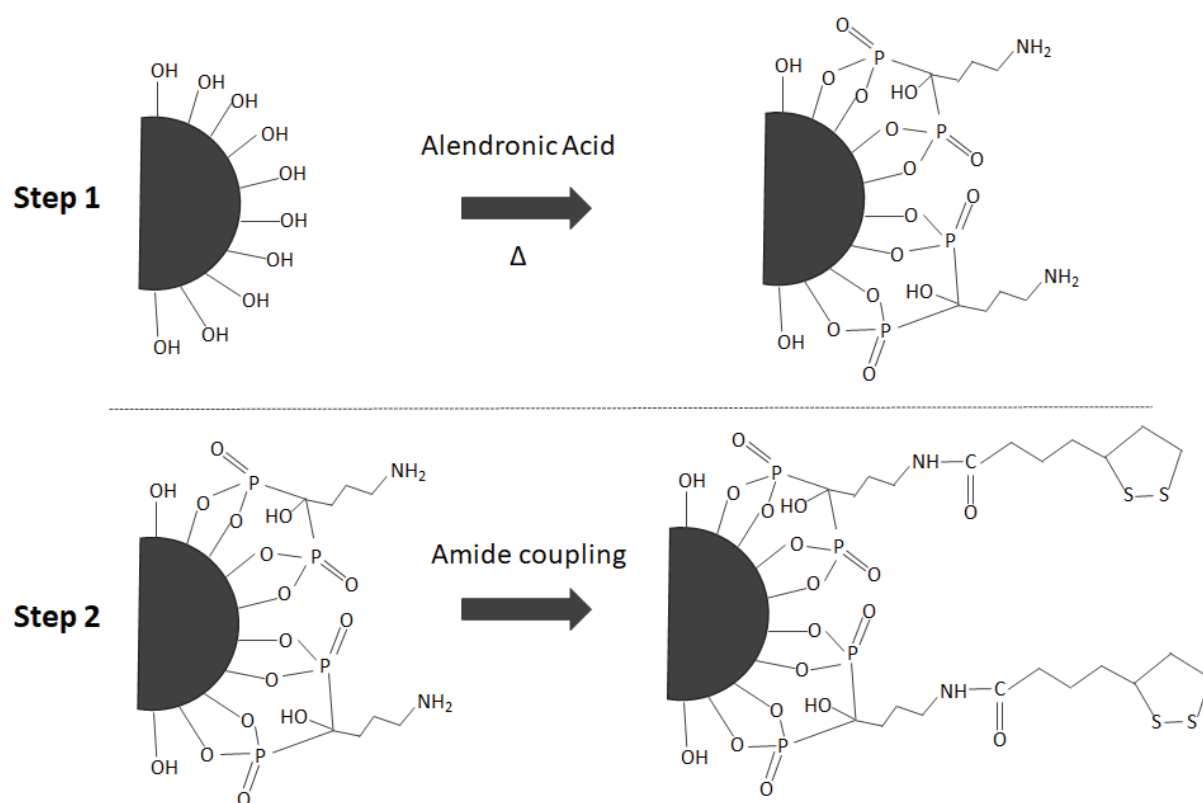


Figure 4-30 – Schematic representation of two-step surface modification of ZrO_2

Pathway 1 : Carbodiimide (TOA/DCC): In this pathway, a mixture of TOA and DCC was prepared with the aim to remove the precipitate of N,N-dicyclohexylurea (DCU) that was the by-product of the reaction between TOA and DCC. The solution that contained O-acylisourea and symmetric anhydrides of TOA was immediately allowed to react with ZrO_2 -AA. The mechanism of this pathway can be described as follows:

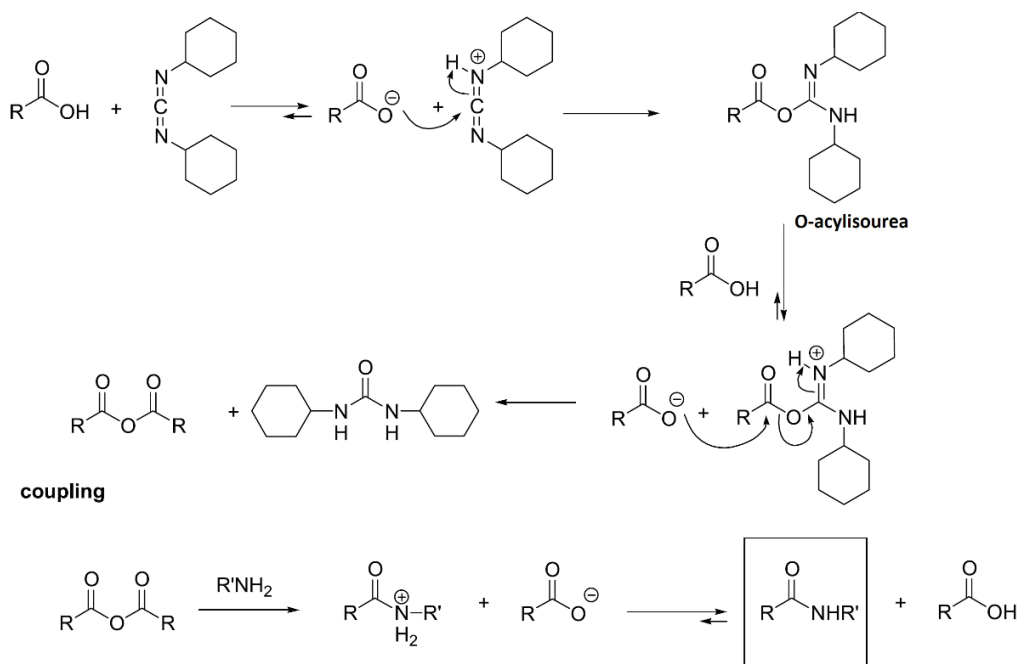


Figure 4-31 – The mechanism of amide coupling reaction mediated by DCC [116]

Pathway 2 : Activated ester (NHS-TOA): One of the drawbacks of the previous carbodiimide pathway was the intermediate derivative N-acylurea, a by-product of the rearrangement of O-acylisourea. In comparison with O-acylisourea, this compound was inert and created in the expense of carboxylic reactant. In order to alleviate this problem, carboxylic could be activated by reacting with substituted phenols or derivatives of hydroxylamine (OHXt) in the presence of carbodiimide compounds. Generally, Xt is chosen with the electron-withdrawing property that causes the acyl moiety to be effectively attacked by nucleophiles (R-NH₂). In this study, N-succinimide active ester of TOA (NHS-TOA) was employed due to its solubility in water that facilitates the washing step.

It is important to highlight that numerous attempts to synthesize the AA-TOA ligand have not been successful.

4.6.1. Fourier-Transform Infrared Spectroscopy

FTIR spectrometry was first used to detect the presence of ligands and retrieve information relevant to bonding nature of the carboxylic and phosphonic acids headgroups to ZrO₂'s surface.

ZrO₂-AA sample was first characterized by ATR-FTIR. Its spectrum showed the presence of phosphonate groups (-PO₃) of AA onto the ZrO₂ surface because of the presence of broad absorption bands at 1130 and 993 cm⁻¹ (blue dash lines). Tridentate bonds could be assumed because of disappearances of P=O and P-OH stretching bands at 1200 and at 917 cm⁻¹, respectively (green dash lines).

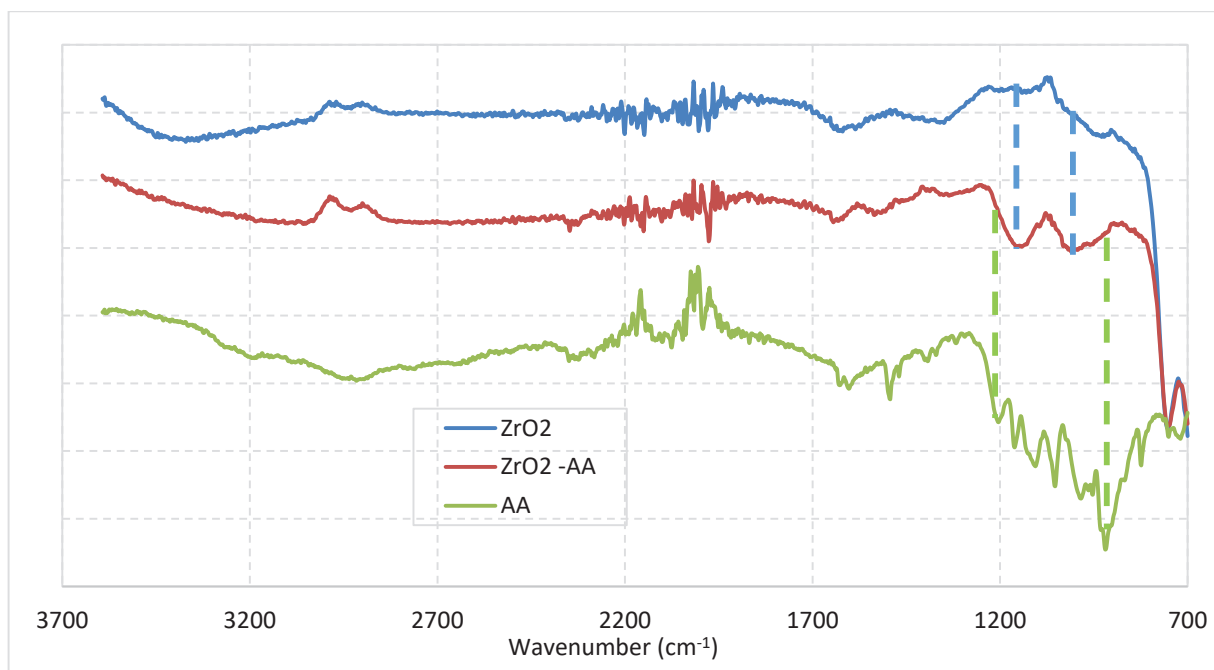


Figure 4-32 – ATR-FTIR spectra of bare ZrO₂, ZrO₂-AA, and AA

DRIFT spectra have confirmed the phosphonate grafting that exhibit a strong absorption band below 1200 cm⁻¹. This technique was also used to collect spectra after amide coupling reaction thanks to higher sensitivity to surface modifications than ATR-FTIR [102]. Generally, it has been suggested that amide I (C=O stretch, at 1600-1700 cm⁻¹) and amide II (N-H bend in-plane and C-N stretch; at 1485-1575 cm⁻¹) bands be indicators of amide bonds; however, the water band (H₂O bend) at 1674 cm⁻¹ in the spectra of ZrO₂-AA and ZrO₂-AA-TOA (Figure 4-33) overlapped with the amide I band. The big difference was the pattern of -CH- stretching band (2830-3000 cm⁻¹) that the spectrum of ZrO₂-AA-TOA showed very similar pattern of -CH- stretching band as did the spectrum of ZrO₂-TOA.

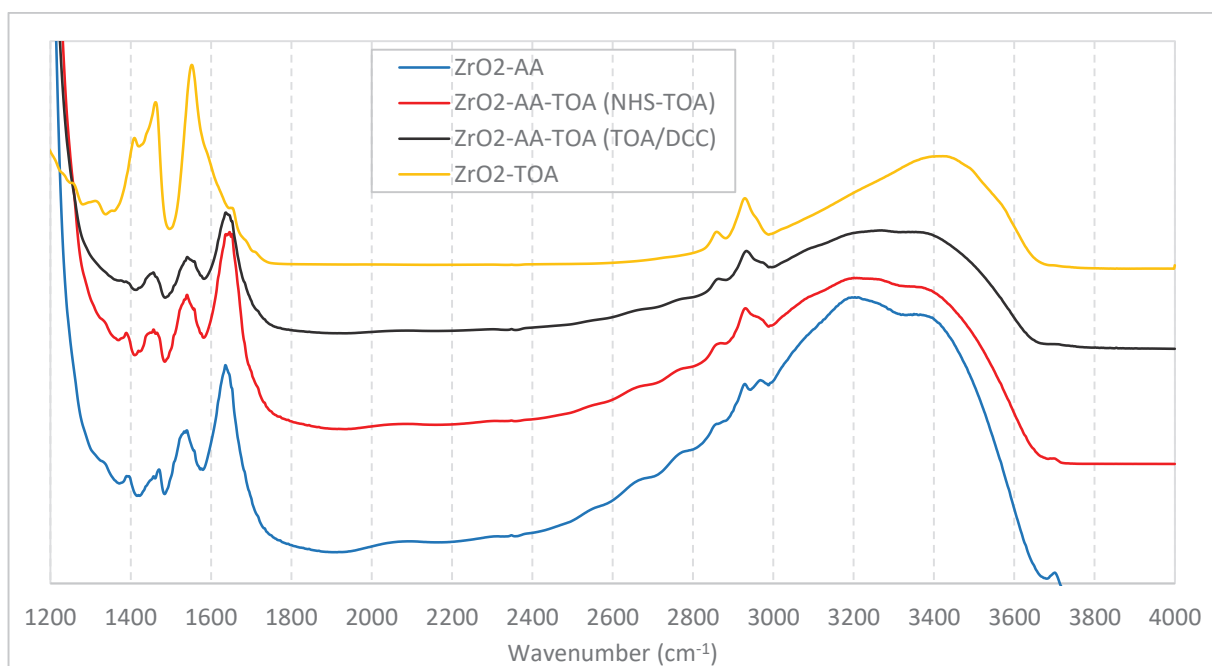


Figure 4-33 – DRIFT spectra of ZrO_2 -AA, ZrO_2 -AA-TOA (NHS-TOA), ZrO_2 -AA-TOA (TOA/DCC) and ZrO_2 -TOA

Assumption on the overlap between water bending and amide I bands was confirmed by recording the spectra after water desorption for ZrO_2 -AA and ZrO_2 -AA-TOA samples at 105°C for 24 hrs under vacuum. Figure 4-34 demonstrated an intense decrease in the intensity of bands at ~ 3400 and $\sim 1630\text{ cm}^{-1}$ in the spectra of ZrO_2 -AA and ZrO_2 -AA-TOA. As such, the residual signal at 1630 cm^{-1} in the ZrO_2 -AA's spectrum was ascribed to -OH group in the AA's structure. Furthermore, intensity of the band at $\sim 1630\text{ cm}^{-1}$ in the spectra of ZrO_2 -AA-TOA is higher than that in the spectrum of ZrO_2 -AA which results from the contribution of amide I (mainly C=O stretching band) created between $-\text{NH}_2$ group of AA and $-\text{COOH}$ group of TOA.

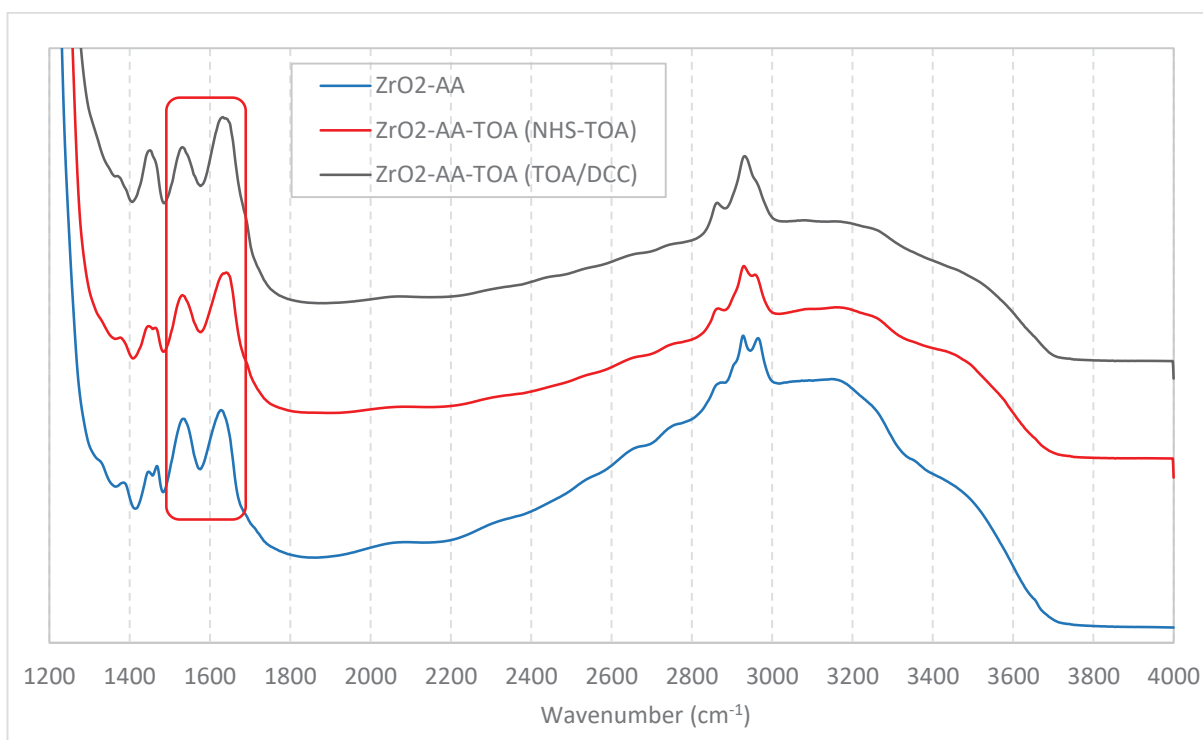


Figure 4-34 – DRIFT spectra of ZrO_2 -AA, ZrO_2 -AA-TOA (NHS-TOA) and ZrO_2 -AA-TOA (TOA/DCC) after water desorption

4.6.2. Thermogravimetric analysis (TGA)

TGA was used to further estimate, to some extent, the organic component content before and after amide coupling reaction in order to calculate the reaction yield (It is important to highlight that phosphate residues were still present after calcination at 900°C). In the Figure 4-35, weight losses between 160 and 800°C of 1.8% wt. (0.073 mmol/g), 2.8% wt. (0.063 mmol/g) and 2.7% wt. (0.061 mmol/g) were assigned to the organic ligand content onto the surface of ZrO_2 -AA, ZrO_2 -AA-TOA (pathways 1 and 2), respectively. Therefore, the reaction yields following two pathways were comparably estimated at about 86% .

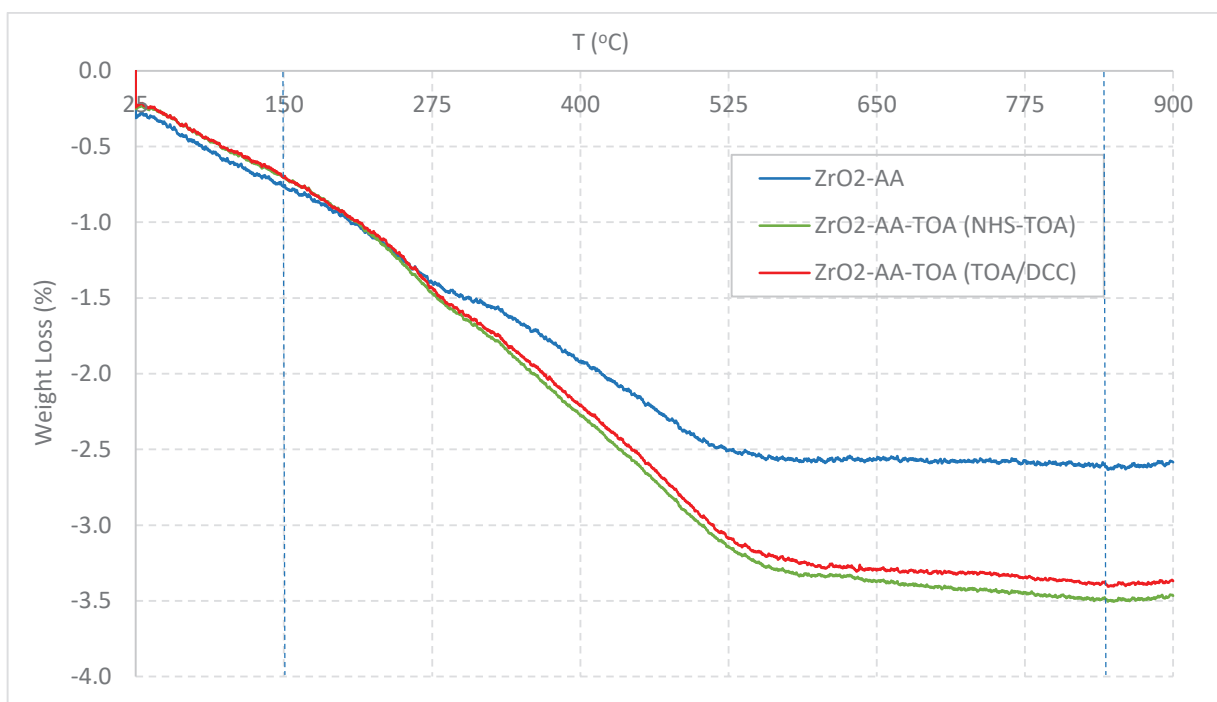


Figure 4-35 – TGA curves of ZrO_2 -AA and ZrO_2 -AA-TOA (NHS-TOA) and ZrO_2 -AA-TOA (TOA/DCC)

4.6.3. ^{31}P MAS solid-state NMR

Many publications have mentioned that ^{31}P MAS solid state NMR characterization of nano-metal oxides modified with phosphonic acids could distinguish among different species of phosphonic acids (physisorbed, chemisorbed, phosphonate) [81, 107]. ^{31}P solid-state NMR is a powerful tool to reveal the covalent linkage between P-OH/P=O to the ZrO_2 's surface. Because alendronic acid (AA) is an amino-biphosphonic acid existing in zwitterionic form that contains one neutral $-P(O)(OH)_2$ and one anionic $-P(O)(O^-)(OH)$ group [117], its NMR spectrum exhibited two sharp resonance peaks at 22.7 ppm and 13.0 ppm, respectively.

In terms of surface-modified nano- ZrO_2 materials (ZrO_2 -AA and ZrO_2 -AA-TOA), the resonance peaks possessed two distinct features that were characteristic of phosphonic acid ligand functionalized metal oxides [118]: (i) they were shifted upfield (12.8 ppm) compared to pure ligand; and (ii) they broadened in the range from -4 to 34 ppm. Basically, the nature of surface modification of metal oxides was driven by condensation between $-P-OH/-P-O^-$ and $-Zr-OH$ or/and $-P-OH/-P-O^-$ and coordinatively unsaturated Zr(IV) because of complex properties of the ZrO_2 's surface that encompassed protonated ($-Zr-OH$), unprotonated ($-Zr-O^-$) or coordinatively unsaturated Zr(IV) sites. Moreover, ^{31}P chemical shifts were greatly

affected by surrounding environment, namely the O-P-O bond length/angle and electronegativity of neighboring atoms. Consequently, the broadness of ^{31}P resonance peak could not be averaged using MAS technique owing to the various bonds of phosphonic acid headgroups to the ZrO_2 's surface [106, 107]. The resonance peaks of ZrO_2 -AA and ZrO_2 -AA-TOA were shifted upfield with respect to neutral $-\text{PO}(\text{OH})_2$ group to 12.8 ppm that was very close to the chemical shift of anionic group. From these observations, alendronic acid probably bonds to ZrO_2 's surface via mono/bidentate tripodal binding modes that came from heterocondensation between $-\text{P-OH}$ head groups and $-\text{Zr-OH}$ to lead Zr-O-P linkages. However, the tridentate bonding mode was likely to be present due to the disappearance of P=O band in ATR-FTIR spectrum and broadening NMR resonance peaks. Interestingly, the downfield shift of resonance peak of ZrO_2 -AA-TOA compared to that of ZrO_2 -AA can plausibly be explained by the amide bond ($-\text{NH-CO}$) that promoted the electron-withdrawing effect, hence deshielding the P atoms.

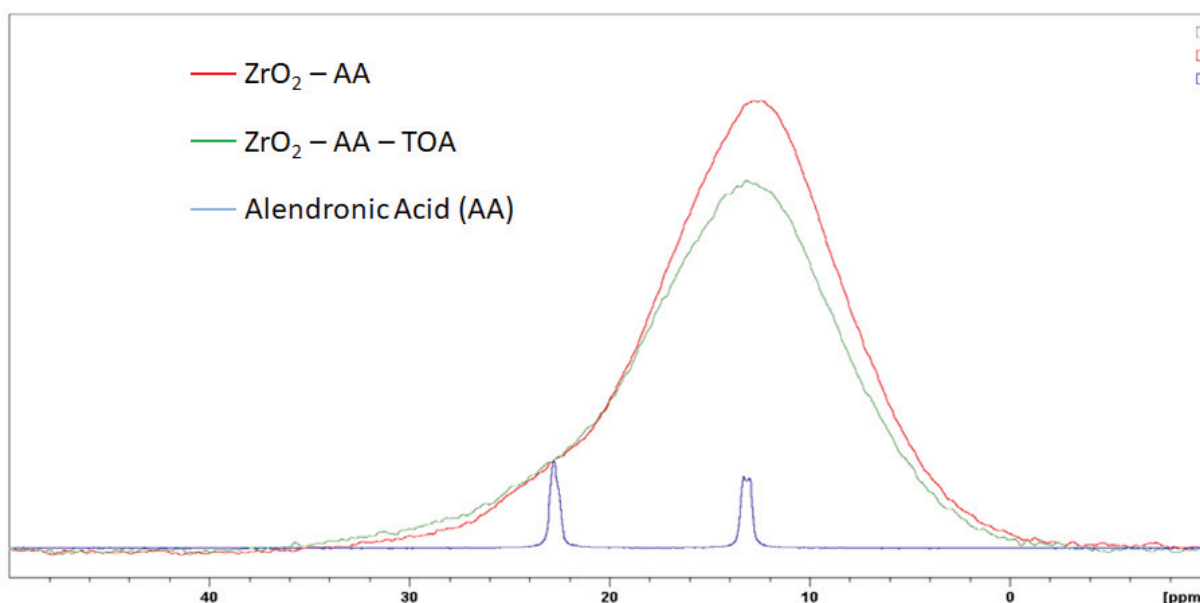


Figure 4-36 – ^{31}P solid-state MAS NMR spectra of ZrO_2 -AA, ZrO_2 -AA-TOA and AA

4.6.4. BET specific surface area

High surface area to volume ratio was of great importance at nanoscale and large specific surface areas (SSA) have been widely sought in applications related to adsorption process. Our results exhibited that BET specific areas were unchanged (around $50 \text{ m}^2/\text{g}$) despite the

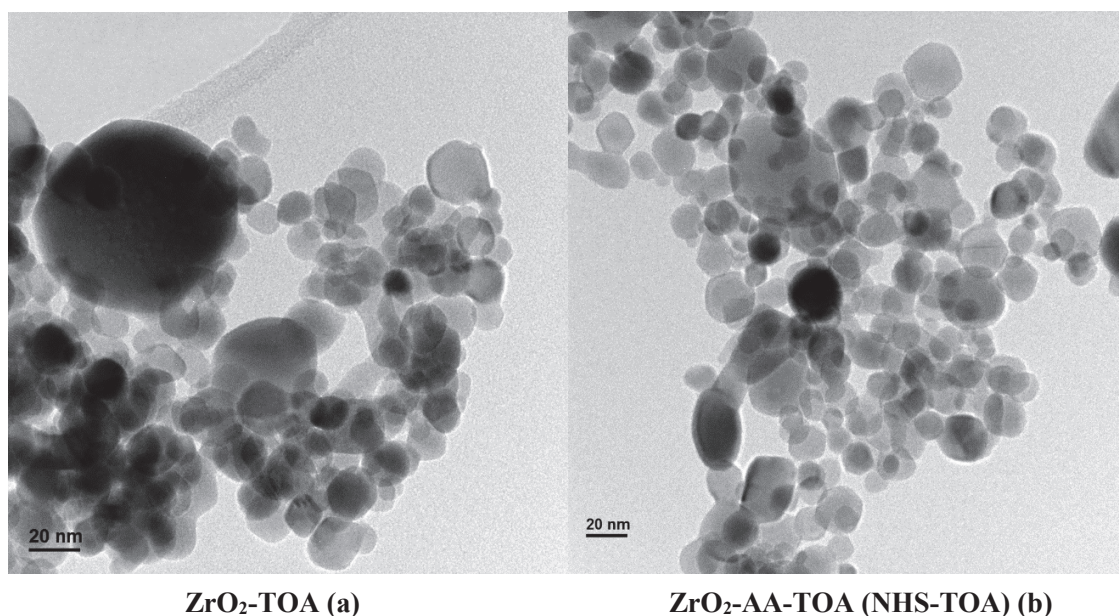
harsh condition of surface modification *via* the two-step surface modification process (Table 4-4).

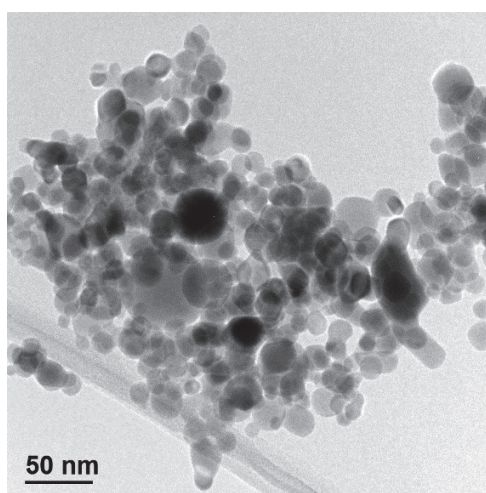
Table 4-4. Specific surface areas of surface-modified ZrO₂ materials determined by BET method

Material	BET specific surface area (m ² /g)
ZrO ₂ (Lotus Synthesis)	52.0 ± 1.0
ZrO ₂ -TOA	50.7 ± 1.7
ZrO ₂ -AA	47.5 ± 1.1
ZrO ₂ -AA-TOA (NHS-TOA)	51.2 ± 1.4
ZrO ₂ -AA-TOA (TOA/DCC)	58.0 ± 1.4

4.6.5. SEM images

SEM images was studied in order to acquire actual morphology of surface-modified nano-ZrO₂ materials and some information on the effect of surface modification processes can be derived. With the aid of EDX technique, the elemental composition of the materials could be determined. The images of surface-modified nano-ZrO₂ in Figure 4-37 showed that nano sizes of surface-modified nano-ZrO₂ materials did not considerably differ from each other (~ 20 nm). This fact demonstrates that surface modification processes did not lead to aggregation of ZrO₂ nanoparticles, in agreement with BET specific area values.





ZrO₂-AA-TOA (TOA/DCC) (c)

Figure 4-37 – SEM images of ZrO₂-TOA (a), ZrO₂-AA-TOA (NHS-TOA) (b), and ZrO₂-AA-TOA (TOA/DCC)

Nevertheless, the results from EDX technique could not reveal P, N content of materials for two main reasons: (i) the sensitivity of EDX technique (limit of detection was approximately 0.1% wt. element) was not sufficient to determine the low content of P and N on ZrO₂-AA-TOA materials; and (ii) L_α energy of Zr (2.044 keV) overlapped K_α energy of P (2.010 keV) (Figure 4-38).

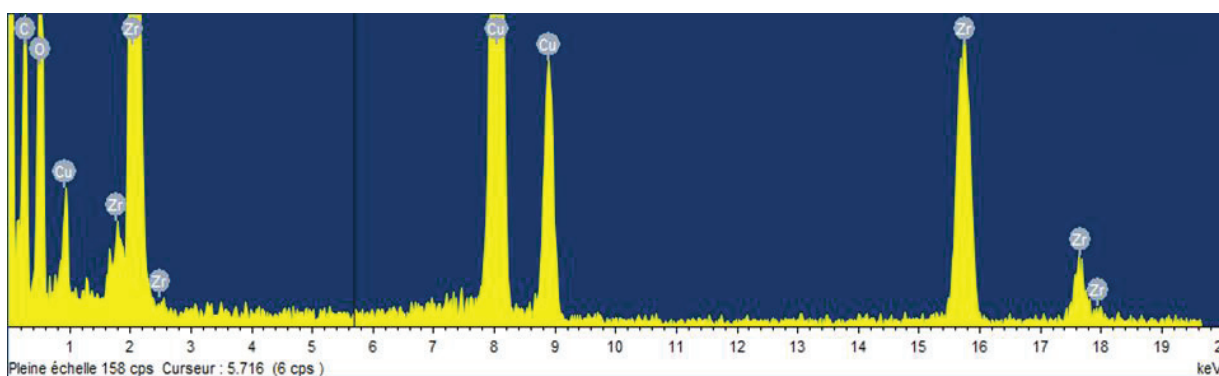


Figure 4-38 – SEM-EDX spectrum of ZrO₂-AA-TOA (NHS-TOA)

4.6.6. Adsorption study of ZrO₂-AA-TOA

4.6.6.1. Maximum adsorption capacities toward Pd and Au

In order to obtain understanding on adsorption capability of ZrO₂-AA-TOA materials, the saturation of ZrO₂-AA-TOA (NHS-TOA) and ZrO₂-AA-TOA (TOA/DCC) with Pd and Au was carried out : 50 mg of ZrO₂-AA-TOA materials were stirred with 25 mL of 25 mg Pd/L

or 25 mL of 135 mg Au/L. The maximum adsorption capacities toward Pd and Au of ZrO₂-AA-TOA are presented in the following table (Table 4-5).

Table 4-5. The maximum adsorption capacities of ZrO₂ surface-modified via NHS-activated ester of TOA and DCC-mediated TOA-amide coupling

Materials	n _{R-S-S-R} (μmol/g)	Adsorption capacity (mg/g)		n _{M(a)} (μmol/g)		n _{R-S-S-R} /n _{M(a)}	
		Pd	Au	Pd	Au	Pd	Au
ZrO ₂ -TOA	129.4	6.3	43.0	59.2	218.3	2.2	0.6
ZrO ₂ -AA-TOA (NHS-TOA)	64	3.2	10.6	30.1	53.8	2.1	1.2
ZrO ₂ -AA-TOA (TOA/DCC)	64	3.5	6.4	32.9	32.5	1.9	2.0

Compared with the adsorption capacities of ZrO₂-TOA toward Pd and Au that were 6.3 mg/g for Pd and 43 mg/g for Au respectively, ZrO₂-AA-TOA materials showed inferior adsorption due to the lower amount of TOA moiety on ZrO₂-AA-TOA materials. Interestingly, in terms of the mole ratio of disulfide moiety (R-S-S-R) to adsorbed metals, some conclusions could be drawn: (i) 1 Pd forms coordinative bonds to 2 R-S-S-R moieties with single bond to each moieties regardless of either the amount of TOA on materials' surface or material types (ZrO₂-TOA or ZrO₂-AA-TOA); (ii) the mole ratio of disulfide to gold tended to fluctuate; interestingly, ZrO₂-TOA with higher amount of TOA on the surface (0.13 mmol/g) 1 R-S-S-R seemed to be able to adsorb 2 atoms of Au that probably resulted from the fact that the standard oxidation potential of [AuCl₄⁻] was somewhat high (1.004V) that could oxidize the R-S-S-R according to the illustration in Figure 4-39. In other words, disulfide moieties of TOA could reduce [AuCl₄⁻] to Au(0).

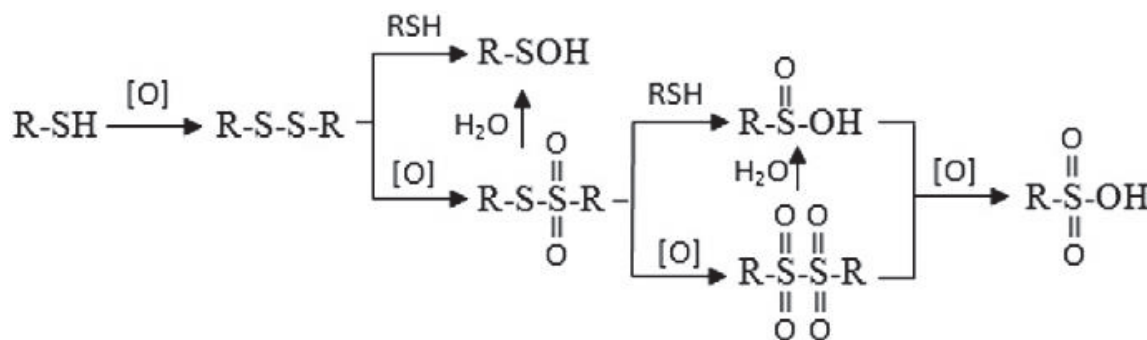
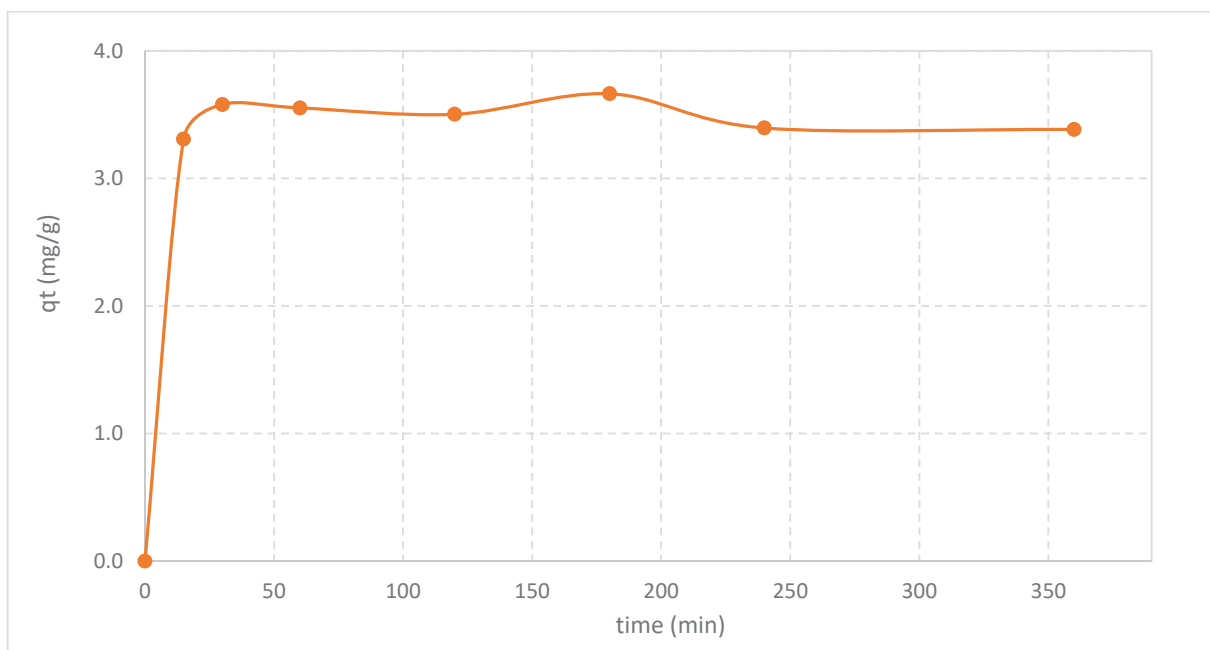


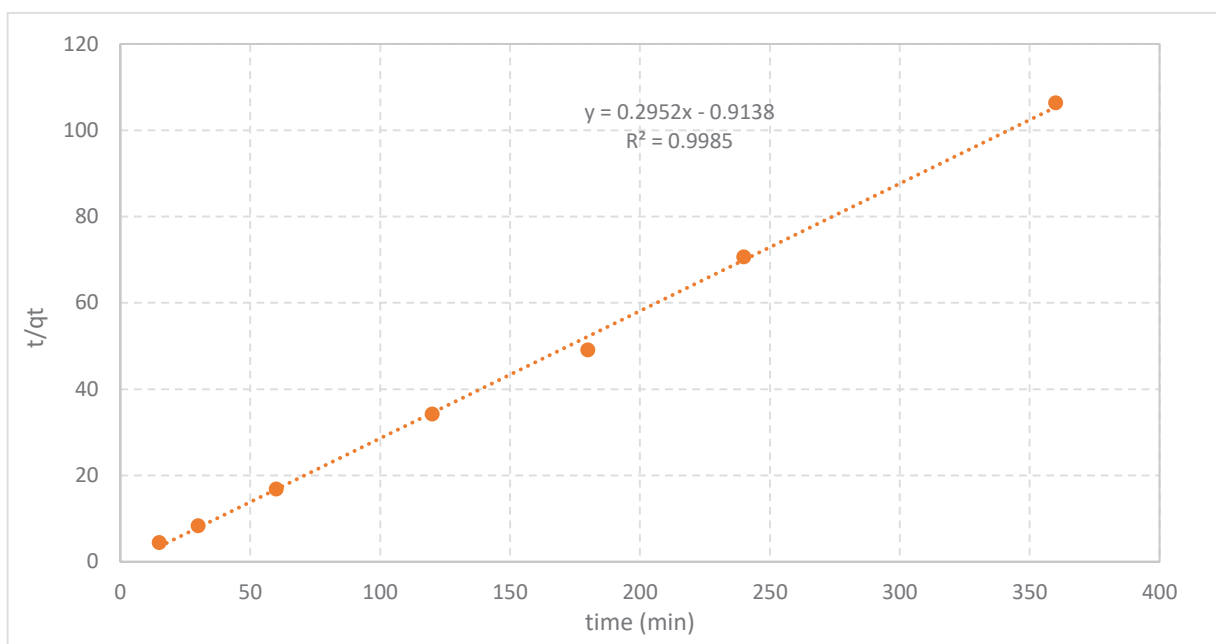
Figure 4-39 – Oxidation process of thiol group [119]

4.6.6.2. Adsorption kinetics of ZrO₂-AA-TOA

Similar to the nano-ZrO₂ directly modified with TOA, the investigation of adsorption kinetics using nano-ZrO₂ modified with TOA through two-step surface modification using NHS activated ester of TOA (pathway 2) was carried out as to whether the surface modification method could alter the adsorption process. For the sake of simplicity, the single solution of 10 mg/L Pd was used to study the adsorption capacity of Pd as a function of contact time. In comparison to the previous experiment about maximum adsorption capacity of ZrO₂-AA-TOA, we observed an agreement in adsorption capacity toward Pd of approximately 3.5 mg/g (Figure 4-40 A). The contact time needed for Pd adsorption to reach saturation (60 min) is shorter than that of ZrO₂-TOA probably due to the lower content of disulfide moiety on ZrO₂-AA-TOA. Moreover, the adsorption data have also demonstrated the similar nature of the adsorption process as that of ZrO₂-TOA because of the suitability of the pseudo-second adsorption kinetics model in describing the adsorption process (Figure 4-40 B).



(A)



(B)

Figure 4-40 – A) The effect of contact time on adsorption capacity and B) pseudo-second order model of Pd adsorption kinetics of ZrO₂-AA-TOA (NHS-TOA)

4.6.6.3. Reusability of ZrO₂-AA-TOA

Two-step surface modification conferred a real improvement in terms of reusability of the final hybrid material. The adsorption percentage (more than 90%) was steadily maintained after 4 cycles of adsorption/stripping (Figure 4-41). Two conclusions could be drawn from these results: (i) the assumption of protonation of sulfur sites of TOA moiety that inhibited coordination between chloro-complex of target metals and sulfur sites was not anymore valid and (ii) phosphonic species on the ZrO₂'s surface after modification with alendronic acid were definitely more resistant to the harsh condition of effluent (high concentration of acids) than carboxylic. Importantly, this observation also consolidated the evidence of amide bond that was created between TOA and AA on ZrO₂'s surface.

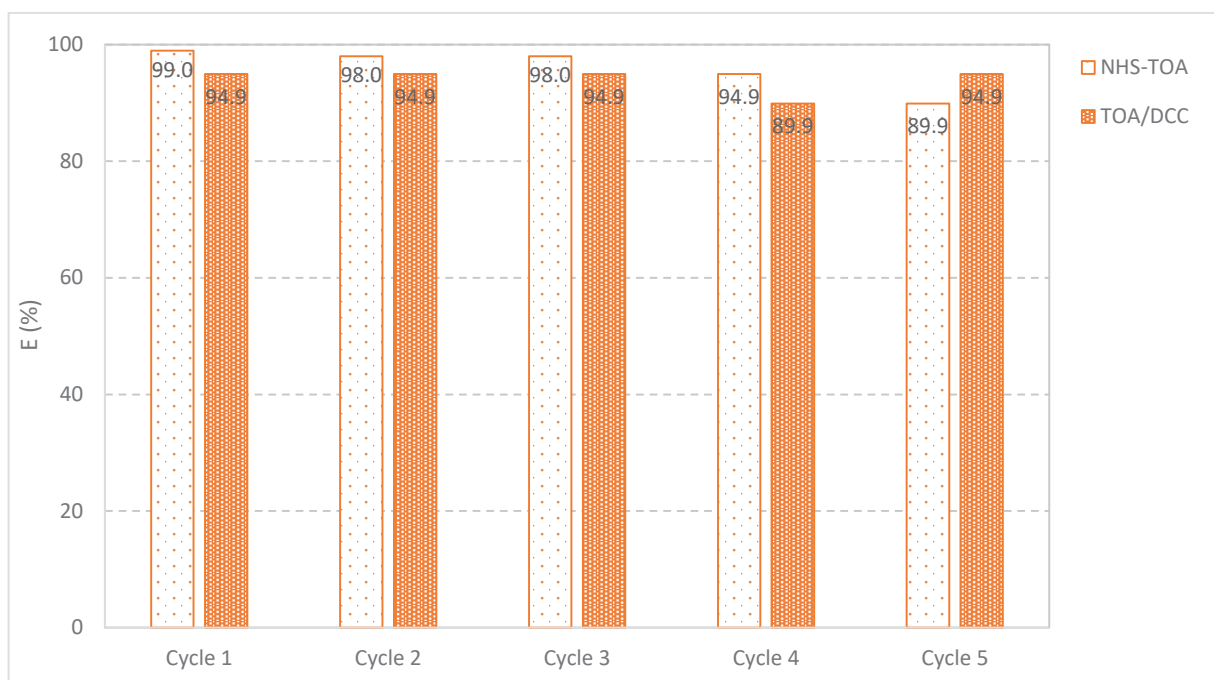


Figure 4-41 – Recyclability of ZrO_2 -AA-TOA materials for capturing Pd in the single solution at 10 mg/L through 5 cycles of adsorption/desorption

Furthermore, the above results demonstrated that both two-step surface modification pathways afforded up resultant materials with same adsorption performances toward Pd in the acidic condition of solution containing hydrochloric acid.

4.6.6.4. Adsorption of surface modified nano- ZrO_2 materials toward Pd and Au in the real e-waste effluent.

The important goal of this study in terms of industrial implementation was to achieve a nanoabsorbent that can be reused in the Pd and Au recovering process from the effluents. In this study, the underlying reason about the difference in bond strength between ligands and the ZrO_2 's surface endows the resulting material with reusability. Figure 4-42 indicates the adsorption capability of ZrO_2 -TOA and ZrO_2 -AA-TOA through 4 cycles of adsorption/desorption that demonstrates the stability of ZrO_2 -AA-TOA in the harsh condition of the effluent with high acid concentration and predominant presence of base metals (Cu, Ni, Fe). The two-step surface modification appeared again to be an alternative pathway that circumvented the shortcoming of ZrO_2 -TOA in reusability.

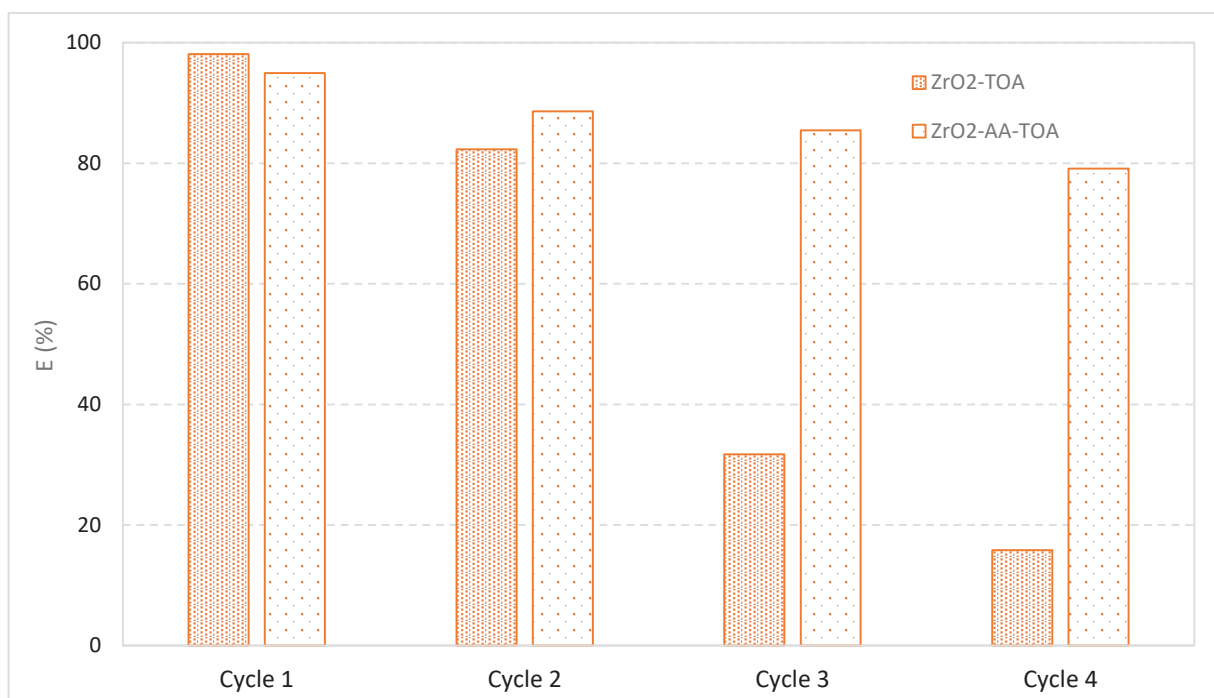


Figure 4-42 – Comparison of surface-modified ZrO₂ materials' recyclability toward Pd

Figure 4-42 illustrates the difference in reusability between nano-ZrO₂ materials directly modified with thioctic acid (ZrO₂-TOA) and nano-ZrO₂ materials two-step modified with thioctic acid (ZrO₂-AA-TOA). Both materials were subjected to 4 cycles of adsorption/desorption in which the adsorption was carried out in the effluent containing 1.6 mg/L Pd and non-detected Au. The observed decreasing tendency derived from the results showed that the matrix of effluent appeared to have an impact on the extraction performance of the resultant materials. In order to clarify this effect, the effluent was spiked with Pd so that the final concentration of Pd was about 12 mg/L and ZrO₂-AA-TOA (NHS-TOA) material was subjected to 5 adsorption/desorption cycles. As indicated in Figure 4-43, the extraction performance was gradually decreasing through adsorption/desorption cycles, especially in the first use of ZrO₂-AA-TOA, its adsorption performance was just about 63% of that in standard solution. Based on this observation, the assumption predicated on the oxidation of disulfide moieties on ZrO₂-AA-TOA was reinforced.

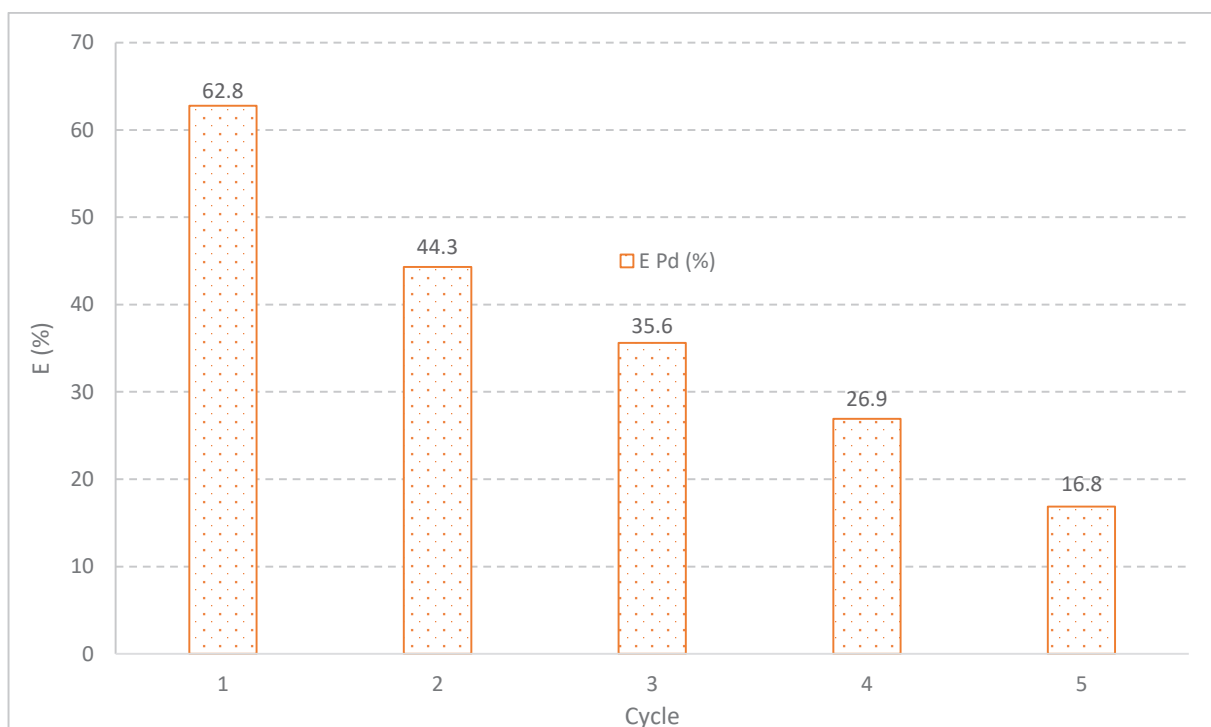


Figure 4-43 – Reusability test of ZrO_2 -AA-TOA (NHS-TOA) in the effluent diluted 5-fold and spiked with Pd

What happened if the Pd and Au coexisted in the e-waste effluent? The scenario of co-existence of Pd and Au in the effluent was designed in which Pd and Au were spiked into the effluent so that the final concentrations of Pd and Au were approximately 10 mg/L after 5-fold dilution. The results in Figure 4-44 showed that the adsorption performance decreases significantly after 2 cycles of adsorption/desorption. Combined with the above result, it was very likely that disulfide moiety of thioctic did not well-suit such a highly oxidizing condition of the e-waste effluent where aqua regia and gold complex can oxidize S-containing ligands.

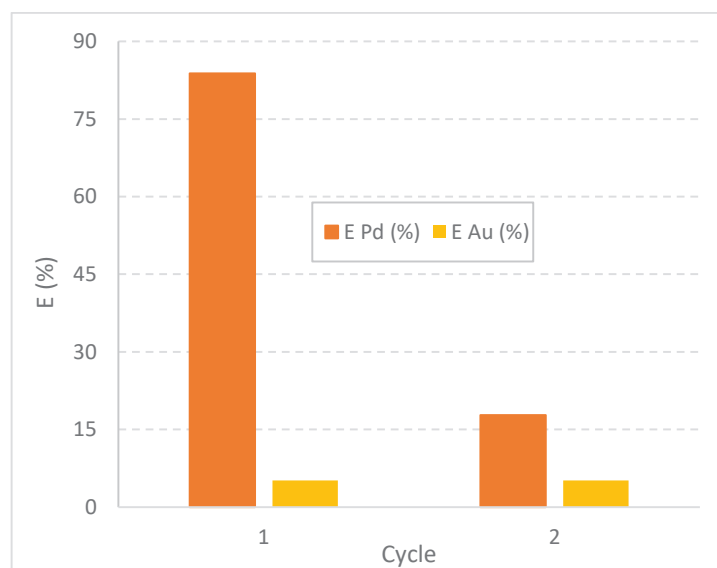


Figure 4-44 – Reusability test of ZrO_2 -AA-TOA (NHS-TOA) in the effluent diluted 5-fold and spiked with Pd and Au

Summary

In this chapter, the key concern was mainly concentrated on elaboration of surface modification process that produces the resultant material with high resistance toward the harsh condition of the e-waste effluent or recyclability through successive cycles of adsorption/desorption. Post-surface modifications of nano- ZrO_2 with different ligands and characterizations of the surface-modified nano- ZrO_2 with the aim to get insights into the bonding nature of ligand were first carried out. Thanks to the screening process of adsorption capability of nano- ZrO_2 modified with different ligands, thioctic surface-modified nano- ZrO_2 appeared to be a promising material in Pd and Au adsorption. Through in-depth investigation of Pd and Au adsorption capability of ZrO_2 -TOA, some thermodynamic and kinetic parameters were acquired to better understand its adsorption behavior. The inevitable instability of carboxylic grafting groups on ZrO_2 's surface led to the two-step surface modification processes including: (i) grafting phosphonic groups of AA to ZrO_2 's surface, (ii) amide-coupling amine group of AA to carboxylic group of TOA. Obviously, via this strategy, thioctic acid was firmly anchored on ZrO_2 's surface and the resultant materials (ZrO_2 -AA-TOA) showed the reusability in a simple matrix of standard solution of Pd. Furthermore, when applied in the harsh conditions of real effluent with the excess amount of competing ions (Co, Ni, Fe), ZrO_2 -AA-TOA showed its selectivity toward Pd and Au. Unfortunately, the presence of aqua regia or/and gold complex in e-waste effluent caused the disulfide moiety to be oxidized, hence its reusability was impeded.

However, the concept of two-step surface modification processes in this study has paved the way for choosing suitable ligands in different media so that the desirable adsorption properties of the resultant materials can be tuned in diverse applications.

CHAPTER 5. DESIGN OF COMPOSITE DEVICE

Nanomaterials have been showing promising capabilities in various applications, such as sensor fabrication, photocatalysis, and membrane design among others. In terms of remediation and wastewater treatment, many studies have been carried out based on different types of nanomaterials and demonstrated the superior properties to the conventional materials including high specific area, accessible active sites and short intra-particle diffusion distance. However, several problems have been addressed when it comes to applications at industrial scale. Firstly, the chemical stability and mechanical durability were considered as the main drawbacks. For instance, nanoparticles can be dissolved in the acidic media of leachate or effluent; nanoparticles can aggregate reducing their specific surface area; hence, decreasing their performance. Secondly, due to their small size, nanoparticles could not be a good choice in high-flux systems (fixed-bed, flow-through systems), due to exhibiting extremely high pressure drop in these systems. Furthermore, complete recovery of nanomaterials or regeneration was a challenging task even in the batch-mode systems apart from magnetic nanoparticles. To tackle the disadvantages thereof, the concept of dispersing nanoparticles into or onto a support or matrix, particularly polymer networks, has been studied and employed and a number of publications have proved the feasibility of this idea [86, 120].

In this study, we aim to develop novel hybrid nanomaterials based on the aforementioned idea which not only carry the advantages of each components, but also complement the downsides of each other. Moreover, from the technical points of view, the synergistic properties of this material enable the regenerability and reusability. Described in the Figure 5-1 is the schematic structure of the hybrid inorganic/organic material; specifically, zirconia nanoparticles dispersed onto a polypropylene network and their modification with selected ligands. In this chapter, dispersion of zirconia is strongly focused with the purpose to obtain the following requirements:

- High durability and nanostructure of zirconia coating.
- Homogeneity of the layer of modified zirconia.
- Presence of voids.

Zirconia nano-coating was to increase highly the specific surface area of the final device and then the quantity of organic trapping agent. It was carried out according two approaches:

single dip coating and layer-by-layer dip coating methods. Decision, on which method was used, depended on the characteristics of polypropylene, such as the swelling degree, and mainly on the density of grafting groups (COOH groups). It is noteworthy to mention that the supply of –COOH surface modified polypropylene is not trivial and has required to investigate different sources of raw materials and to collaborate with the research group of Prof. Dirk HEGEMANN at EMPA in Switzerland. At the beginning of this project we had access to CREAT facilities and products and in particular to PP-COOH with high density of carboxylic group (2.7 meq/g). Unfortunately, the company shut down and we could not find same product elsewhere. This prompted us to learn and to develop LbL method while using PP-COOH with low COOH group density.

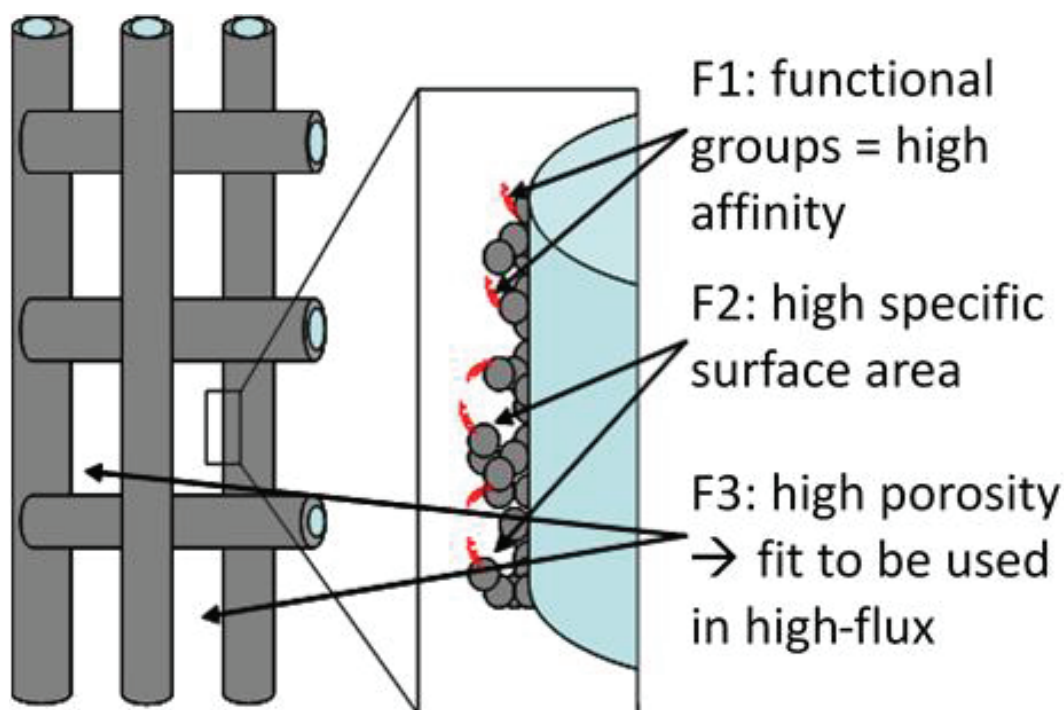


Figure 5-1 – Schematic structure of the aimed inorganic/organic material

The complete synthetic procedure is summarized in the Figure 5-2 which includes the coating step and surface modification step. On the other hand, when it comes to layer-by-layer method, parameters relevant to coating process were investigated, including the effect of NaCl concentration, the influence of polyacrylic acid's molecular weight...

In this work, LbL method was performed using two kinds of polyelectrolytes including zirconia nanoparticles suspension and polyacrylic acid (PAA). Many parameters related to the LbL method were studied, namely:

- (i) Effect of the number or layers of (ZrO₂/PAA)
- (ii) Effect of the type of zirconia nanosuspension: 2 samples of ZrO₂ nanosuspension with pH 10 and pH 1 provided by Lotus Synthesis Company and a commercial product of Sigma Aldrich Company (pH 5).
- (iii) Influence of molecular weight of PAA.
- (iv) Influence of ionic strength in the aqueous solution of PAA.

All polypropylene samples coated, regardless of methods, were thoroughly characterized by infrared spectroscopy (ATR-FTIR), scanning electron microscopy (SEM), thermogravimetric analysis (TGA) and powder X-ray diffraction technique (XRD).

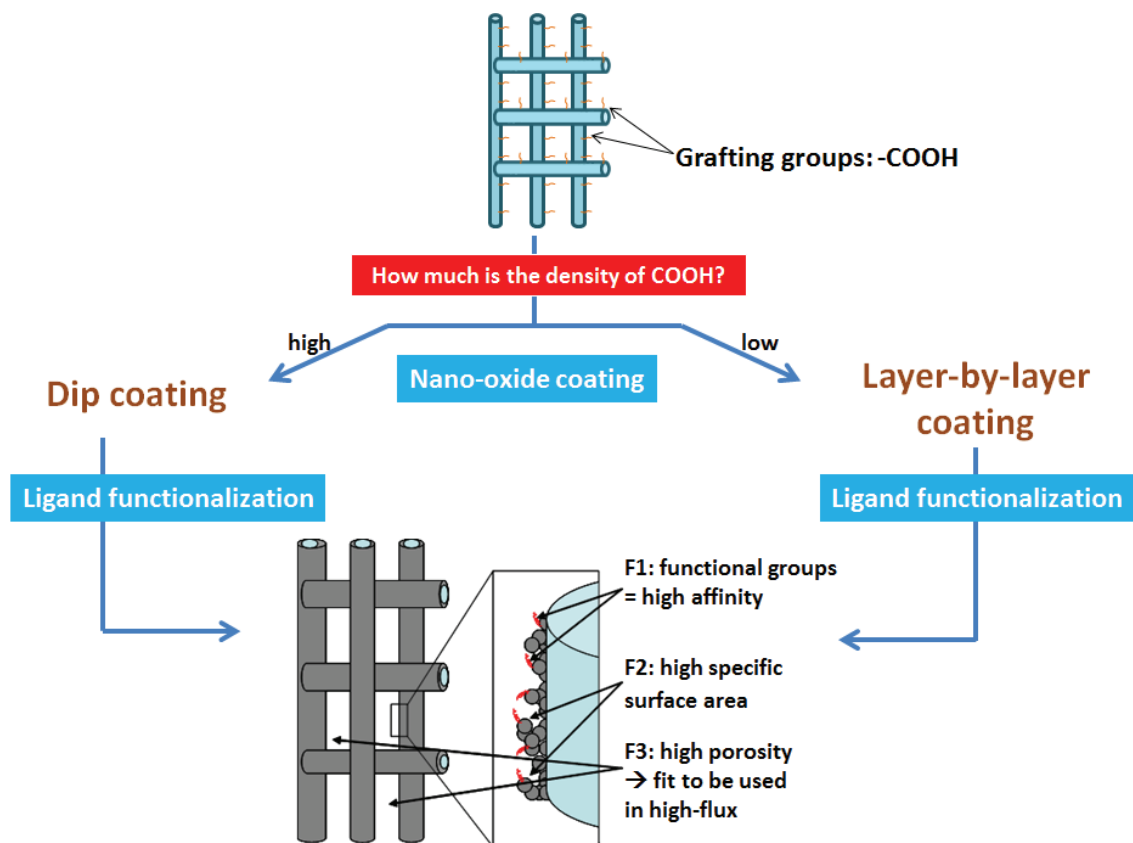


Figure 5-2 – Different approaches to zirconia coating on the polypropylene

5.1. Deposition of nano-zirconia coating on the polypropylene with high density of grafting group (single dip coating)

The dip coating process accompanying with some investigated parameters is depicted in Figure 5-3. Aspects of the process which strongly impact on the structure and amount of zirconia on the polypropylene were carefully examined, namely the effect of grafting groups on the polypropylene fibers, soaking conditions (time, temperature, pH...).

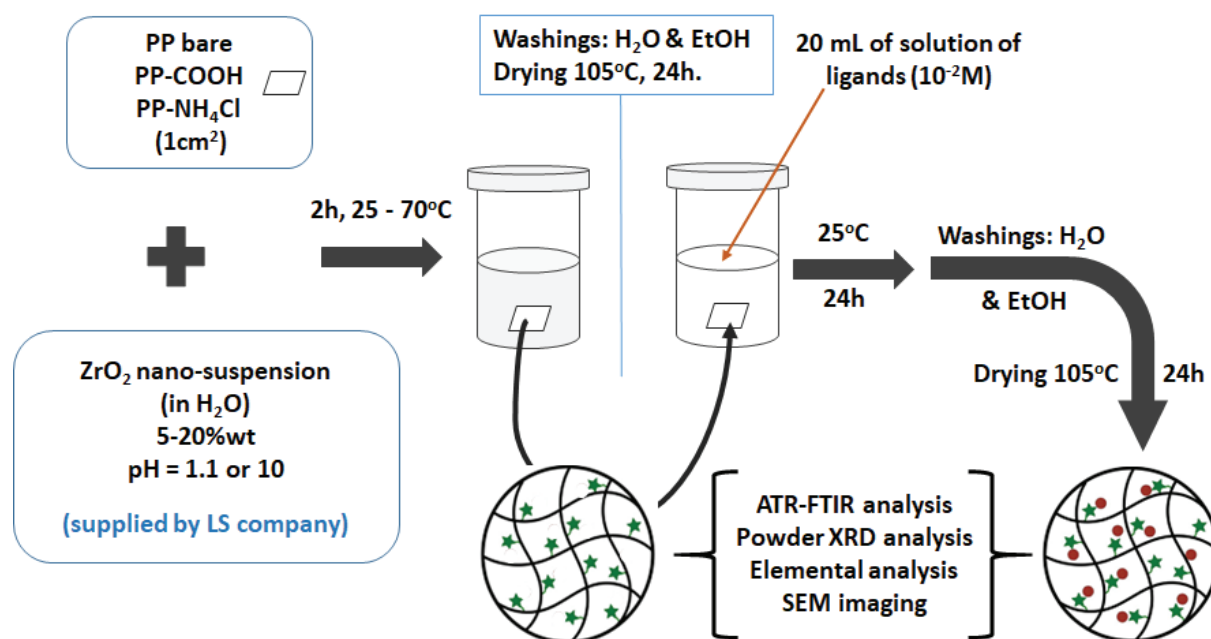


Figure 5-3 – Schematic representation of single dip-coating approach

The studied range of parameters:

- pH of ZrO₂ nanosuspension: 1 and 10
- ZrO₂ nanosuspensions' concentration: 5-20% wt.
- Impregnating temperature: 25 – 70°C
- Impregnating duration: 2 hrs
- [TOA] = 10⁻² M

The ATR-FTIR spectra show that the presence of ZrO₂ on PP-COOH was confirmed by the appearance of a broad band below 500 cm⁻¹. Nanoparticles could not be deposited on the surface of bare PP and PP-NH₃⁺, so the surface of PP must be modified with carboxylic functional groups. After nano-ZrO₂ deposited on PP-COOH, the intensity of carboxylic's stretching band (ν_{COOH}) at 1703 cm⁻¹ decreased dramatically due to the interaction between

-COOH groups and ZrO_2 . Bands at 1580 cm^{-1} and 1464 cm^{-1} attributed to $\nu_{as}(\text{COO})$ and $\nu_s(\text{COO})$, respectively, exhibited traditional bridging bonding of the carboxylic group.

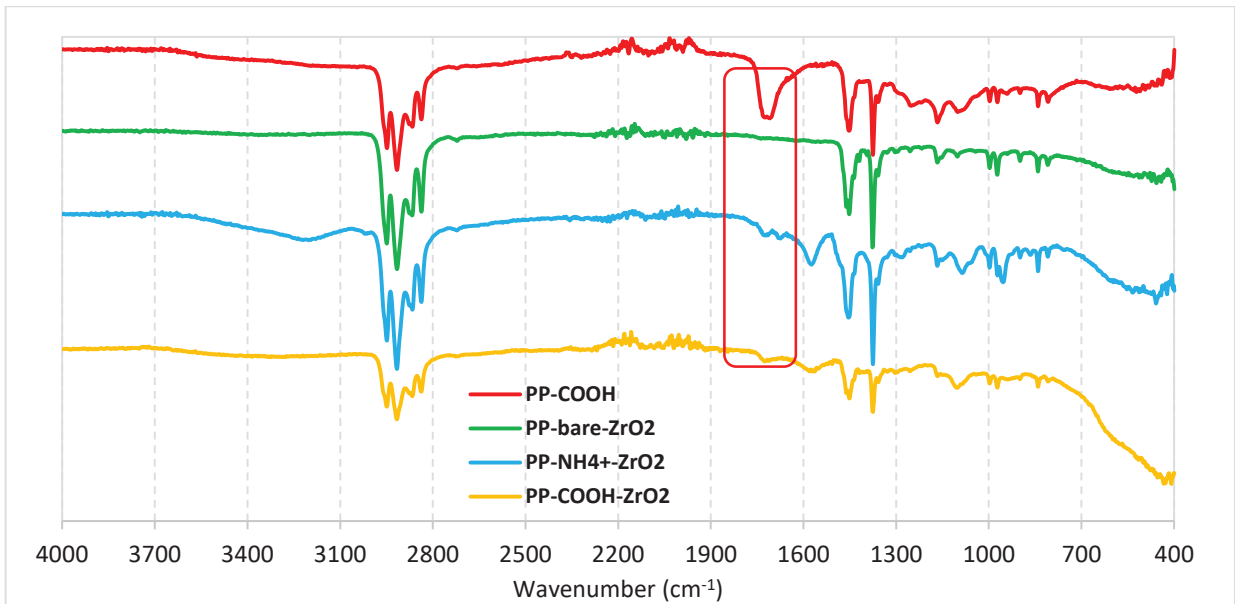


Figure 5-4 – ATR-FTIR spectra of carboxylic-modified polypropylene (red), ZrO_2 -coated bare polypropylene (green), ZrO_2 -ammonium-modified polypropylene (blue) and ZrO_2 -coated carboxylic-modified polypropylene (yellow).

5.1.1. Effect of pH of zirconia nanosuspension to dip coating process

The performance of the grafting process was studied while using LOTUS SYNTHESIS nanosuspensions at initial pH of 1 or 10.

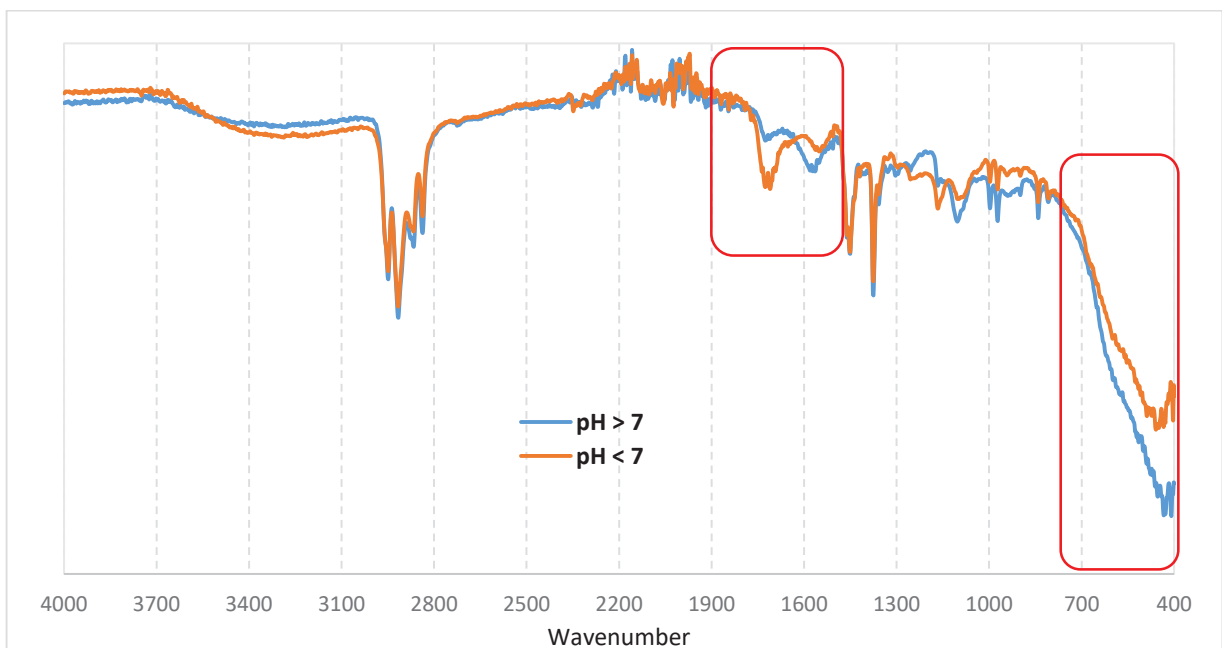


Figure 5-5 – ATR-FTIR spectra ZrO_2 -coated PP-COOH samples using ZrO_2 nanosuspension with pH 10 and pH 1

The data demonstrated that both could be used because of the broad band below 500 cm^{-1} . However, the nanosuspension at pH 10 was more efficient as demonstrated in ATR-FTIR by the large decrease of the ν_{COOH} band at 1703 cm^{-1} (Figure 5-5). This is probably because of higher degree of COOH deprotonation and ZrO_2 attraction due to opposite surface charge. It is noteworthy to mention that basic ZrO_2 nanosuspensions stands in a formulation using polyethylene glycol (PEG) as the dispersant (stabilizer) and PEG was incorporated onto the surface of ZrO_2 by hydrogen bonds. Therefore, PEG can play a role as a “bridge” to connect ZrO_2 nanoparticles and surface of PP-COOH, followed by the bonding of COOH groups to ZrO_2 via mono or bidentate modes. In the following experiments, the basic ZrO_2 suspensions from LOTUS SYNTHESIS was the only one to be used.

5.1.2. Effect of zirconia nanosuspensions concentration

Powder XRD spectra (Figure 5-6) indicate that tetragonal polymorph was the main phase of ZrO_2 's lattice with characteristic diffraction peaks at $2\theta = 30.2^\circ$, 34.5° , 50.2° and 60.2° for the (101), (002), (112) and (221) lattice planes. The intensity of the characteristic peaks was higher with higher concentration of ZrO_2 nanosuspension.

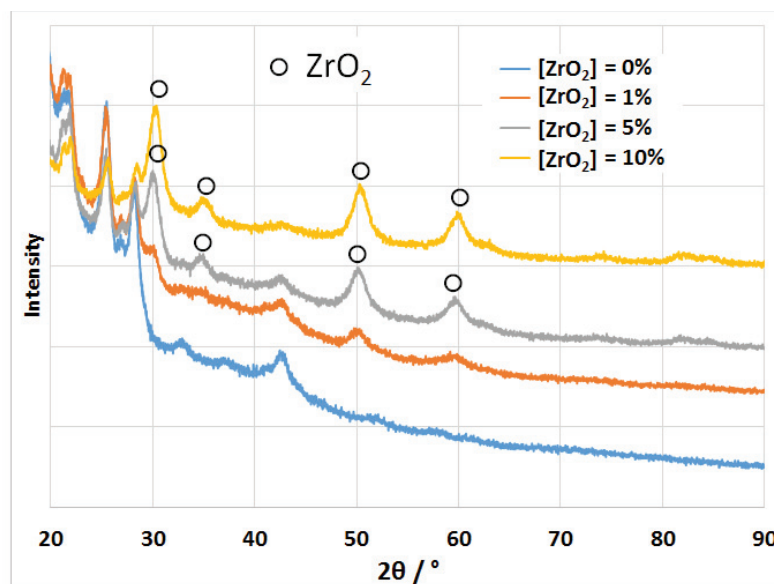


Figure 5-6 – XRD spectra of different ZrO_2 -coated PP-COOH

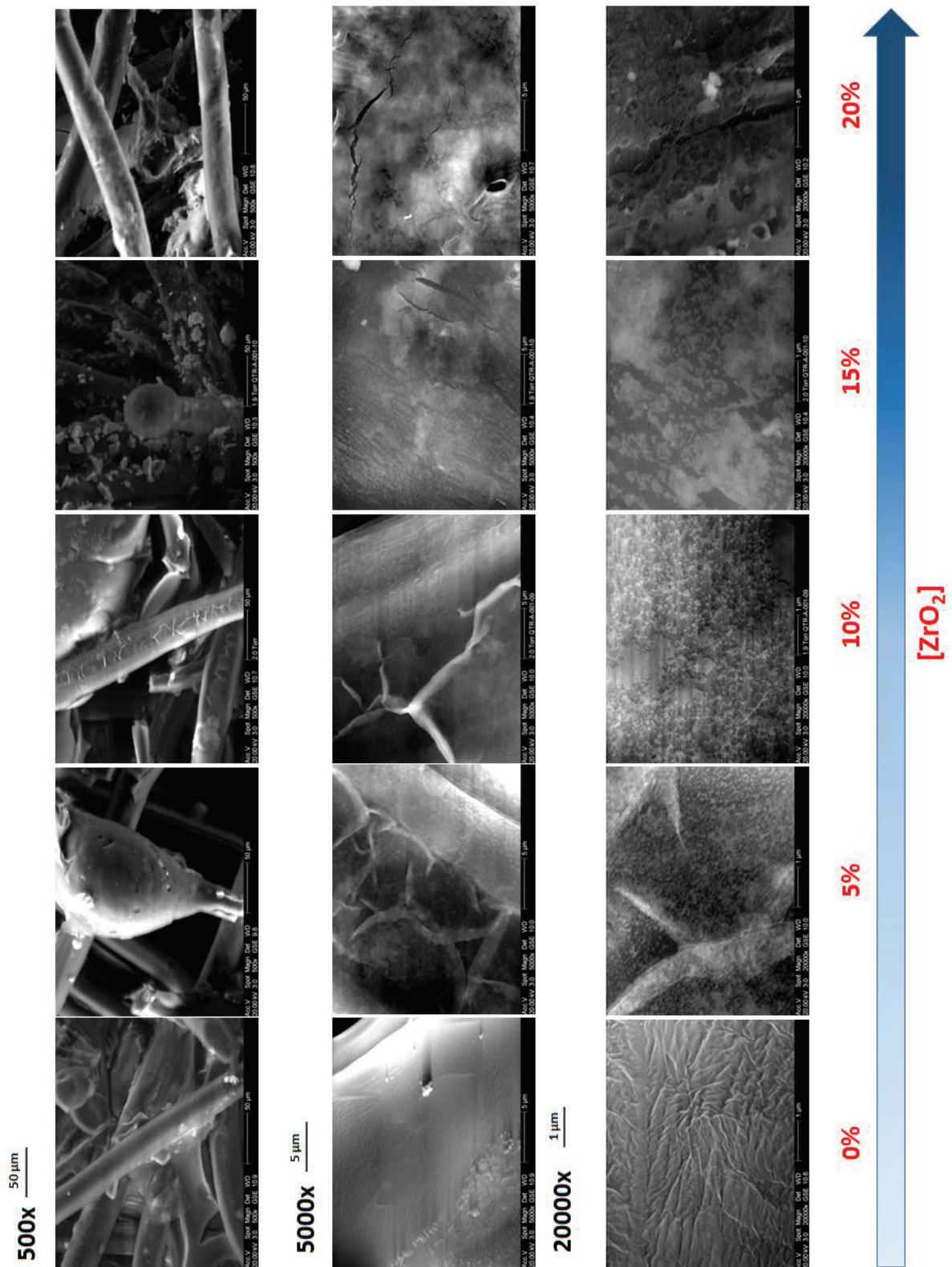


Figure 5-7 – SEM images of different ZrO₂-coated PP-COOH

By investigating the surface morphology using SEM technique at high magnification (Figure 5-7), uniform layer of ZrO_2 without cracks and visible interconnected voids were obtained using ZrO_2 nanosuspension at 10% wt.

5.1.3. Effect of temperature

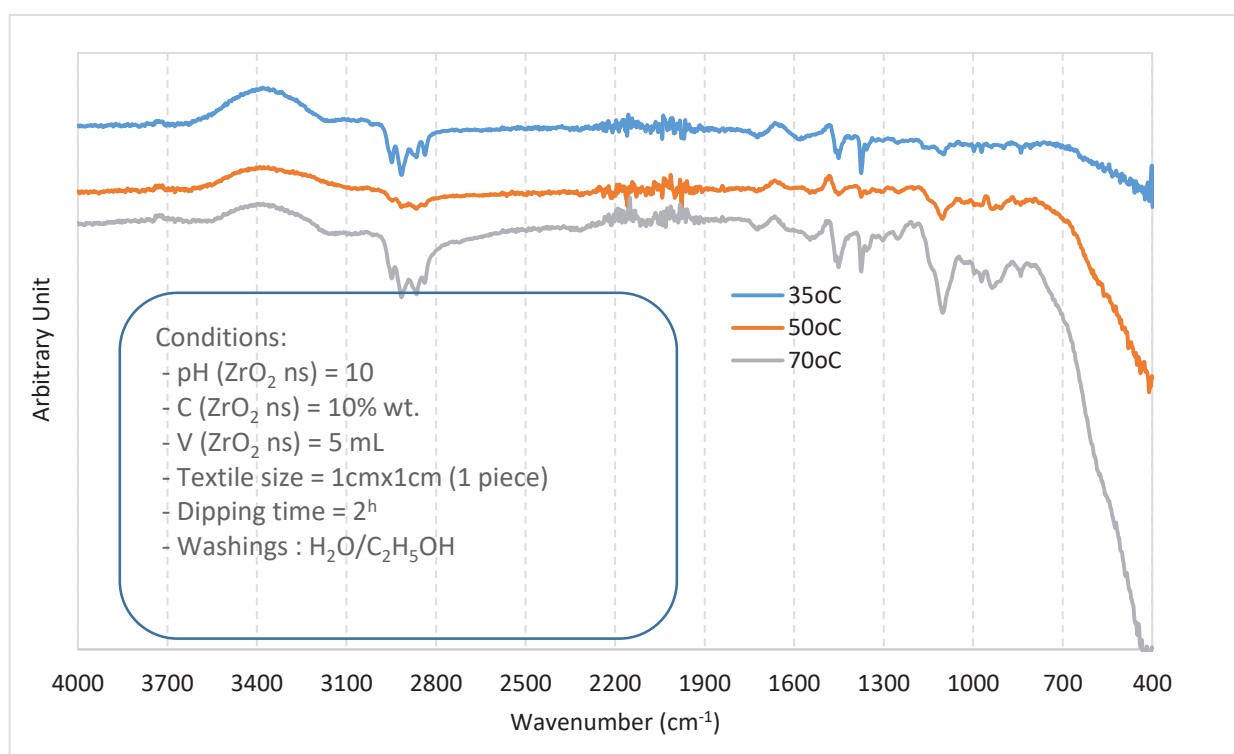


Figure 5-8 – ATR-FTIR of PP-COOH coated ZrO_2 at different temperatures

The Figure 5-8 shows that the higher the temperature of soaking process is, the higher amount of ZrO_2 on the surface of PP-COOH corresponding to the increasing intensity of the band below 500 cm^{-1} is. However, temperature in the range of $25\text{-}35^\circ\text{C}$ was chosen in terms of simplicity of the process, and the limitation of PP-COOH's mechanical strength.

5.1.4. Investigation into adsorption capability of PP-COO- ZrO_2 (dip coating) impregnated with thiocetic acid

In this experiment, one piece of PP-COO- ZrO_2 samples impregnated with TOA was contacted for 24 hrs with 20 mL of Pd standard solution containing 10 ppm (mg/L), the concentration of HCl was maintained at 0.5M. Specifically, the time of impregnating PP-COOH- ZrO_2 with TOA was increased from 5 min, 30 min, 2^h and 24^h.

Table 5-1. The results of Pd concentration after adsorption after using PP-COO-ZrO₂ impregnated with TOA for 5 min, 30 min, 2 hrs and 24 hrs.

Description	[Pd] (mg/L)	Extraction percentage (%)
Initial solution containing Pd	10.6	-
PP-COO-ZrO ₂ soaked into TOA 10 ⁻² M for 5 min	6.7	37.0
PP-COO-ZrO ₂ soaked into TOA 10 ⁻² M for 30 min	5.6	47.3
PP-COO-ZrO ₂ soaked into TOA 10 ⁻² M for 2 hrs	5.4	52.0
PP-COO-ZrO ₂ soaked into TOA 10 ⁻² M for 24 hrs	2.7	74.5

The results in the Table 5-1 first proved the feasibility of the concept. Longer soaking time in TOA solutions led to better performance of Pd extraction. However, PP-COOH supplied by CREAT swelled up and became highly breakable during adsorption process, meaning that mechanical stability of polypropylene decreased drastically (Figure 5-9).

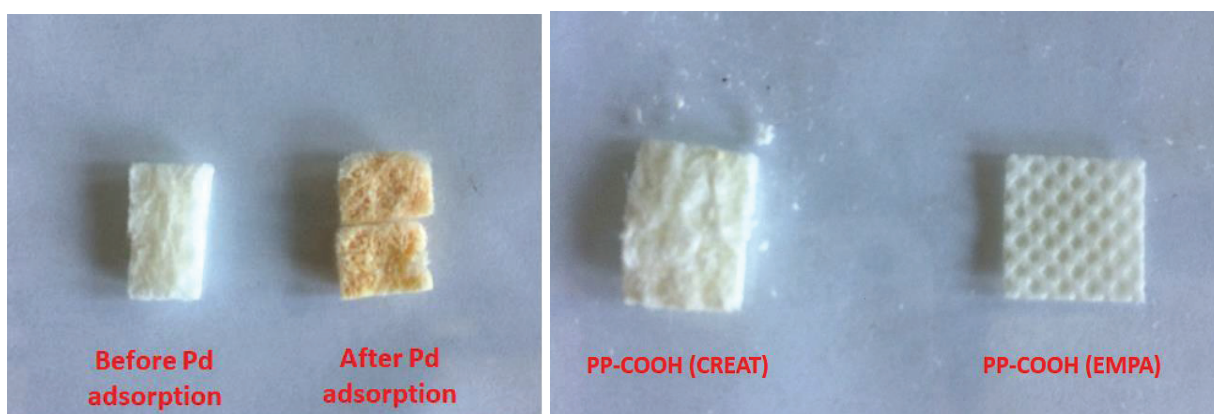


Figure 5-9 – Photos of PP-COOH-ZrO₂ impregnated with TOA before and after Pd adsorption process (left), and PP-COOH-ZrO₂ textiles from CREAT and EMPA

Therefore, PP supplied by SAATI and EMPA were selected as alternatives.

5.2. Deposition of ZrO₂ on the polypropylene with low density of grafting group (layer-by-layer dip coating method)

5.2.1. The difference in carboxylic group density

FTIR spectra (Figure 5-10) illustrate the difference in intensity of the ν_{COO} at $\sim 1700 \text{ cm}^{-1}$ of different surface-modified polypropylene (PP) provided by CREAT, EMPA and SAATI. For the sake of clarity, SAATI company supplied us PP substrates and then these substrates were modified through the plasma coating process at EMPA. According to Figure 5-10, CREAT substrate has higher quantity of -COOH group than does EMPA substrate. However, the former one displayed lower mechanical strength (presence of fibers in the media) and the closure of the CREAT company during this study were taken into consideration for the continuation of the thesis. Fortunately, EMPA (Swiss Federal Laboratories for Materials Science and Technology, Advanced Fibers, Plasma & Coating team) directed by Dr. Dirk HEGEMANN provided us different COOH surface-modified PP obtained by plasma activation. It is noteworthy that some ketone and aldehyde groups can also be present in the sample. Furthermore, the presence of band $\sim 1700 \text{ cm}^{-1}$ in the spectrum of PP SAATI after plasma-coated by EMPA also demonstrated the feasibility of this process.

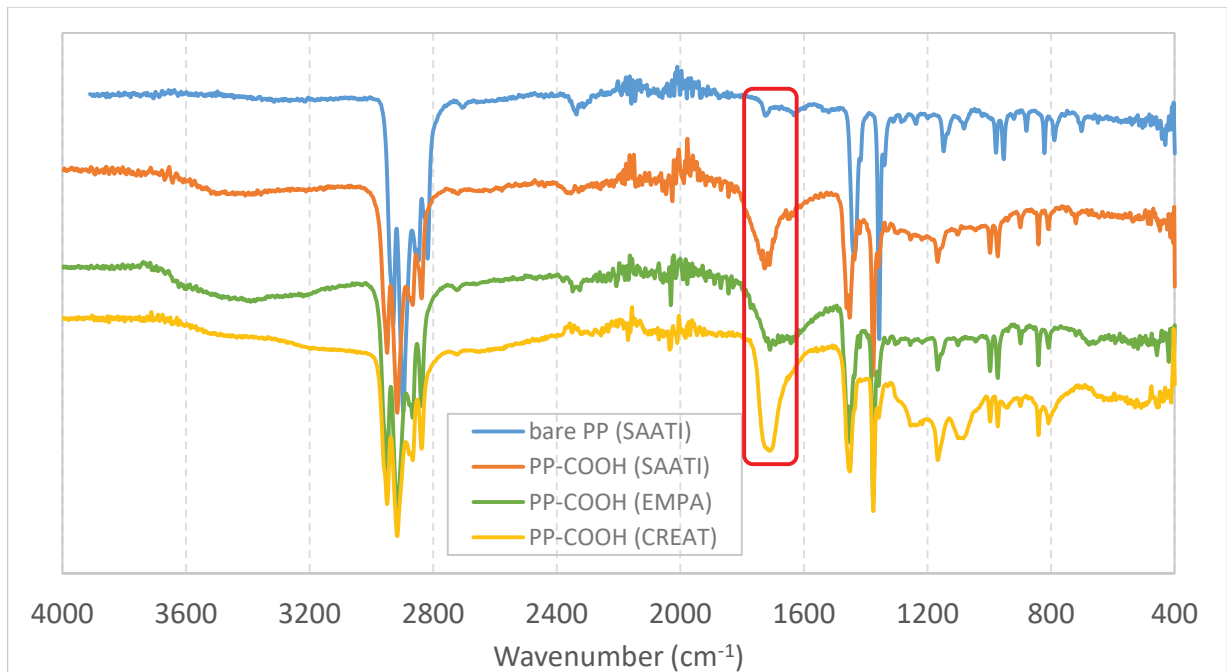


Figure 5-10 – FTIR spectra of carboxylic-modified polypropylene samples from EMPA and CREAT.

5.2.2. Effect of the type of nanosuspension of zirconia to the coating process

Figure 5-11 shows that we can obtain higher quantity of ZrO_2 on novel PP-COOH supports when using Sigma Aldrich nanosuspension. One possible reason for that is the nanoparticles' size in the suspension of Lotus Synthesis (LS) (10 – 30 nm) is much smaller than that of Sigma Aldrich (~100 nm). Generally speaking, the smaller nanoparticles have higher surface charge density and the bigger ones have lower surface charge density, so fewer ZrO_2 nanoparticles will be needed to compensate the opposite charge on the surface of substrate if LS nanosuspensions are used. On the other hand, pH of nanosuspension affects quite seriously, especially just 1.25 % wt. of ZrO_2 is obtained because of the negative surface charge of ZrO_2 nanoparticles in pH 10.

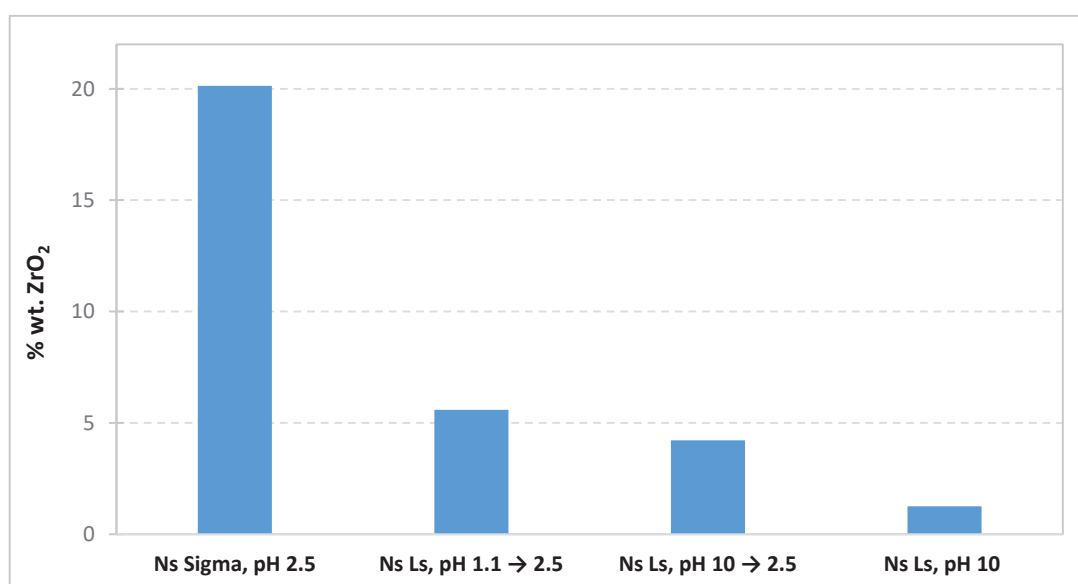


Figure 5-11 – The content of ZrO_2 deposited on PP substrate by LbL method using different sources of nanosuspension

In order to reinforce the assumptions thereof, surface charge's behavior of nanosuspensions, PAAH ($M_w \sim 100.000$) and substrates were studied via the changes of surface potential as a function of pH. As indicated in Figure 5-12, PAAH ($M_w \sim 100.000$) bears negative charges in the whole selected pH range, while ZrO_2 nanosuspension shows a charge sign's reversal around their pH_{PIC} (7.5 for ZrO_2 ns (LS) pH 1, 5.2 for ZrO_2 ns (LS) pH 10, 8.7 for ZrO_2 (SA)). Therefore, the electrostatic interaction is likely the main driving force in the LbL coating. Specially, the surface charge of PP substrate, which is characterized by streaming potential technique (conducted at ISA Institute with the support of Dr. Claire BORDES and Ms. Marie HANGOUET) became more negative after plasma modification that is the plausible reason why the ZrO_2 deposition is viable (Figure 5-13).

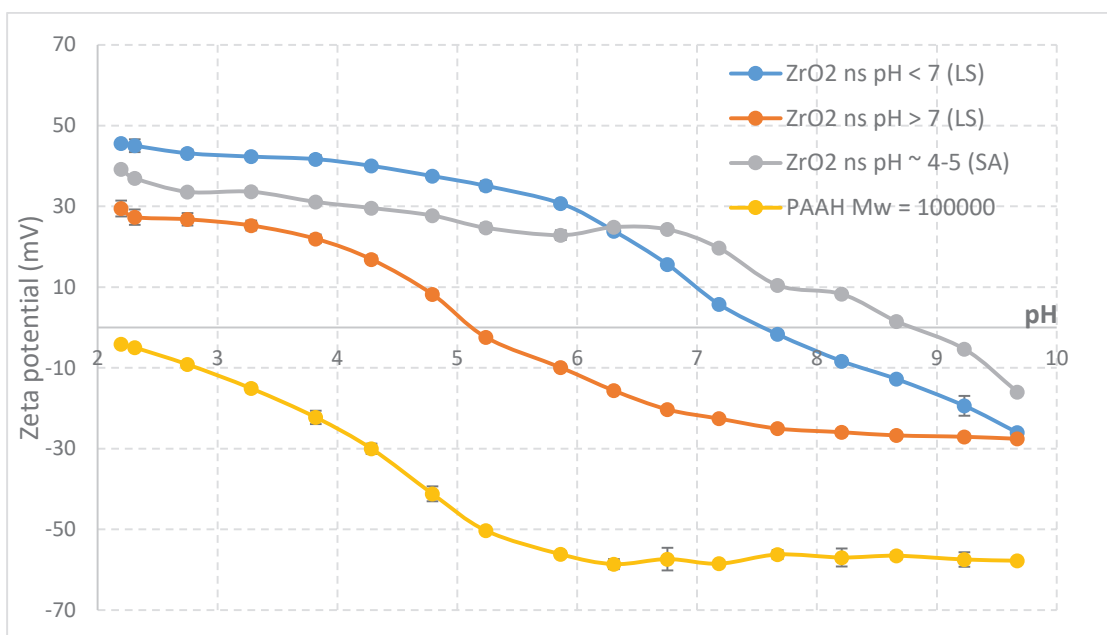


Figure 5-12 – Surface zeta potential curves of the used nanosuspensions and PAAH

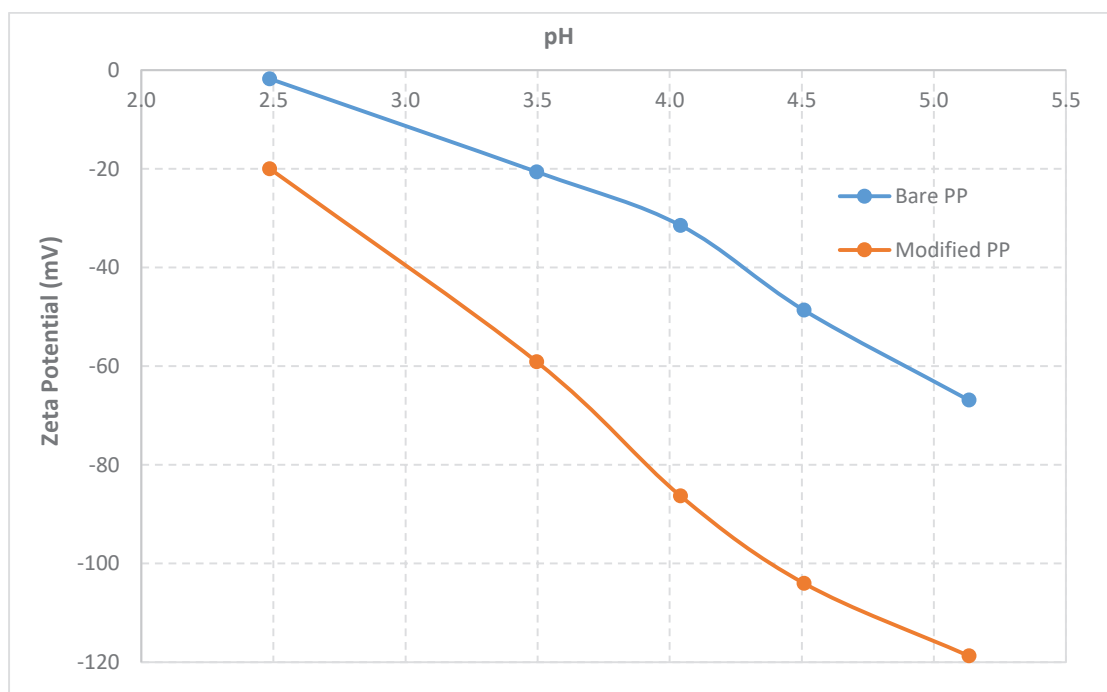


Figure 5-13 – Surface zeta potential curves of textiles based on streaming potential measurement

The hypothesis on electrostatic interaction that plays the main role in LbL coating method led to a question: based on different types of ZrO_2 ns, would it be possible to create a coating

layer with 100% of ZrO₂? In order to answer this question, LbL coating process was carried out on PP-COOH textiles from EMPA, but ZrO₂ nanosuspensions (pH 1 and pH 10) from Lotus Synthesis were used instead of using ZrO₂ ns (SA) and PAAH. Both ZrO₂ nanosuspensions were diluted to 1% wt. and their pHs were adjusted to 6 in order that their surface were counter charged to each other. The content of ZrO₂ on textiles was determined by TGA and the results shown in Figure 5-14 demonstrate that 100%-ZrO₂ layer can be coated on PP-COOH textiles. The maximum amount of ZrO₂ on PP-COOH textiles appears to have reached the value of approximately 5.7 % wt that corresponds to 15 layers of ZrO₂(+)/ZrO₂(-).

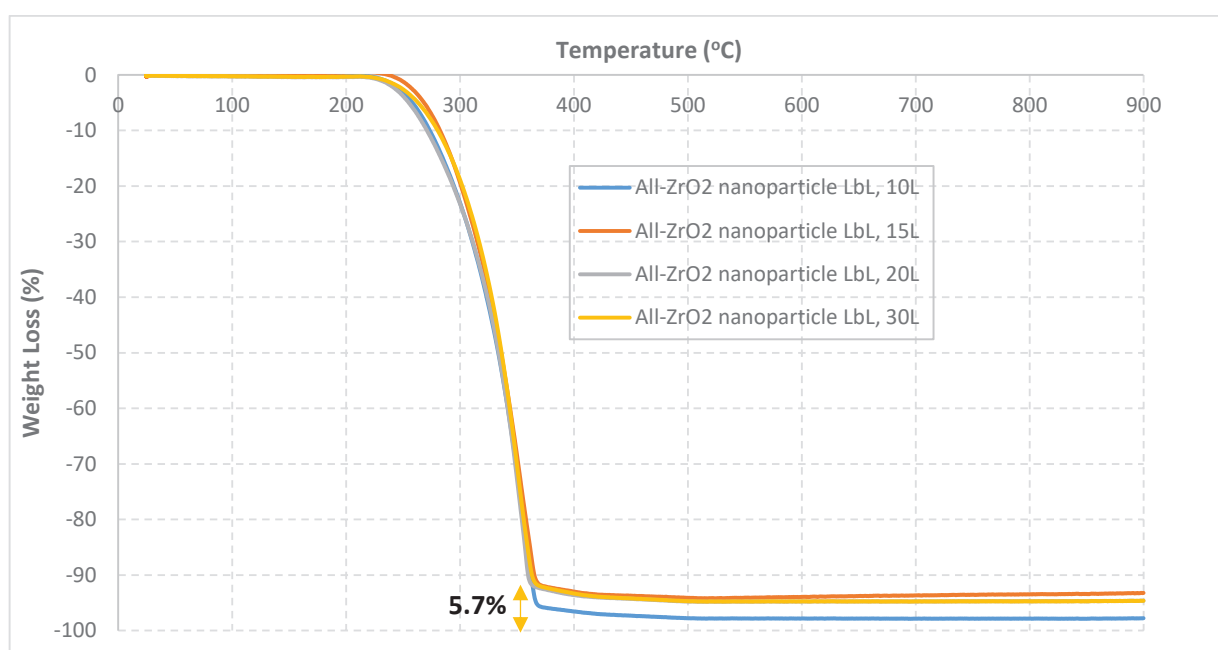


Figure 5-14 – TGA curves of PP-COOH coated with 100% ZrO₂ by LbL method

5.2.3. Effect of the number of layers

Basically, the more layers of (ZrO₂/PAAH) is deposited, the higher content of ZrO₂ is coated on PP-COOH. In this experiment, 3 batches of PP-COOH (4 pieces of 1cm x 1cm dimension) were LbL coated with the increasing number of layers from 10 to 30 layers of (ZrO₂/PAAH). The exact content of ZrO₂ and morphology of ZrO₂-coated PP-COOH were determined by ATR-FTIR, TGA, elemental analysis and SEM, respectively.

By ATR-FTIR (Figure 5-15), one could detect the presence of zirconia on polypropylene, particularly, because of a broad and intense band below 700 cm^{-1} corresponding to inorganic component or zirconia.

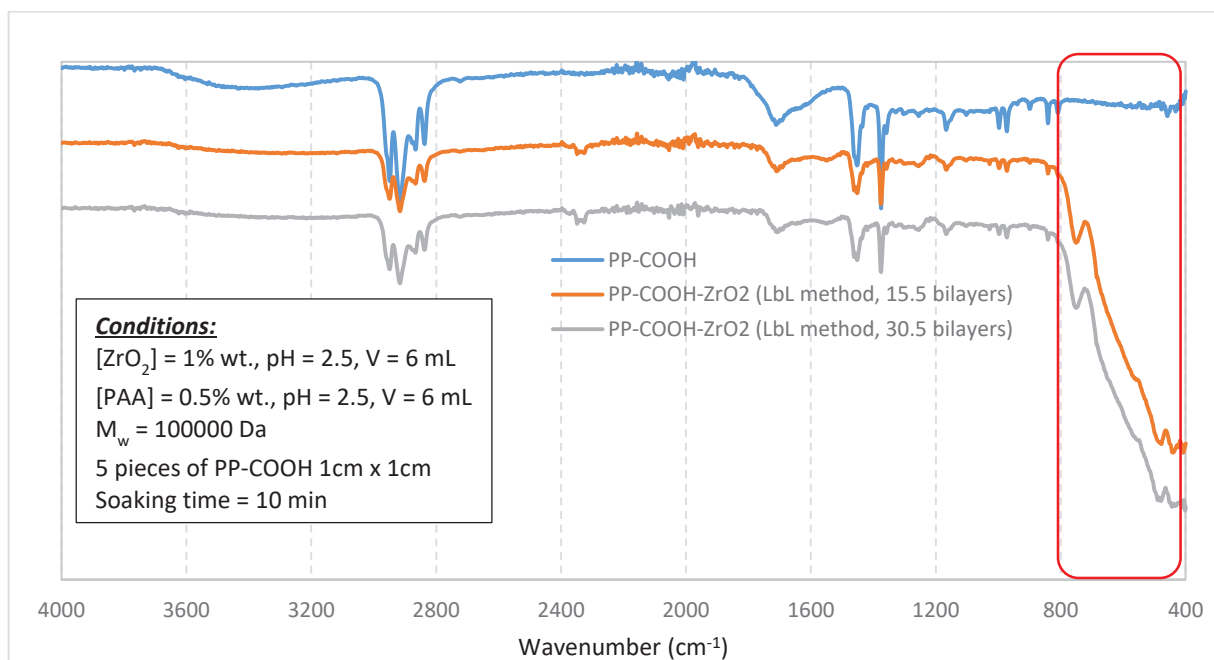


Figure 5-15 – ATR-FTIR spectra of bare PP-COOH, PP-COOH coated with 15 layers and 30 layers of (ZrO₂/PAAH)

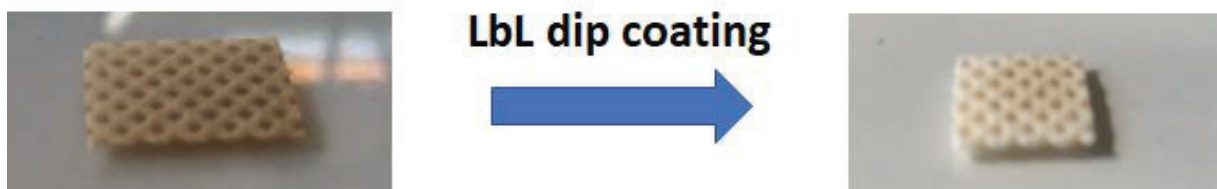


Figure 5-16 – Illustration of PP-COOH (EMPA) textiles before (left) and after (right) LbL coating with nano-ZrO₂. The change of textile's color from brown to white after LbL process has been indicative of the presence of ZrO₂ on textile's fibers

SEM images of samples (Figure 5-17) with increasing layers of (ZrO₂/PAAH) have shown that higher the number of layers were, the more uniform the coating was. Moreover, the results of ZrO₂ content given by TGA and Zr EA matched up quite properly. Especially, with 15 layers of ZrO₂/PAAH, about 20% wt. of zirconia was deposited on the PP-COOH.

Table 5-2. The content of ZrO₂ coated on PP-COOH

# layers	% wt. ZrO ₂ (TGA)	% wt. ZrO ₂ (EA)
10	12.0	10.6
15	20.1	17.3
30	24.5	22.7

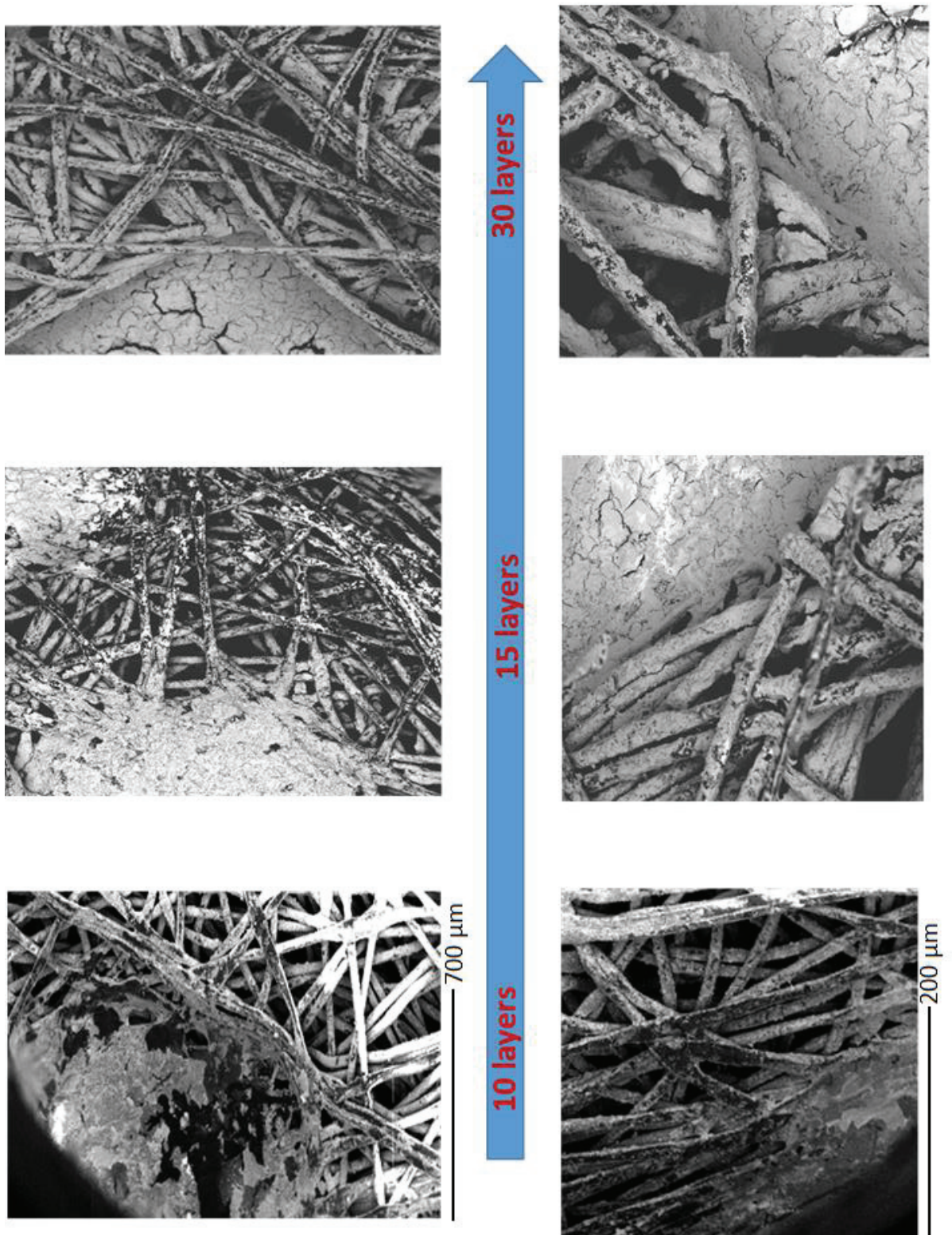


Figure 5-17 – SEM images of PP-COOH coated with 10, 15, and 30 layers of (ZrO₂/PAAH)

As the best compromise in terms of time and reactant consumption, polypropylene coated with 15 layers of (ZrO₂/PAA) was selected for the next investigations when it comes to homogeneity, porosity and coating time.

5.2.4. Effect of molecular weight of polyacrylic acid

As illustrated in Figure 5-18, with the same number of (ZrO₂/PAAH) layers (15 layers), the higher the molecular weight of PAAH was, the higher amount of ZrO₂ on the surface of PP was. A plausible explanation was that longer PAAH chain beared more -COOH and COO⁻ groups, thereby higher amount of ZrO₂ was needed to overcompensate to reverse the surface charge of multilayer coatings. Nevertheless, a decrease of M_w of PAAH from 5000 to 2000 did not cause a further decrease of ZrO₂'s quantity that likely results from the non-electrostatic interactions (hydrophobic interaction, hydrogen bonding) between ZrO₂ and -COOH groups of PAAH.

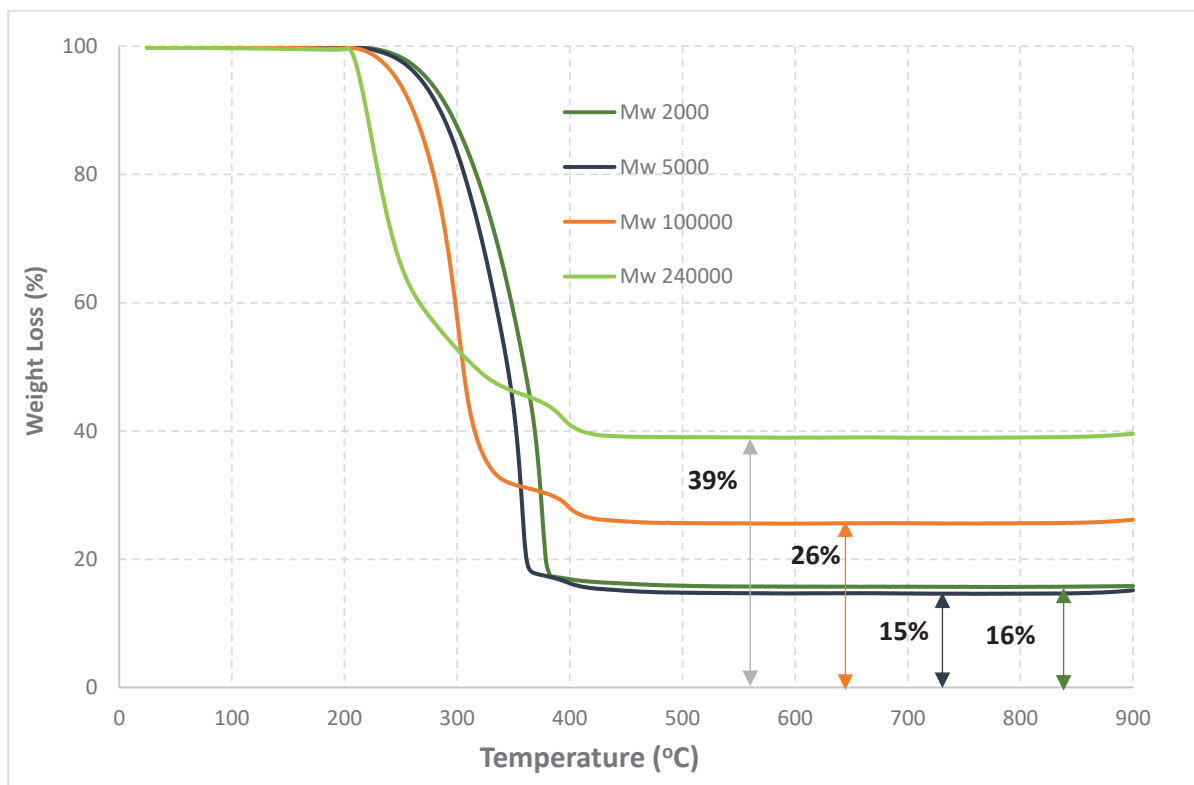


Figure 5-18 – TGA curves of PP-COOH samples coated with (ZrO₂/PAAH) using PAAH solutions with different M_w.

5.2.5. The role of sodium chloride

It has been reported that the activity of salt in the solution significantly impacts on the thickness, roughness, swelling and growth mechanism of the LbL coating process. As illustrated in the Figure 5-19 is the scheme of interaction between polyelectrolytes that has been of particular interest in the studies of Joseph B. Schlenoff et al. [121]

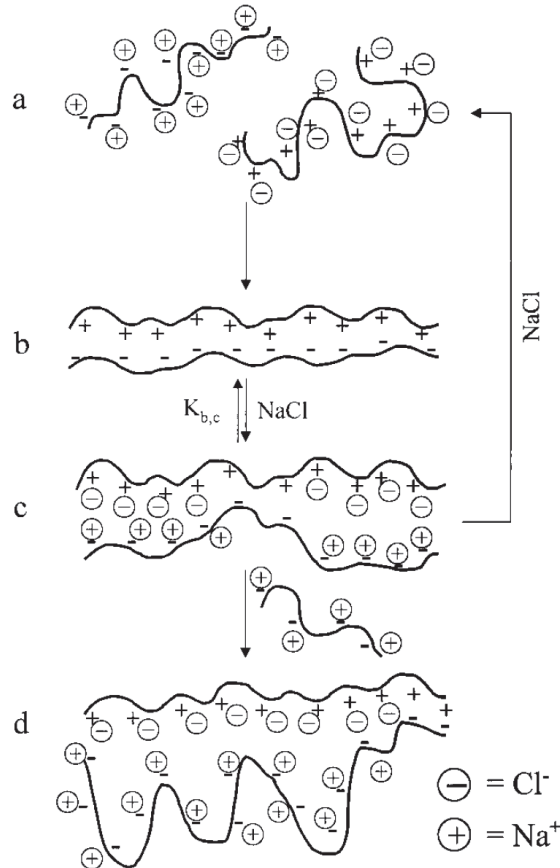


Figure 5-19 – Schematic representation of the LbL build-up process [122]

Throughout their publication, polyelectrolytes (PEs) exist in the solution with charges compensated by counter-ions **(a)**. During the LbL coating process, the polyelectrolytes interact with each other via electrostatic attraction and charge overcompensation without intervention of other small ions (“intrinsic” compensation) **(b)**. If salt is added to the solution, such as NaCl, cation Na^+ and anion Cl^- will compensate PEs’ charges (“extrinsic compensation”) **(c)**. To the larger extent of effect, counter-ions could cause swelling and destroy the LbL assembly into the free PEs coating if the salt’s concentration is sufficiently high. In the presence of subsequent PE, for instance negative PE, the surface charge of LbL coating was reversed and LbL coating process continues to proceed **(d)** [122].

Apparently, much of attention has been paid to morphology of LbL coating, so in this experiment we aimed at acquiring some understanding on the effect of salt in PAAH solution on ZrO_2 's quantity of LbL coating. Specifically, 15-layer coatings were deposited on EMPA substrates using 4 PAAH solutions containing different salt's concentrations at 0, 0.05, 0.5 and 1.5 M, respectively. According to the Figure 5-20, the amount of ZrO_2 did not change substantially ranging from 25 to 28 % wt. Then, it could be concluded that in our condition the presence of salt in the PAAH solution does not impact on the amount of ZrO_2 . However, some other parameters including thickness, roughness and porosity can be affected [121, 123].

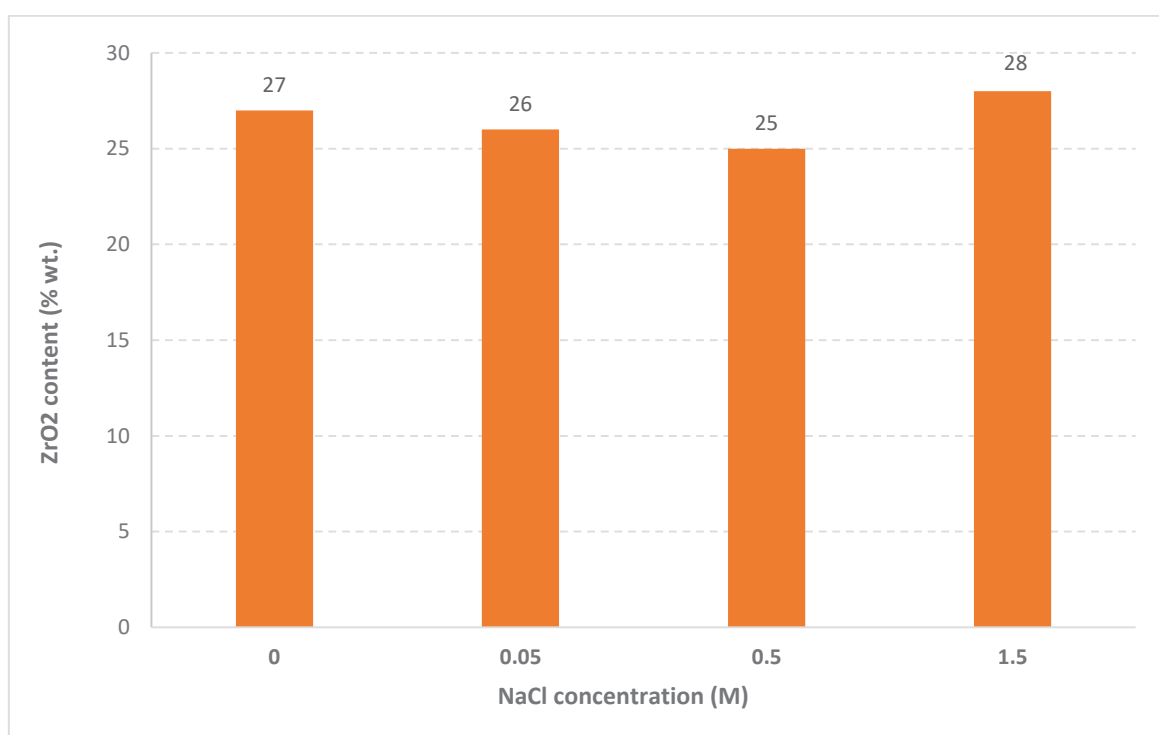


Figure 5-20 – Effect of NaCl in PAAH solution on ZrO_2 content (% wt.). Conditions: $[ZrO_2] = 1\%$ wt. pH 2.5; $[PAAH] = 0.5\%$ wt. pH 2.5 with $[NaCl]$ varied from 0 to 1.5 M

5.2.6. Effect of the ZrO_2 nanosuspension's concentration

It was evident that the concentration of the ZrO_2 nanosuspension influenced the ZrO_2 content within LbL coating (Figure 5-21). When it comes to thermodynamics and kinetics of the process, the higher the concentration of nanosuspension was, the higher the content of ZrO_2 's amount on the substrates was (assuming the same number of layers and soaking time of 15 minutes in ZrO_2 nanosuspension and PAAH solution). Therefore, the amount of

ZrO₂ within LbL coating on the substrate could be easily tuned through varying the concentration of ZrO₂ nanosuspension.

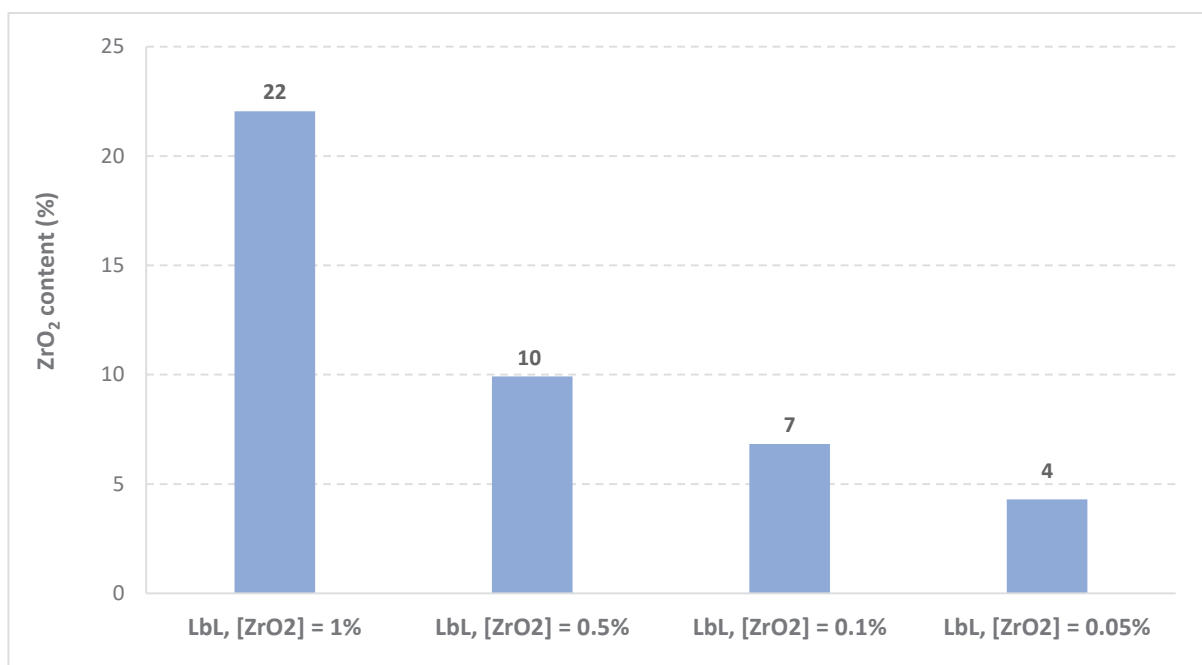


Figure 5-21 – Effect of ZrO₂ nanosuspension's concentration. Conditions: [ZrO₂] = 1 - 5% wt. pH 2.5; [PAAH] = 0.5% wt. pH 2.5 with [NaCl] = 0 M

5.2.7. Stability test of LbL coating on the PP-COOH substrate

Apart from the consideration of the strength of bond between ligands and ZrO₂'s surface, the mechanical and chemical durability of LbL coating on the substrate has been of crucial importance in this thesis because of possible industrial implementation with our industrial partner MORPHOSIS. The final hybrid nanocomposite device (PP-COO-ZrO₂-TOA) was expected to be reusable; in other words, ZrO₂ must not be released into the solution. In order to confirm the stability of the final material, PP-COOH pieces coated with ZrO₂ via LbL dip-coating were subject to the reusability test in which PP-COOH pieces were alternately soaked in HCl 0.5M and the stripping mixture of thiourea 0.2 M and HCl 0.5 M.

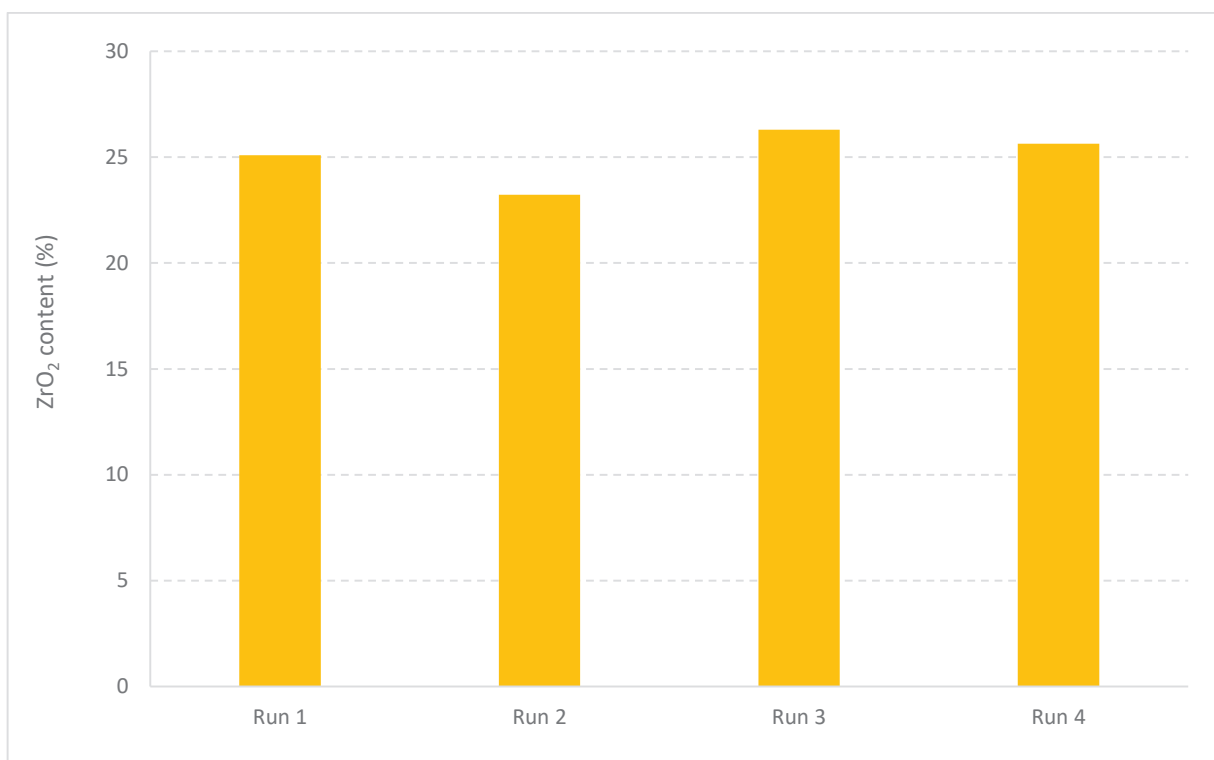


Figure 5-22 – Stability test of ZrO₂ on PP substrate

The results in Figure 5-22 show that the ZrO₂ content was maintained intact (23-26% wt.) in spite of the high acidic concentration and the hazardous agents used. Moreover, one could conclude that other types of interactions, such as covalent bonding, H-bonding get involved in the build-up process of LbL coating [97, 100].

5.2.8. Application of LbL dip-coating to commercial SAATI polypropylene textiles

Thanks to coating procedure using cold plasma of CO₂/C₂H₄ from EMPA laboratory, naked PP textiles from SAATI company (Figure 5-3) were surface-modified with carboxylic group, then ZrO₂ nanoparticles were coated onto these PP-COOH textiles (Figure 5-10). SEM images (Figure 5-23 to Figure 5-25) showed an homogeneous coating of nano-ZrO₂ on both types of textiles, yet some differences could be observed at higher magnification. PP textiles PP 297/35 with higher mesh (opening) appeared to possess thicker and rougher ZrO₂ nanocoating due probably to higher density of ZrO₂ nanoparticles in every voids that led to higher degree of aggregation.

Table 5-3. Specifications of SAATI PP textiles

	PP 106/26	PP 297/35
Mesh (sieve) opening (μm)	106	297
Mesh count (n/cm)	47	20
Thread diameter (μm)	100	200
Thickness (μm)	195	425

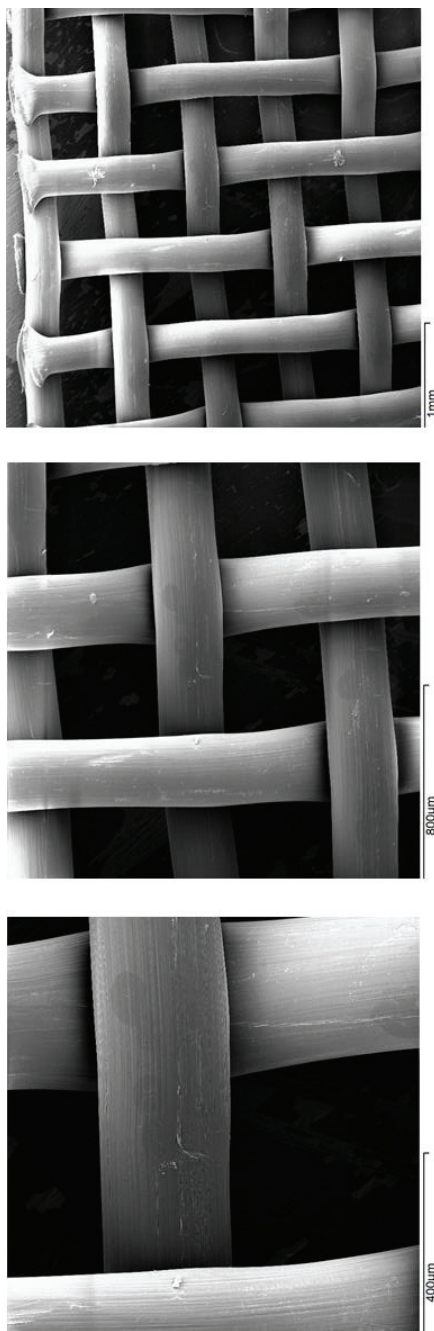


Figure 5-23 – SEM images of naked PP substrates 106/26

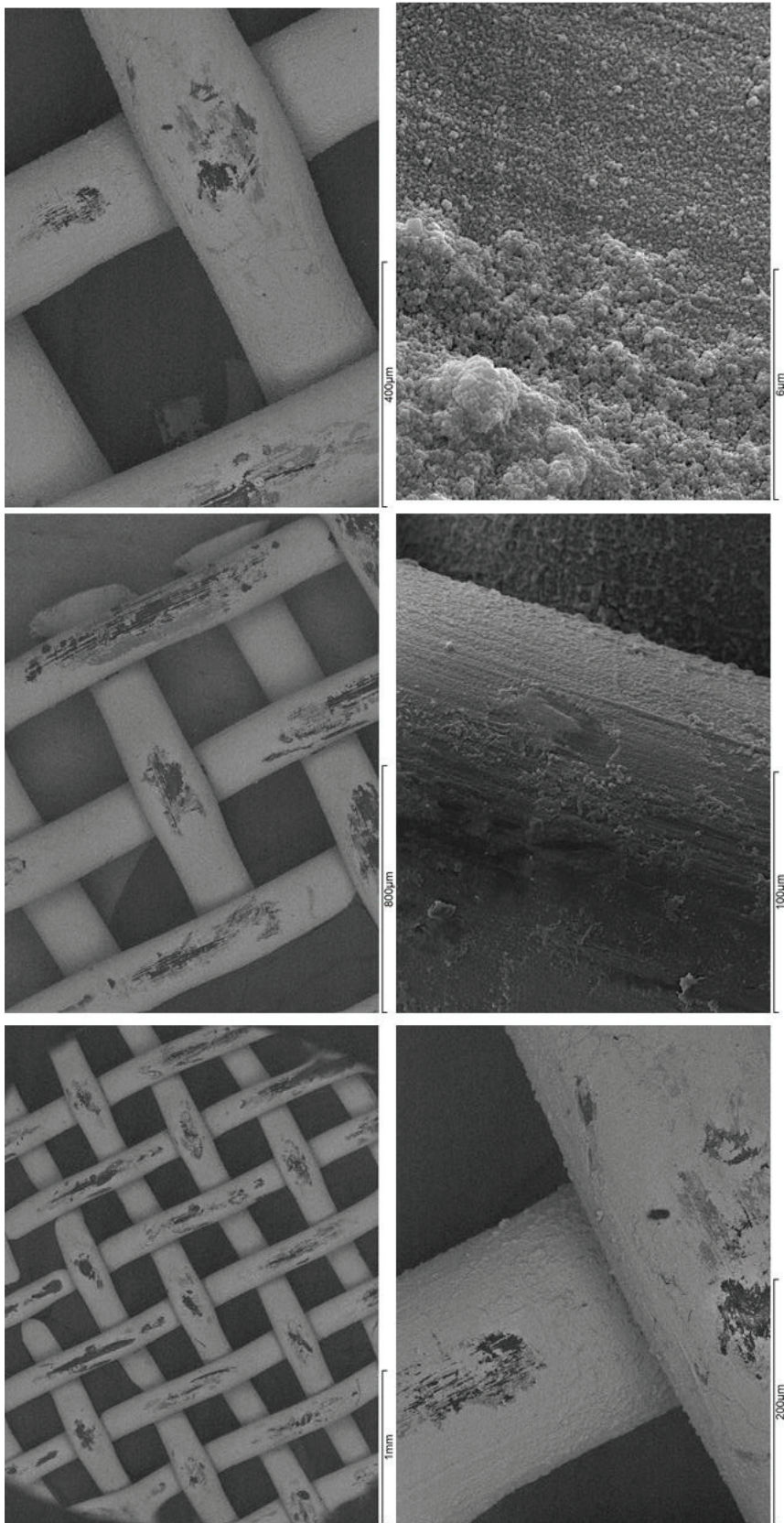


Figure 5-24 – SEM images of ZrO₂-coated PP substrates 106/26

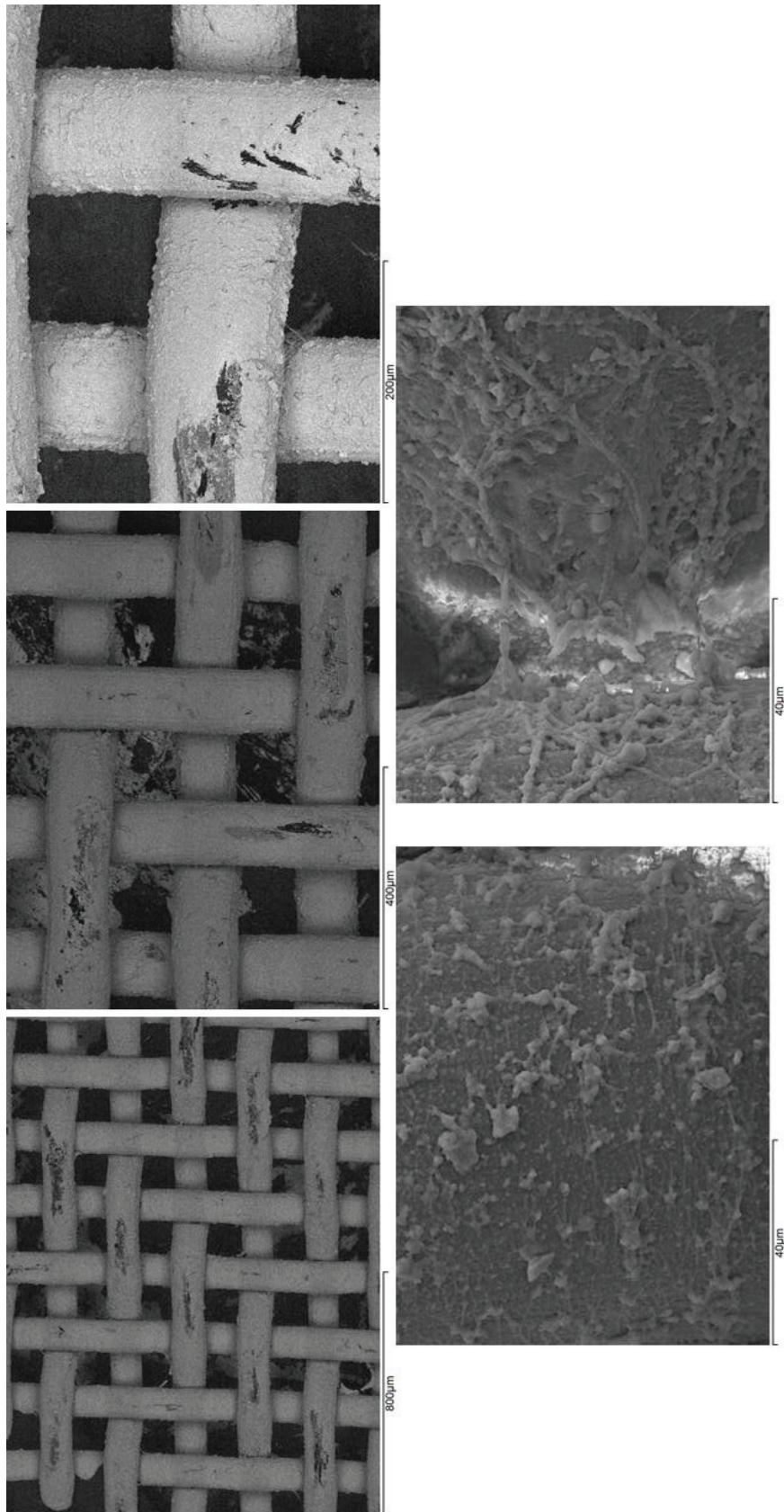


Figure 5-25 – SEM images of ZrO₂-coated PP substrates 297/35

5.2.9. Investigation of adsorption capability of LbL-made PP-COO-ZrO₂ impregnated with TOA

The versatility of the design concept of material in this study was investigated by soaking PP-COO-ZrO₂ textiles with TOA for cycles of adsorption/desorption. At first glance, the selectivity toward Pd over Au and the decreasing tendency in adsorption performance were similar to those of ZrO₂-TOA. Although the adsorption performance was lower than that of ZrO₂-TOA because of lower content of TOA on material's surface, this data demonstrated the potential of the proposed concept of material design.

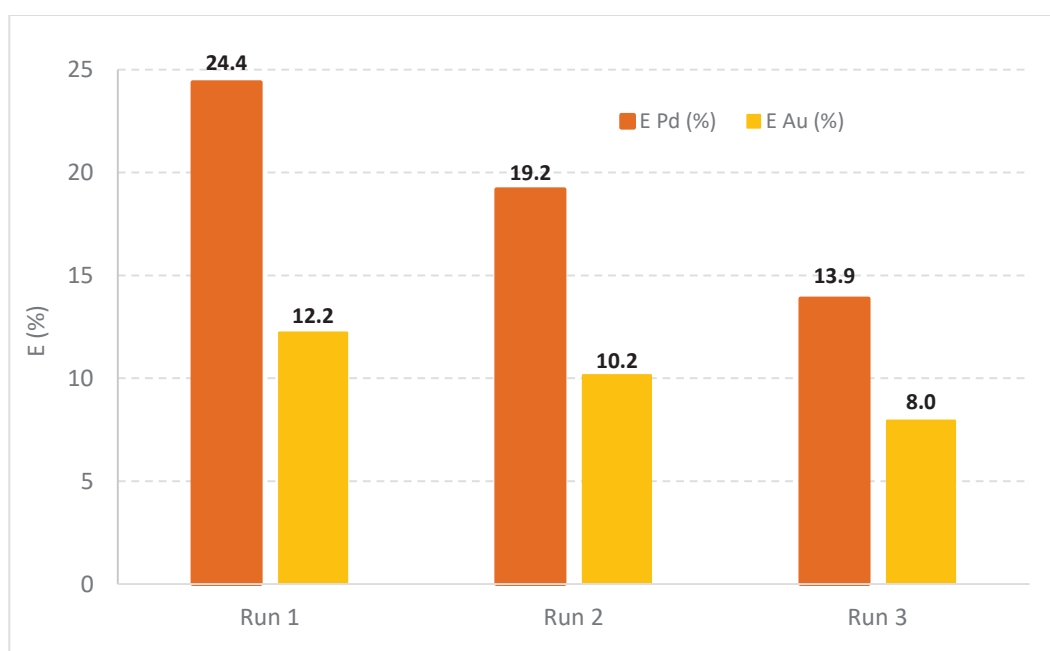


Figure 5-26 – Reusability test of PP-COOH-ZrO₂ impregnated with thioctic acid

The uses of two-step surface modification should be taken in further consideration in this case. According to Figure 5-26, the extraction percentages of the final material being just about 24.4 % for Pd and 12.2 % for Au indicated that surface area of ZrO₂ decreased after coating process. Therefore, from our perspective, it was not worth carrying out the two-step surface modification while the adsorption performance of the final material has not yet been improved.

Summary

Chapter 5 mainly focused on dip-coating processes that could endow the resultant material with properties mentioned in chapter 2. The research for a suitable substrate for nano-ZrO₂ coating was a huge challenge in this part of the study. Most of endeavors were dedicated to seeking an available, and abundant resource of polypropylene with surface modified with carboxylic functional groups. To date, carboxylic surface modification for polypropylene textiles supplied by SAATI company using cold plasma (CO₂/C₂H₄) surface modification technology developed by EMPA has been an acceptable solution.

Basically, the idea of LbL coating process was rooted in the purpose to obtain the homogenous ZrO₂'s coating on PP-COOH textiles and inspired by the LbL method that has been studied since 1997. All concerns in term of parameters were gravitated toward the aim to acquire a malleable, stable, affordable ZrO₂ layer and environmentally friendly process.

The layer-by-layer dip coating has shown its versatility in nano-ZrO₂ coating on PP-COOH that imparted the stability of nano-ZrO₂ layer to the resultant material. Nevertheless, the surface area of nano-ZrO₂ layer on PP-COOH textile has been reduced considerably via this approach, so it is required that further investigation into the porosity of nano-oxides (SiO₂@ZrO₂ core-shell) should be conducted so that two-step surface modification can ensure the adequate density of ligand on resultant material's surface.

GENERAL CONCLUSIONS & PERSPECTIVES

Throughout this study, all work-packages were essentially arranged and conducted into two main parts that turned around the objectives described in chapter 2, including (i) functionalizing nano-ZrO₂'s surface with ligands and (ii) grafting nano-ZrO₂ on polypropylene textiles. Our findings can be summarized as follows:

Functionalizing nano-ZrO₂'s surface with ligands

Diverse ligands, including carboxylic acid (TOA, DODGA) and phosphonic ones (PMIDAA, DEHCOMPA, and DOCMPA) were selected to post-modify nano-ZrO₂'s surface and were screened to figure out the suitable ligand in Pd and Au adsorptions. All these hybrid systems were thoroughly characterized by different methods, such as ATR-FTIR, ³¹P MAS solid-state NMR, and elemental and thermogravimetric analyses to get understanding on the nature of bonding modes of carboxylic and phosphonic groups on nano-ZrO₂'s surface. Among the surface-modified nano-ZrO₂ materials, thioctic acid surface-modified nano-ZrO₂ (ZrO₂-TOA) emerged as a fulfilling material in Pd and Au adsorptions.

In the case of the ZrO₂-TOA with 2.2% wt of TOA, its adsorption capability toward Pd and Au was extensively scrutinized with respect to adsorption isotherm and adsorption kinetics. Thermodynamically, the adsorption process of ZrO₂-TOA follows Langmuir adsorption model and the adsorption capacities of ZrO₂-TOA toward Pd and Au are 6.3 mg/g and 43 mg/g, respectively. Recently, a tendency of employing nanoadsorbents based on thiol and amine surface-modified mesoporous SiO₂ and Fe₃O₄@SiO₂ in the adsorption of Au or/and Pd has emerged and provided comparable performance. For instance, considering pH of the adsorption medium at 1, the adsorption capacities toward Au of thiol group-modified Fe₃O₄@SiO₂ in studies of Q. Xu and R. Roto [73, 74] are approximately 40-50 mg/g. Kinetically, pseudo-second-order model best describes the adsorption behavior of ZrO₂-TOA toward Pd and Au. In terms of the reusability of ZrO₂-TOA, the weak bonding of carboxylic groups to ZrO₂'s surface was observed because of acidic hydrolysis of Zr-O-C. Furthermore, the adsorption experiment using N,N-dioctylcarbamoylphosphonic acid - surface-modified nano-ZrO₂ through successive cycles of adsorption/desorption that showed an unchanged tendency in adsorption performance highlighted the necessity of surface modification of nano-ZrO₂ with phosphonic-containing ligand.

When it comes to improvement of stability of TOA on ZrO₂'s surface, the surface of ZrO₂ was tailored via two steps modification: (i) grafting alendronic acid (AA) on the surface and (ii) amide coupling between -NH₂ groups of AA and -COOH groups of TOA. Two pathways of amide coupling reaction were investigated so that yield, ease of handling, and feasibility were evaluated and compared.

Pathway	Amide coupling via NHS-activated ester of TOA	Amide coupling with TOA mediated by DCC
Yield	~ 86%	
Ease of handling	NHS-TOA was prepared in DMF and reaction was conducted in DMF with ZrO ₂ -AA in 24 hrs. at 25°C. Washing: DMF and C ₂ H ₅ OH	TOA was mixed with DCC in C ₂ H ₅ OH, then DCU precipitate was filtered. The mixture was stirred with ZrO ₂ -AA in 24 hrs. at 25°C. Washing: C ₂ H ₅ OH
Feasibility	NHS-TOA was provided by ICSM Institute.	TOA, DCC were respectively purchased from ACROS Organics TM and Sigma Aldrich.

Demonstrated in chapter 4, the reusability of the resultant materials synthesized via two pathways was improved significantly in the hydrochloric acid matrix. The applicability of these materials to the highly oxidizing conditions, however, should be taken into consideration because disulfide moiety of TOA was unavoidably oxidized by strong oxidants, such as nitric acid or chloro-gold complex that can co-exist in the e-wastewater. From our own perspectives, ligands containing carboxylic and dialkyl-amido-phosphonate groups or amino phosphine groups are recommended as replacements of TOA.

Grafting nano-ZrO₂ on polypropylene textiles

Based on dip-coating method to deposit nano-ZrO₂ polypropylene textiles. Preliminary investigation into the parameters affecting the process was conducted and the conditions are given as follows:

- pH of ZrO₂ ns: 10 (Lotus Synthesis)
- Concentration of ZrO₂ ns: 10% wt. in H₂O
- Volume of ZrO₂ ns: 5 mL
- Type of textile: COOH surface-modified non-woven polypropylene textiles from **CREAT**
- The number of textiles: 5 1cmx1cm pieces/batch
- Temperature = 25°C
- Dipping time = 2^h
- Washing: H₂O/C₂H₅OH

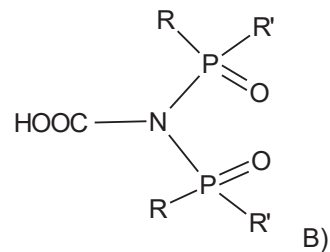
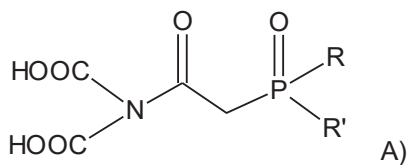
ZrO₂-grafted PP-COOH impregnated with TOA (PP-COOH-ZrO₂) proved to be able to adsorb Pd in the acidic solution (HCl), but the limited mechanical stability and the shortage of CREAT textiles became obstacles to further development.

With the aim to control the content of ZrO₂ and to improve ZrO₂ nano-coating process on the new polypropylene textile which was modified via cold-plasma coating and provided by **EMPA, layer-by-layer method (LbL)** was studied by using successive deposition of acidic ZrO₂ nanosuspension (pH ~2.5, Sigma Aldrich), and polyacrylic acid (PAAH, M_w = 100000). The results showed that this process could be controlled in terms of the quantity of ZrO₂, for instance, the amount of ZrO₂ is around 20-23%wt with 15 layers of (ZrO₂/PAAH).

Incessant seeking an available supplier of Polypropylene textiles brought about the provision of two new types of polypropylene textiles from **SAATI** that were suitable for nano-ZrO₂ coating via LbL method. The smoothness and homogeneity illustrated by SEM depended on the void's size of textile. In other words, the probability of nano-ZrO₂ access to the voids and aggregation affects the quality of the ZrO₂ coating, especially the ZrO₂ coating on PP textile with mesh size of 297 μm is thicker and rougher than that on PP textile with mesh size of 106 μm.

Apparently, the accomplishments thereof pave the way for next studies and developments of two-step surface modification and layer-by-layer coating method to scale up the recovery process, yet fundamental questions still need to be addressed:

- i. Is it possible and practical to design a structure including carboxylic groups for amide coupling and carbamoyl phosphonate or phosphine oxide for precious metals removal?



Schematic representation of the proposed structures: A) amide-phosphonate group-containing and B) amino phosphine group-containing

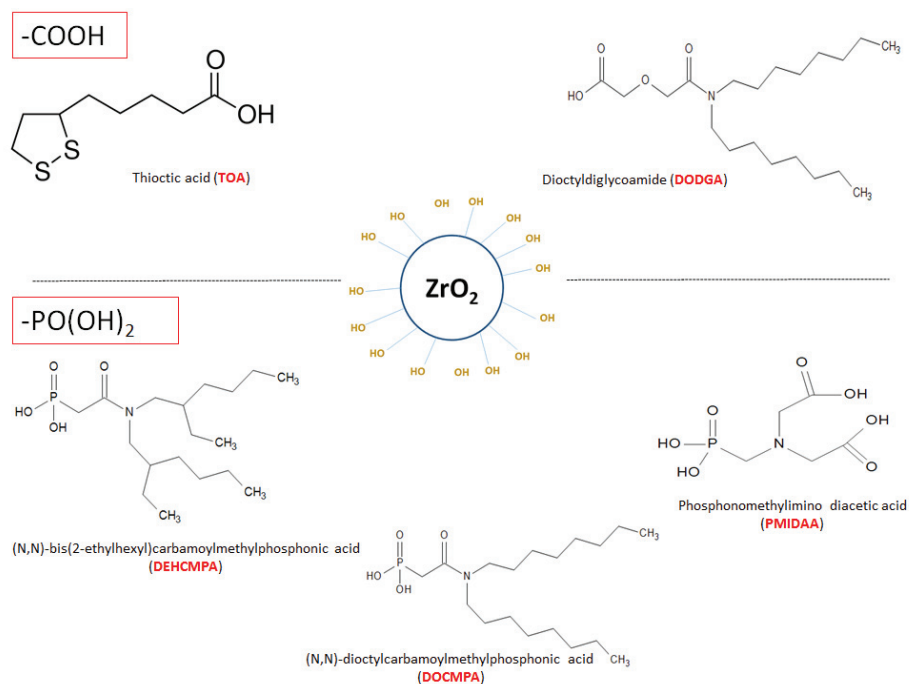
- ii. Can porosity of nano-oxide materials be tuned to obtain the coating with adequate density of M-OH groups for succeeding two-step surface modification?

RÉSUMÉ GENERAL & PERSPECTIVES

Tout au long de cette étude, l'ensemble des travaux a été essentiellement organisé et conduit en deux parties principales en fonction des objectifs décrits au chapitre 2: (i) fonctionnaliser la surface de nano-ZrO₂ avec des ligands complexants pour l'or et le palladium et (ii) greffer les nano-ZrO₂ en surface de textiles de polypropylène (PP). Nos résultats peuvent être résumés comme suit:

Fonctionnaliser la surface de nano-ZrO₂ avec des ligands complexants :

Divers ligands tels que des acides carboxyliques (TOA, DODGA) et phosphoniques (PMIDAA, DEHCPMPA, et DOCMPA) ont été sélectionnés (Figure 1) pour modifier la surface de nano-ZrO₂ et ont été testés pour déterminer les ligands appropriés pour l'adsorption de Pd et d'Au. Tous ces systèmes hybrides ont été caractérisés de façon univoque par différentes méthodes, telles que l'ATR-FTIR, la RMN MAS à l'état solide du ³¹P, l'analyse élémentaire, et l'analyse thermogravimétrique pour comprendre la nature des liaisons des groupes carboxyliques et phosphoniques à la surface des nano-ZrO₂. Parmi les matériaux modifiés, les nano-ZrO₂ modifiés en surface avec l'acide thioctique (ZrO₂-TOA) sont apparus comme étant le matériau le plus efficace pour l'adsorption de Pd et d'Au.

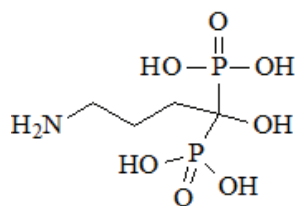


Structures des ligands complexants utilisés dans cette étude

Dans le cas du ZrO_2 modifié en surface avec 2,2 %w de TOA, sa capacité d'adsorption en Pd et en Au a fait l'objet d'une étude approfondie via la description des isothermes et des cinétiques d'adsorption. D'un point de vue thermodynamique, le procédé d'adsorption de ZrO_2 -TOA suit le modèle d'adsorption de Langmuir et les capacités d'adsorption de ZrO_2 -TOA pour le Pd et l'Au sont respectivement de 6,3 mg/g et 43 mg/g. Ces valeurs sont comparables avec celles reportées dans la littérature pour des résines échangeuses d'ions ou des oxydes mésoporeux tels que SiO_2 ou $Fe_3O_4@SiO_2$ modifiés avec des groupements thiol et amine. Par exemple, Q. Xu et R. Roto ont montré que les capacités d'adsorption de l'Au par $Fe_3O_4@SiO_2$ modifié avec des groupements thiol étaient d'environ 40-50 mg/g à pH 1 [73, 74].

En milieu acide et d'un point de vue cinétique, le modèle de pseudo-second ordre a permis de décrire le comportement d'adsorption de ZrO_2 -TOA envers le Pd et l'Au. Généralement, si le transfert de masse et la diffusion dans les pores de nanoparticules sont négligeables, l'adsorption vis-à-vis des molécules cibles sera régit par l'interaction entre les sites actives sur l'adsorbant. Grâce au modèle de pseudo-second ordre, on peut conclure que l'adsorption est régie par l'interaction entre la surface de l'adsorbant et les molécules cibles [72]. Afin de réutiliser le nano-matériau ZrO_2 -TOA, le Pd et l'Au ont été récupérés à l'aide d'un mélange optimisé de thiourea 0.2 M et HCl 0.5 M.

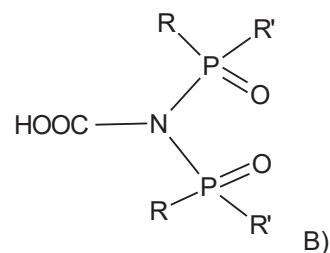
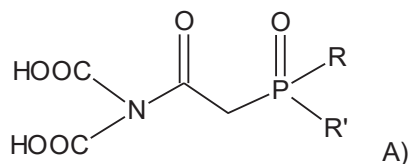
En ce qui concerne la réutilisation du nano-matériau ZrO_2 -TOA, nous nous sommes confrontés à l'instabilité de la liaison des groupements carboxyliques ZrO_2 -OOCR à la surface du matériau en raison de son hydrolyse en milieu fortement acide (réaction acide-base de Brönsted). Cette difficulté a été surmontée via l'utilisation de nano- ZrO_2 modifié en surface par l'acide N,N-dioctylcarbamoylephosphonique lors des cycles successifs d'adsorption/désorption, expériences qui ont mises en évidence la nécessité de modifier la surface du nano- ZrO_2 avec un ligand comportant une fonction plus robuste tel qu'un acide phosphonique. Dans ce contexte, nous avons mis au point un procédé en deux étapes pour améliorer la stabilité du TOA en surface de ZrO_2 : (i) greffage d'acide alendronique (AA) (Figure 2) en surface de ZrO_2 et (ii) réaction de couplage peptique entre les groupements $-NH_2$ de AA et les groupements $-COOH$ de TOA. Une étude paramétrique des paramètres de synthèse a été effectuée afin de comparer les rendements, la facilité et la faisabilité de la réaction (Tableau suivant).



Structure de l'acide alendronique (AA)

Voie	Via un ester de TOA activé par NHS	Via TOA catalysé par DCC
Rendement	~ 86%	
Facilité de manipulation	NHS-TOA a été préparé dans le DMF et la réaction a été réalisée dans le DMF avec ZrO ₂ -AA pendant 24 hrs à 25°C. Lavage: DMF et C ₂ H ₅ OH	TOA a été mélangé avec DCC dans C ₂ H ₅ OH, puis le précipité de DCU a été filtré. Le mélange a été agité avec ZrO ₂ -AA pendant 24 hrs à 25°C. Lavage: C ₂ H ₅ OH
Faisabilité	NHS-TOA fourni par l'ICSM	TOA, DCC ont été achetés respectivement chez ACROS Organics™ et Sigma Aldrich

La réutilisation des nano-matériaux synthétisés via les deux voies a été significativement améliorée dans une solution modèle comportant seulement de l'acide chlorhydrique. L'applicabilité de ces matériaux en conditions hautement oxydantes a été prise en compte lors de l'extraction de Pd et d'Au dans des solutions réelles fournies par la société MORPHOSIS. Ces conditions ont montré que la fonction disulfure du TOA était inévitablement oxydée par des oxydants puissants, tels que l'acide nitrique ou les complexes chlorés de l'or pouvant coexister dans les solutions industrielles. Suite à ces résultats, nous proposons comme alternatives des ligands contenant des groupes carboxyliques et dialkylamido-phosphonates (Figure A suivante) ou des groupes amino phosphine comme substitués de TOA (Figure B suivante).



Molécules alternatives au TOA

Dépôts de nano-ZrO₂ sur des textiles en polypropylène

Les nano-ZrO₂ ont été déposés, soit par dip-coating soit par la technique dite Layer-by-Layer (LbL), sur des textiles en polypropylène (PP) modifié en surface par des fonctions acides carboxyliques. Une difficulté majeure fut de pérenniser le sourcing en PP-COOH suite à l'arrêt d'exploitation de la société qui avait fourni les premiers échantillons de textile. La mise en place d'une collaboration avec le laboratoire du professeur Dirk HEGEMANN de l'EMPA (Swiss Federal Laboratories for Materials Science and Technology, Advanced Fibers, Plasma & Coating team) a permis la fonctionnalisation efficace par plasma de textile issu de la société SAATI.

Le choix du dépôt de nanoparticules de ZrO₂ sur PP-COOH par simple dip-coating (immersion dans la suspension de ZrO₂) s'est avéré efficace lorsque la densité de fonctions acide carboxyliques était importante comme dans le cas du textile fourni par la société CREAT. Une étude paramétrique concernant les paramètres de dépôt a été menée et a permis d'établir les conditions idéales comme suit :

- pH de nano-ZrO₂: 10 (Lotus Synthesis)
- Concentration de nano-ZrO₂ : 10%w dans H₂O
- Volume de nano-ZrO₂: 5 mL
- Type de textile: textiles en polypropylène non-tissé, COOH-modifié (**CREAT**)
- Le nombre de textiles: 5 pièces de 1cmx1cm/lot
- Température = 25°C
- Temps d'immersion = 2^h
- Lavage: H₂O/C₂H₅OH

La surface du nano-coating de ZrO₂ fut ensuite post-fonctionnalisée par l'acide thioctique par simple immersion à nouveau dans une solution de TOA à 10⁻² M. Le nano-composite

final (PP-COOH-ZrO₂-TOA) s'est avéré capable d'adsorber le Pd dans la solution modèle acide (HCl), mais la stabilité mécanique limitée (fibres non tissées) et la pénurie de textiles CREAT sont devenus des obstacles au développement de notre technologie.

Dans le but de contrôler la teneur et d'améliorer le procédé de revêtement de ZrO₂ sur un nouveau support textile en polypropylène modifié en surface par un procédé de plasma-froid par l'EMPA, une méthode couche par couche (LbL) a été également développée. Une autre étude paramétrique a permis de mettre au point les conditions de dépôt par immersions successives dans une nano-suspension de ZrO₂ acide (pH ~ 2.5, Sigma Aldrich) et d'acide polyacrylique (PAAH, M_w = 100 000) :

- Concentration de nano-ZrO₂ : 1%w dans H₂O, pH = 2.5, V = 6 mL
- Concentration de PAAH : 0.5%w dans H₂O, pH = 2.5, V = 6 mL
- M_w = 100000 Da
- Le nombre de textiles: 5 pièces de 1cmx1cm/lot
- Temps d'immersion = 10 min

Les résultats en microscopie et en analyses thermiques ont montré que ce procédé permettait de contrôler finement la quantité de ZrO₂ et d'atteindre d'importantes quantités de ZrO₂ [20-23 %w avec 15 couches de (ZrO₂/PAAH)]. Nous avons également mis au point un dépôt purement inorganique de ZrO₂ par immersion successive de différentes nanosuspensions de ZrO₂ en jouant sur les charges de surfaces des nano-crystallites en fonction du pH de la solution de dépôt.

Nous avons observé sur les clichés MEB que la finesse et l'homogénéité des dépôts dépendaient de la taille de la maille du textile. En d'autres termes, la probabilité d'agrégation de nano-ZrO₂ semblait plus élevée dans un espace restreint, ce qui affecte la qualité du revêtement. Par exemple, le revêtement sur un textile PP possédant une taille de maille de 297 µm est plus épais et plus rugueux que sur un textile PP avec une taille de maille de 106 µm. Il conviendrait dans le futur d'étudier l'impact des caractéristiques de différents textiles (grammage, taille des fils ...) sur la cinétique d'adsorption et les performances du process.

Les résultats précédents ouvrent la voie à de nouveaux développements concernant la modification de surface de nano-crystallites de ZrO₂ en deux étapes ainsi qu'à la méthode

de revêtement couche par couche (LbL) pour améliorer le procédé de recyclage. Mais des questions fondamentales doivent encore être abordées: La porosité des matériaux à base de nano-oxyde peut-elle être ajustée pour obtenir un revêtement avec une densité adéquate de groupements M-OH pour la modification de surface en deux étapes?

REFERENCES

- [1] J.R. Dodson, A.J. Hunt, H.L. Parker, Y. Yang, J.H. Clark, Elemental sustainability: Towards the total recovery of scarce metals, *Chemical Engineering and Processing: Process Intensification*, 51 (2012) 69-78.
- [2] D. Peck, P. Kandachar, E. Tempelman, Critical materials from a product design perspective, *Materials & Design*, 65 (2015) 147-159.
- [3] R. Widmer, H. Oswald-Krapf, D. Sinha-Khetriwal, M. Schnellmann, H. Böni, Global perspectives on e-waste, *Environmental Impact Assessment Review*, 25 (2005) 436-458.
- [4] C. Hagelüken, Recycling the Platinum Group Metals: A European Perspective, *Platinum Metals Review*, 56 (2012) 29-35.
- [5] I. Oswald, A. Reller, E-Waste: A Story of Trashing, Trading, and Valuable Resources, *GAIA - Ecological Perspectives for Science and Society*, 20 (2011) 41-47.
- [6] B.K. Reck, T.E. Graedel, Challenges in Metal Recycling, *Science*, 337 (2012) 690-695.
- [7] S. Zhang, Y. Ding, B. Liu, C.-c. Chang, Supply and demand of some critical metals and present status of their recycling in WEEE, *Waste Management*, 65 (2017) 113-127.
- [8] A. Manhart, International Cooperation for Metal Recycling From Waste Electrical and Electronic Equipment, *Journal of Industrial Ecology*, 15 (2011) 13-30.
- [9] Y. Lu, Z. Xu, Precious metals recovery from waste printed circuit boards: A review for current status and perspective, *Resources, Conservation and Recycling*, 113 (2016) 28-39.
- [10] J. Ruan, Z. Xu, Constructing environment-friendly return road of metals from e-waste: Combination of physical separation technologies, *Renewable and Sustainable Energy Reviews*, 54 (2016) 745-760.
- [11] A. Khaliq, M. Rhamdhani, G. Brooks, S. Masood, Metal Extraction Processes for Electronic Waste and Existing Industrial Routes: A Review and Australian Perspective, *Resources*, 3 (2014) 152.
- [12] A. Kasper, A. Gabriel, E. de Oliveira, N. de Freitas Juchneski, H. Veit, Electronic Waste Recycling, in: H.M. Veit, A. Moura Bernardes (Eds.) *Electronic Waste*, Springer International Publishing, 2015, pp. 87-127.
- [13] Y.J. Park, D.J. Fray, Recovery of high purity precious metals from printed circuit boards, *Journal of hazardous materials*, 164 (2009) 1152-1158.
- [14] J. Cui, L. Zhang, Metallurgical recovery of metals from electronic waste: A review, *Journal of hazardous materials*, 158 (2008) 228-256.
- [15] L. Jing-ying, X. Xiu-li, L. Wen-quan, Thiourea leaching gold and silver from the printed circuit boards of waste mobile phones, *Waste Management*, 32 (2012) 1209-1212.
- [16] V.H. Ha, J.-c. Lee, J. Jeong, H.T. Hai, M.K. Jha, Thiosulfate leaching of gold from waste mobile phones, *Journal of hazardous materials*, 178 (2010) 1115-1119.

- [17] T. Kinoshita, S. Akita, N. Kobayashi, S. Nii, F. Kawaizumi, K. Takahashi, Metal recovery from non-mounted printed wiring boards via hydrometallurgical processing, *Hydrometallurgy*, 69 (2003) 73-79.
- [18] R. Poirot, D. Bourgeois, D. Meyer, Palladium Extraction by a Malonamide Derivative (DMDOHEMA) from Nitrate Media: Extraction Behavior and Third Phase Characterization, *Solvent Extraction and Ion Exchange*, 32 (2014) 529-542.
- [19] A.P. Paiva, G.I. Carvalho, M.C. Costa, A.M.R.d. Costa, C. Nogueira, The Solvent Extraction Performance of N,N'-Dimethyl-N,N'-Dibutylmalonamide Towards Platinum and Palladium in Chloride Media, *Separation Science and Technology*, 49 (2014) 966-973.
- [20] M.C. Costa, A. Assunção, A.M.R. da Costa, C. Nogueira, A.P. Paiva, Liquid-Liquid Extraction of Platinum from Chloride Media by N,N'-Dimethyl-N,N'-Dicyclohexyltetradecylmalonamide, *Solvent Extraction and Ion Exchange*, 31 (2013) 12-23.
- [21] P. Malik, A.P. Paiva, A Novel Solvent Extraction Route for the Mutual Separation of Platinum, Palladium, and Rhodium in Hydrochloric Acid Media, *Solvent Extraction and Ion Exchange*, 28 (2010) 49-72.
- [22] S.A. Ansari, P. Pathak, P.K. Mohapatra, V.K. Manchanda, Chemistry of Diglycolamides: Promising Extractants for Actinide Partitioning, *Chemical Reviews*, 112 (2012) 1751-1772.
- [23] J.A. Shusterman, H.E. Mason, J. Bowers, A. Bruchet, E.C. Uribe, A.B. Kersting, H. Nitsche, Development and Testing of Diglycolamide Functionalized Mesoporous Silica for Sorption of Trivalent Actinides and Lanthanides, *ACS applied materials & interfaces*, 7 (2015) 20591-20599.
- [24] P. Malik, A. Paula Paiva, Solvent Extraction of Rhodium from Chloride Media by N,N'-Dimethyl-N,N'-Diphenyltetradecylmalonamide, *Solvent Extraction and Ion Exchange*, 26 (2008) 25-40.
- [25] P. Malik, A.P. Paiva, Solvent Extraction Studies for Platinum Recovery from Chloride Media by A N,N'- Tetrasubstituted Malonamide Derivative, *Solvent Extraction and Ion Exchange*, 27 (2009) 36-49.
- [26] G.H. Rizvi, J.N. Mathur, M.S. Murali, R.H. Iyer, Recovery of Fission Product Palladium from Acidic High Level Waste Solutions, *Separation Science and Technology*, 31 (1996) 1805-1816.
- [27] A.P. Paiva, G.I. Carvalho, M.C. Costa, A.M.R. da Costa, C. Nogueira, Recovery of Platinum and Palladium from Chloride Solutions by a Thiodiglycolamide Derivative, *Solvent Extraction and Ion Exchange*, 32 (2014) 78-94.
- [28] A. Das, R. Ruhela, A.K. Singh, R.C. Hubli, Evaluation of novel ligand dithiodiglycolamide (DTDGA) for separation and recovery of palladium from simulated spent catalyst dissolver solution, *Separation and Purification Technology*, 125 (2014) 151-155.

- [29] R. Ruhela, J.N. Sharma, B.S. Tomar, M.S. Murali, R.C. Hubli, A.K. Suri, Dithiodiglycolamide: novel ligand with highest selectivity and extractability for palladium, *Tetrahedron Letters*, 52 (2011) 3929-3932.
- [30] A.B. Kanagare, K.K. Singh, M. Kumar, M. Yadav, R. Ruhela, A.K. Singh, A. Kumar, V.S. Shinde, DTDGA-Impregnated XAD-16 Beads for Separation of Gold from Electronic Waste Solutions, *Industrial & Engineering Chemistry Research*, 55 (2016) 12644-12654.
- [31] C. Fontàs, E. Anticó, F. Vocanson, R. Lamartine, P. Seta, Efficient thiocalix[4]arenes for the extraction and separation of Au(III), Pd(II) and Pt(IV) metal ions from acidic media incorporated in membranes and solid phases, *Separation and Purification Technology*, 54 (2007) 322-328.
- [32] M. Yamada, M. Rajiv Gandhi, Y. Kondo, F. Hamada, Synthesis and characterisation of p-diethylaminomethylthiocalix[4]arene for selective recovery of platinum from automotive catalyst residue, *Supramolecular Chemistry*, 26 (2014) 620-630.
- [33] S. Singh, K.C. Barick, D. Bahadur, Functional Oxide Nanomaterials and Nanocomposites for the Removal of Heavy Metals and Dyes, *Nanomaterials and Nanotechnology*, (2013).
- [34] D. Dupont, W. Brullot, M. Bloemen, T. Verbiest, K. Binnemans, Selective uptake of rare earths from aqueous solutions by EDTA-functionalized magnetic and nonmagnetic nanoparticles, *ACS applied materials & interfaces*, 6 (2014) 4980-4988.
- [35] J. Veliscek-Carolan, K.A. Jolliffe, T.L. Hanley, Selective sorption of actinides by titania nanoparticles covalently functionalized with simple organic ligands, *ACS applied materials & interfaces*, 5 (2013) 11984-11994.
- [36] N. Das, Recovery of precious metals through biosorption — A review, *Hydrometallurgy*, 103 (2010) 180-189.
- [37] A. Nakajima, Accumulation of gold by microorganisms, *World Journal of Microbiology and Biotechnology*, 19 (2003) 369-374.
- [38] D. Parajuli, C.R. Adhikari, M. Kuriyama, H. Kawakita, K. Ohto, K. Inoue, M. Funaoka, Selective Recovery of Gold by Novel Lignin-Based Adsorption Gels, *Industrial & Engineering Chemistry Research*, 45 (2006) 8-14.
- [39] D. Parajuli, H. Kawakita, K. Inoue, M. Funaoka, Recovery of Gold(III), Palladium(II), and Platinum(IV) by Aminated Lignin Derivatives, *Industrial & Engineering Chemistry Research*, 45 (2006) 6405-6412.
- [40] M. Gurung, B.B. Adhikari, S. Alam, H. Kawakita, K. Ohto, K. Inoue, Persimmon tannin-based new sorption material for resource recycling and recovery of precious metals, *Chemical Engineering Journal*, 228 (2013) 405-414.
- [41] M. Gurung, B.B. Adhikari, H. Kawakita, K. Ohto, K. Inoue, S. Alam, Selective Recovery of Precious Metals from Acidic Leach Liquor of Circuit Boards of Spent Mobile Phones Using Chemically Modified Persimmon Tannin Gel, *Industrial & Engineering Chemistry Research*, 51 (2012) 11901-11913.

- [42] Y. Xiong, C.R. Adhikari, H. Kawakita, K. Ohto, K. Inoue, H. Harada, Selective recovery of precious metals by persimmon waste chemically modified with dimethylamine, *Bioresource Technology*, 100 (2009) 4083-4089.
- [43] M. Gurung, B.B. Adhikari, H. Kawakita, K. Ohto, K. Inoue, S. Alam, Recovery of Au(III) by using low cost adsorbent prepared from persimmon tannin extract, *Chemical Engineering Journal*, 174 (2011) 556-563.
- [44] M. Gurung, B.B. Adhikari, H. Kawakita, K. Ohto, K. Inoue, S. Alam, Recovery of gold and silver from spent mobile phones by means of acidothiourea leaching followed by adsorption using biosorbent prepared from persimmon tannin, *Hydrometallurgy*, 133 (2013) 84-93.
- [45] S.Y. Bratskaya, A.Y. Ustinov, Y.A. Azarova, A.V. Pestov, Thiocarbamoyl chitosan: Synthesis, characterization and sorption of Au(III), Pt(IV), and Pd(II), *Carbohydrate Polymers*, 85 (2011) 854-861.
- [46] M.E. Romero-González, C.J. Williams, P.H.E. Gardiner, S.J. Gurman, S. Habesh, Spectroscopic Studies of the Biosorption of Gold(III) by Dealginated Seaweed Waste, *Environmental science & technology*, 37 (2003) 4163-4169.
- [47] A.V. Pethkar, S.K. Kulkarni, K.M. Paknikar, Comparative studies on metal biosorption by two strains of *Cladosporium cladosporioides*, *Bioresource Technology*, 80 (2001) 211-215.
- [48] I. Savvaidis, Recovery of gold from thiourea solutions using microorganisms, *Biometals*, 11 (1998) 145-151.
- [49] I. de Vargas, E. Macaskie Lynne, E. Guibal, Biosorption of palladium and platinum by sulfate-reducing bacteria, *Journal of Chemical Technology & Biotechnology*, 79 (2003) 49-56.
- [50] V.N. Losev, E.V. Elzufiev, O.V. Buyko, A.K. Trofimchuk, R.V. Horda, O.V. Legenchuk, Extraction of precious metals from industrial solutions by the pine (*Pinus sylvestris*) sawdust-based biosorbent modified with thiourea groups, *Hydrometallurgy*, 176 (2018) 118-128.
- [51] A. Sari, D. Mendil, M. Tuzen, M. Soylak, Biosorption of palladium(II) from aqueous solution by moss (*Racomitrium lanuginosum*) biomass: Equilibrium, kinetic and thermodynamic studies, *Journal of hazardous materials*, 162 (2009) 874-879.
- [52] M. Ruiz, A.M. Sastre, E. Guibal, Palladium sorption on glutaraldehyde-crosslinked chitosan, *Reactive and Functional Polymers*, 45 (2000) 155-173.
- [53] D. Parajuli, H. Kawakita, K. Inoue, K. Ohto, K. Kajiyama, Persimmon peel gel for the selective recovery of gold, *Hydrometallurgy*, 87 (2007) 133-139.
- [54] Z. Hubicki, A. Wołowicz, Adsorption of palladium(II) from chloride solutions on Amberlyst A 29 and Amberlyst A 21 resins, *Hydrometallurgy*, 96 (2009) 159-165.

- [55] Z. Hubicki, A. Wołowicz, M. Wawrzekiewicz, Application of commercially available anion exchange resins for preconcentration of palladium(II) complexes from chloride–nitrate solutions, *Chemical Engineering Journal*, 150 (2009) 96-103.
- [56] N.V. Nguyen, J. Jeong, M.K. Jha, J.-c. Lee, K. Osseo-Asare, Comparative studies on the adsorption of Au(III) from waste rinse water of semiconductor industry using various resins, *Hydrometallurgy*, 105 (2010) 161-167.
- [57] Z. Hubicki, M. Leszczyńska, B. Łodyga, A. Łodyga, Palladium(II) removal from chloride and chloride–nitrate solutions by chelating ion-exchangers containing N-donor atoms, *Minerals Engineering*, 19 (2006) 1341-1347.
- [58] P. Liu, G.-f. Liu, D.-l. Chen, S.-y. Cheng, N. Tang, Adsorption properties of Ag(I), Au(III), Pd(II) and Pt(IV) ions on commercial 717 anion-exchange resin, *Transactions of Nonferrous Metals Society of China*, 19 (2009) 1509-1513.
- [59] S.H. Lee, H. Chung, Ion Exchange Characteristics of Palladium and Ruthenium from a Simulated Radioactive Liquid Waste, *Separation Science and Technology*, 38 (2003) 3459-3472.
- [60] S.H. Lee, H. Chung, Ion Exchange Characteristics of Palladium and Rhodium from a Simulated Radioactive Liquid Waste, *Journal of Nuclear Science and Technology*, 37 (2000) 281-287.
- [61] M. Yamada, M.R. Gandhi, Y. Kondo, K. Haga, A. Shibayama, F. Hamada, Selective sorption of palladium by thiocarbamoyl-substituted thiacalix[n]arene derivatives immobilized on amberlite resin: application to leach liquors of automotive catalysts, *RSC Advances*, 5 (2015) 60506-60517.
- [62] T. Kimuro, M.R. Gandhi, U.M.R. Kunda, F. Hamada, M. Yamada, Palladium(II) sorption of a diethylphosphate-modified thiacalix[6]arene immobilized on amberlite resin, *Hydrometallurgy*, 171 (2017) 254-261.
- [63] M. Yamada, M. Rajiv Gandhi, U.M.R. Kunda, F. Hamada, Thiacalixarenes: emergent supramolecules in crystal engineering and molecular recognition, *Journal of Inclusion Phenomena and Macrocyclic Chemistry*, 85 (2016) 1-18.
- [64] J.M. Sánchez, M. Hidalgo, V. Salvadó, A Comparison of the Separation Behavior of Some New Coordinating Resins and Commercial Quaternary Ammonium Resins with Reference to Their Separation of Gold(III) and Palladium(II) in Hydrochloric Acid Media, *Solvent Extraction and Ion Exchange*, 22 (2004) 285-303.
- [65] A. Muşină, V. Bocokić, V. Lavric, S. van Zutphen, Phosphorus-Based Polymers for Selective Capture of Platinum Group Metals, *Industrial & Engineering Chemistry Research*, 53 (2014) 13362-13369.
- [66] A. Musina, S. van Zutphen, V. Lavric, Late transition metal recovery from a silver nitrate electrolyte using a phosphine-oxide bearing scavenger, *New Journal of Chemistry*, (2018).

- [67] J.M. Sánchez, M. Hidalgo, V. Salvadó, The selective adsorption of gold (III) and palladium (II) on new phosphine sulphide-type chelating polymers bearing different spacer arms: Equilibrium and kinetic characterisation, *Reactive and Functional Polymers*, 46 (2001) 283-291.
- [68] J.M. Sánchez, M. Hidalgo, V. Salvadó, Synthesised phosphine sulphide-type macroporous polymers for the preconcentration and separation of gold (III) and palladium (II) in a column system, *Reactive and Functional Polymers*, 49 (2001) 215-224.
- [69] T.A. Kurniawan, M.E.T. Sillanpää, M. Sillanpää, Nanoadsorbents for Remediation of Aquatic Environment: Local and Practical Solutions for Global Water Pollution Problems, *Critical Reviews in Environmental Science and Technology*, 42 (2012) 1233-1295.
- [70] S. Mallakpour, M. Madani, A review of current coupling agents for modification of metal oxide nanoparticles, *Progress in Organic Coatings*, 86 (2015) 194-207.
- [71] P. Homchuen, R.D. Alorro, N. Hiroyoshi, R. Sato, H. Kijitani, M. Ito, A Study on the Utilization of Magnetite for the Recovery of Platinum Group Metals from Chloride Solution, *Mineral Processing and Extractive Metallurgy Review*, 37 (2016) 246-254.
- [72] N.F. Abd Razak, M. Shamsuddin, S.L. Lee, Adsorption kinetics and thermodynamics studies of gold(III) ions using thioctic acid functionalized silica coated magnetite nanoparticles, *Chemical Engineering Research and Design*, 130 (2018) 18-28.
- [73] R. Roto, Y. Yusran, A. Kuncaka, Magnetic adsorbent of Fe₃O₄@SiO₂ core-shell nanoparticles modified with thiol group for chloroauric ion adsorption, *Applied Surface Science*, 377 (2016) 30-36.
- [74] Y. Zhang, Q. Xu, S. Zhang, J. Liu, J. Zhou, H. Xu, H. Xiao, J. Li, Preparation of thiol-modified Fe₃O₄@SiO₂ nanoparticles and their application for gold recovery from dilute solution, *Separation and Purification Technology*, 116 (2013) 391-397.
- [75] T. Kang, Y. Park, K. Choi, J.S. Lee, J. Yi, Ordered mesoporous silica (SBA-15) derivatized with imidazole-containing functionalities as a selective adsorbent of precious metal ions, *Journal of Materials Chemistry*, 14 (2004) 1043-1049.
- [76] K. Lam, C. Fong, K. Yeung, Separation of precious metals using selective mesoporous adsorbents, *Gold Bull*, 40 (2007) 192-198.
- [77] S.P. Pujari, L. Scheres, A.T.M. Marcelis, H. Zuilhof, Covalent Surface Modification of Oxide Surfaces, *Angewandte Chemie International Edition*, 53 (2014) 6322-6356.
- [78] P.H. Mutin, G. Guerrero, A. Vioux, Organic-inorganic hybrid materials based on organophosphorus coupling molecules: from metal phosphonates to surface modification of oxides, *Comptes Rendus Chimie*, 6 (2003) 1153-1164.
- [79] M.R. Awual, T. Yaita, S.A. El-Safty, H. Shiwaku, Y. Okamoto, S. Suzuki, Investigation of palladium(II) detection and recovery using ligand modified conjugate adsorbent, *Chemical Engineering Journal*, 222 (2013) 172-179.

- [80] Y.-P. Zhu, T.-Y. Ma, Y.-L. Liu, T.-Z. Ren, Z.-Y. Yuan, Metal phosphonate hybrid materials: from densely layered to hierarchically nanoporous structures, *Inorganic Chemistry Frontiers*, 1 (2014) 360-383.
- [81] C.S. Pauly, A.-C. Genix, J.G. Alauzun, M. Sztucki, J. Oberdisse, P. Hubert Mutin, Surface modification of alumina-coated silica nanoparticles in aqueous sols with phosphonic acids and impact on nanoparticle interactions, *Physical Chemistry Chemical Physics*, 17 (2015) 19173-19182.
- [82] A.K. Bhattacharya, G. Thyagarajan, Michaelis-Arbuzov rearrangement, *Chemical Reviews*, 81 (1981) 415-430.
- [83] N. Bou Orm, Y. Dkhissi, S. Daniele, L. Djakovitch, Synthesis of 2-(arylamino)ethyl phosphonic acids via the aza-Michael addition on diethyl vinylphosphonate, *Tetrahedron*, 69 (2013) 115-121.
- [84] G.A. Seisenbaeva, I.V. Melnyk, N. Hedin, Y. Chen, P. Eriksson, E. Trzop, Y.L. Zub, V.G. Kessler, Molecular insight into the mode-of-action of phosphonate monolayers as active functions of hybrid metal oxide adsorbents. Case study in sequestration of rare earth elements, *RSC Advances*, 5 (2015) 24575-24585.
- [85] M. Hood, M. Mari, R. Muñoz-Espí, Synthetic Strategies in the Preparation of Polymer/Inorganic Hybrid Nanoparticles, *Materials*, 7 (2014) 4057.
- [86] S. Sarkar, E. Guibal, F. Quignard, A.K. SenGupta, Polymer-supported metals and metal oxide nanoparticles: synthesis, characterization, and applications, *J Nanopart Res*, 14 (2012) 1-24.
- [87] M.L.P. Dalida, A.F.V. Mariano, C.M. Futralan, C.-C. Kan, W.-C. Tsai, M.-W. Wan, Adsorptive removal of Cu(II) from aqueous solutions using non-crosslinked and crosslinked chitosan-coated bentonite beads, *Desalination*, 275 (2011) 154-159.
- [88] Q. Xu, P. Yin, G. Zhao, G. Yin, R. Qu, Synthesis and characterization of silica gel microspheres encapsulated by salicylic acid functionalized polystyrene and its adsorption of transition metal ions from aqueous solutions, in: *Open Chemistry*, 2010, pp. 214.
- [89] G.N. Manju, K. Anoop Krishnan, V.P. Vinod, T.S. Anirudhan, An investigation into the sorption of heavy metals from wastewaters by polyacrylamide-grafted iron(III) oxide, *Journal of hazardous materials*, 91 (2002) 221-238.
- [90] A.E. Chávez-Guajardo, J.C. Medina-Llamas, L. Maqueira, C.A.S. Andrade, K.G.B. Alves, C.P. de Melo, Efficient removal of Cr (VI) and Cu (II) ions from aqueous media by use of polypyrrole/maghemite and polyaniline/maghemite magnetic nanocomposites, *Chemical Engineering Journal*, 281 (2015) 826-836.
- [91] L.H. Cumbal, A.K. SenGupta, Preparation and Characterization of Magnetically Active Dual-Zone Sorbent, *Industrial & Engineering Chemistry Research*, 44 (2005) 600-605.

- [92] M. Hua, Y. Jiang, B. Wu, B. Pan, X. Zhao, Q. Zhang, Fabrication of a New Hydrous Zr(IV) Oxide-Based Nanocomposite for Enhanced Pb(II) and Cd(II) Removal from Waters, *ACS applied materials & interfaces*, 5 (2013) 12135-12142.
- [93] E. Repo, J.K. Warchoń, A. Bhatnagar, M. Sillanpää, Heavy metals adsorption by novel EDTA-modified chitosan–silica hybrid materials, *Journal of Colloid and Interface Science*, 358 (2011) 261-267.
- [94] J. Pérez, L. Toledo, C.H. Campos, B.L. Rivas, J. Yañez, B.F. Urbano, Organic–inorganic interpenetrated hybrids based on cationic polymer and hydrous zirconium oxide for arsenate and arsenite removal, *Chemical Engineering Journal*, 287 (2016) 744-754.
- [95] G. de Falco, M. Barczak, F. Montagnaro, T.J. Bandosz, A New Generation of Surface Active Carbon Textiles As Reactive Adsorbents of Indoor Formaldehyde, *ACS applied materials & interfaces*, 10 (2018) 8066-8076.
- [96] J. Dobrzyńska, R. Dobrowolski, R. Olchowski, E. Zięba, M. Barczak, Palladium adsorption and preconcentration onto thiol- and amine-functionalized mesoporous silicas with respect to analytical applications, *Microporous and Mesoporous Materials*, 274 (2019) 127-137.
- [97] N. Joseph, P. Ahmadiannamini, R. Hoogenboom, I.F.J. Vankelecom, Layer-by-layer preparation of polyelectrolyte multilayer membranes for separation, *Polymer Chemistry*, 5 (2014) 1817-1831.
- [98] H. Lee, R. Mensire, R.E. Cohen, M.F. Rubner, Strategies for Hydrogen Bonding Based Layer-by-Layer Assembly of Poly(vinyl alcohol) with Weak Polyacids, *Macromolecules*, 45 (2012) 347-355.
- [99] E. Pál, D. Sebök, V. Hornok, I. Dékány, Structural, optical, and adsorption properties of ZnO₂/poly(acrylic acid) hybrid thin porous films prepared by ionic strength controlled layer-by-layer method, *Journal of Colloid and Interface Science*, 332 (2009) 173-182.
- [100] K. Vermöhlen, H. Lewandowski, H.D. Narres, M.J. Schwuger, Adsorption of polyelectrolytes onto oxides — the influence of ionic strength, molar mass, and Ca²⁺ ions, *Colloids and Surfaces A: Physicochemical and Engineering Aspects*, 163 (2000) 45-53.
- [101] H.J. Choi, K.-C. Park, H. Lee, T. Crouzier, M.F. Rubner, R.E. Cohen, G. Barbastathis, G.H. McKinley, Superoleophilic Titania Nanoparticle Coatings with Fast Fingerprint Decomposition and High Transparency, *ACS applied materials & interfaces*, 9 (2017) 8354-8360.
- [102] G. Haberhauer, M.H. Gerzabek, Drift and transmission FT-IR spectroscopy of forest soils: an approach to determine decomposition processes of forest litter, *Vibrational Spectroscopy*, 19 (1999) 413-417.
- [103] M.M. Beasley, E.J. Bartelink, L. Taylor, R.M. Miller, Comparison of transmission FTIR, ATR, and DRIFT spectra: implications for assessment of bone bioapatite diagenesis, *Journal of Archaeological Science*, 46 (2014) 16-22.

- [104] V. Lafond, C. Gervais, J. Maquet, D. Prochnow, F. Babonneau, P.H. Mutin, 17O MAS NMR Study of the Bonding Mode of Phosphonate Coupling Molecules in a Titanium Oxo-Alkoxo-Phosphonate and in Titania-Based Hybrid Materials, *Chemistry of Materials*, 15 (2003) 4098-4103.
- [105] F. Brodard-Severac, G. Guerrero, J. Maquet, P. Florian, C. Gervais, P.H. Mutin, High-Field 17O MAS NMR Investigation of Phosphonic Acid Monolayers on Titania, *Chemistry of Materials*, 20 (2008) 5191-5196.
- [106] W. Gao, L. Dickinson, C. Grozinger, F.G. Morin, L. Reven, Self-Assembled Monolayers of Alkylphosphonic Acids on Metal Oxides, *Langmuir*, 12 (1996) 6429-6435.
- [107] C. Schmitt Pauly, A.-C. Genix, J.G. Alauzun, G. Guerrero, M.-S. Appavou, J. Pérez, J. Oberdisse, P.H. Mutin, Simultaneous Phase Transfer and Surface Modification of TiO₂ Nanoparticles Using Alkylphosphonic Acids: Optimization and Structure of the Organosols, *Langmuir*, 31 (2015) 10966-10974.
- [108] M.J. Lundqvist, M. Nilsing, S. Lunell, B. Åkermark, P. Persson, Spacer and Anchor Effects on the Electronic Coupling in Ruthenium-bis-Terpyridine Dye-Sensitized TiO₂ Nanocrystals Studied by DFT, *The Journal of Physical Chemistry B*, 110 (2006) 20513-20525.
- [109] G. Guerrero, P.H. Mutin, A. Vioux, Anchoring of Phosphonate and Phosphinate Coupling Molecules on Titania Particles, *Chemistry of Materials*, 13 (2001) 4367-4373.
- [110] A.N. Nikoloski, K.-L. Ang, Review of the Application of Ion Exchange Resins for the Recovery of Platinum-Group Metals From Hydrochloric Acid Solutions, *Mineral Processing and Extractive Metallurgy Review*, 35 (2014) 369-389.
- [111] S. Shen, T. Pan, X. Liu, L. Yuan, Y. Zhang, J. Wang, Z. Guo, Adsorption of Pd(II) complexes from chloride solutions obtained by leaching chlorinated spent automotive catalysts on ion exchange resin Diaion WA21J, *Journal of Colloid and Interface Science*, 345 (2010) 12-18.
- [112] R. Ruhela, K. Singh, B.S. Tomar, T.K. Shesagiri, M. Kumar, R.C. Hubli, A.K. Suri, Amberlite XAD-16 Functionalized with 2-Acetyl Amide Group for the Solid Phase Extraction and Recovery of Palladium from High Level Waste, *Industrial & Engineering Chemistry Research*, 52 (2013) 5400-5406.
- [113] Y.-S. Ho, Review of second-order models for adsorption systems, *Journal of hazardous materials*, 136 (2006) 681-689.
- [114] E. Aghaei, D.R. Alorro, N.A. Encila, K. Yoo, Magnetic Adsorbents for the Recovery of Precious Metals from Leach Solutions and Wastewater, *Metals*, 7 (2017).
- [115] S. Azizian, Kinetic models of sorption: a theoretical analysis, *Journal of Colloid and Interface Science*, 276 (2004) 47-52.
- [116] C. Montalbetti, V. Falque, Amide bond formation and peptide coupling, *Tetrahedron*, 61 (2005) 10827-10852.

- [117] J. Mao, S. Mukherjee, Y. Zhang, R. Cao, J.M. Sanders, Y. Song, Y. Zhang, G.A. Meints, Y.G. Gao, D. Mukkamala, M.P. Hudock, E. Oldfield, Solid-State NMR, Crystallographic, and Computational Investigation of Bisphosphonates and Farnesyl Diphosphate Synthase–Bisphosphonate Complexes, *Journal of the American Chemical Society*, 128 (2006) 14485-14497.
- [118] S.K. Davidowski, G.P. Holland, Solid-State NMR Characterization of Mixed Phosphonic Acid Ligand Binding and Organization on Silica Nanoparticles, *Langmuir*, 32 (2016) 3253-3261.
- [119] B. Fotoohi, L. Mercier, Some insights into the chemistry of gold adsorption by thiol and amine functionalized mesoporous silica in simulated thiosulfate system, *Hydrometallurgy*, 156 (2015) 28-39.
- [120] R.C. Smith, J. Li, S. Padungthon, A.K. Sengupta, Nexus between polymer support and metal oxide nanoparticles in hybrid nanosorbent materials (HNMs) for sorption/desorption of target ligands, *Frontiers of Environmental Science & Engineering*, 9 (2015) 929-938.
- [121] J.B. Schlenoff, S.T. Dubas, Mechanism of Polyelectrolyte Multilayer Growth: Charge Overcompensation and Distribution, *Macromolecules*, 34 (2001) 592-598.
- [122] S.T. Dubas, J.B. Schlenoff, Polyelectrolyte Multilayers Containing a Weak Polyacid: Construction and Deconstruction, *Macromolecules*, 34 (2001) 3736-3740.
- [123] S.T. Dubas, J.B. Schlenoff, Swelling and Smoothing of Polyelectrolyte Multilayers by Salt, *Langmuir*, 17 (2001) 7725-7727.